

AD628796



## SHOCK ATTENUATION IN SOLID AND DISTENDED MATERIALS

J. R. Rempel  
D. N. Schmidt  
J. O. Erkman  
W. M. Isbell

Stanford Research Institute  
Menlo Park, California  
Contract AF 29(601)-6040

TECHNICAL REPORT NO. WL-TR-65-119

February 1966

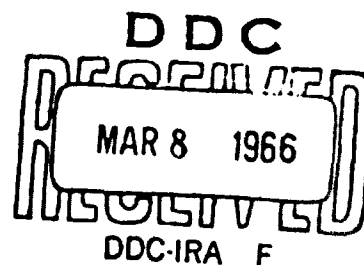
AIR FORCE WEAPONS LABORATORY  
Research and Technology Division  
Air Force Systems Command  
Kirtland Air Force Base  
New Mexico

CLEARINGHOUSE  
FOR JOURNAL SCIENTIFIC AND  
TECHNICAL INFORMATION  
Microfilm

5.00 \$ 0.75 162-00

REPRODUCTION COPY

Circle 1



PAGES \_\_\_\_\_  
ARE  
MISSING  
IN  
ORIGINAL  
DOCUMENT

Research and Technology Division  
AIR FORCE WEAPONS LABORATORY  
Air Force Systems Command  
Kirtland Air Force Base  
New Mexico

When U. S. Government drawings, specifications, or other data are used for any purpose other than a definitely related Government procurement operation, the Government thereby incurs no responsibility nor any obligation whatsoever, and the fact that the Government may have formulated, furnished, or in any way supplied the said drawings, specifications, or other data, is not to be regarded by implication or otherwise, as in any manner licensing the holder or any other person or corporation, or conveying any rights or permission to manufacture, use, or sell any patented invention that may in any way be related thereto.

This report is made available for study with the understanding that proprietary interests in and relating thereto will not be impaired. In case of apparent conflict or any other questions between the Government's rights and those of others, notify the Judge Advocate, Air Force Systems Command, Andrews Air Force Base, Washington, D. C. 20331.

Distribution of this document is unlimited.

SHOCK ATTENUATION IN SOLID AND DISTENDED MATERIALS

J. R. Rempel  
D. N. Schmidt  
J. O. Erkman  
W. M. Isbell

Stanford Research Institute  
Menlo Park, California  
Contract AF29(601)-6040

TECHNICAL REPORT NO. WL-TR-64-119

Distribution of this document  
is unlimited.

## FOREWORD

This report was prepared by the Stanford Research Institute, Menlo Park, California, under Contract AF29(601)-6040. The research was performed under Program Element 7.60.06.01.D, Project 5710, Subtasks 15.018 and 15.032, and was funded by the Defense Atomic Support Agency (DASA).

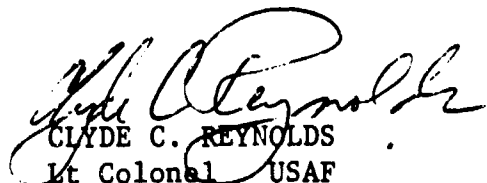
Inclusive dates of research are 1 August 1963 through 1 November 1965. The report was submitted 1 December 1965 by the AFWL Project Officer, Lieutenant George P. Crotwell, Jr., (WLRP).

The work was performed and is reported here in two distinct phases: 1, Foams; 2, Solids. Principal project scientists on Phase 1 were John Rempel and David Schmidt; those on Phase 2 were John Erkman and William Isbell. G. R. Fowles acted as project supervisor. Many other staff members of Poulter Research Laboratories contributed to various aspects of the work. The assistance of Captain William Niles of the Air Force Weapons Laboratory is gratefully acknowledged.

This report has been reviewed and is approved.



GEORGE P. CROTWELL, JR.  
1Lt USAF  
Project Officer



CLYDE C. REYNOLDS  
Lt Colonel USAF  
Chief, Physics Branch



WILLIAM H. STEPHENS  
Colonel USAF  
Chief, Research Division

## ABSTRACT

---

### PHASE 1: FOAMS

Results of optical measurements of peak pressures in the 0.1- to 6-kbar range transmitted through 3- to 12-mm-thick layers of certain foams, namely, 0.7 to 1.4 g/cc aluminum, 0.67 g/cc polyurethane, 1.1 g/cc beryllium, 1.1 and 1.7 g/cc graphite, and 1.0 g/cc silica, are presented. Superficial impact momentum densities are in the range of 0.6 to  $3 \times 10^4$  taps and are delivered by explosive propulsion of a thin sheet of aluminum.

Within the range of study, peak pressures scale approximately linearly with the ratio of superficial momentum density to superficial mass density of foam; the range of validity of the scaling and the scale factor depend strongly on the kind of foam. The effect of degree of distention on scaling relations in aluminum is slight but is somewhat greater in graphite. Of the foams considered, polyurethane transmits the least peak pressure per unit of added weight but shows the greatest tendency to increase the delivered momentum through rebound.

Through the use of parameter values measured in shock experiments an elementary theory predicts fairly reliably the conditions under which the transmitted shock structure consists of an elastic forerunner alone without a following locking wave. Presently available theory fails to predict accurately either observed peak pressures or wave shapes.

### PHASE 2: SOLIDS

Attenuation of shock waves is studied in specimens made of 1060 and 2024 aluminum, OFHC copper, gold, and Armstrong C-7 epoxy. The strains induced in the specimens are virtually one-dimensional. Comparison of experimental and calculated results indicate that an elastoplastic model for the relation between stress and strain should be used for aluminum,

copper, and the epoxy. Such a relation permits the prediction of the observed attenuation more exactly than does a relation in which rigidity is neglected.

Results for gold show that the shock is also attenuated more rapidly than predicted by the use of a stress-strain relation which neglects rigidity. More data are needed before a more appropriate stress-strain relation can be obtained for gold.

## CONTENTS

---

### PHASE 1: FOAMS

1. INTRODUCTION . . . . .	3
2. SUMMARY . . . . .	5
A. Experimental Methods and Results . . . . .	5
B. State of Our Understanding of Foam Behavior under Shock Loading . . . . .	8
1. The Forerunner . . . . .	8
2. The Main Wave . . . . .	17
C. The Best Foam . . . . .	34
D. Quasi-Static Compression of Foam . . . . .	36
E. The Effect of Heat . . . . .	36
3. MAJOR EXPERIMENTS . . . . .	41
A. Description of Two-Dimensional Techniques . . . . .	41
B. Quasi-Static Measurements . . . . .	51
C. Experiments in Preheated Foam . . . . .	59
D. After-Shot Observations . . . . .	64
E. Value of Explosive Momentum . . . . .	66
F. Foam Uniformity . . . . .	67
4. THEORY . . . . .	71
A. General . . . . .	71
B. Calculation by the Method of Characteristics . . . . .	72
C. Calculation by the Method of Artificial Viscosity . . . . .	
D. Interpretation of Experimental Results by the Simple Theory . . . . .	77
E. Foam Effectiveness as a Function of Parameters from the Simple Theory . . . . .	79
5. CONCLUSIONS AND FURTHER DIRECTIONS . . . . .	83
REFERENCES . . . . .	85



## CONTENTS

### PHASE 2: SOLIDS

1. INTRODUCTION . . . . .	89
2. SUMMARY . . . . .	91
3. EXPERIMENTAL ARRANGEMENT FOR STUDYING ATTENUATION OF SHOCKS IN SOLIDS . . . . .	93
A. Flyer Plate Assemblies . . . . .	93
B. Methods of Recording Attenuation Experiments . . . . .	100
4. RESULTS OF WEDGE EXPERIMENTS . . . . .	109
A. C-7 Epoxy Wedge-Shaped Specimen . . . . .	109
B. Aluminum Wedge-Shaped Specimen . . . . .	111
C. Copper Wedge-Shaped Specimen . . . . .	116
D. Gold Wedge-Shaped Specimen . . . . .	118
5. RESULTS OF EXPERIMENTS USING GAGES . . . . .	120
A. C-7 Epoxy Specimens . . . . .	120
B. Aluminum Specimens . . . . .	120
C. Copper Specimens . . . . .	124
6. CALCULATION OF ATTENUATING SHOCK WAVES . . . . .	130
7. COMPARISON OF RESULTS OF CALCULATIONS AND RESULTS OF EXPERIMENTS . . . . .	136
A. C-7 Epoxy . . . . .	136
B. Aluminum . . . . .	143
C. Copper . . . . .	148
D. Gold . . . . .	148
APPENDIX I MECHANISM CAUSING FLYER PLATES TO SPALL . . . . .	151
APPENDIX II THE OPTICAL LEVER ARM TECHNIQUE . . . . .	154
REFERENCES . . . . .	159
DISTRIBUTION. . . . .	160

## ILLUSTRATIONS

### PHASE 1: FOAMS

Fig. 1	Cross-Sectional View of General Experimental Arrangement . . . . .	6
Fig. 2	Typical Smear Camera Record . . . . .	7
Fig. 3	Approximate Wave Shapes . . . . .	11
Fig. 4	Effectiveness of Aluminum Foam . . . . .	21
Fig. 5	Pressure Attenuation in Four Foams . . . . .	22
Fig. 6	Observed Pressure History in Anvil Contrasted with that Forecast by Artificial Viscosity—Shot 9155 . . . . .	28
Fig. 7	Locking Solid Equation of State . . . . .	29
Fig. 8	Pressure Profile in a Foam According to Methods of Characteristics and of Artificial Viscosity . . . . .	30
Fig. 9	Distribution of Particle Speed in a Foam According to Methods of Characteristics and Artificial Viscosity . . . . .	31
Fig. 10	Quasi-Static, One-Dimensional Compression of Polyurethane . . . . .	37
Fig. 11	Smear Camera Record Showing Fast-Rising Forerunner—Shot 9832 . . . . .	41
Fig. 12	Outrunning in a Slab . . . . .	45
Fig. 13	Containment Tank Used with Foamed Beryllium . . . . .	47
Fig. 14	Experiments Mounted on Cover Plate . . . . .	52
Fig. 15	Quasi-Static Compression of Polyurethane Including Relaxation . . . . .	54
Fig. 16	Effect of Preheating on Compression of Polyurethane . . . . .	55
Fig. 17	Compression of Polyurethane under Various Length-to-Diameter Ratios . . . . .	57
Fig. 18	Effect of Preheating on Compression and One-Dimensional Strain of Closed-Cell Aluminum . . . . .	58
Fig. 19	Effect of Preheating on Compression of Open-Cell Aluminum . . . . .	60
Fig. 20	Effect of Preheating on Compression of ATJ Graphite . . . . .	61
Fig. 21	Effect of Preheating on Compression of Silica . . . . .	62
Fig. 22	View of Experiment with Thermal Isolation . . . . .	63
Fig. 23	Microphotodensitometer Survey of X-Ray Shadowgrams of a Foam Layer . . . . .	68
Fig. 24	Relation Between Pressure and Particle Speed Just Behind the Locked Front in Polyurethane Foam, Half-Space Struck by Aluminum Flyer . . . . .	74
Fig. 25	Modifications of Equation of State for Q-Calculations . . . . .	76

## ILLUSTRATIONS

### PHASE 2: SOLIDS

Fig. 1	Flyer Plate Assembly . . . . .	94
Fig. 2	Results of Flyer Plate Planarity Tests . . . . .	95
Fig. 3	X-Ray Pictures of Flyer Plates in Motion . . . . .	97
Fig. 4	X-Ray Picture of Spalled Flyer Plate . . . . .	99
Fig. 5	Wedge and Light Source Cover Mounted on Vacuum Chamber . . . . .	102
Fig. 6	Smear Camera Record of an Optical Lever Shot . . . . .	103
Fig. 7	Construction of Manganin Wire Transducer . . . . .	104
Fig. 8	Arrangement of Three Transducers for a Single Shot . . . . .	105
Fig. 9	Typical Transducer Record . . . . .	107
Fig. 10	Pressure in C-7 Epoxy vs. $x/x_0$ . . . . .	110
Fig. 11	Record of Motion of Free Surfaces of Aluminum and Copper Wedges . . . . .	112
Fig. 12	Peak Particle Velocity in Aluminum vs. $x/x_0$ . . . . .	114
Fig. 13	Peak Particle Velocity in Copper vs. $x/x_0$ . . . . .	117
Fig. 14	Peak Particle Velocity in Gold vs. $x/x_0$ . . . . .	119
Fig. 15	Pressure vs. Time from Gages Hit with Aluminum Plates . . . . .	121
Fig. 16	Pressure in C-7 Epoxy vs. $x/x_0$ . Results from Optical and Transducer Shots . . .	123
Fig. 17	Pressure from Gages on Aluminum Specimens vs. Time . . . . .	125
Fig. 18	Pressure from Gages on Copper Specimens vs. Time . . . . .	127
Fig. 19	Elastoplastic Equation of State . . . . .	131
Fig. 20	Comparison of Calculated Wave Profiles with Results of Gages for C-7 Epoxy . . .	137
Fig. 21	Comparison of Calculated Wave Profiles with Results of Gages for C-7 Epoxy. Elastoplastic Equation of State for Aluminum ( $M = 0.055$ ) . . . . .	139
Fig. 22	Pressure in C-7 Epoxy vs. $x/x_0$ from Experiments and Calculations . . . . .	141
Fig. 23	Comparison of Calculated Wave Profiles with Results of Gages for Aluminum Targets . . . . .	145
Fig. 24	Comparison of Calculated Wave Profiles with Results of Gages for Copper Targets . . . . .	149
Fig. I-1	( $x, t$ ) Diagram of Flyer Plate Driven by a Brass Buffer Plate . . . . .	152
Fig. II-1	Geometry for Optical Lever Arrangement . . . . .	154
Fig. II-2	Diagram of Two-Dimensional Shot . . . . .	156

## TABLES

---

### PHASE 1: FOAMS

Table 1	Results of Major Experiments . . . . .	9
Table 2	Comparison of Measurements of Forerunner Speed in Foams with Predictions . . .	18
Table 3	Forerunner Strength of Foams Compared with Quasi-Static Yield Strength . . . .	19
Table 4	Experimentally Observed Impulse Gains . . . . .	24
Table 5	Calculated and Observed Stopping Power of Foam . . . . .	35
Table 6	Quasi-Static One-Dimensional Compression of Foams . . . . .	38
Table 7	After-Shot Densities and Sound Speeds of Foams . . . . .	65
Table 8	Deduction of Shock Speed in Locked Polyurethane (0.67 g/cc) from Main Wave Pressure and Reverberation Time . . . . .	78

### PHASE 2: SOLIDS

Table 1	Values of Constants for Murnaghan Equation of State . . . . .	130
Table 2	Values of Constants for Elastoplastic Equations of State . . . . .	132

**PHASE 1: FOAMS**

*By*

J. R. REMPEL

*and*

D. N. SCHMIDT

## 1. INTRODUCTION

An interposed layer of porous or foamed material can often sharply reduce the peak stress reached in a hard body as a result of deposition of X-ray energy. The foam may then be a means of protecting the body against pressure damage. We have studied this property in several widely different foams useful in lowering impact stresses due to collisions lasting 10 to 100  $\mu\text{sec}$  in which momentum densities in the neighborhood of  $1 \times 10^4 \text{ dyne sec cm}^{-2}$  (taps) are exchanged. The first goal has been exploration of the effect; the second, semiquantitative prediction using easily accessible physical properties of foams; and the third, understanding of the detailed flow within the foam during the impact. Methods of investigation have included measurements of static properties of foams, observations of foam behavior under shock, and calculations.

The work on this and on previous contracts<sup>1,2</sup> has yielded considerable exploratory information on distended plastics, silica, graphite, beryllium, and several kinds of aluminum. In all these materials it is established that there is a protective effect and that there are two mechanisms responsible: the two-wave nature of the flow in certain distention ranges of these foams and the relatively large disparity between crushing wave speed and speed of overtaking rarefactions. A heavy enough impact upon a foam layer gives rise at the struck surface to a wave of pronounced change moving into the foam; the voids are removed, and the density greatly increased. If high stress is not kept on the struck surface, release waves start from that surface toward the shock front and, because of the large changes in the nature of the material brought about by the crushing or main wave, these release waves quickly overtake the impact wave and steadily reduce its speed and pressure. This tends to lower the pressure finally delivered to the protected structure. Sometimes splitting off from and moving ahead of the main wave, another wave of much less density change may carry off at high speed an important part of the total impact momentum at the first or outer foam interface and deliver it to the structure to be protected at a relatively low, constant pressure applied for a relatively long time; this wave is related to the linear or proportional region in a statically measured stress-strain

diagram. Since, when it is present, it comes to the structure ahead of the main or crushing wave we call it the first or forerunning wave.

As is plain from the summary in Section 2 of this report, much remains to be learned of the generally true details of flow in foams. The further research outlined in the fifth and last section would help to throw light on these details. Sections 3 and 4 contain descriptions of this year's experiments and calculations, respectively.

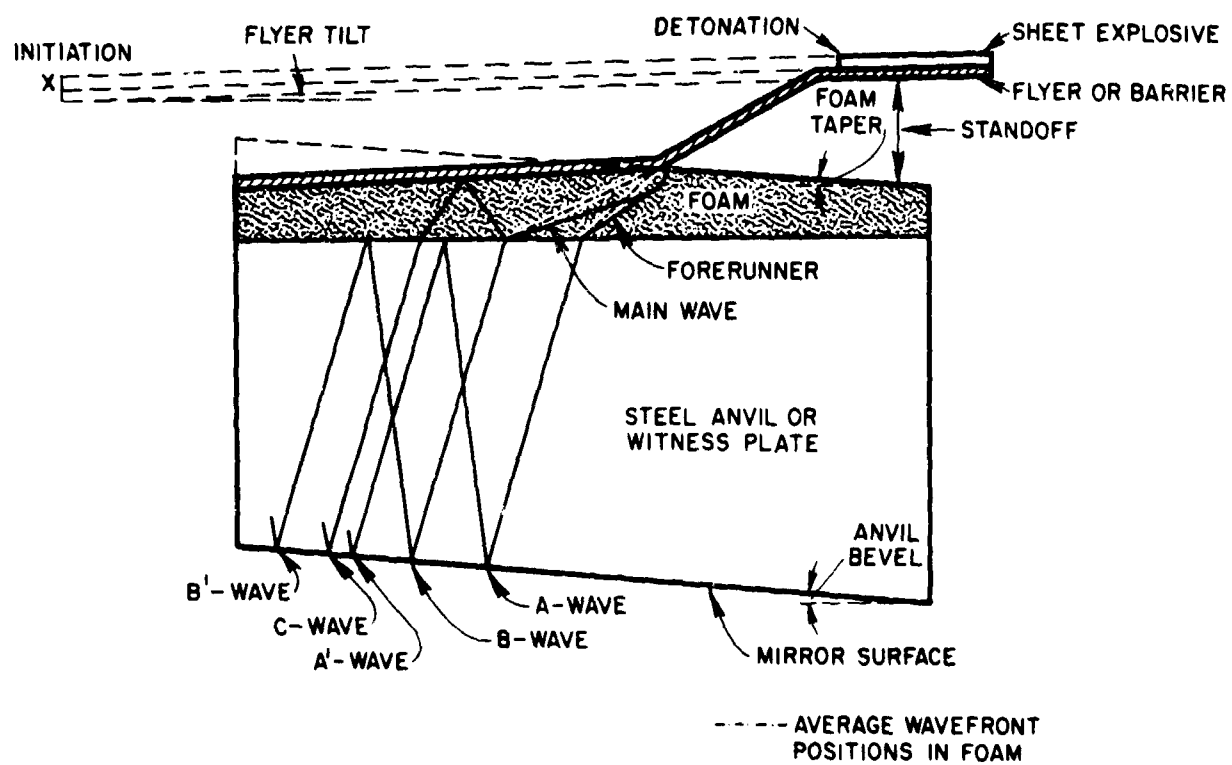
## 2. SUMMARY

### A. EXPERIMENTAL METHODS AND RESULTS

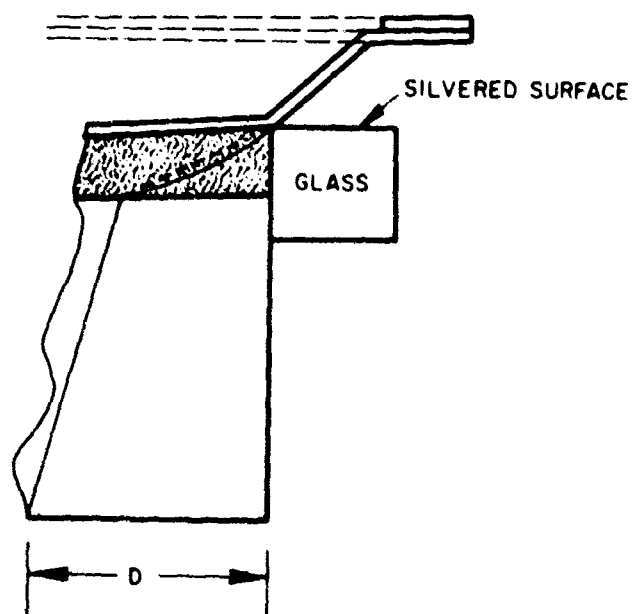
We explosively put a certain amount of momentum per unit area in the range  $0.5$  to  $5 \times 10^4$  taps into one side of a foam layer 3 to 12 mm thick and by high-speed photography of light images formed in a polished surface measured the shapes, pressures, and speeds of stress waves in a steel anvil in contact with the opposite side of the foam. The basic method is the optical lever arm described by Fowles.<sup>3</sup> Except for a few cases in which the explosive lay directly against the foam, momentum was delivered by an aluminum sheet, 0.012 to 0.040 inch thick. For one-dimensional (1-D) symmetry the sheet was driven by an explosive lens across a vacuum gap onto the foam; in this arrangement the anvil is wedge-shaped.<sup>2</sup> The more usual arrangement allowed a small amount of obliquity and involved a running detonation front in sheet explosive lying against the aluminum sheet; these are called two-dimensional (2-D) experiments.<sup>2</sup> For the 1-D experiments we know accurately the value of momentum density applied to the foam; in the 2-D the relation between the momentum density and the explosive thickness is known only to an accuracy of  $\pm 10$  percent.<sup>4</sup> Because of its ease of performance and because of a wish to survey behavior in a wide variety of foams, we used the 2-D arrangement this year in all experiments. Figure 1 is an illustration of the arrangement including all its variations; Fig. 2 is a record made with the basic arrangement, i.e., flyer in contact with a plane parallel slab of foam lying on a plane parallel steel anvil. The light source responsible for the images seen in the figure is an explosive argon bomb with a ruled translucent grid described by Pressman.<sup>5</sup> The small amount of obliquity must always be kept in mind when comparing peak pressures and wave shapes in 1-D and 2-D experiments in the same thicknesses of the same material; however, in the survey comparing results in widely different materials, obliquity is not critically important.

The kinds of foam studied this year have been polyurethane, open- and closed-cell aluminum, silica, beryllium, and graphite.





(a)



(b)

68 463 43

FIG. 1 CROSS-SECTIONAL VIEW OF GENERAL EXPERIMENTAL ARRANGEMENT

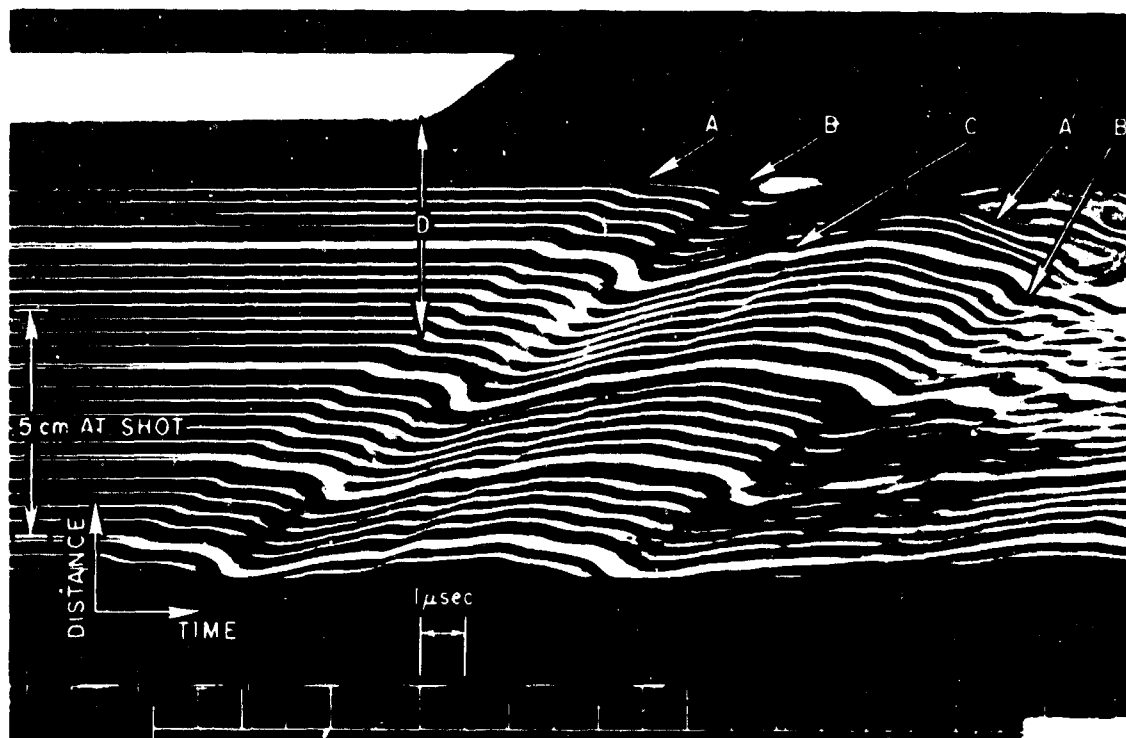


FIG. 2 TYPICAL SMEAR CAMERA RECORD

For each shot Table 1 lists foam kind, density, and thickness, then explosive thickness (approximately 0.016 inch provides  $1 \times 10^4$  taps, except when there is an air gap between flyer and foam 0.0243 inch =  $1 \times 10^4$  taps), and anvil thickness. Sometimes we measured detonation speed with time-of-arrival switches or "pins" on the explosive; always the smear camera photographed the motion of images in the anvil free surface. When the aluminum sheet (called "flyer" or "barrier") was separated by an air gap from the foam or when the foam was preheated, "standoff" or "hot," respectively, was entered in the column headed "Type of Experiment." Two anvils with nonparallel surfaces are also noted in this column.

In Table 1 the emergent waves are identified by the letter A for elastic forerunner and B for main or locking wave. When the first wave is double, its parts may be signaled by A-1 or A-2. Pressure jumps (not peak pressures) in each wave are entered after each wave designation and are presumed to exist at the foam-anvil interface although they are measured at the anvil free surface. Apparent wave speed means the speed of the front along this free surface and within experimental error should equal detonation speed ( $7.35 \pm 0.07$  mm/ $\mu$ sec at ordinary temperatures) unless a beveled anvil, tapered slab, or tilted flyer is used. In each

experiment involving a preheated specimen detonation speed was measured again, and these results are noted in Table 1. Average wave speed (in the foam) is inferred from the separation [D in Fig. 1(b)] along the anvil mirror surface between detonation and point of wave emergence by assuming a planar wave front in the foam as well as in the anvil.

Because this deduced value depends strongly on the value taken for the apparent wave speed,  $7.35 \text{ mm}/\mu\text{sec}$  is used whenever the experimental measurement of apparent speed agrees with that value within the uncertainty of the measurements. In computing the pressure jumps from the camera record the same rule is followed, although the computation is much less sensitive to apparent speed. It should be noted that the average speed of a forerunner as read in Table 1 will be higher than its characteristic speed by an amount increasing with the delay between initial impact and forerunner emergence ahead of the main shock.

Figure 3 shows approximate pressure histories at the foam-anvil interface sketched from the smear camera photographs. Written beside each outline is the total impulse showing in it up to the point on the time-axis marked by the arrow, when the observation was interrupted by reverberations or the pressure returned finally to zero.

## B. STATE OF OUR UNDERSTANDING OF FOAM BEHAVIOR UNDER SHOCK LOADING

### 1. THE FORERUNNER

In some solids a single impact may give rise to a train of two shock fronts of which the speed and pressure of the first are characteristic of the material.<sup>6</sup> Elastic-rigid foams often support two successive waves stemming from the same impact. Noticing that strain in quasi-static, 1-D compression of elastic-rigid foam is proportional to stress up to a certain limit (defined as the stress where strain falls out of proportionality by 0.2 percent) or yield stress, we have sought to identify this elastic or proportional limit state with the state behind the first or forerunning wave; but in the one elastic-rigid foam examined accurately<sup>2</sup> for the correlation (0.67 g/cc polyurethane) we have forecast a forerunner speed from the modulus of linear compression which is 20 percent lower than measured. This discrepancy may be due to lack of uniformity in the physical properties among specimens of the same kind and similar density. In none of the several foams studied has the proportional limit or yield

Table 1  
RESULTS OF WIND EXPERIMENTS

SHOT NO.	TEST ITEM MATERIAL		SPECIFIC GRAVITY	THICKNESS (in)	TYPE OF EXPLOSIVE	OTHER DESCRIPTION	SHOT NO.	WIND PRESSURE (lb/ft <sup>2</sup> )		APPROXIMATE WIND SPEED (ft/sec)	WIND DIRECTION (deg)	REMARKS
	Type	Average Density (g/cc)										
9792	MB-AI	0.76	1.46 ± 0.005	0.030	2-D slab	Specimen 4" x 6" Explosive 4" x 12" point initiated Barrier 0.020" AI Avail 4" x 6" x 1" 4340 steel	H	20.1 -1.7 +1.3	7.7 ± 0.3	10.50 ± 0.1		Sharp jump, return was to flat for 1 sec. then pressure rapidly increased
9793	P-I	0.64	Variable 17.61 to 2.90 ± 0.15	0.016	2-D slab tapered	Specimen 4" x 12" Explosive 4" x 12" point initiated Barrier 0.020" Nylon 2 Avail 4" x 6" x 1" 4340 steel	A	1.05 ± 0.2 Using $U_0 = 11.0 ± 2.0$	11.0 ± 2.0	1.5 ± 0.1 from taper and $U_0 = 11.0 ± 2.0$		A-front sharp. Possible weak failure at throat end of foam. Unstable slight trend toward weaker A-front as foam thickens. Indication of turbulent appeared near end.
9800	MB-AI	0.96	4.09 ± 0.02	0.025	2-D slab	Specimen 4" x 6" Explosive 4" x 12" point initiated Barrier 0.012" AI Avail 4" x 6" x 1" 4340 steel	B	12 ± 2	7.1 ± 0.1	1.01 ± 0.05		Indication of turbulence in early part of record. Sharp jump, wave flat for less than 1 sec. Rapid decay to zero.
9801	MB-AI	0.95	6.11 ± 0.02	0.025	2-D slab	Same as Shot 9800	B	5.0 ± 0.5	7.1 ± 0.1	0.70 ± 0.15		Wave taken ~2.5 msec. to reach maximum stress less than 1 msec.
9802	MB-AI	0.990 ± 0.007	8.05 ± 0.03	0.025	2-D slab	Same as Shot 9800	A	0.33 ± 0.03	7.5 ± 0.1	Failed		Both faces gradual. B-front wave in 2.5-3.0 msec. to peak above pressure wave ~4 msec.
9803	MB-AI	0.960 ± 0.001	5.94 ± 0.03	0.015	2-D slab	Same as Shot 9800	B	1.9 ± 0.5	7.4 ± 1.0	Failed		Both waves gradually rising. B-front taken 2.5 msec. to reach peak, stays 4 msec.
							A	0.37 ± 0.05	7.3 ± 0.3	Failed		
9804	P-I	0.67	Variable 18.21 to 2.64 ± 0.10	0.025	2-D slab tapered	Same as Shot 9794 except barrier was 0.012" AI	A	0.77 ± 0.10 Using $U_0 = 11. ± 1.1$	11.0 ± 1.1	1.7 ± 0.2 -0.1 from taper and $U_0 = 11. ± 1.1$		A-wave sharp. B gradual, accumulating up to foam thickness increased. Possible slight trend toward lower pressure in A-front with thickness of foam.
							B	~1 to ~4.3 Using $U_0 = 25 to 10$	~25 to ~10			
9809	MB-AI	0.688 ± 0.024	4.47 ± 0.14	0.0165	2-D slab	Same as Shot 9800	B	6.6 ± 0.4	7.05 ± 0.1	0.605 ± 0.08		Sharp jump; steady return to zero through disturbed record.
9832	P-I	0.645 ± 0.007	12.67 ± 0.05	0.050	2-D slab	Specimen 4" x 12" Explosive 4" x 12" point initiated Barrier 4" x 12" 0.012" AI Avail 1" x 4" x 12" 4340 steel	A	1.0 ± 0.0 -0.2 Using $U_0 = 7.54$	7.54 ± 0.15	1.65 ± 0.1 Using $U_0 = 7.54$		Probably apparent B-strength raised by re-orientation of A-front to wall. Wave trend toward higher stress at later times.
							B	5.0 ± 0.1 -0.7 Using $U_0 = 7.54$	7.5 ± 0.3			
9833	P-I	0.644 ± 0.007	12.69 ± 0.002	0.050	2-D slab	Same as Shot 9832 except avail 2" thick	A	1.0 ± 0.22 Using $U_0 = 8.0$	8.0 ± 0.1	1.0 ± 0.3 Using $U_0 = 8.0$		Both waves gradually rising. B-front taken 2.5 msec. to reach peak, stays ~4 msec.
							B	3.4 ± 0.0 Using $U_0 = 8.0$	8.0 ± 0.1			
9834	MB-AI	0.925 ± 0.004	6.10 ± 0.02	0.017	2-D slab	Same as Shot 9800	A	0.29 ± 0.04	7.4 ± 0.3	0.57 ± 0.08		Both waves gradually rising. B-front taken 2.5 msec. to reach peak, stays ~4 msec.
							B	0.01 ± 0.17	7.4 ± 0.3			
9835	MB-AI	0.927 ± 0.004	6.07 ± 0.01	0.017	2-D slab	Same as Shot 9800 except avail 2" x 6" x 8"	Failed					
9801	N <sub>2</sub>	1.049	6.50 ± 0.005	0.0115	2-D slab	Same as Shot 9800	A1	0.36 ± 0.04	7.27 ± 0.21	2.13 ± 0.10		Both waves gradually rising.
							A2	0.10 ± 0.07				
9892	MB-AI	1.445	4.09 ± 0.15	0.018	2-D slab	Same as Shot 9800	A	1.49 ± 0.05	7.325 ± 0.13	2.14 ± 0.27		Sharp A-front. A wave flat for ~7 msec. then falls slowly. Possible gradual reflection off floor or B-wave ~8 msec after A-arrival.
9893	N <sub>2</sub>	1.053	6.46 ± 0.005	0.0175	2-D slab	Same as Shot 9800	A1	0.39 ± 0.04 Using $U_0 = 0.91 ± 0.10$	0.91 ± 0.10	1.8 ± 0.4 Using $U_0 = 0.91 ± 0.10$ 2.2 ± 0.1 Using $U_0 = 7.35 ± 0.05$		2-step jump in A-wave. Both waves rise slowly.
							A2	0.28 ± 0.03 Using $U_0 = 0.91 ± 0.02$				
							B	1.8 ± 0.2 Using $U_0 = 0.91 ± 0.02$				
9894	MB-AI	1.458	4.01 ± 0.01	0.025	2-D slab	Same as Shot 9800	A1	2.4 ± 0.30	7.3 ± 0.5	2.45 ± 0.1		Both jumps sharp. A displacement falls about 2% before B-arrival. B-wave flat for ~1 msec. Possible reflection of B-wave off floor ~8 msec after B-arrival. Stability in each wave reached only near end of detonation run.
							A2	2.0 ± 0.4				
							B	4.5 ± 0.5		1.04 ± 0.1		
9895	MB-AI	1.48	1.82 ± 0.05	0.0172	2-D slab	Specimen 4" x 6" Explosive 4" x 12" point initiated Barrier 4" x 12" 0.012" AI Avail 4" x 6" x 2" 4340 steel	A	Not reliable	Not reliable	Not reliable		B-front overshoots A-wave about 2" from top of wall. B-front sharp. Both very gradual reflection off floor occurring ~1 msec after B-front. B-wave exceeds after jump.
9896	N <sub>2</sub>	1.048	6.11 ± 0.02	0.0174	2-D slab	Same as Shot 9890	A1	0.835 ± 0.10 Using $U_0 = 7.15$	7.15 ± 0.15	2.9 ± 0.1 Using $U_0 = 7.15$		A-fronts gradual. B sharp. B-wave flat for 2.5 msec. Magnitude of jump less in early half of record.
							A2	0.94 ± 0.10 Using $U_0 = 7.15$				
							B	2.52 ± 0.10 Using $U_0 = 7.15$	7.22 ± 0.24			
9897	MB-AI	1.41	1.05 ± 0.05	0.025	2-D slab	Same as Shot 9890	A	0.40 ± 0.05	8.11 ± 0.8	2.40 ± 0.22		Gradual A-wave sharp. B-front B-wave flat for less than 1 msec. Possible weak reflection off floor ~7 msec after B-arrival.

Table 1 continued

SHOT NO.	SPECIMEN MATERIAL			EXPLOSIVE THICKNESS (inch)	TYPE OF EXPERIMENT	OTHER DIMENSIONS	WAVE IDENTITY	$\Delta P$ MAXIMUM PRESSURE JUMP <sup>†</sup> (kbar)	$U_a$ APPARENT WAVE SPEED (mm/ $\mu$ sec)	$\bar{U}$ AVERAGE WAVE SPEED (mm/ $\mu$ sec)	REMARKS
	Type	Average Density (g/cc)	Thickness (mm)								
9933	MD-AO	1.279	8.11 $\pm$ 0.01	0.050	2-D slab	Same as Shot 9930	A	0.60 $\pm$ 0.05 Using $U_a = 6.84$	6.84 $\pm$ 0.23	2.89 $\pm$ 0.23 Using $U_a = 7.35$ 1.99 $\pm$ 0.45 Using $U_a = 6.84$	Gradual A-rise, sharp B-front. B-wave flat for less than 1 $\mu$ sec. Reflection off flyer 6.7 $\mu$ sec after B-arrival.
10035	C-PT0114	1.15	5.10 $\pm$ 0.03	0.0165	2-D slab	Specimen 5" $\times$ 8" Explosive 5" $\times$ 12" point initiated Barrier 5" $\times$ 12" $\pm$ 0.012" Al Avail 2" $\times$ 6" $\times$ 8" 4340 steel	B	8.1 $\pm$ 1.3 3.86 $\pm$ 0.20	7.30 $\pm$ 0.90 7.14 $\pm$ 0.26	1.24 $\pm$ 0.10	Sharp B-front, steady long decay. Clear reflection off barrier 5.25 $\mu$ sec after B-arrival.
10036	C-PT0114	1.15	8.10 $\pm$ 0.02	0.0165	2-D slab	Same as Shot 10035	B	3.0 $\pm$ 0.2 Using $U_a = 7.7$	7.7 $\pm$ 0.1	1.0 $\pm$ 0.1	Possible forerunner over-run by ray from bottom of record. B-front sharp, gradual steady decay. Possible weak reflection off barrier either 6.7 or 10.6 $\mu$ sec after B-arrival.
10037	C-PT0114	1.15	8.07 $\pm$ 0.03	0.0106	2-D slab	Same as Shot 10035	A	0.6 $\pm$ 0.2	Not reliable	Not reliable	Indication of A-wave instability gradually rising A front.
							B	0.695 $\pm$ 0.09	7.5 $\pm$ 0.3	0.82 $\pm$ 0.03	Sharp B-front followed by steady, long relaxation. Possible weak barrier reflection either 6.7 or 10.4 $\mu$ sec after B-arrival.
10082	C-ATJ	1.73	6.00 $\pm$ 0.03	0.0165	2-D slab	Same as Shot 10035 except specimen 5" $\times$ 12"	A	0.665 $\pm$ 0.04	7.1 $\pm$ 0.3	1.7 $\pm$ 0.1	Stability reached only near middle of record. A-front gradual, B-front sharp, long gradual relaxation. Possible weak reflection off flyer.
10083 <sup>§</sup>	C-ATJ	1.73	6.02 $\pm$ 0.05	0.016	2-D slab	Same as Shot 10082	A	0.715 $\pm$ 0.07 0.74 $\pm$ 0.07 edge	7.2 $\pm$ 0.3 7.5 $\pm$ 0.3	1.8 $\pm$ 0.15 1.6 $\pm$ 0.15	No significant difference seen between reflection waves 1/2" wide, 1/2" apart. Pressure transducer has not enough time resolution.
							B	1.7 $\pm$ 0.2 1.4 $\pm$ 0.2 edge			
10084	C-ATJ	1.73	4.00 $\pm$ 0.01	0.0165 $\pm$ 0.0005	2-D slab	Same as Shot 10082	B	5.7 $\pm$ 0.1	7.84 $\pm$ 0.75	1.1 $\pm$ 0.2	Weak reflection off flyer. B-wave flat on top for $\sim$ 1 $\mu$ sec, very sharp rise.
10260	P-C (CPN)	0.71	5.02 $\pm$ 0.02	0.021	2-D slab	Specimen 5" $\times$ 10" Explosive 4" $\times$ 13" point initiated Barrier 5" $\times$ 12" $\pm$ 0.012" Al Avail 2" $\times$ 6" $\times$ 8" 4340 steel (aluminized)	A	2.2 $\pm$ 0.2	7.6 $\pm$ 0.3	1.2 $\pm$ 0.1 Using $U_a = 7.35$	Sharp A-jump, gradual B-jump. Decay of B-wave begins almost immediately after arrival. A-B interval $\sim$ 4.8 $\mu$ sec. Usual smallness in forerunner traces.
							B	0.50 $\pm$ 0.03		1.4 $\pm$ 0.1 Using $U_a = 7.6$	
10261	P-C (CPN)	0.71	5.03 $\pm$ 0.02	0.021	2-D slab with standoff	Specimen 5" $\times$ 10" Explosive 4" $\times$ 12" point initiated Flyer 4" $\times$ 12" $\pm$ 0.012" Al Avail 2" $\times$ 6" $\times$ 8" 4340 steel (aluminized) Paper spacer 3/16"	A	1.6 $\pm$ 0.4 Using $U_a = 8.0$	8.0 $\pm$ 0.3	Not reliable	A-jump sharper than in Shot 10331 and 10332. B-front more gradually rising and more slowly decaying. Reflection off flyer about 2.5 $\mu$ sec after B-arrival. High apparent speed probably due to flyer and target foam not being parallel. A-B interval $\sim$ 1.8 $\mu$ sec.
							B	0.9 $\pm$ 0.2 Using $U_a = 8.0$	8.5 $\pm$ 0.2		
10331	P-C (CPN)	0.71	4.99 $\pm$ 0.01	0.020	Not 2-D slab with standoff	Same as Shot 10261 Foam temperature 107°C	A	1.08 $\pm$ 0.07 Using $U_a = 7.2$ or 7.7	7.2 $\pm$ 0.5	2.2 $\pm$ 0.5 Using $U_a = 7.2$	C-wave 3.8 $\mu$ sec behind B-front. B-wave flat $\sim$ 0.5 $\mu$ sec then gradually decays. A-B interval $\sim$ 1.7 $\mu$ sec (same as unheated Shot 10261).
							B	3.13 $\pm$ 0.09 Using $U_a = 7.13$	7.13 $\pm$ 0.15		
10332	P-C (CPN)	0.7025 $\pm$ 0.002	5.02 $\pm$ 0.02	0.0213	Not 2-D slab with standoff	Same as Shot 10261 Foam temperature 116°C	A	1.4 $\pm$ 0.1 Using $U_a = 7.13$	7.13 $\pm$ 0.30	1.33 $\pm$ 0.29 Using $U_a = 7.13$	Same as Shot 10331 except indication of semi-formity in temperature or material since both waves became weaker at later times.
							B	2.7 $\pm$ 0.5 Using $U_a = 7.13$ 2.4 $\pm$ 0.5 Using $U_a = 7.35$	7.3 $\pm$ 0.4		
10360	MD-AK	1.40 $\pm$ 0.01	5.00 $\pm$ 0.03	0.0235	Not 2-D slab with standoff	Same as Shot 10261 Foam temperature 318°C	A	0.72 $\pm$ 0.06	7.25 $\pm$ 0.46	Not reliable	Strong blurring of record by convection currents. Results doubtful.
							B	0.5 $\pm$ 0.15	7.5 $\pm$ 0.3		
10361	Si	0.521 $\pm$ 0.002	5.01 $\pm$ 0.01	0.0155	2-D slab with standoff	Same as Shot 10261	A	Not reliable	8.1 $\pm$ 0.3	Not reliable	Anomalous record.
							B	Not reliable			
10446	Bz	1.122	5.95	0.026	2-D slab bevelled avtil, standoff	Specimen 5" $\times$ 8" Explosive 4" $\times$ 12" Flyer 4" $\times$ 12" $\pm$ 0.012" Al Avail 2" $\times$ 6" $\times$ 8" bevelled 8" 22 Paper spacer 3/16"	A	1.4 $\pm$ 0.15 Using $U_a = 7.2$	7.2 $\pm$ 0.2	Not measured	
							B	3.1 $\pm$ 0.2 Using $U_a = 7.25$	7.25 $\pm$ 0.15		
10453	Bz	1.134	3.96	0.0117	2-D slab bevelled avtil, standoff	Same as Shot 10446	A	1.6 Using $U_a = 6.8$	6.8 $\pm$ 0.2	Not measured	
							B	2.1 $\pm$ 0.2 Using $U_a = 6.8$	6.8		

<sup>§</sup> All explosives type EL-5040 from Du Pont.

<sup>†</sup> Pressure ( $\Delta P$ ) and average wave speed ( $\bar{U}$ ) reduced from data using the value  $U_a = 7.35 \pm 0.05$  mm/ $\mu$ sec unless otherwise noted.

<sup>§</sup> Sapphire pressure gage and 2 camera slits were used in Shot 10001.

MD-AK Closed-cell aluminum foam } from Emerson and Cuming Inc., Gardena, Calif.

MD-AO Open-cell aluminum foam }

Si Silicon foam }

C-PT0114 Graphite foam } from National Carbon Co., Division of Union Carbide, Los Angeles, Tenn.

C-ATJ Graphite foam }

Bz Beryllium foam } from Brush Beryllium Co., Hayward, Calif.

P-C Closed-cell polyurethane, made by Petersen Products, Inc., Burlingame, Calif. from materials supplied by Polystyrene Corp., Richmond, Calif.

P-C (CPN) Closed-cell polyurethane, made by Petersen Products, Inc., Burlingame, Calif. from materials supplied by C-P-R Division of the Upjohn Co., Los Angeles, Calif.

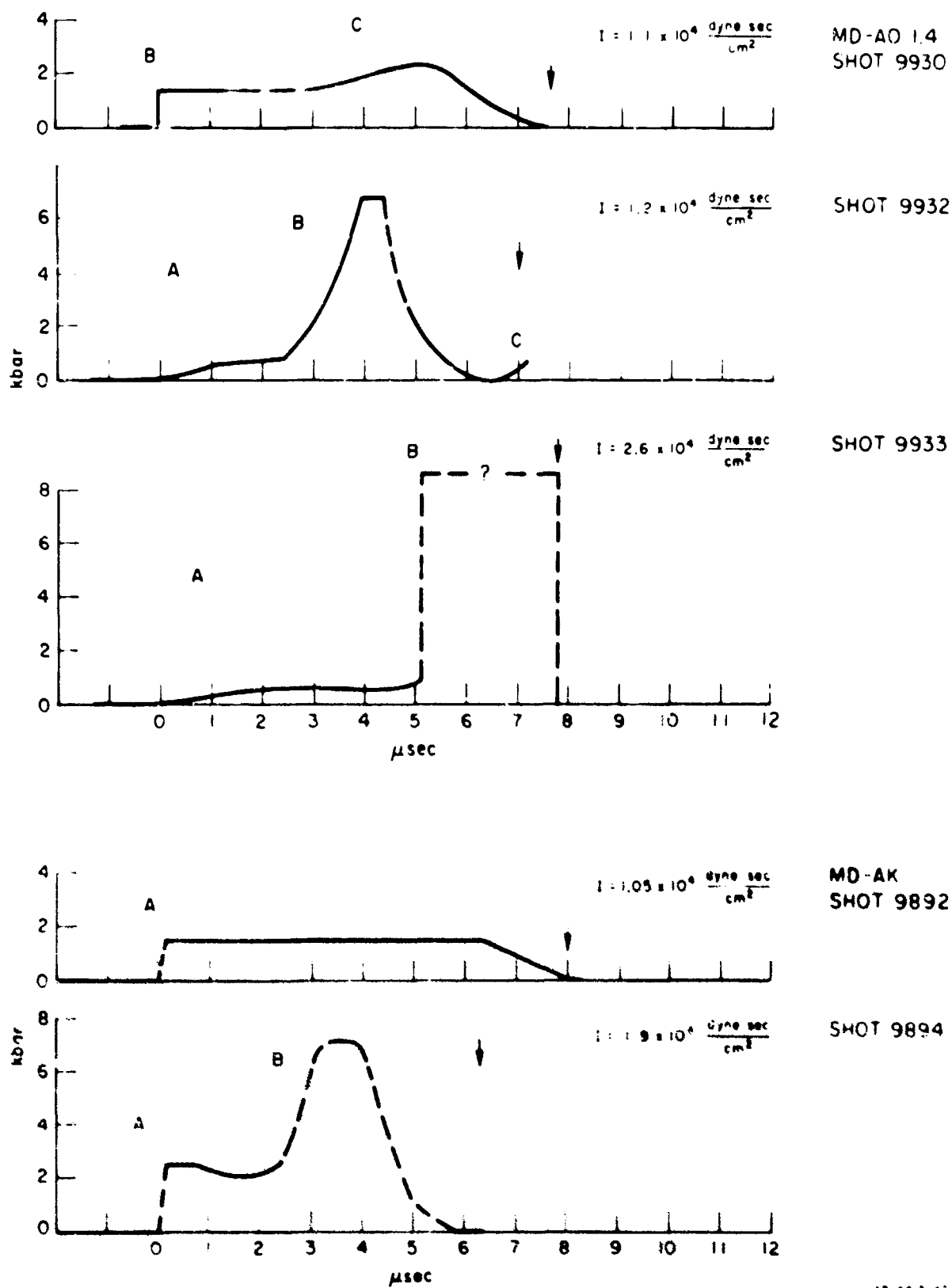
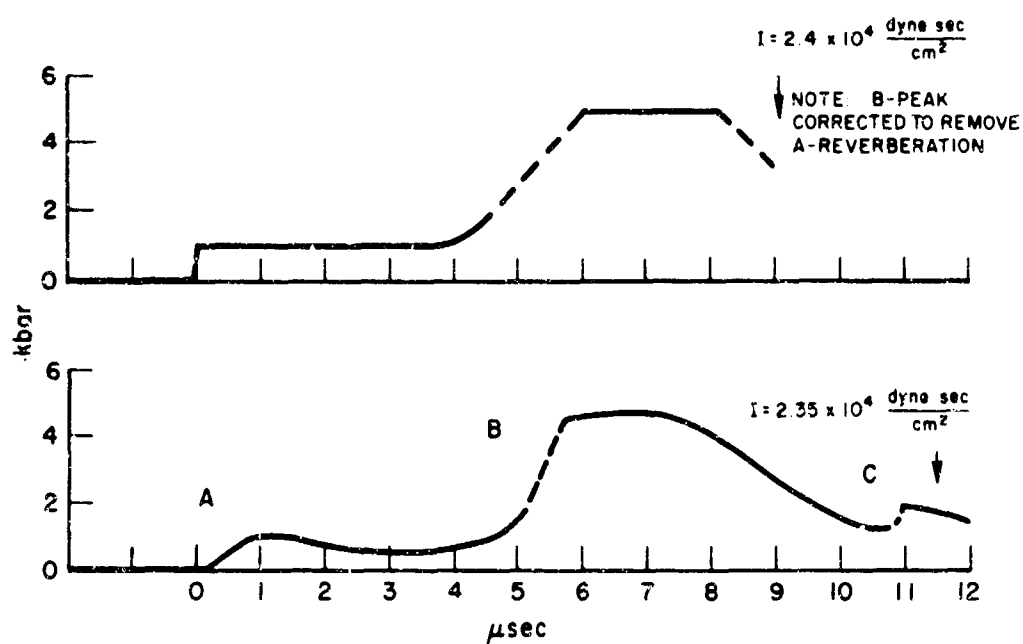
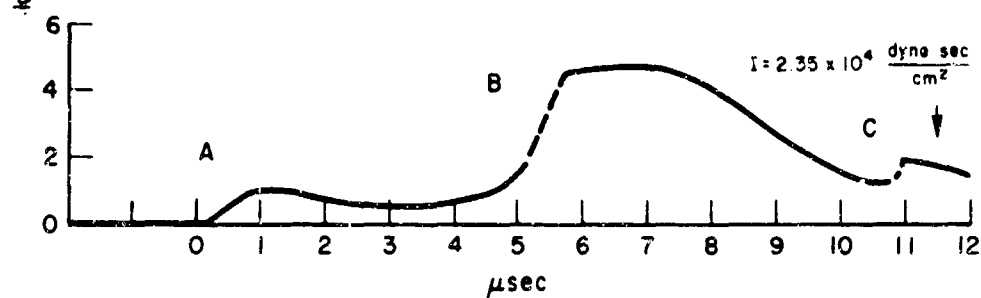


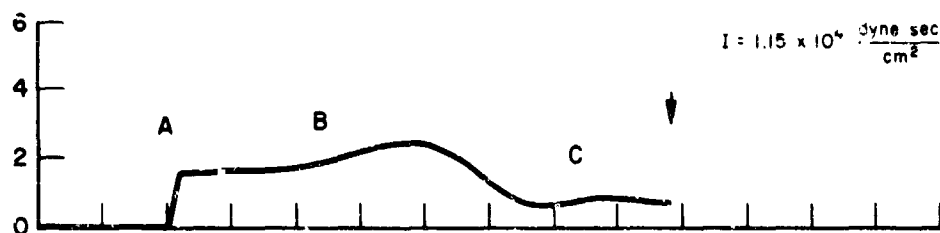
FIG. 3 APPROXIMATE WAVE SHAPES



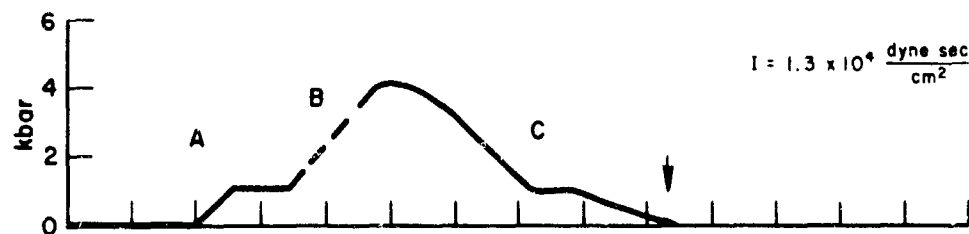
P-C (POLYTRON)  
SHOT 9832



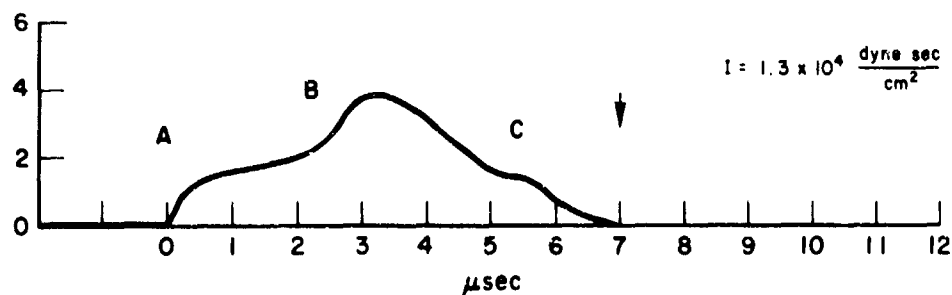
SHOT 9833



P-C (CPR)  
SHOT 10261



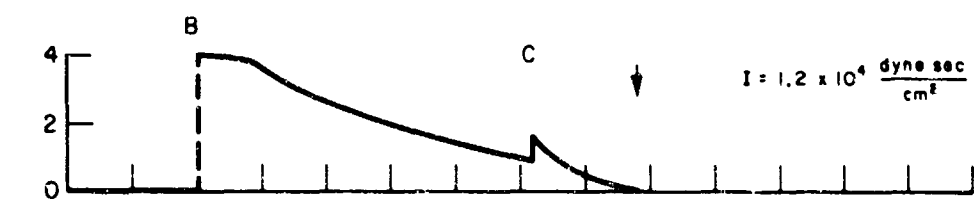
SHOT 10331



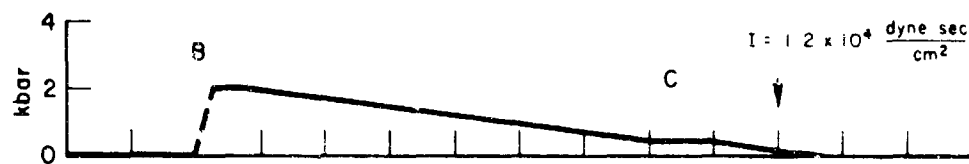
SHOT 10332

88-4613-48

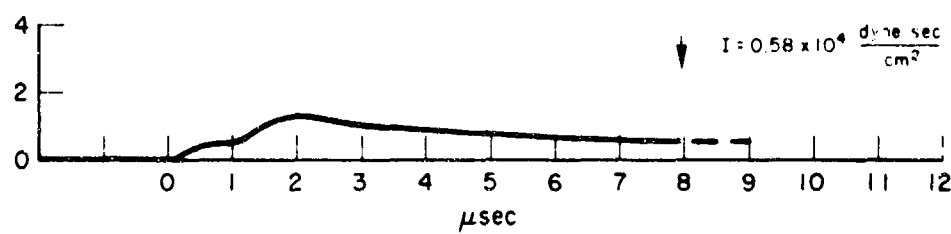
FIG. 3 APPROXIMATE WAVE SHAPES (Cont'd)



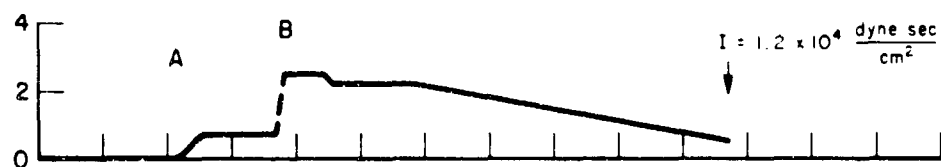
C (PT 1104)  
SHOT 10035



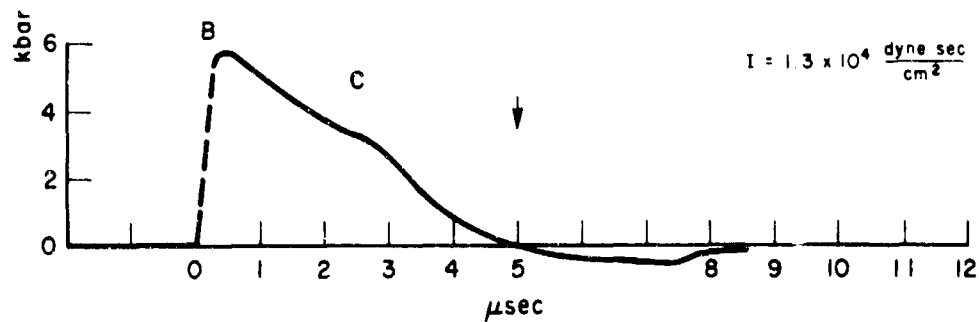
SHOT 10036



SHOT 10037



C (AT J)  
SHOT 10082



SHOT 10084

68-4613-49

FIG. 3 APPROXIMATE WAVE SHAPES (Cont'd)



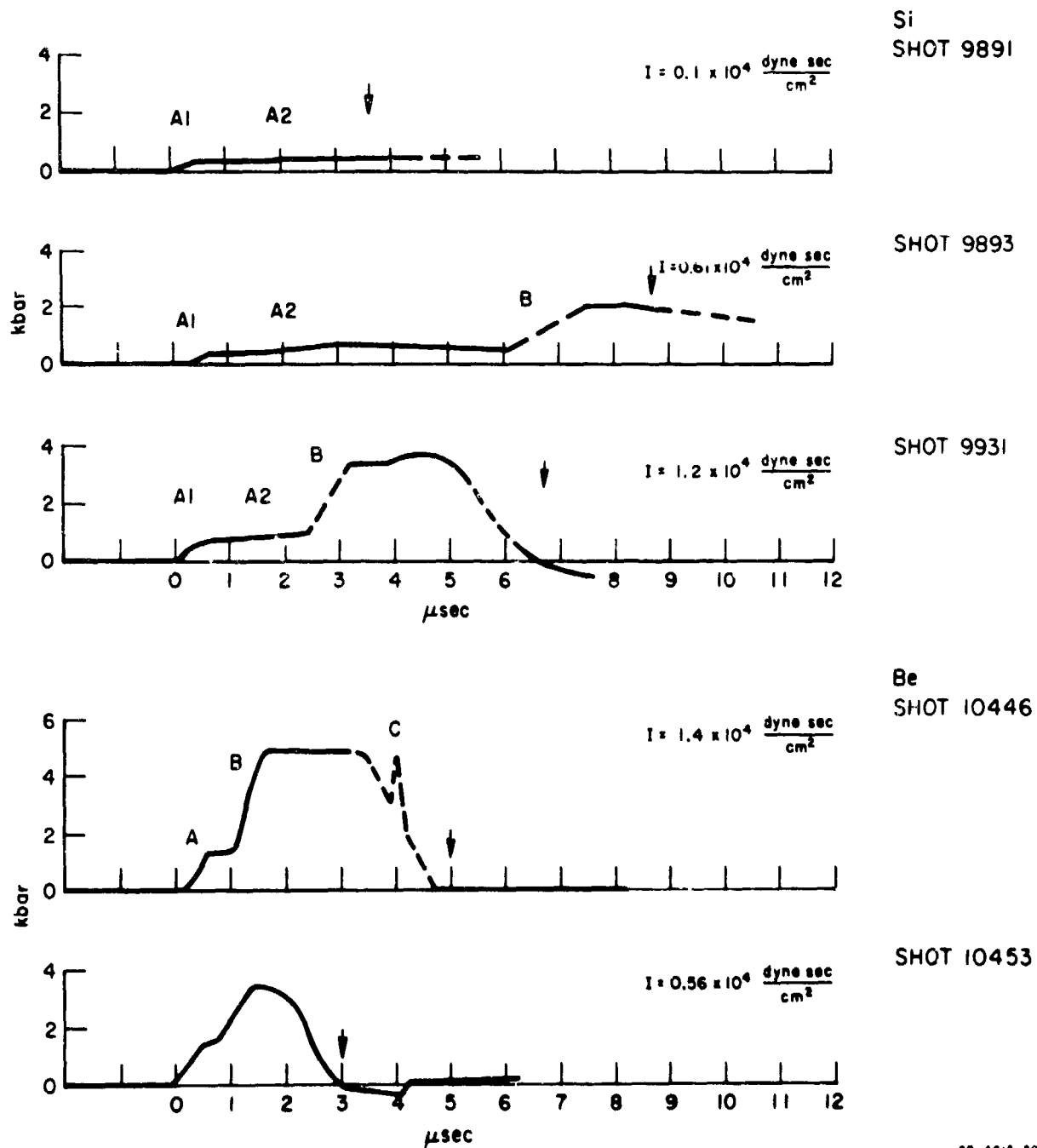
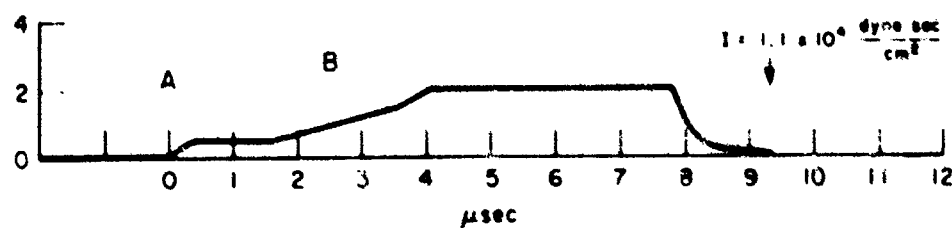
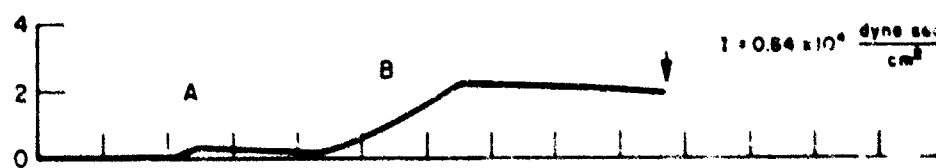
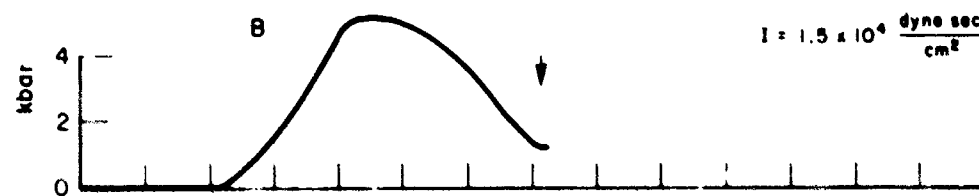
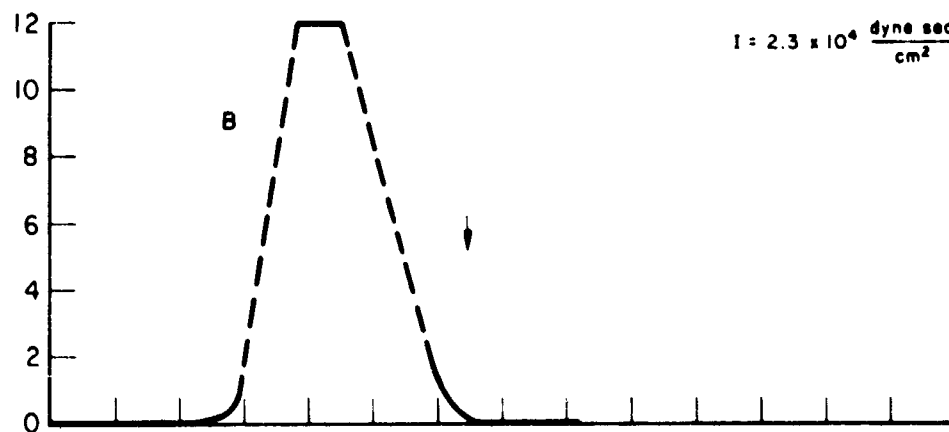
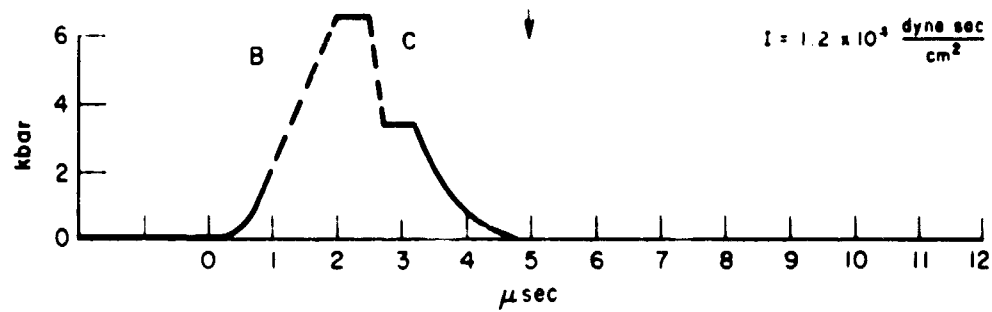


FIG. 3 APPROXIMATE WAVE SHAPES (Cont'd)



00 48.5 51

FIG. 3 APPROXIMATE WAVE SHAPES (Concl'd)

stress amounted to more than half the stress seen in a steel anvil struck by the forerunner. This can only be due to the effect of the rate of strain although the magnitude of the effect may be less than appears in the disparity between the pressure induced by the forerunner in the anvil and the yield stress, since the free-running forerunner stress is enhanced upon reflection from the wall. Because the anvil is relatively motionless under the impact, the product of pressure and volume increments across the reflected shock must equal the same product across the forerunner; hence for any likely equation of state the first wave stress cannot more than double itself at the wall.

Although we have observed forerunner speed in only one foam material, e.g., polyurethane, we have measured average speeds (Table 1 of first waves in several foams by an addition to the experiments by which we observed pressure histories. Since the forerunner may not break out ahead of the main wave until the main wave has slowed to the characteristic forerunner speed, observed average first wave speeds are upper limits upon this characteristic speed. In all experiments except one involving 0.9 g/cc open-cell aluminum and another in polyurethane (C-P-R), observed average wave speeds agree within experimental uncertainty with modulus speed or are higher than modulus speed. If strain-rate affects forerunner speed the influence must be less than 20 percent.

As the forerunner front moves through polyurethane it tends to lose its abruptness or discontinuous character.<sup>7</sup> Silica foam has never shown a steep pressure rise in the forerunner but regularly transmits first waves reaching end stress in two distinct, gradual stages usually more than a microsecond apart.<sup>8</sup> Such behavior suggests a compound nature of the first wave a purely elastic wave may be only a part of the forerunner. Or the loss of sharpness may be a feature of stress relaxation in the forerunner<sup>9</sup> of which we also have evidence in both polyurethane and aluminum.<sup>10</sup> Closed-cell aluminum on the other hand has always given a sharp forerunner; open-cell aluminum and graphite have shown both.

Evidence for the compound nature of the forerunner is our observation that measured sound speed<sup>\*</sup> has invariably been significantly higher than the speed predicted from the modulus of linear compression. The ratio of sound speed to modulus speed ranges from 3 in 0.9 g/cc open-cell

---

\* We timed the passage of a burst of 1 Mc supersonic energy through a thickness of foam.

aluminum and 1.2 g/cc beryllium to about 1 1/3 in 0.67 g/cc polyurethane. One measurement of modulus in silica yields a speed agreeing with sound speed.

Most of the average wave speeds are, however, lower than sound speed in the same kind and density of material, which is further evidence for the complex nature of the forerunner.

The foregoing comments on the forerunner are summarized in Tables 2 and 3. In Table 2 for each kind and density of foam studied appears a sound speed (column 2), one to three observed shock speeds (columns 3, 4, and 5) and the forerunner speed forecast from the modulus. Of the observed shock speeds that under Method A (column 3) is from a flash X-ray shadowgram reported by Fowles and Curran,<sup>1</sup> that under Method B (column 4) stems from simultaneous optical measurements of stress and speed in a foam wedge reported by Rempel,<sup>2</sup> and those under Method C (column 5) are the average wave speeds in Table 1.

Table 3 lists for each kind and density of foam a value of static yield stress (column 3). The tangent to the quasi-static stress-strain curve at the point where the second derivative of stress with respect to strain vanishes meets the extension of the linear portion at the stress value shown in column 4. Column 5 reports the observed stresses in a steel anvil resulting from forerunner impact; and in column 6 are the values of stress induced in a rigid wall if the foam Hugoniot followed the linear portion to the intersection in column 4 and then fell onto the tangent.

Except for the peak pressure behind it we know nothing of the nature of the wave reflected by the forerunner off the anvil. It would be a broad compression fan if the shock equation of state were like the quasi-static in shape and, if it were, we could understand why we have not seen the shadow of the wall-reflected wave in X-ray shadowgrams.<sup>11</sup>

## 2. THE MAIN WAVE

Two aspects of the main wave are important for our protective purposes: what is the peak pressure and momentum it brings to the foam-covered structure and how much foam is needed to stop it completely? Our experimental answers to these questions in specific cases have appeared in Table 1 and Fig. 3. We have generalized these results

Table 2  
COMPARISON OF MEASUREMENTS OF FORERUNNER SPEED  
IN FOAMS WITH PREDICTIONS

MATERIAL AND DENSITY (g/cc)	SOUND SPEED (mm/μsec, ± 1%)	SHOCK WAVE SPEED (mm/μsec)			
		Measured			Forecast from Modulus (3)
		Method A*	Method B†	Method C‡ (average)	
P-C ~0.6 (Poly- tron) 0.66 0.644 0.645	1.73 (1)△	1.74	1.65 ± 0.05	1.8 ± 0.3 1.65 ± 0.10	1.40 ± 0.10
P-C 0.714 (CPR) 0.798	2.11 (3)			1.2 ± 0.10	1.50 ± 0.08
Si ~1.1 1.02 0.931 1.048 1.053	1.35 (1)			1.4 ± 0.3 1.8 ± 0.4	1.0 ± 0.05 1.3 ± 0.065
MD-AK 1.41 1.445 1.458	4.6 (3)			2.14 ± 0.27 2.45 ± 0.30	2.06 ± 0.10
MD-AO 0.948 0.925 1.30 1.279 1.41 1.38	2.54 (3)    4.75 (3)			0.57 ± 0.01 1.99 ± 0.45 2.69 ± 0.22	0.83 ± 0.04 2.08 ± 0.10
C-ATJ 1.78 ~1.73	2.32 (3)			1.6 ± 0.15	1.32 ± 0.13
C-PT- 1.18 0114 ~1.15	1.8 (3)			1.6 ± 0.15	1.02 ± 0.09
Be 1.195	6.71 (3)				2.175 ± 0.36

\* Fowles and Curren.<sup>1</sup>

† Rempel.<sup>2</sup>

‡ From work done this year. The average wave speeds are from Table 1, and are those of the leading elements in the disturbance.

△ Numbers in parentheses indicate the first report of the measurement.

All entries are based on consideration of a single measurement or experiment except the first entry in the last column. This forecast is computed from the average ratio of density to modulus speed among 5 measurements (Table 1). The uncertainty limits correspond to the standard deviation of the 5 ratios from the mean.

Table 3  
FORERUNNER STRENGTH OF FOAMS COMPARED  
WITH QUASI-STATIC YIELD STRENGTH

MATERIAL	DENSITY (g/cc)	STATIC YIELD STRESS (0.2% Offset) ( $\pm 0.01$ kbar)	INTERSECTION OF TANGENTS TO STATIC CURVE (kbar)	PRESSURE INDUCED IN STEEL BY FORERUNNER (kbar)	MAXIMUM PRESSURE IN RIGID WALL EXPECTED FROM STATIC COMPRESSION (kbar)
P-C (Polytron)	0.660 ~0.67 0.644 0.668	0.33	0.38	0.91 $\pm$ 0.15 1.0 $\pm$ 0.20	0.48
P-C(CPR)	~0.714 0.798 0.697	0.55	0.70	1.9 $\pm$ 0.32	0.96
Si	1.02 0.931 1.05	0.165 0.097	0.152	0.66 $\pm$ 0.15	0.19
MD-AK	1.41 1.46 1.445 1.405	0.76	0.945	2.6 $\pm$ 0.3 1.49 $\pm$ 0.05	1.11
MD-AO	0.948 0.939 0.960	0.069		0.33 $\pm$ 0.03 0.37 $\pm$ 0.05	0.10
C-ATJ	1.78 ~1.73	0.50	0.54	0.665 $\pm$ 0.04	0.80
C-PT-0114	1.18 ~1.15	0.055	0.06	0.72 $\pm$ 0.07	0.10
MD-AO	1.30 1.28 1.41 1.445 1.34	0.345	0.61	0.60 $\pm$ 0.05 0.90 $\pm$ 0.04 1.49 $\pm$ 0.05	0.73
Be	1.195	0.28	0.46	1.5 $\pm$ 0.15	0.62

somewhat in Fig. 4, where all our experiments in aluminum foam we plot the peak observed pressure in the anvil against the quantity

$$\frac{I_0}{l\rho_0}$$

where  $I_0$  is the thickness of sheet explosive converted to momentum density according to the relation 0.016 inch of explosive (EL-506D) equals  $1 \times 10^4$  taps,  $l$  is the original foam thickness, and  $\rho_0$  original foam density. In Fig. 4 we have tried to allow for errors in effective foam thickness arising from the obliquity of impact and for the uncertainty

in the conversion factor between explosive thickness and input momentum density by the addition of horizontal uncertainty bars through the data points.

All data points in Fig. 4 stemming from open-cell aluminum lie near a straight line; that is, within the ranges of parameter variations studied, peak pressure passing into a wall depends linearly upon  $I_0/\rho_0 l$ . It is probably oversimplifying to draw a single straight line through data points for such a wide variety of densities of foams; but certainly distortion does not sharply affect the relation between peak pressure and  $I_0/\rho_0 l$ . Figure 4 may show a small difference due to the closed- or open-cell structure. Furthermore, the value of  $I_0/\rho_0 l$  at which the main wave stops just short of the wall is near the intersection of the straight line mentioned above and the pressure level induced in the anvil by the forerunner. In the figure this intersection lies between  $I_0/\rho_0 l = 1.95$  and  $2.7 \times 10^4$  cm/sec for 1.4 g/cc closed-cell aluminum and below  $1.6 \times 10^4$  cm/sec in 0.9 g/cc open cell foam.

In Fig. 5 we have similarly organized experimental results in polyurethane, beryllium, silica, and two kinds of graphite. All experiments providing information for Fig. 4 were 2-D; in Fig. 5, despite the fact that values of momentum and foam thickness are not strictly comparable between 1-D and 2-D experiments, we have included data from 1-D experiments described earlier<sup>2</sup> (Shots 9155, 9180, 9216, 9228, and 9217 in polyurethane, and Shots 9325 and 9345 in silica) as well as data from 2-D shots. Values of input momentum for 2-D experiments were calculated by means of the theory described in Section 3E below. For 1-D experiments input momentum was computed from measured flyer speed and mass.

Polyurethane (0.67 g/cc) data from the three 1-D experiments can easily be represented by a straight line which crosses the ordinate for forerunner strength in the anvil at  $I_0/\rho_0 l = 1.98 \times 10^4$  cm/sec. Except for Shots 8775 and 8863<sup>\*</sup> the 2-D shots in this material give results consistent with this straight line. We do not know the reason for the inconsistent results from Shots 8775 and 8863; they may indicate breakdown of the scaling law in the region of high thicknesses and momenta.

---

\* Since the excursion of the anvil mirror due to the main wave in Shots 8775 and 8863 was enhanced by coincidence with the first reverberation in the anvil of the forerunner, the values for main wave peak strength reported earlier<sup>2</sup> have been reduced by forerunner strength (1 kbar) in Fig. 5.

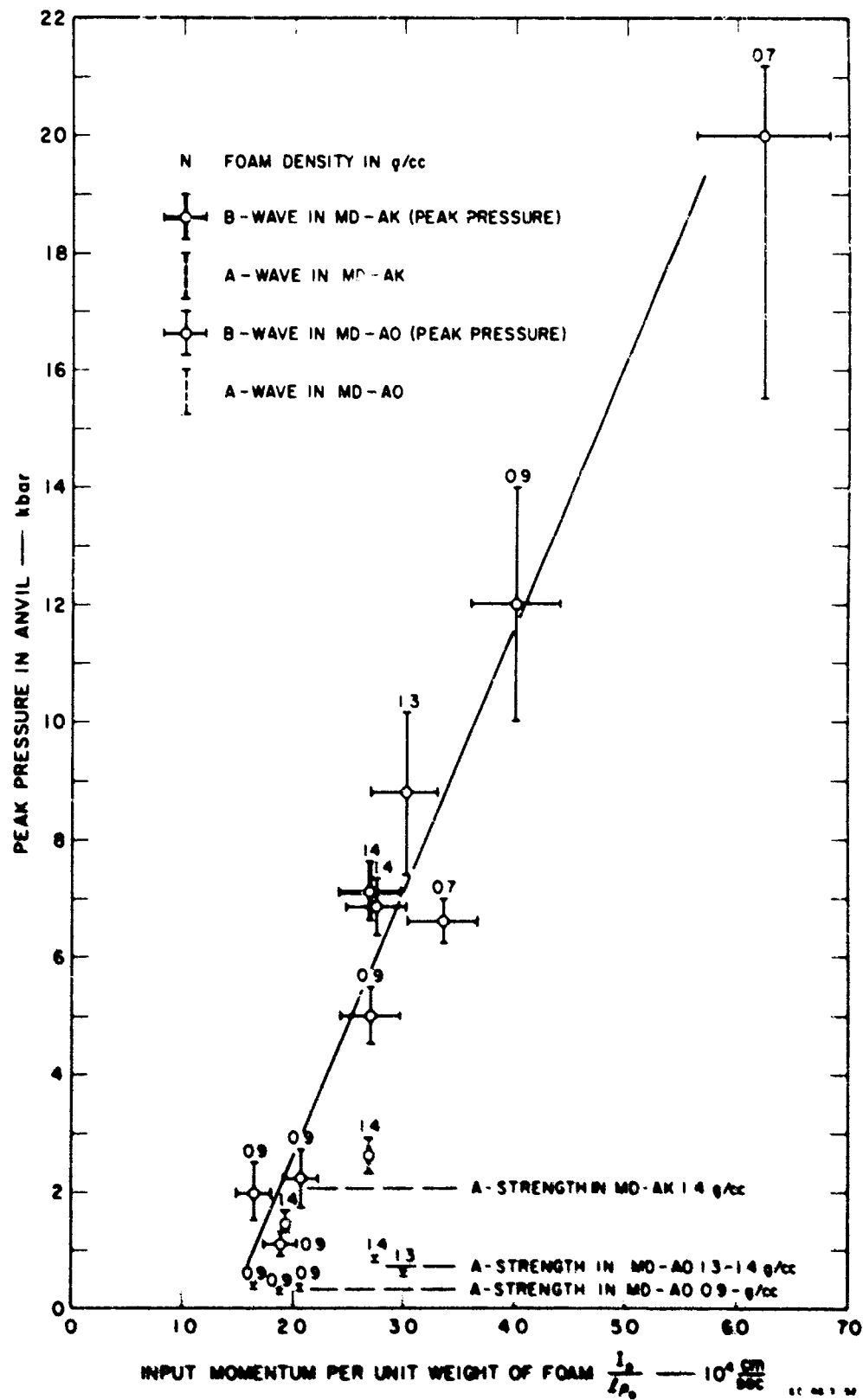


FIG. 4 EFFECTIVENESS OF ALUMINUM FOAM





Judging from the one experiment in 0.335 g/cc polyurethane (Shot 9228), in which there was no main wave, the line summarizing peak pressures may lie significantly to the right of that for 0.67 g/cc material.

A strong anomaly appears in the silica data represented in Fig. 5. Shots 9325, 9893, and 9891 are consistent in the sense established above for polyurethane and aluminum; there is a linear relation (Silica 1 in Fig. 5) between peak anvil pressure and the quantity  $I_0/\rho_0 l$  that indicates the main wave is just held off the wall near  $I_0/\rho_0 l = 1.24 \times 10^4$  cm/sec. But data from Shots 9931, 9893, and 9345 seem to fall along another wholly different line (Silica 2 in Fig. 5) which does not cross the ordinate for forerunner strength at any point in the first quadrant. A degree of consistency would arise from discarding the results of Shot 9931 but we know of no reason that experiment should not be considered. We propose as a tentative explanation that the value of the quantity  $I_0/\rho_0 l$  corresponding to emergence of the first wave from main wave just at the wall may separate regions of different rates of change of peak pressure with  $I_0/\rho_0 l$ . Shot 9325 had no forerunner; Shot 9931 did. Since the forerunner draws off momentum from the main wave, it is reasonable that peak pressure falls faster with increasing foam thickness in the neighborhood of the first appearance of the forerunner than elsewhere.

Results in both kinds of graphite are consistent in the sense described above. ATJ graphite (1.73 g/cc) stops the main wave at  $I_0/\rho_0 l \approx 0.7 \times 10^4$  cm/sec; PT-0114 graphite (1.1 g/cc) at  $I_0/\rho_0 l \approx 0.4 \times 10^4$  cm/sec. Neither of these crossings is confirmed by experimental data from shots in which the main wave is completely held off the wall.

A straight line through the two data points in beryllium crosses the ordinate corresponding to forerunner strength at  $I_0/\rho_0 l \approx 0.2 \times 10^4$  cm/sec. As in graphite this generalization of foam "stopping power" is tentative. Since the forerunner broke away from the main wave very close to the wall in Shot 10,446, the line summarizing the beryllium information in Fig. 5 may be less steep than it would be if there were data for higher values of the abscissa.

Experimentally observed momentum information, extracted from Table 1 and Fig. 3 and Rempel,<sup>2</sup> is collected in Table 4. Reports by Abrahamson that explosive impulse delivered to a slab lying against sheet explosive depends on the density of the slab have led us to convert thickness of

Table 4  
EXPERIMENTALLY OBSERVED IMPULSE GAINS

MATERIAL, NOMINAL DENSITY, SHOT NO.	INPUT MOMENTUM DENSITY, $I_0$ ( $10^4$ taps)	IMPULSE IN SMEAR CAMERA RECORD, $I_R$ ( $10^4$ taps)	IMPULSE GAIN $\frac{I_R}{I_0}$
Polyurethane, (Polytron) (0.67 g/cc)			
9832*	3.1	2.4, incomplete†	--
9833	3.1	2.35, incomplete	--
8863	3.1	2.5, incomplete	--
9155 (1-D)§	1.1	1.6, incomplete	--
9180 (1-D)	1.1	0.9, incomplete	--
9216 (1-D)	2.2	1.1, incomplete	--
9217 (1-D)	1.1	1.2, incomplete	--
Polyurethane (C-P-R) (0.71 g/cc)			
10261 (standoff)Δ	0.95	1.15	1.3
10331 (standoff) (109°C)	0.94	1.3	1.6
10332 (standoff)	0.99	1.3	1.3
		Average	1.3
Open-cell Aluminum (0.7 g/cc)			
9809	1.0	1.2	1.2
Open-cell Aluminum (0.9 g/cc)			
9800	1.6	2.3	1.4
9801	1.6	1.5, incomplete	--
9802	1.6	0.84, incomplete	--
9803	0.94	1.1	1.2
Open-cell Aluminum (1.4 g/cc)			
9930	1.1	1.1	1.0
9932	1.6	1.2, incomplete	--
Closed-cell Aluminum (1.4 g/cc)			
9892	1.1	1.05	1.0
9894	1.6	1.9	1.2
Silica (1.0 g/cc)			
9891	0.72	0.1, incomplete	--
9893	1.1	0.61, incomplete	--
9931	1.1	1.2	1.1
9345 (1-D)	0.68	0.52, incomplete	--

Table 4 concluded

MATERIAL, NOMINAL DENSITY, SHOT NO.	INPUT MOMENTUM DENSITY, $I_0$ ( $10^4$ taps)	IMPULSE IN SMEAR CAMERA RECORD, $I_R$ ( $10^4$ taps)	IMPULSE GAIN $\frac{I_R}{I_0}$
Graphite, (ATJ) (1.7 g/cc)			
10082	1.0	1.2	1.2
10084	1.0	1.3	1.3
Graphite, (PT 0114) (1.0 g/cc)			
10035	1.0	1.2	1.2
10936	1.0	1.2	1.2
10037	0.66	0.58, incomplete	--
Beryllium, (1.1 g/cc)			
10446 (standoff)	1.12	1.4	1.3
10453 (standoff)	0.64	0.56	0.87
		Average	1.0

## Notes:

\*  $I_0 = (t/0.016) 10^4$  taps where  $t$  is explosive thickness in inches for all shots except those marked standoff and 1-D.

† When the impulse in smear camera record,  $I_R$ , is marked "incomplete" the record was broken off by reverberations in 2-D shots or by driver arrival in 1-D experiments before pressure returned to zero at the foam-anvil interface.

§ For 1-D shots  $I_0 = (t'/0.020) 1.13 \times 10^4$  taps where  $t'$  is flyer thickness in inches. Descriptions of these experiments and of Shot 8863 appear in Rempel.<sup>2</sup>

△ When standoff used  $I_0$  is calculated from the Gurney formula by treating flyer as a free plate.

EL-506D sheet explosive to input momentum density  $I_0$  in two different ways, depending upon whether the explosive impact drives the aluminum flyer alone and the impact on the foam is secondary, or whether barrier and foam are arranged in contact with each other before detonation. Unfortunately, the camera records of the pressure histories in the 1-D experiments, in which input momentum is more accurately known than in the 2-D shots, were interrupted before pressure returned to zero at the foam-anvil interface; so all our observations of impulse gain depend on uncertain values for input momentum  $I_0$ . The table does furnish evidence, however, that the momentum gain, the ratio of observed impulse in the anvil  $I_R$  to  $I_0$ , is lower for 1.4 g/cc aluminum, both open- and closed-cell, than for any other material except possibly silica, and that the gain for polyurethane

is higher. If the foamed aluminum and beryllium lock to crystal density, it is certainly reasonable that their shock impedances are the nearest to that of steel of the materials tested. Locked silica also probably has a relatively high shock impedance. Taking shock impedances  $m_1$  and  $m_2$  of impacting plates as constants, the momentum gain in the forward direction is  $2m_2/(m_1 + m_2)$  if  $m_2$  is the impedance of the plate initially at rest. It is clear that our results for gain generally vary among themselves in the way expected from this formula.

Just as we related certain features of the forerunner to quasi-static compression data by a theory of double shock structure, we seek bases for forecasting such important characteristics of the main wave as peak pressure and total impulse or wave shape. We have developed three theoretical tools for this task: a simplified characteristics method,<sup>1,2</sup> a more complete characteristics method, and the (Q) method of artificial viscosity.<sup>12,13</sup> As data for use with these tools we have the value of the unfoamed density of the material constituting the foam and the values of final strain in quasi-static compression. As a check on these values foam samples under shock compression were flash X-rayed, but due to edge effects both in the compression and in the X-ray beam passing through the locked mass, the results have so far been difficult to interpret exactly, although they clearly show compression to near undistended density behind the main wave.<sup>1,2</sup>

For several foams the simplified characteristics theory predicts approximately the greatest value of the quantity  $I_0/\rho_0 l$  corresponding to the transmission to a wall of the forerunner without the main wave. We calculate the particular value  $S$  of  $I_0/\rho_0 l$  corresponding to collision of the locked wall reflection and the oncoming locked wave at the time  $t^*$  when pressure and particle speed jump in the main wave disappears:<sup>14</sup>

$$S = U_e \left[ \frac{V_0 - V_1}{V_0} \right] \left[ \frac{1}{1 + \left( \frac{V_0 - V_1}{V_0 - V_e} \right)^{1/2} - \left( \frac{V_0 - V_e}{V_0 - V_1} \right)^{1/2}} \right] . \quad (1)$$

In this formula  $V_0$  = initial specific volume,  $V_1$  = locked specific volume,  $V_e$  = specific volume in the forerunner, and  $U_e$  = forerunner speed. In theory when  $I_0/\rho_0 l = S$ , there is a second pressure pulse delivered to the wall, but the rate of reduction of peak pressure with foam thickness in

the neighborhood of  $I_0/\rho_0 l = S$  is high and experimentally it is a good estimate of conditions needed to avoid the main wave.

Except for premature but unimportant interruption of the record, 1-D Shot 9155<sup>2</sup> produced an excellent pressure history (Fig. 6) and we can use our study of it to illustrate many general features of our findings. First, we chose an elastic pressure-volume locus of the slope and peak pressure to give the observed forerunner stress in the anvil (1 kbar) and the observed forerunner speed (1.65 mm/ $\mu$ sec), and to give the original foam specific volume 1.515 cm<sup>3</sup>/g. Next by calculations with the simple theory we found a locked specific volume which predicted the observed time interval between first and second wavefronts (i.e., 1.7 to 2.6  $\mu$ sec) a good compromise value is 1.0 cm<sup>3</sup>/g.<sup>15</sup> Next we chose a value for wave speed in locked foam which would give the observed value of the time interval between the main (B) and reverberation (C) wave; this value can be 2.11 mm/ $\mu$ sec. By assuming the locked equation of state is a straight line passing through the point  $P = 1$  kbar and  $V = 1.00$  cc/g with slope related to assumed shock speed in the locked mass, we then had an energy-independent equation of state (Fig. 7). (Actually for unimportant reasons the slightly curved, solid line in Fig. 7 was used in the Q-method calculations; the straight, dotted line described in the text was used in the computations by characteristics.) Using this equation of state for the foam and a simple straight line  $P$ - $V$  equation of state for the aluminum in the flyer, we carried out calculations graphically by the characteristics method and electronically by the Q-method. Pressure and particle speed distributions resulting from these two methods at time 2.47  $\mu$ sec after flyer impact are plotted in Figs. 8 and 9. Since the characteristics and artificial viscosity solutions agreed closely, we used the artificial viscosity method to compute the pressure history in a rigid wall behind 5 mm of the foam whose equation of state is represented in Fig. 7. This history is shown in Fig. 6 alongside the observed history.

There are a number of striking and obvious discrepancies between the two curves of Fig. 6. About 10 percent of the peak pressure by the Q-method can be attributed to the false assumption of rigidity in the wall. To get better agreement shock speed in the locked material would have to be lowered to about 0.9 mm/ $\mu$ sec which would, of course, separate the B and C fronts far beyond the observed relation unless we attribute to the reverberation front a much higher speed during its return from the flyer than during its trip from wall to flyer. This is quite reasonable

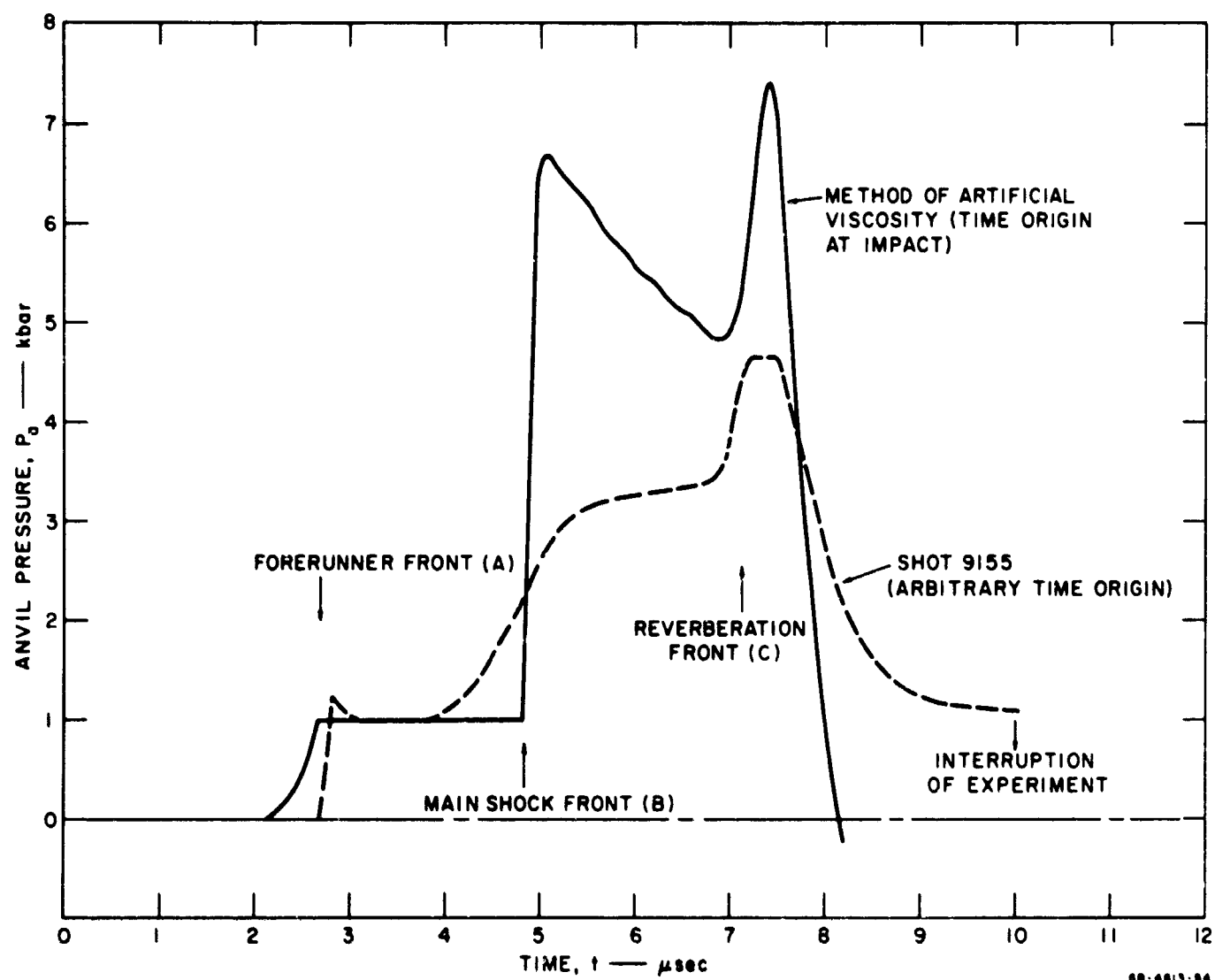


FIG. 6 OBSERVED PRESSURE HISTORY IN ANVIL CONTRASTED WITH THAT FORECAST BY ARTIFICIAL VISCOSITY — SHOT 9155

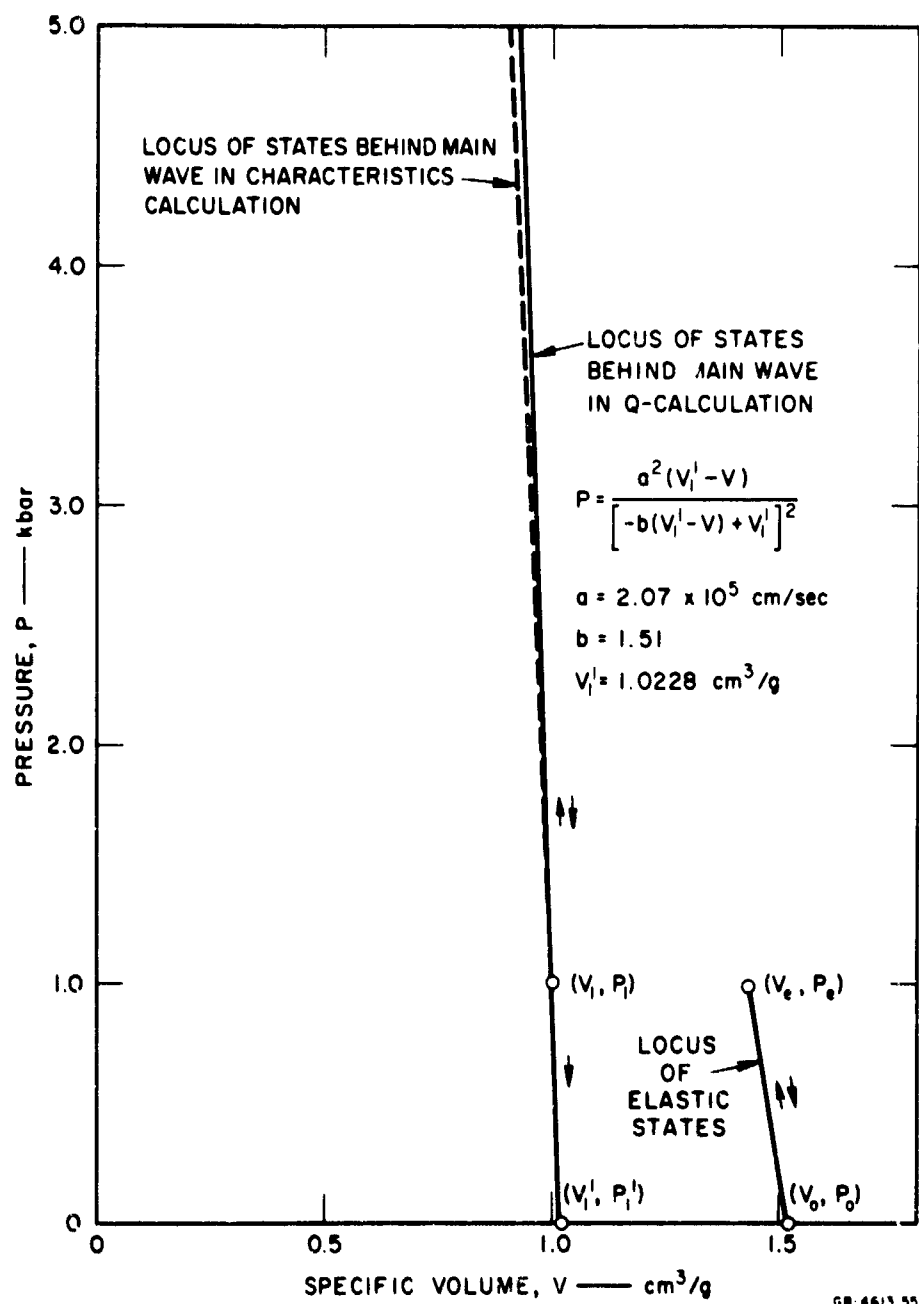


FIG. 7 LOCKING SOLID EQUATION OF STATE



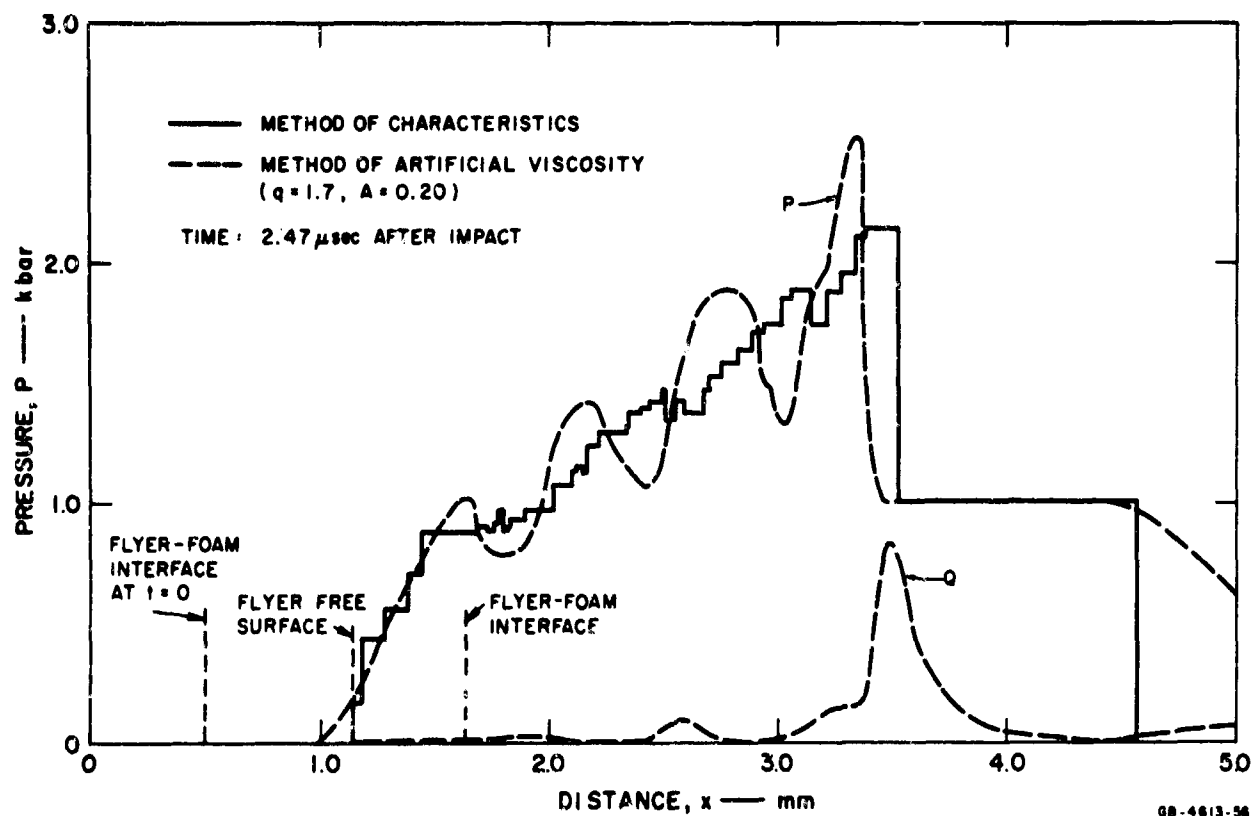


FIG. 8 PRESSURE PROFILE IN A FOAM ACCORDING TO METHODS OF CHARACTERISTICS AND OF ARTIFICIAL VISCOSITY

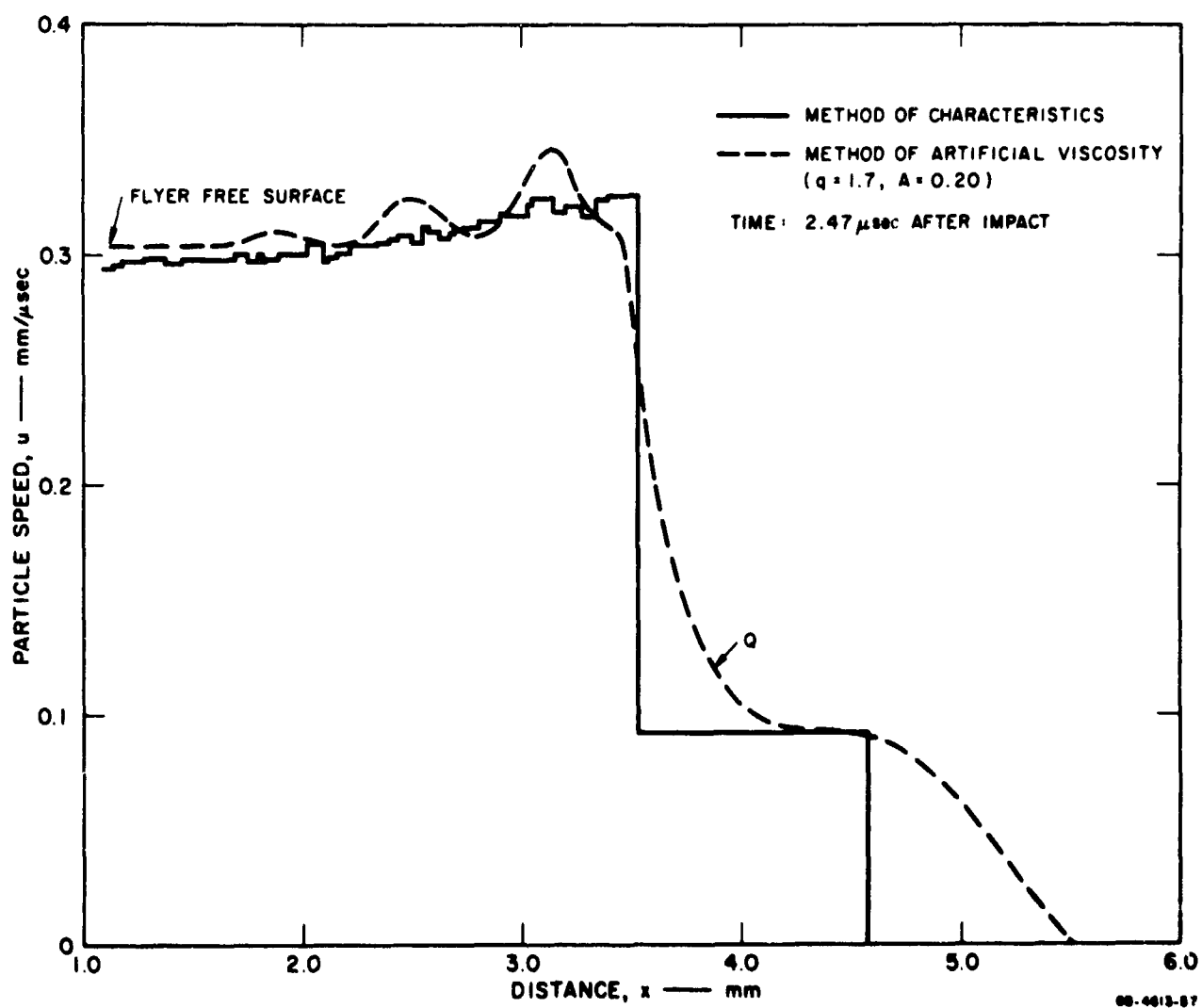


FIG. 9 DISTRIBUTION OF PARTICLE SPEED IN A FOAM ACCORDING TO METHODS OF CHARACTERISTICS AND ARTIFICIAL VISCOSITY

but would involve a serious modification of the equation of state. The relaxation behind the *C* front seen in Shot 9155 is much slower than that calculated, but this discrepancy could be removed by alteration of the equation of state to provide gradual isentropic relaxation from the locked state ( $P = 1$  kbar,  $V = 1.0$  cc/g) to some state near ( $P = 0$ ,  $V = 1.515$  cc/g). Neither the characteristics method nor the *Q*-method is expected to give information on shock width, of course, but the rise time in the main wave is unusually long compared to ordinary materials, and the pressure plateau behind the main wave is completely unexpected. Since waves in the flyer make between three and ten round trips each microsecond, there should be a pressure gradient across the locked foam layer, and we expect as a result to see a gradient behind the main wave in the anvil.

The pressure plateau is frequently but not always found in experiments involving polyurethane, silica, and aluminum but never in graphite where steady pressure relaxation is the rule. The phenomenon is particularly striking in Shot 9931 in silica, Shot 9803 in aluminum, Shot 10,446 in beryllium, and Shot 9832 in polyurethane (Fig. 3). Both the unusually long rise time in the main front and the plateau must be connected with the porous nature of the material, although there is the possibility in some experiments of an interaction between main wave and a simple compression wave moving back into the foam from the wall after forerunner arrival. This would give the appearance of a thick shock front. (Shots 9800, 9801, and 9809 in aluminum showed slow rises to main wave pressure in the absence of a forerunner.) Since graphite is porous but shows no main wave plateau, there may be another factor or factors contributing to the flatness.

Since there are pores against the anvil and since the full pressure in a wave cannot be passed into the anvil until these are closed, rise time may be simply this closing time. Pores in 0.67 g/cc polyurethane measured microscopically are 0.3 to 0.6 mm in diameter; since locking wave rise time in Shot 9155 is  $1.5 \mu\text{sec}$ , a  $0.2 \text{ mm}/\mu\text{sec}$  particle speed would be needed to close all the pores during rise time. This is indeed the particle speed expected behind the main wave at the time of its arrival at the anvil, see Fig. 9 for example.

As the main wave becomes stronger its plateau character tends to become less pronounced (Shots 9894, 9809, 9800, and 9932 in Fig. 3). This is reasonable because the lack in uniformity in porous material becomes less important as shock and particle speeds become more nearly alike.

By comparing the results of a few very simple calculations with observed peak pressures, it can be shown that the so-called "locked states" in aluminum and beryllium, as in polyurethane, do not have the same shock impedances as do the same materials in undistended form. The disparity appears to be greater for light-weight foams than for the more dense. If the impedance of both solid aluminum and beryllium is assumed to be  $1.60 \times 10^6 \text{ g cm}^{-2} \text{ sec}^{-1}$  and the impedance of steel is  $2.25 \times 10^6 \text{ g cm}^{-2} \text{ sec}^{-1}$ , and if it is noted that all the material (including flyer) behind the locking front moves at nearly the same speed, we can calculate a lower bound to the pressure expected upon meeting of steel wall and a main wave front behind which the aluminum or beryllium is in the normal undistended state. In cases where there is a forerunner ahead of the main front we subtract from the total input momentum the momentum passing into the steel before main wave arrival and in computing the mass of locked material we neglect the mass piled up at the wall by the forerunner. To estimate the lower bound we also neglect the pressure behind the main front just before impact. Comparisons of these calculated lower bounds with experimental observations are shown below:

MATERIAL	ESTIMATED LOWER BOUND ON PRESSURE (kbar)	OBSERVED PEAK PRESSURE (kbar)	UPPER BOUND ON OBSERVED IMPEDANCE ( $10^6 \text{ g cm}^{-2} \text{ sec}^{-1}$ )	SHOT NO.
0.7 g cc MD-AO	24	6.6	0.29	9.809
0.9 g cc MD-AO	21	5.0	0.24	9.801
0.9 g cc MD-AO	16	2.2	0.14	9.802
0.9 g cc MD-AO	13	2.0	0.15	9.803
1.4 g cc MD-AO	18	6.9	0.43	9.932
1.4 g cc MD-AO	11	7.0	0.79	9.894
1.1 g cc Be	12	4.5	0.405	10.446
1.1 g cc Be	9.5	3.7	0.45	10.453

The fourth column above contains values of shock impedance computed from the observed interface pressures (in the third column) and the foregoing assumptions. Actual impedances in the locked foam should be lower than entries in the fourth column.

Graphite, especially the ATJ, appears to be more nearly truly "locked" behind the main wave than any of the above materials.

MATERIAL	ESTIMATED LOWER BOUND ON PRESSURE (kbar)	OBSERVED PEAK PRESSURE (kbar)	UPPER BOUND ON OBSERVED IMPEDANCE ( $10^6 \text{ g cm}^{-2} \text{ sec}^{-1}$ )	SHOT NO.
1.1 g/cc C-PT0114	6.7	3.9	0.29	10,035
1.1 g/cc C-PT0114	4.3	2.0	0.22	10,036
1.1 g/cc C-PT0114	2.7	1.3	0.25	10,037
1.7 g/cc C-ATJ	5.75	5.7	1.6	10,084
1.7 g/cc C-ATJ	3.5	2.6	0.39	10,082

Estimates above are based on an assumed undistended impedance for carbon of  $0.55 \times 10^6 \text{ g cm}^{-2} \text{ sec}^{-1}$ . This better agreement between estimated and observed pressures may be connected with the more conventional wave shapes seen in graphite and noted earlier in this report.

Choice of an assumed "locked" impedance for 1.1 g/cc silica is not so clear but if we take that of a quartzite,  $1.63 \times 10^6 \text{ g cm}^{-2} \text{ sec}^{-1}$ , we find:

ESTIMATED LOWER BOUND ON PRESSURE (kbar)	OBSERVED PEAK PRESSURE (kbar)	UPPER BOUND ON OBSERVED IMPEDANCE ( $10^6 \text{ g cm}^{-2} \text{ sec}^{-1}$ )	SHOT NO.
1.8	7.0	0.445	9,325
8.8	2.4	0.295	9,893
7.5	2.2	0.33	9,345

### C. THE BEST FOAM

In our present terms, the best foam holds the peak pressure on a structure stemming from an impact carrying a certain momentum density below a certain limit by adding the least mass per unit area to the structure. The choice of the best foam may also depend on environmental conditions, the properties of the protected structure, and other factors not considered here.

When momentum is deposited in the foam layer instantaneously, the full forerunner stress (greater than the characteristic pressure  $P_c$  because of reflection) will be felt in the structure. In other cases it may be possible to hold the peak stress below this level but it is not likely these cases will be of practical interest when protection by the use of elastic-rigid foams is sought. The least stress that can be expected then is what we have called forerunner pressure in the anvil.

Of the foams studied, polyurethane is the best in the sense of the above definition. Its ability to stop the main wave is the highest, and the rate of increase of peak pressure with increasing  $I_0/\rho_0 l$  lowest (Fig. 5). Judging from the relative independence of  $I_0/\rho_0 l$  on foam distention seen in Fig. 4, the demands of a structural tolerance lower than the forerunner stress of a given density of polyurethane would better be met by increasing the distention of polyurethane instead of substituting a material such as graphite with a lower forerunner pressure. The effect of distention on foam effectiveness is less than the effect of the kind of material (within our range of materials). The single data point from 0.33 g/cc polyurethane (Shot 9228)<sup>2</sup> indicates that the effect of distention may be greater in polyurethane than in aluminum, but in our experience it is true that the influence of distention on foam quality is less than the effect of kind of material. Polyurethane, however, has a greater tendency to rebound (thus increasing momentum delivered to structure) than have materials of higher shock impedance.

We have had fair success roughly judging peak pressures in widely different kinds of foams from the calculated values of the quantity  $S$ . This success may possibly become greater as more accurate values of the parameters upon which  $S$  depends become known. In Table 5 appear the calculated values of  $S$  and the observed values of  $I_0/\rho_0 l = S'$  separating 1- and 2-wave shock systems. Also listed are the parameter values used in the computation of  $S$ . This scheme is useful only in locating the general area in a plot such as Fig. 5 in which to expect observed peak pressures.

Table 5  
CALCULATED AND OBSERVED STOPPING POWER OF FOAMS

MATERIAL	$U_0$ (mm/ $\mu$ sec)	$P_0$ (kbar)	$V_0$ (cc/g)	$V_1$ (cc/g)	$S$ ( $10^4$ cm/sec)	$S'$ ( $10^4$ cm/sec)
Polyurethane	1.65	1.0	1.515	1.00	2.2	1.6 - 2.4
Aluminum (open-cell)	0.77	0.28	1.05	0.37	1.15	<1.6
Aluminum (closed-cell)	2.3	2.0	0.715	0.37	2.1	1.95 - 2.7
Silica	1.35	0.65	0.95	0.50	2.0	1.25 - 1.35
Graphite (ATJ)	1.3	0.71	0.58	0.50	0.33	0.75(?)
Graphite (PT0114)	1.0	0.70	0.87	0.50	0.85	<0.70
Beryllium	2.0	1.5	0.83	0.55	1.3	<0.8

#### D. QUASI-STATIC COMPRESSION OF FOAMS

Several cylinders of each of the foams studied were carefully dimensioned and weighed, encased in hollow steel cylinders, and compressed hydraulically at a rate of 6,000 psi/min. At ordinary temperatures stress is linearly related to strain below a certain limit of proportionality. At higher stress the rate of change of stress with strain becomes much smaller until a point is reached at which this rate becomes zero (point of inflection). As stress rises still higher, the rate increases again. The compression curve in Fig. 10 shows results for polyurethane.

Data reduced from quasi-static testing appears in Table 6. The predicted elastic wave speed is the square root of the ratio of the modulus of linear compression to density. Some foam specimens were heated and compressed at temperatures above ambient.

#### E. EFFECT OF HEAT

Although our experiments with preheated foams have been too few for close calculation of the amount of change, it is clearly established that heat tends to reduce elastic modulus, elastic yield, and forerunner strength. One experiment with preheated closed cell aluminum (1.4 g/cc) shows a considerably larger lowering of this strength than might be forecast from the weakening of the static yield strength; the forerunner stress in the anvil seems to be reduced more than 50 percent under preheating from ambient to 318°C, and the static proportional limit falls only 30 percent under heating to 426°C.<sup>16</sup> In fact, the first wave stress in the anvil is quite near the static yield of the heated specimen. As a result, the value of  $S$  for this foam is reduced by preheating. Since the measured peak pressure is higher as a result of preheating it is also likely the experimentally defined stopping power  $S'$  of the foam is lowered; that is, if the more or less linear relation between peak pressure in the anvil and  $I_0/l\rho_0$  continues to hold in the preheated material, preheating displaces this line leftward toward lower values of  $I_0/\rho_0 l$ .

The preheated foam also shows stress relaxation in the forerunner similar to the relaxation seen in the unheated samples. Observation of first wave speed in the preheated aluminum failed.

Preheating polyurethane does not seem to have so strong an effect on shock behavior as expected from static observations; the decline in

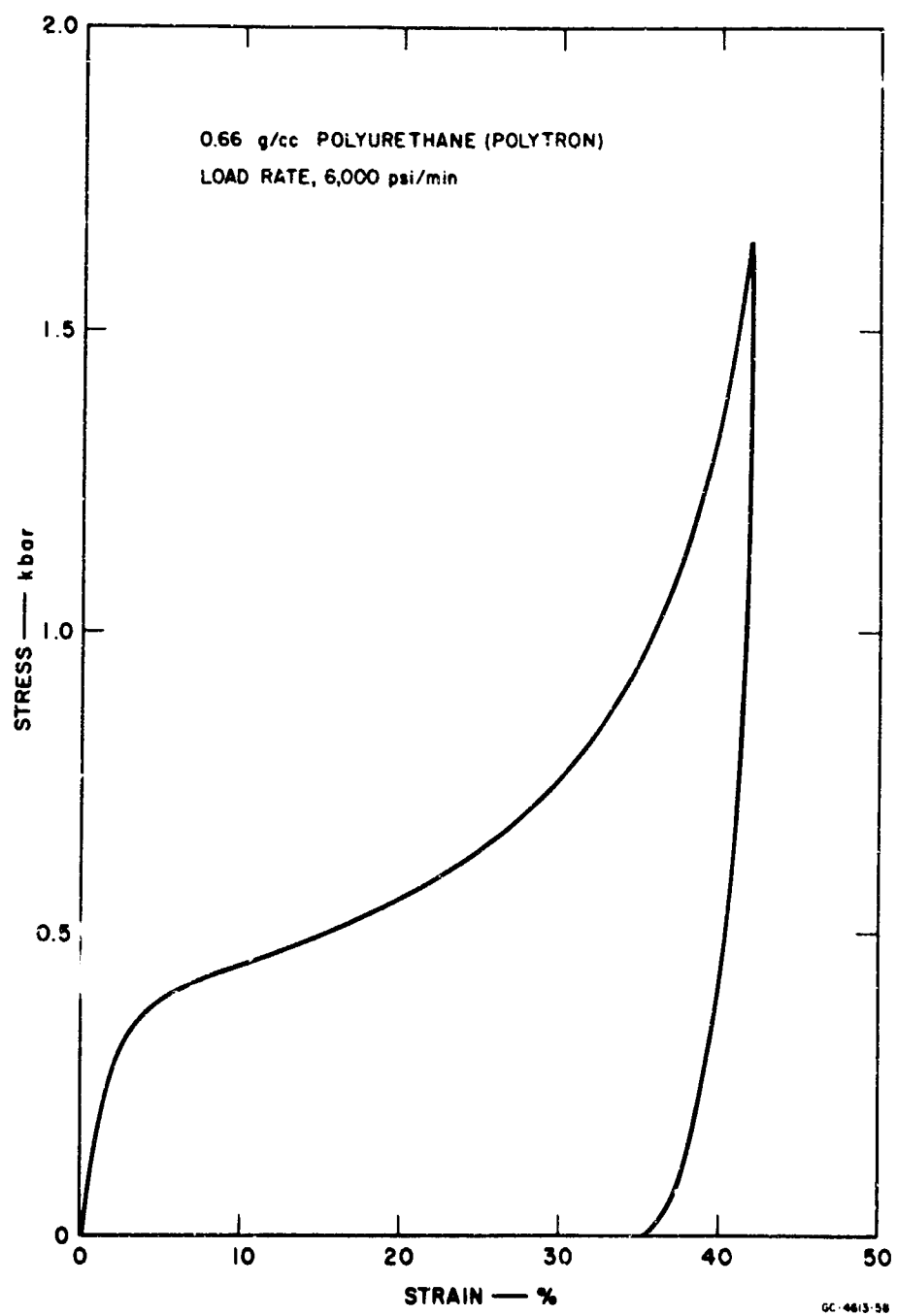


FIG. 10 QUASI-STATIC, ONE-DIMENSIONAL COMPRESSION  
OF POLYURETHANE



Table 6  
QUASI-STATIC ONE-DIMENSIONAL COMPRESSION OF FOAMS

MATERIAL	INITIAL DENSITY (g/cc)	TEST TEMPERATURE (°C)	ELASTIC MODULUS (kbar)	PREDICTED ELASTIC WAVE SPEED (mm/μsec)	YIELD STRESS 0.2% OFFSET (kbar)	COMPRESSION AT 1.5 kb (%)	MODULUS AT 1.5 kb (kbar)
Polyurethane (closed-cell, Polytron)	0.660	Ambient	11.9	1.34 ± 0.07	0.331 ± 0.007	41.8	12.3
	0.664	Ambient	12.9	1.40 ± 0.08	0.304 ± 0.007	41	Not measured
	0.659	Ambient	16.4	1.58 ± 0.08	0.310 ± 0.007	41	Not measured
	0.661	Ambient	12.3	1.37 ± 0.07	0.296 ± 0.007	41	Not measured
	0.654	Ambient	12.0	1.35 ± 0.07	0.331 ± 0.007	43	Not measured
	0.900	Ambient	21.6	1.58 ± 0.08	0.807 ± 0.007	17.4	0.711
	0.667	120	4.57	0.830 ± 0.05	0.138 ± 0.007	47.5	32.4
	0.668	157	Negligible			51.5	30.8
	0.893	120	8.76	1.00 ± 0.05	0.372 ± 0.007	27.3	12.5
	0.880	200	Negligible			31.4	37.6
Polyurethane (closed cell, CPR)	0.798	Ambient	17.8	1.50 ± 0.08	0.551 ± 0.007	27.8	8.07
	0.697	120	5.69	0.905 ± 0.045	0.151 ± 0.007	45.2	13.9
Aluminum (open cell)	0.553	Ambient	Very small		0.0172 ± 0.004	68.0	20.8
	0.780	Ambient	6.61	0.936 ± 0.047	0.0276 ± 0.007	62.0	17.9
	0.948	Ambient	6.51	0.826 ± 0.041	0.0690 ± 0.007	55.0	8.96
	1.30	Ambient	56.5	2.08 ± 0.10	0.345 ± 0.007	34.5	8.68
	1.30	200	23.6	1.37 ± 0.07	0.248 ± 0.007	36.8	10.9
	1.30	426	16.9	1.14 ± 0.06	0.186 ± 0.007	39.0	8.82
Aluminum (closed cell)	1.41	Ambient	60.0	2.06 ± 0.10	0.759 ± 0.007	22.2	83.4
	1.43	426	17.6	1.11 ± 0.05	0.690 ± 0.007	27.6	41.9
Silica (first lot)	1.02	Ambient	10.55	1.01 ± 0.05	0.165 ± 0.007	36.7	17.7
Silica (second lot)	0.585	Ambient	Not measured		0.0552 ± 0.007	60.5	27.0
	0.931	Ambient	15.7	1.30 ± 0.065	0.0965 ± 0.007	42.5	17.65
	0.945	426	7.86	0.915 ± 0.045	0.206 ± 0.007	28.0	13.0
Graphite (electrode)	0.975	Ambient	2.20	0.142 ± 0.013	0.0482 ± 0.007	50.0	35.8
Graphite (PT-0114)	1.18	Ambient	13.1	1.02 ± 0.092	0.0551 ± 0.007	21.2	14.3
Graphite (Aij)	1.78	Ambient	31.5	1.32 ± 0.13	0.497 ± 0.007	12.9	11.8
	1.78	426	14.5	0.905 ± 0.090	0.504 ± 0.007	19.6	9.69
Beryllium	1.195	Ambient	56.5	2.175 ± 0.36	0.276 ± 0.007	15.0	10.6
	1.215	Ambient	50.9	2.045 ± 0.04	0.641 ± 0.007	Not measured	

NOTES:

All specimens compressed into tight-fitting steel dies.

Uncertainty limits above refer to a particular measurement and do not include the likely variation between samples.

All densities measured at ambient temperature.

static strength is near 70 percent at 120°C, but the forerunner is weakened by less than 40 percent in two experiments with preheated material.<sup>17</sup> In these experiments main wave stress is raised from about 0.7 to 3.0 kbar by preheating, and the peak pressure *vs.*  $I_0/\rho_0 l$  relation is displaced to the left in Fig. 5. Although the effect of preheating on elastic modulus at 120°C was strong, our investigation of the influence of preheating on forerunner speed was inconclusive.

Preheating slows the forerunner pressure rise, and the effect was more dramatic in our experiment with closed-cell aluminum than in our polyurethane shots.

### 3. MAJOR EXPERIMENTS

#### A. DESCRIPTION OF TWO-DIMENSIONAL TECHNIQUES

In all experiments a detonation front in sheet explosive moving normal to itself generated a line impact traveling across one face of a thin slab of foam; the waves in the foam stemming from this impact passed into a hardened steel anvil in close contact with the other side of the slab. The resultant angular displacement of images reflected in a mirror free surface on the anvil was photographed with a high-speed smear camera. Because the waves meet the interface and the free surface obliquely, the technique<sup>2</sup> is called two-dimensional (2-D). Figure 1(a) illustrates both the general arrangement and several special features such as flyer tilt, anvil bevel, standoff, and foam taper which were used in various experiments. (The figure shows the barrier on flyer plate tilted with respect to the foam free surface. When sound speed in the foam is close to or above detonation speed, this tilt must be used to achieve impact speed higher than sound speed. This feature has not yet been needed in our work.) Usually the surfaces and interfaces were parallel to each other. When the foam pores are connected with each other, detonation products may flow into the slab to confuse the response, so in every experiment except the first two we put a thin, solid aluminum barrier (or flyer) between the sheet of explosive and the impacted surface of the foam. When the effect of preheating foams was studied, we wanted to insulate the explosive from the hot foam as much as possible, so a 3/16-inch-wide standoff was kept between barrier and foam surfaces by means of a thin paper spacer on edge. In certain experiments we did not make the mirror surface of the anvil parallel to the impacted surface, but beveled it to change the collision angle between wavefront and free surface. As a means of measuring wave speed in foam, in two shots we beveled or tapered the foam slab. Finally, as a more general means of measuring wave speed in foam, we let the explosive shock in every experiment interrupt reflection in a glass mirror at the end of the detonation run. Figure 1(b) illustrates this feature and Table 1 gives details of each experiment. Since the value of the rate of travel of the initial impact along the foam slab is important in

data reduction, we frequently put time-of-arrival switches on the free surface of the sheet explosive.

To measure the angular displacement of the mirror we used an optical lever arm<sup>3</sup> generally about 20 feet long with a 40-inch focal-length lens placed about 20 feet from the mirror. A typical smear camera record appears in Fig. 2 (Shot 10,331). The lines are images of points on translucent grid lines ruled at known separations on opaque glass covering one end of an explosive argon light source.<sup>5</sup> The vertical scale in Fig. 2 is computed from the grid line spacings and the optical distances in the experiment;<sup>\*</sup> the horizontal or time scale comes from the known rotation speed of a mirror in the smear camera. Two long, narrow, mutually perpendicular apertures are used in the optical system: the larger is usually 5/16 inch wide and stands between lens and mirror to limit the reflection zone of a point in the source to a strip about 4 mm wide in the direction perpendicular to the run of the detonation; the smaller aperture, 0.05 mm wide, lies in the focal plane to pass on to the film only light from essentially one point in each grid line. The mirror or polished area of the anvil face is itself only 3/4 inch wide in a direction normal to the detonation travel but extends the whole length of the anvil in the direction parallel to the detonation run.

Thus we see in the lines of Fig. 2 the result of a train of wavefronts sweeping across the steel mirror and moving successively into reflection zones for successive grid lines. The speed of this motion in terms of distance on the mirror we call in this report "apparent wave speed." To each effective light-source point and for each wavefront at least two images correspond, one from the undisturbed reflection zone and the second from the tilted zone at the end of the angular motion. If the rise time in the front were zero, there would be only two images.<sup>†</sup> Because rise time is usually quite an appreciable part of a microsecond, the sharp separation between these two images is not often seen. Judging from the duration<sup>\*</sup> of intermediate images in Fig. 2, the rise time of the

<sup>\*</sup> Time intervals between events in a wave train must be measured from horizontal distances in Fig. 2 between sloping lines drawn through images marking those events. After the mirror surface is tilted the reflection zone of a given line is moved in the direction opposite to the detonation run; because of the 2-D geometry this displacement implies a change in origin of the time scale. By drawing straight lines through images of corresponding events falling in successive grid point loci we can correct for this shift in origin. When measured in the coordinate system shown in Fig. 2, the slope of all lines joining corresponding event-images is the apparent wave speed.

<sup>†</sup> The time separation between the first appearance of one and the last of the other in this ideal case depends on the width of a reflection zone, the separation of the two reflection zones, the apparent speed of the wave along the mirror, film sensitivity, and amount of light.

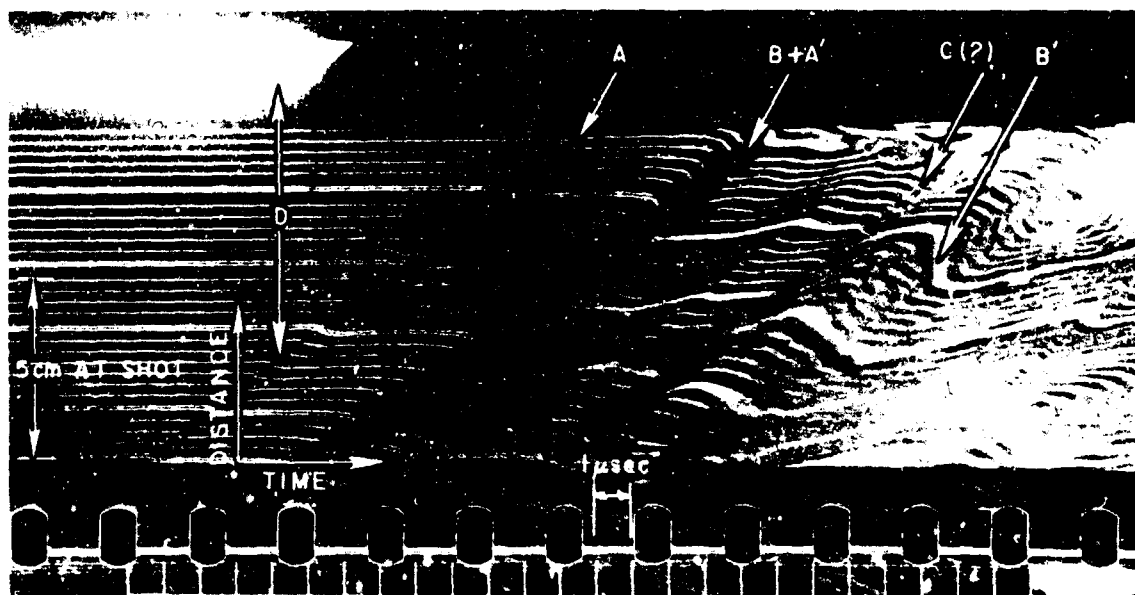


FIG. 11 SMEAR CAMERA RECORD SHOWING FAST-RISING FORERUNNER —  
SHOT 9832

forerunner or *A*-wave is at least  $0.67 \mu\text{sec}$ , and of the main or *B*-wave at least  $1.5 \mu\text{sec}$ . Presumably the forerunner rise time is much less in Fig. 11 (Shot 9,832) where the *A*-wave images are much more clearly separated.

Most likely the *C*-wave in Fig. 2 stems from the double reflection of the main wave off the anvil and again off the barrier. The following disturbances, *A'* and *B'*, are reverberations of the first and second waves entirely within the anvil. One part of the light-source cover is not ruled but is completely translucent. Light passing through there is reflected in the glass mirror abutting the head of the anvil and, as is seen above the grid lines in Fig. 2, exposes the top of each film until the detonation of the explosive lying against the glass mirror destroys its silver surface. The distance *D* on the anvil is read off the calibrated film record and is used to calculate average wave speed in the foam as illustrated in Fig. 1(b). We have measured sound speed at several temperatures in our hardened steel anvils ( $5.88 \pm 0.01 \text{ mm}/\mu\text{sec}$ ), and

in this calculation we assume that all waves in the anvils move at that speed. In all experiments using parallel surfaces, i.e., those not using tapered slabs, beveled anvils, or tilted flyers, the apparent wave speed is assumed to be detonation speed, i.e.,  $7.35 \pm 0.05$  mm/ $\mu$ sec at ambient temperatures, unless the apparent speed seen in the record does not agree with this value within experimental error, in which case the apparent speed seen in the camera record is used.

The interval A-A' (Fig. 2) generally marks the observation time available in this method and depends on the anvil thickness. Useful experiment time is, of course, also limited by the incoming rarefactions from the sides of the foam slab and of the anvil which parallel the detonation run; in the experiment represented by Fig. 2, A-A' is about 8.7  $\mu$ sec and the limit to useful time after A-wave arrival set by side rarefactions is about 10.5  $\mu$ sec.

If rarefactions from the ends of the anvil or slab are important, in principle the camera records a change in either or both apparent wave speed and stress in the same wave while detonation or impact is going on, although if the effect is strong at every point within camera view this visible change may be slight. There are a number of stages in designing an experiment where these ending and starting edge effects can be avoided. To establish the stability of the first wave in the anvil is simple: no ending edge effect is possible and the anvil is made at least a cot  $\theta$  long, where  $a$  is the anvil thickness,  $\cos \theta = c/D$ ,  $c$  is sound speed in the anvil and  $D$  is impact speed on the anvil. A wave moving at steady speed  $D$  along the length of the anvil will be stable everywhere in the anvil mirror beyond a distance  $a \cot \theta$  from the starting edge. There is no ending edge effect for the elastic wave in the foam and the starting edge release waves are outrun in a distance  $a' \cot \theta'$  where  $a'$  is foam thickness,  $\cos \theta' = U_e/D'$ , and  $D'$  is the impact speed along the length of the foam. After stability, of course,  $D = D'$ . Thus in our experiments the forerunner should be stable after a run equal to  $(a \cot \theta + a' \cot \theta')$  along the mirror. In an anvil 2 inches thick and with 0.67 g/cc polyurethane 5 mm thick impacted by explosive lying against it, this distance is 2.7 inches.

To discuss stability in waves trailing the forerunner, we will imagine an impact moving at speed  $D'$  along the length of a slab of thickness  $a'$ ; wave speed of interest will be  $U$  but release wave speed will

be in general  $R''$ . Outrunning begins at a time  $t_0''$  after start of impact:

$$t_0'' = \frac{a''}{U''} \left\{ \left( 1 - \frac{U^2}{D^2} \right)^{1/2} - \left( \frac{R^2}{D'^2} - \frac{U'^2}{D'^2} \right)^{1/2} \right\}^{-1}$$

Also proportional to  $a''$  is the corresponding distance  $b'$  along the unpacted surface:

$$b'' = \left\{ t_0''^2 R''^2 - a''^2 \right\}^{1/2}$$

Figure 12 illustrates these quantities.

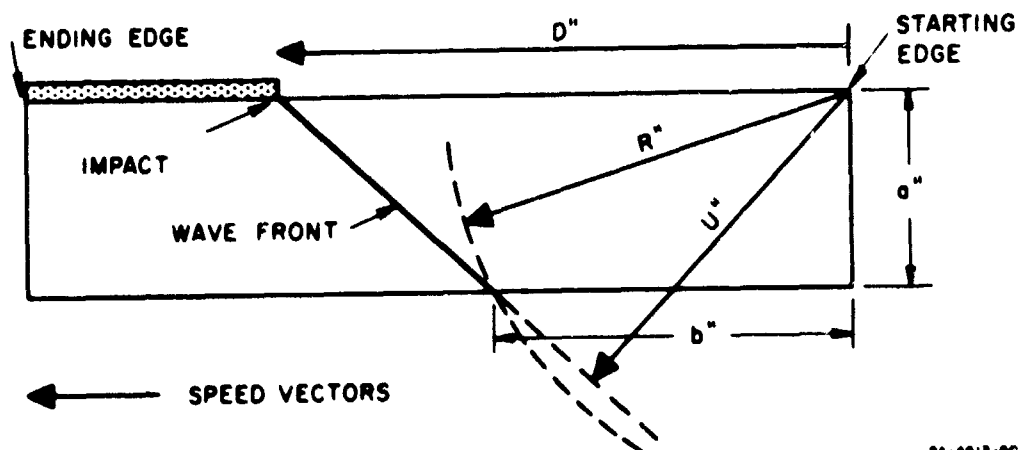


FIG. 12 OUTRUNNING IN A SLAB

A point a distance  $Z''$  from the starting edge of the mirror will be free of relief waves aroused by this wave at the starting edge for a time interval  $\tau'$ :

$$\tau = \frac{(Z^2 + a^2)^{1/2}}{R''} - \left[ \frac{Z'' - b}{D''} + t_0 \right]$$

or

$$Z'' = \frac{\frac{R}{D} \left[ \gamma'' + t_0' - \frac{b'}{D} \right] + \left\{ R^2 \left( \gamma'' + t_0' - \frac{b'}{D} \right)^2 + a^2 \left( \frac{R^2}{D^2} - 1 \right) \right\}^{1/2}}{1 - \frac{R^2}{D^2}}$$

Unless  $R'' > U''/[1 - U''^2/D''^2]^{1/2}$ , end edge effect cannot interfere with observations of the wave causing it. If such interference begins at a distance  $g''$  from the end edge at time  $t_e''$  after the wave first reaches edge, then

$$t_e'' = \frac{a''}{U'' \left(1 - \frac{U''^2}{D''^2}\right)^{1/2} + \left(\frac{R''^2}{D''^2} - \frac{U''^2}{D''^2}\right)^{1/2}}$$

and

$$g'' = \left[R''^2 t_e''^2 - a''^2\right]^{1/2}.$$

When  $R'' \leq U''/[1 - U''^2/D''^2]^{1/2}$ , the end edge disturbance begins a time  $[a''/U''] [1 - U''^2/D''^2]^{1/2}$  after first arrival of the wave at the edge, and moves from the end edge of the slab along the interface or the free surface toward the start edge at speed  $R'' [1 - R''^2/U''^2 + R''^2/D''^2]^{-1/2}$  until the distance

$$h'' = \frac{a'' \left[1 - \frac{R''^2}{U''^2} + \frac{R''^2}{D''^2}\right]^{1/2}}{\frac{R''}{U''} \left[1 - \frac{U''^2}{D''^2}\right]^{1/2}}$$

has been covered, when the disturbance slows. A point on the interface or free-surface distant  $\xi''$  from the end edge will be free of end edge effect for a time  $\mu''$  after the appearance there of the wave causing the effect:

$$\mu'' = \frac{\xi'' - a'' \left[\frac{D''^2}{U''^2} - 1\right]^{1/2}}{D''} + \frac{[\xi''^2 + a''^2]^{1/2}}{R''}$$

Each of these quantities has a meaning both in foam slab and in the anvil, also each may have a distinct meaning depending on which wave is considered. We will leave terms referring to the anvil unprimed, corresponding foam quantities will be singly primed. If the wave considered to be



causing the edge effect is the forerunner or the main wave, terms will carry the subscript 1 or 2, respectively. Immediately we can write  $R_1 = R_2 = U_1 = U_2$  and  $R'_1 = U'_1$ . If we are to make observations on the main wave in the mirror at a distance  $Z$  from the starting edge, the mirror surface must be "clear" of forerunner edge effect at  $Z$  until the main wave reaches  $Z$ , and the foam-anvil interface must be clear of forerunner edge effect at

$$Z' = Z - a \cot \theta$$

until the main wave reaches  $Z'$ . However, in all practical cases, observation of the main wave will be limited by those release waves in the foam behind the main wave, i.e., the condition for stability of the main wave against its own rarefactions will dominate the condition for stability against forerunner relief waves in the foam. Thus we require:

$$Z' \geq b'_2, \quad \text{or} \quad Z \geq b'_2 + a \cot \theta,$$

and

$$\tau_1 \geq \frac{a'(\tan \theta'_2 - \tan \theta'_1)}{D}$$

Both  $U'_1$  and  $U'_2$  are average speeds for the particular experimental conditions considered.

As an example we will find the length of a steel anvil for use with a 5-mm slab of 0.67 g/cc polyurethane. If the anvil is 1 inch thick,  $a = 25.4$  mm; other parameters are  $U = R = 5.88$  mm/ $\mu$ sec,  $U'_1 = R'_1 = 1.65$  mm/ $\mu$ sec,  $R'_2 \approx 2$  mm/ $\mu$ sec,  $a' = 5$  mm, and  $U'_2 \approx 1$  mm/ $\mu$ sec. If the barrier or explosive is in contact with the foam,  $D = 7.35$  mm/ $\mu$ sec. Thus forerunner stability is reached  $(a \cos \theta + a' \cos \theta'_1) = 35.05$  mm = 1.38 inches from the starting edge. Equilibrium of the main wave at the interface comes

$$t'_{02} = \frac{a'}{U'_2} \left\{ \left( 1 - \frac{U'_2}{D^2} \right)^{1/2} - \left( \frac{R'_2}{D^2} - \frac{U'_2}{D^2} \right)^{1/2} \right\}^{-1} = 6.6 \mu\text{sec}$$

after the start, or a distance

$$b'_2 = \left\{ t_{02}'^2 R_2'^2 - a'^2 \right\}^{1/2} = 12.3 \text{ mm} = 0.485 \text{ inch}$$

along the interface. The stable B-front will then first appear in the anvil mirror

$$Z = b'_2 + a \cot \theta = 46.2 \text{ mm} = 1.82 \text{ inches}$$

from the starting edge, but the forerunner stress ahead of it in this region of the anvil will have been weakened by starting edge effect. This will not destroy the main wave data but can be avoided by using parts of the mirror yet farther from the starting edge. Such a region must be clear for

$$\tau_1 = \frac{a' (\tan \theta'_2 - \tan \theta'_1)}{D} = \frac{a'}{D} \left[ \tan \cos^{-1} \frac{U'_2}{D} - \tan \cos^{-1} \frac{U'_1}{D} \right] = 2.0 \text{ } \mu\text{sec}$$

after the passage of the first wave; hence it will be found at distances Z along the mirror satisfying the inequality:

$$Z \geq \frac{\frac{U^2}{D} \left[ \tau_1 + t_{01} - \frac{b_1}{D} \right] + \left\{ U^2 \left( \tau_1 + t_{01} - \frac{b_1}{D} \right)^2 + a^2 \left( \frac{U^2}{D^2} - 1 \right) \right\}^{1/2}}{1 - \frac{U^2}{D^2}}$$

in which

$$t_{01} = \frac{a}{U \left( 1 - \frac{U^2}{D^2} \right)^{1/2}} = 7.2 \text{ } \mu\text{sec}$$

$$b_1 = \{ t_{01}^2 U^2 - a^2 \}^{1/2} = 34 \text{ mm}$$

Thus  $Z \geq 120 \text{ mm} = 4.7 \text{ inches}$ . For a 2-inch-thick anvil this clear area lies beyond a distance

$$Z \geq 172 \text{ mm} = 6.8 \text{ inches}$$

from the starting edge. Since reverberations in the anvil may be more annoying than starting edge effect ahead of the main wave, frequently this lower limit on anvil length has been ignored.

End edge effect in locked foam influences the main wave at the interface in the region within

$$g'_2 = [(R'_2 t'_{e2})^2 - a'^2]^{1/2} = 6.4 \text{ mm} = 0.25 \text{ inch}$$

of the end edge. Since  $a \cot \theta > g'_2$  for both the 1- and 2-inch anvils, this influence does not reach the main-wave jump in the mirror. In the 1-inch anvil the fast end edge effect extends a distance

$$h_1 = \frac{aU}{D} \frac{1}{\left[1 - \frac{U^2}{D^2}\right]^{1/2}} = 33.9 \text{ mm} = 1.33 \text{ inches}$$

from the end edge; and  $h_1 = 67.8 \text{ mm} = 2.66 \text{ inches}$  in the 2-inch anvil. In this region the interval between a wave and its end edge reflection is

$$\frac{2\zeta}{D} = 0.272\zeta \leq 0.272h_1 ,$$

that is,  $9.22 \mu\text{sec}$  when  $a = 1 \text{ inch}$  and  $18.4 \mu\text{sec}$  when  $a = 2 \text{ inches}$ . Outside this region the interval is of course longer. Since the main wave follows about  $2.0 \mu\text{sec}$  behind the first, end edge effect will appear ahead of the main front only for

$$\zeta \leq D = 7.35 \text{ mm} = 0.29 \text{ inch} .$$

Since an area of the steel mirror near the end edge was always masked, Fig. 2 shows no end edge influence on the first two wavefronts. The anvil used in the experiment of which Fig. 2 is the record was 2 inches

thick and  $8\frac{1}{2}$  inches long in the direction of the detonation run. Under these conditions only the last nine or ten grid images, between the first and second fronts, should escape rarefactions stemming from the starting edge, but the record does not seem to show any effect of that kind anywhere. We do not think this lateral release within the anvil is important in any of our experiments, and we have tentatively interpreted any such apparent relaxation of stress in the A-wave that we have seen as arising from stress relaxation behind the forerunner in the foam<sup>18</sup> — due either to an internal mechanism in the elastically strained material,<sup>9</sup> or to sound waves moving from a free edge at speeds higher than forerunner speed.

For reasons not understood, A-wave apparent speed failed to coincide within the uncertainty limits with detonation or impact speed in three experiments, Shots 9,893 and 9,931 in silica, Shot 9,933 in open-cell aluminum. In all three the first wave rose extremely slowly, so perhaps either the experimental error was larger than expected or components of the forerunner were subject to unknown edge effects. These apparent wave speeds were lower than impact speed; a wave in the mirror surface outrunning starting edge effect should be moving faster than its stable speed.

If for 1.3 g/cc aluminum we estimate that  $U'_2 = 2.5$  mm/ $\mu$ sec and  $R'_2 = 6.0$  mm/ $\mu$ sec, we find for a specimen 4 mm thick (Shots 9,930 and 9,932) that the main front will be stable at the interface a distance 46 mm or 1.8 inches from the starting edge. In a 2-inch anvil this instability should disappear about 4.5 inches from the starting edge, and thus would not be photographed in our experiments. We cannot explain the seeming contradiction between A-wave behavior in Shots 9,930 and 9,932: in the first the B-front overtook the A-front, yet in the second, when more explosive was used, a stable A-front appeared throughout the record.

The lighter aluminum, though, may be heavily affected by release waves in the locked foam. Here we estimate  $U'_2 = 0.8$  mm/ $\mu$ sec and  $R'_2 = 6.0$  mm/ $\mu$ sec. In a typical experiment  $a' = 6.0$  mm, hence  $b'_2 = 493$  mm = 19.4 inches; that is, the main wave may never outrun release waves behind it in any of our experiments with this material. Yet the points in Fig. 4 stemming from these experiments do not seem far out of agreement with points from heavier material.

We do not know what part of the relaxation behind the *B*-front seen in the smear records should be attributed to starting edge effect.

Because of the toxicity of pulverized beryllium we impacted foamed specimens of this metal within an airtight steel tank, a photograph of which appears in Fig. 13. To help the containment, air pressure in the tank was held below 500  $\mu$  during the explosion. Both beryllium shots were on beveled anvils, but the foam slabs were not tapered and the flyers not tilted because the expected high forerunner speed was not indicated in preliminary static testing. The experiments were mounted on the tank cover plate as sketched in Fig. 14.

## B. QUASI-STATIC MEASUREMENTS

To make the quasi-static measurements reported in Table 6, we hydraulically compressed\* machine-cut cylinders of foam encased in close-fitting steel dies. (Since minimum wall thickness was 3/8 inch, die expansion was completely negligible in our tests.) Displacement and pressure-sensing gages connected to remote writing equipment made a simultaneous plot of stress in the hydraulic chamber *vs.* engineering strain in the cylinder.

Without exception all the stress-strain relations in quasi-static (0.172 kbar/minute), 1-D compression took the form shown for polyurethane in Fig. 15: a seemingly straight or "elastic" region from zero to the limit of proportionality, followed by a region of gradually falling second derivative of stress with respect to strain. There is a point of inflection when this derivative becomes zero, then a region where it rises until the end of the compression. Most of our tests ended at 1.72-kbar stress, but in a few we went to over 4.14 kbar. Except in the case of 1.4 g/cc closed-cell aluminum, density at 1.72 kbar is in the neighborhood of that of the undistended solid; density of closed-cell aluminum is only 2.39 g/cc at 4.14 kbar (crystal density 2.70 g/cc). Points of inflection always fall below 1.72 kbar. To show the "locking" nature of the compression, relaxation behavior is included in Fig. 15 for another sample of the same kind and approximately the same density of foam. Preheating the specimen of foam generally lowers both the elastic modulus and yield, as shown in Fig. 16 for polyurethane. The

---

\* Baldwin Press Model MA1B operated at 6,000 psi/min. on the specimen.

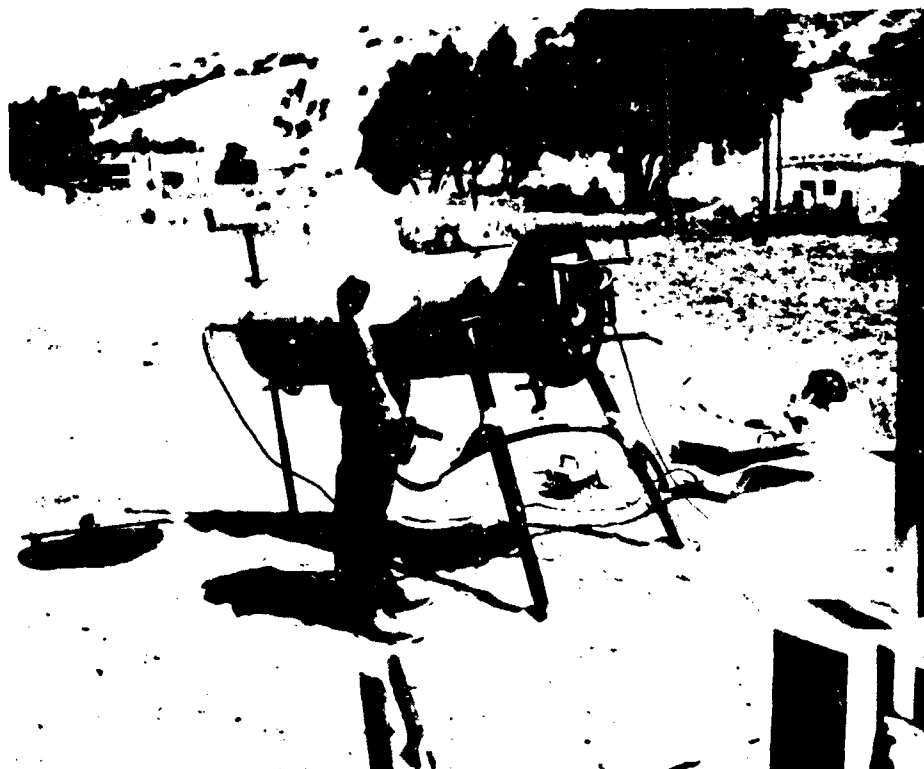


FIG. 13 CONTAINMENT TANK USED WITH FOAMED BERYLLIUM

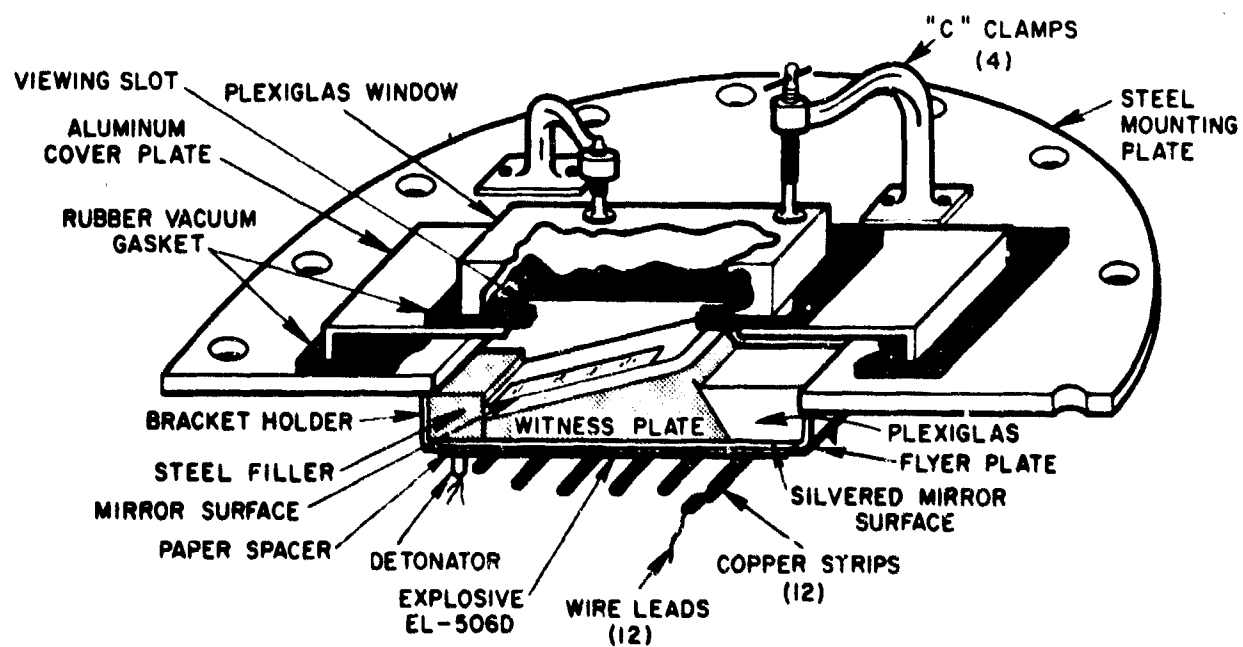


FIG. 14(a) EXPERIMENTS MOUNTED ON COVER PLATE

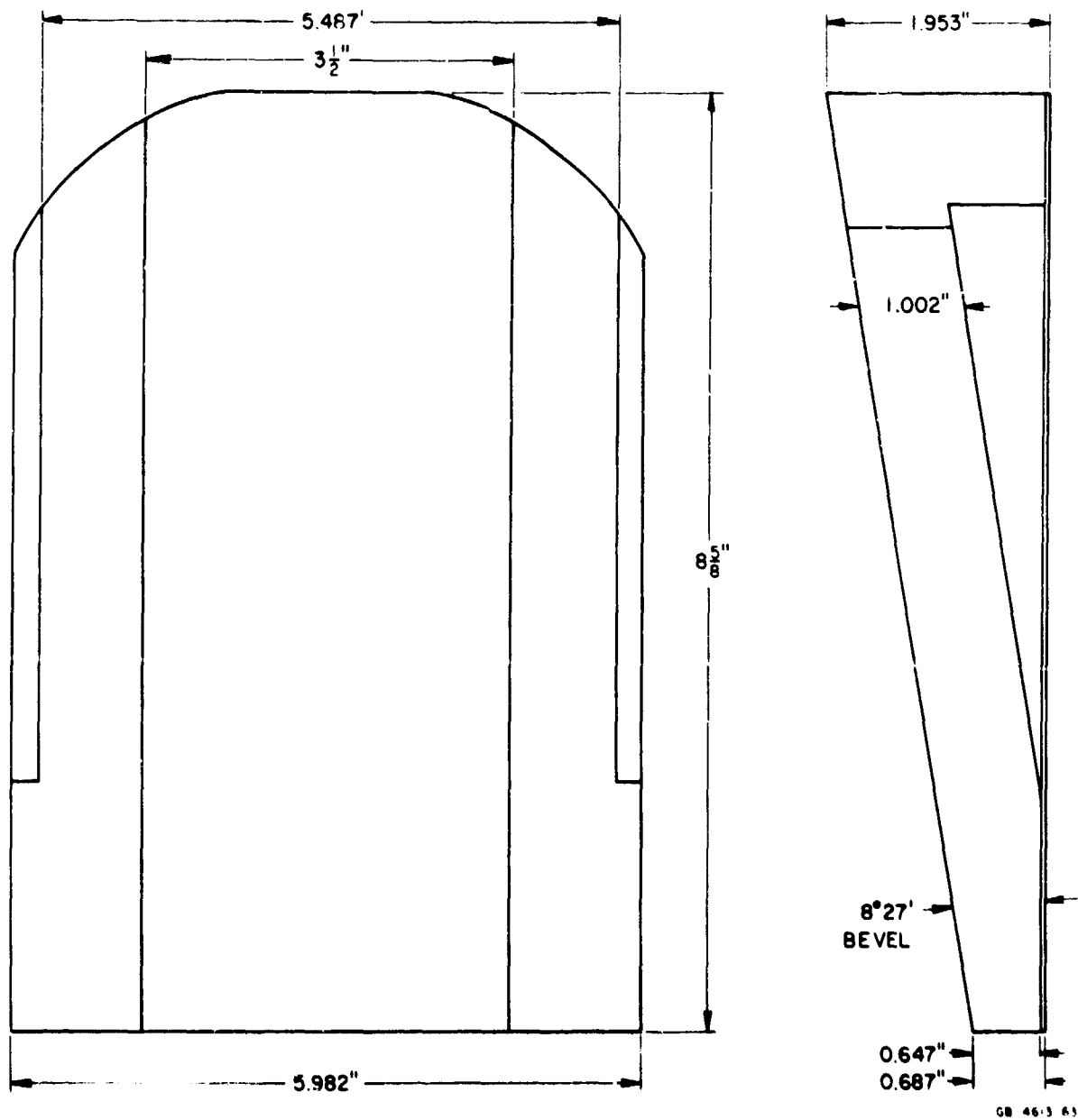


FIG. 14(b) EXPERIMENTS MOUNTED ON COVER PLATE

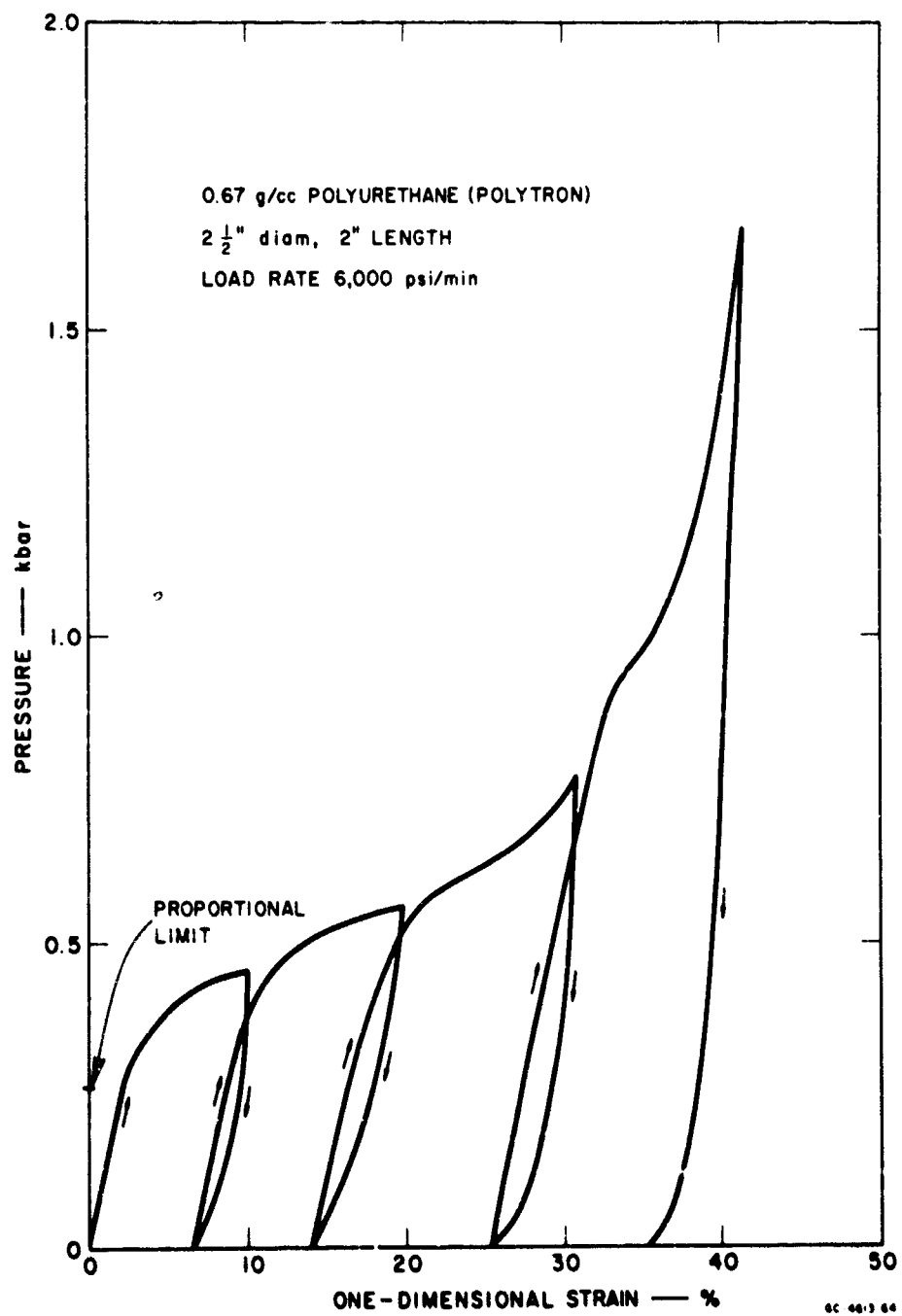


FIG. 15 QUASI-STATIC COMPRESSION OF POLYURETHANE INCLUDING RELAXATION



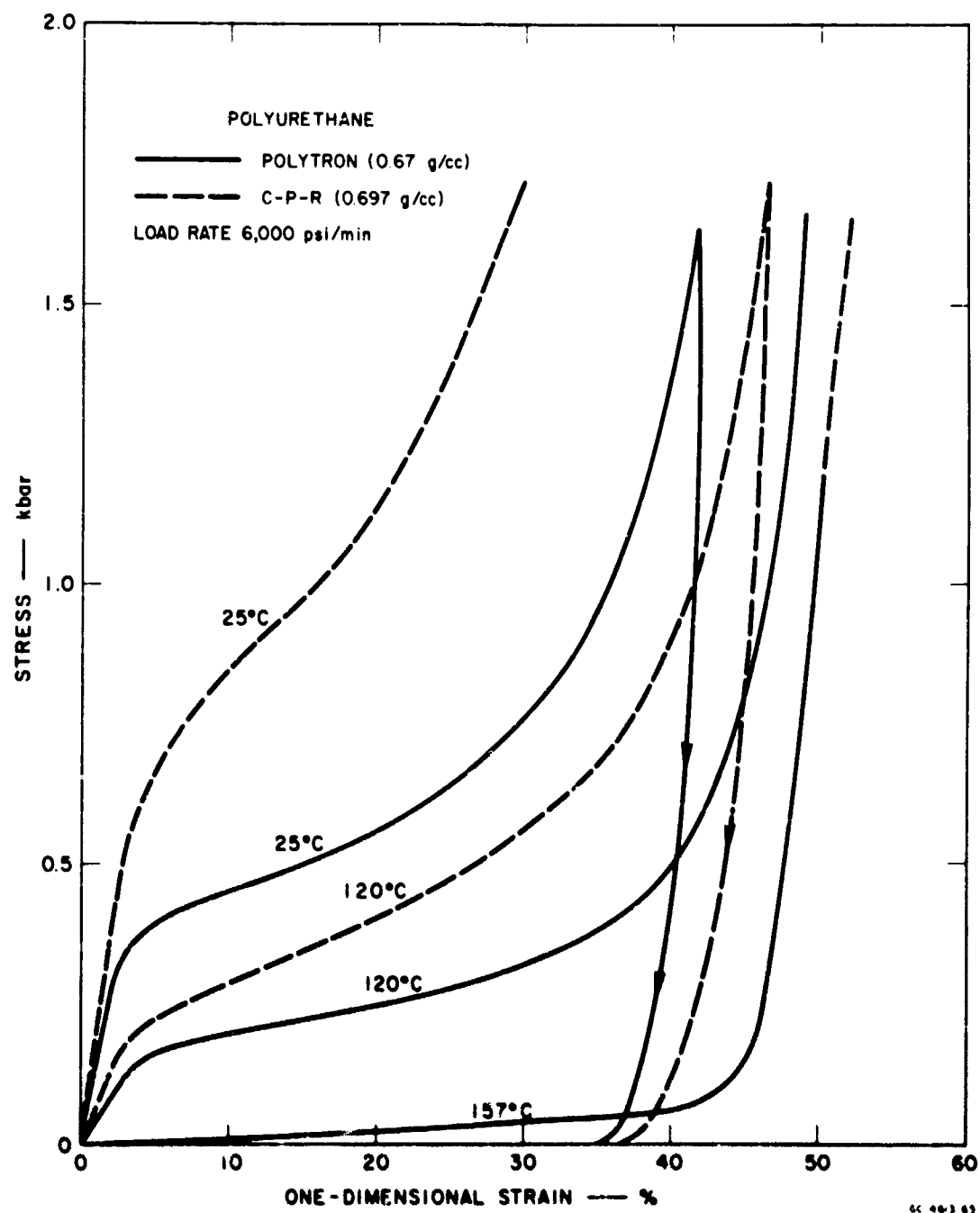


FIG. 16 EFFECT OF PREHEATING ON COMPRESSION OF POLYURETHANE

difference among the compression curves depending on the manufacturer of the samples in Fig. 16 is typical of this material.

Most of the quasi-static properties we found in our foams appear in Table 6. Predicted elastic wave speeds are simply the square roots of the ratio of modulus to starting density. Yield stress is defined as the stress at which the departure from a linear relation between stress and strain amounts to 0.2 percent of stress or strain. Also appearing in the table are compression, the slope of the stress-strain curve at 1.5-kbar stress, and our measurements of sound speeds. Uncertainty limits refer to the single measurements and not to the variation that is likely among different specimens of the same kind and density of material. From our values it appears that yield in silica is raised by preheating and is little affected in closed-cell aluminum. Otherwise results are as expressed in Fig. 16.

To assess the proportion of apparent stress arising in friction between the specimen foam and the wall of the die, we did two things: (1) compressed various samples of the same polyurethane foam but of different length-to-diameter ratios and (2) during very slow, stepwise compression of aluminum in a special apparatus held lateral expansion to zero by increasing hydrostatic pressure on the sides of the specimen. Compression under various length-to-diameter ratios in polyurethane is reported in Fig. 17; behavior of closed-cell aluminum under 1-D strain has been shown in Fig. 18 by points lying very close to the elastic portion of a stress-strain curve found from a die-held sample of the same material. Quasi-static behavior at 425°C is included in the same figure. Differences between curves for various length-to-diameter ratios in Fig. 17 are statistically significant but are seemingly randomly related to any possible influence of die friction, which should increase with increasing ratio. We think the effect of variation in sample properties probably masks the friction effect in Fig. 17.

By making a die of smaller diameter we were able to reach higher stresses during quasi-static testing of one specimen each of polyurethane and closed-cell aluminum. Results showed the usual divergences from tests to lower stress limits due to differences in the physical properties of samples; but final strain reached in aluminum was considerably higher than in earlier tests. Maximum stress was 4.35 kbar at which strain in 1.432 g/cc aluminum was 40.5 percent (89.2 percent of crystal density) and in 0.698 g/cc CPR polyurethane, 48.2 percent (final density 1.34 g/cc).

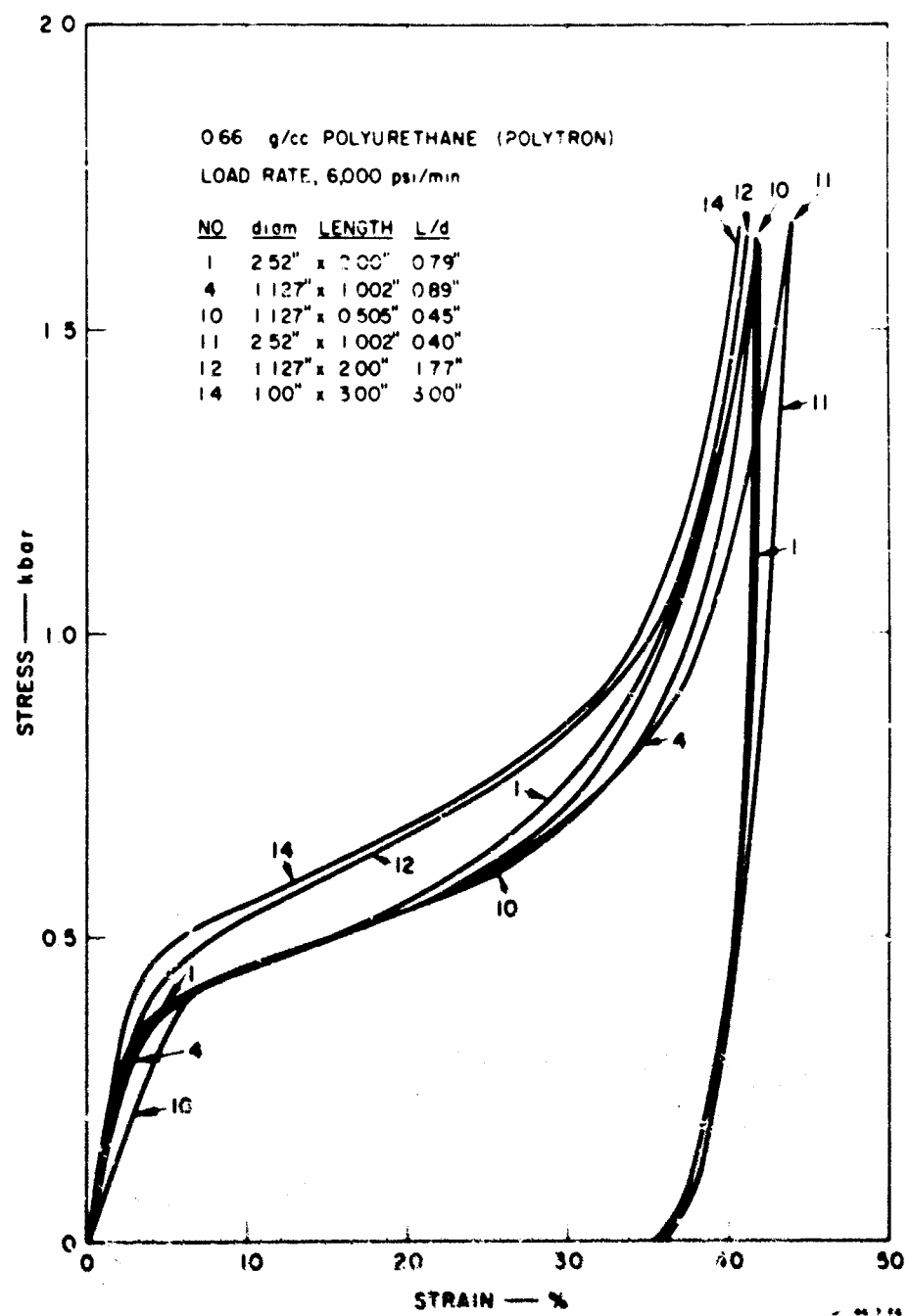


FIG. 17 COMPRESSION OF POLYURETHANE UNDER VARIOUS LENGTH-TO-DIAMETER RATIOS

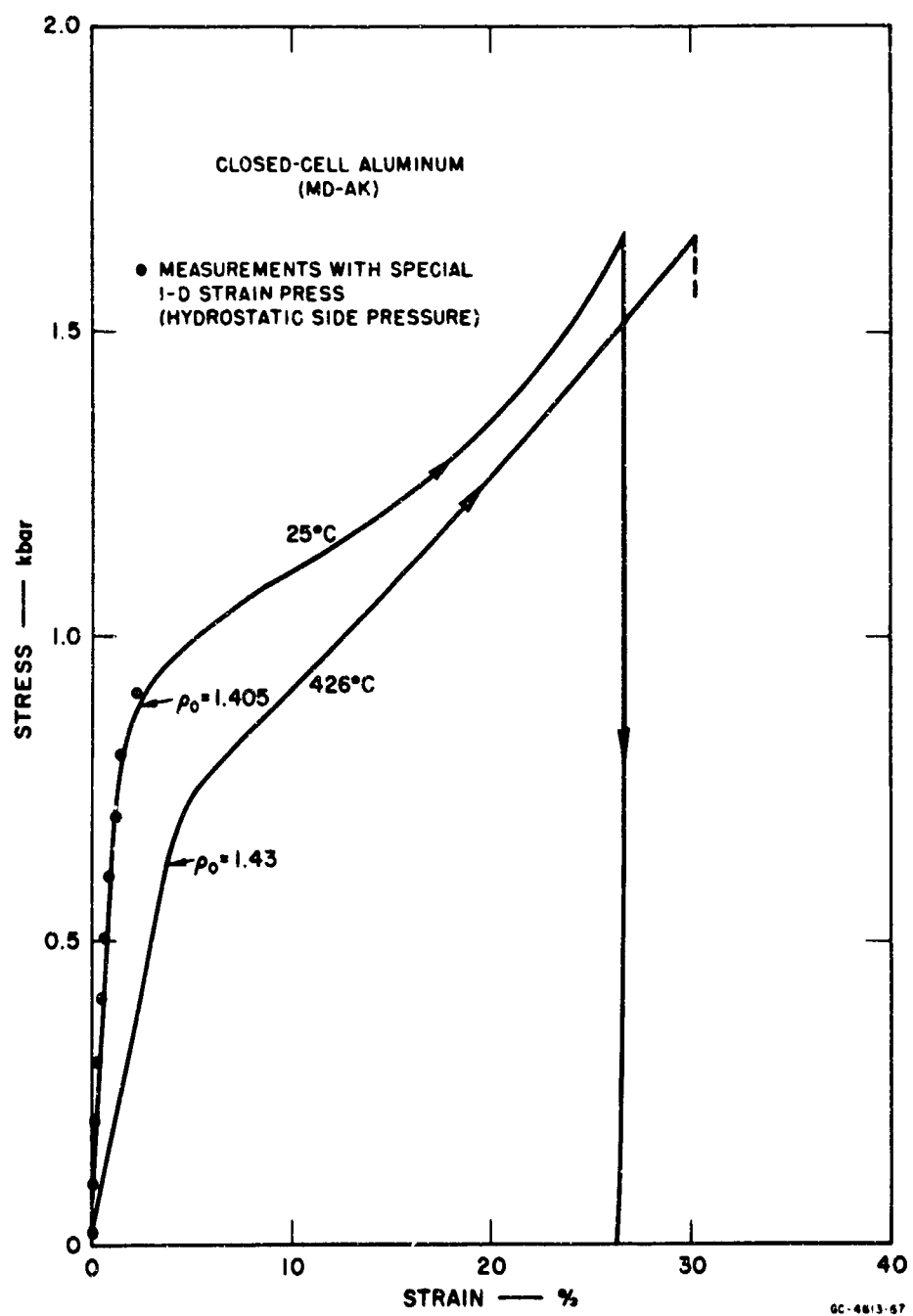


FIG. 18 EFFECT OF PREHEATING ON COMPRESSION AND ONE-DIMENSIONAL STRAIN OF CLOSED-CELL ALUMINUM

Figures 19 and 20, showing the temperature effect on compressive behavior in open-cell aluminum and graphite, respectively, are similar to Figs. 16 and 18. The curves above 1.0-kbar stress show that there is considerable structural rigidity left in the foam even though the proportional limit has been greatly exceeded, and that this rigidity is reduced both below and above the limit by heat. The pressure-volume equation of state of an ordinary solid or liquid generally shows, of course, an opposite pressure dependence on temperature than that seen in these figures. Figure 21, taken from compression data in silica, is then remarkable above the static yield point in showing the direction of temperature-pressure relation expected of an ordinary material. Since the apparent "Grüneisen constant" corresponding to the temperature dependence of pressure in this foam is of the order of 0.2, i.e., approximately one-tenth that of ordinary solids and liquids, there must be some structural weakening due to heating. (Pure silica fuses above 1,000°C.) Except for temperature of sample and die and slight difference in sample densities, the conditions of the tests leading to the two curves in Fig. 21 were the same. The samples were taken from neighboring locations in the same large block.

### C. EXPERIMENTS IN PREHEATED FOAM

To explore the effect of preheating on the shock response of foams, the usual 2-D experiments were enclosed within asbestos insulating boxes fitted with electrical heating wire. Power was slowly applied until thermocouples on the free surfaces of both foam and anvil read the same temperature. Figure 22 shows the arrangement of this apparatus. During the heating, the flyer and explosive drawn in Fig. 22, of course, were replaced by an insulating cover; when a temperature slightly above the wanted level had been reached the flyer and explosive were put in place along with a cold, removable heat shield. With this precaution we never found the temperature in the explosive just before initiation above 60°C. However, because the explosive was hotter than usual, its detonation speed was measured in every experiment involving preheating. (Results are entered in Table 1 in the Apparent Wave Speed column.) To reach foam temperatures near 300°C we heated for approximately 1 hour with 800 watts.

Preliminary static work had shown which temperatures should have a marked effect of foam behavior without melting or decomposing the material

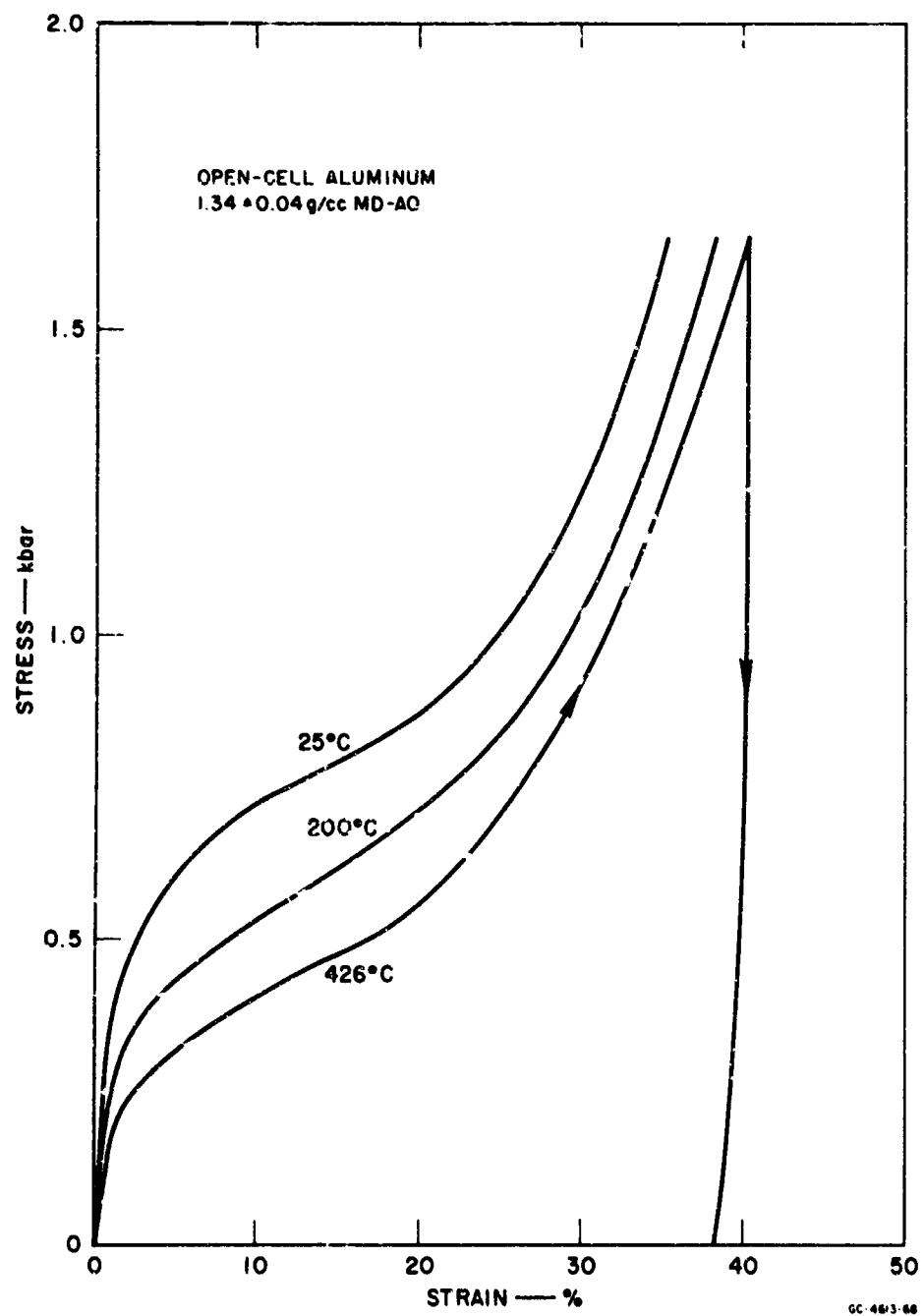


FIG. 19 EFFECT OF PREHEATING ON COMPRESSION OF OPEN-CELL ALUMINUM

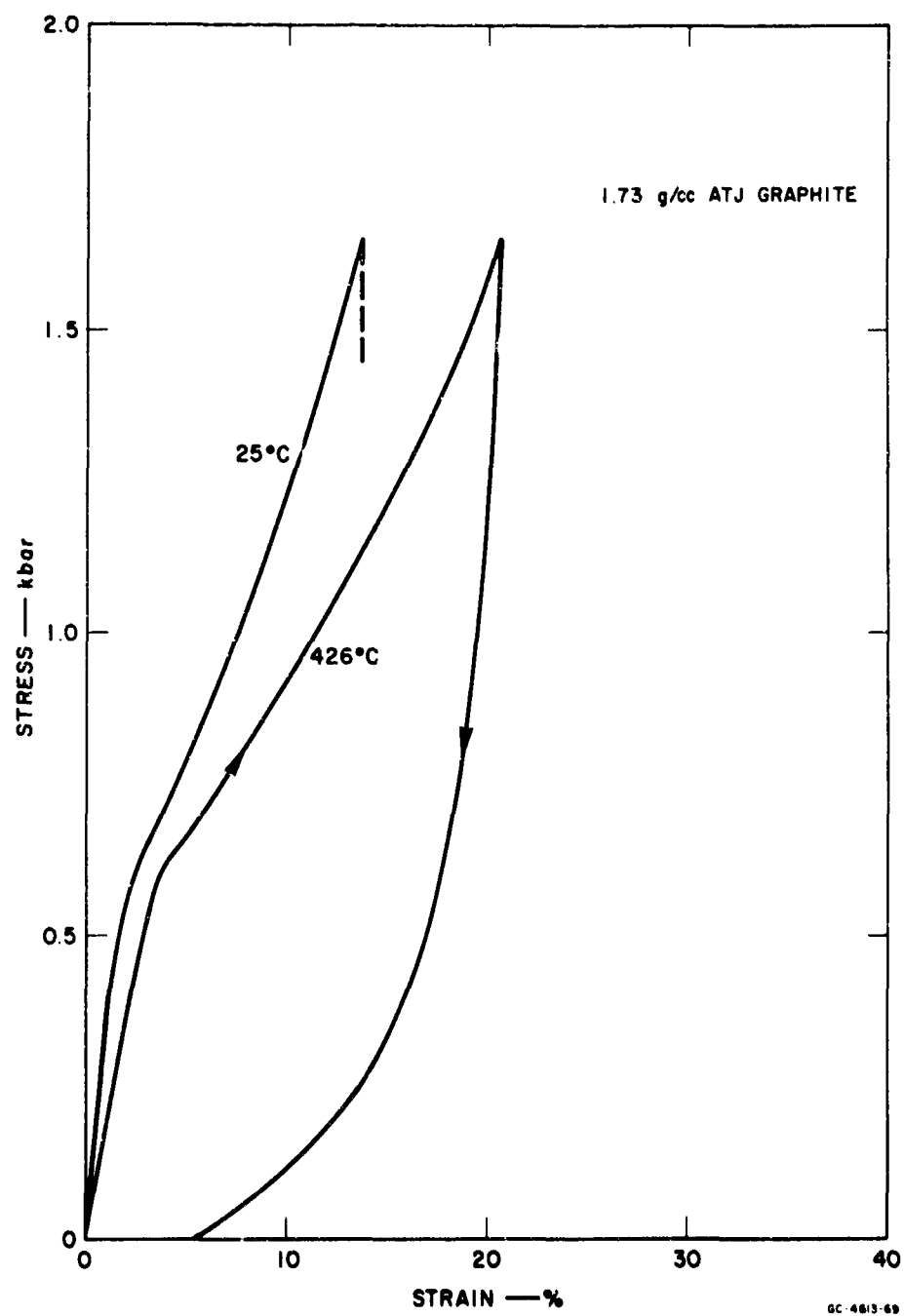


FIG. 20 EFFECT OF PREHEATING ON COMPRESSION OF ATJ GRAPHITE

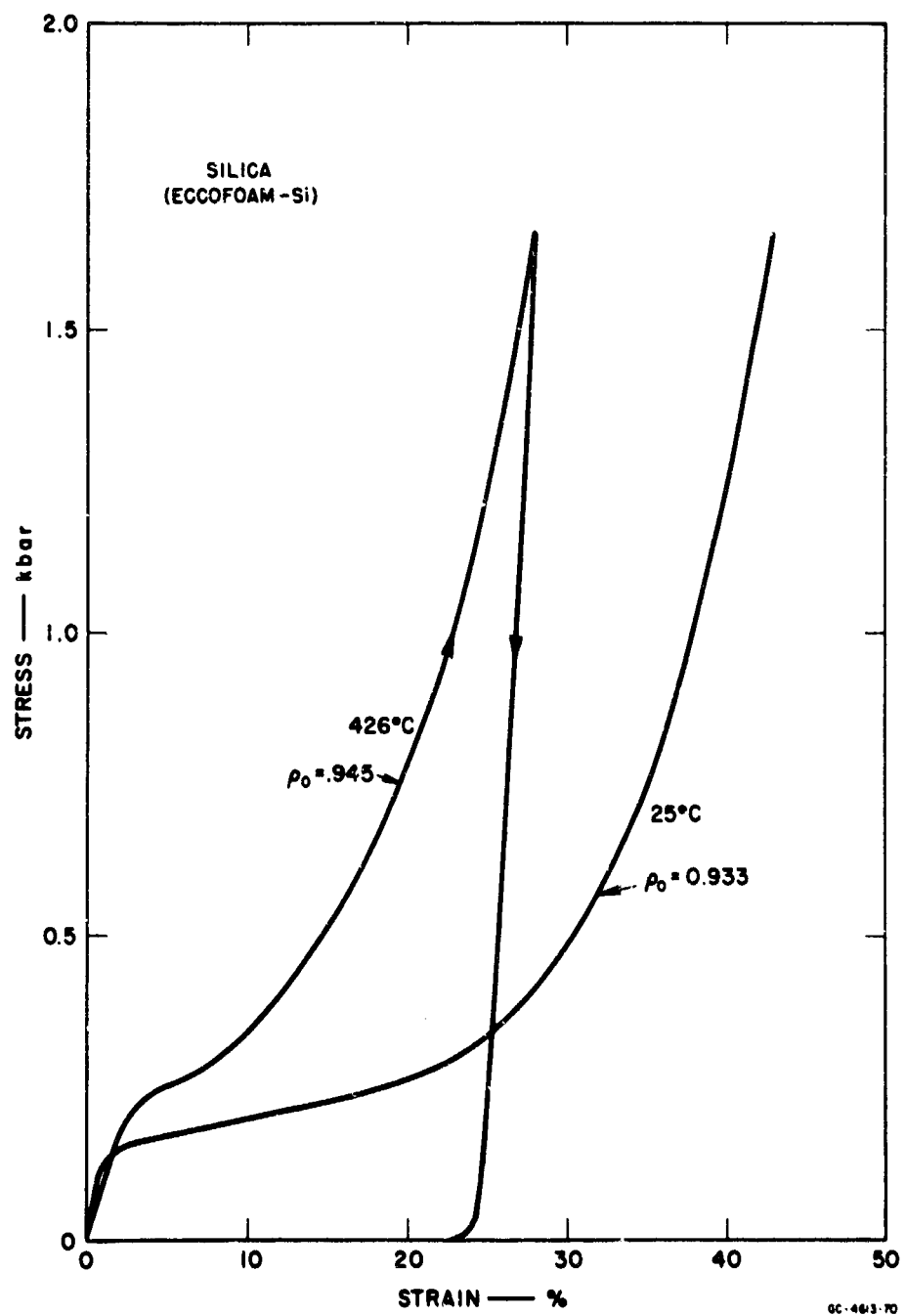


FIG. 21 EFFECT OF PREHEATING ON COMPRESSION OF SILICA



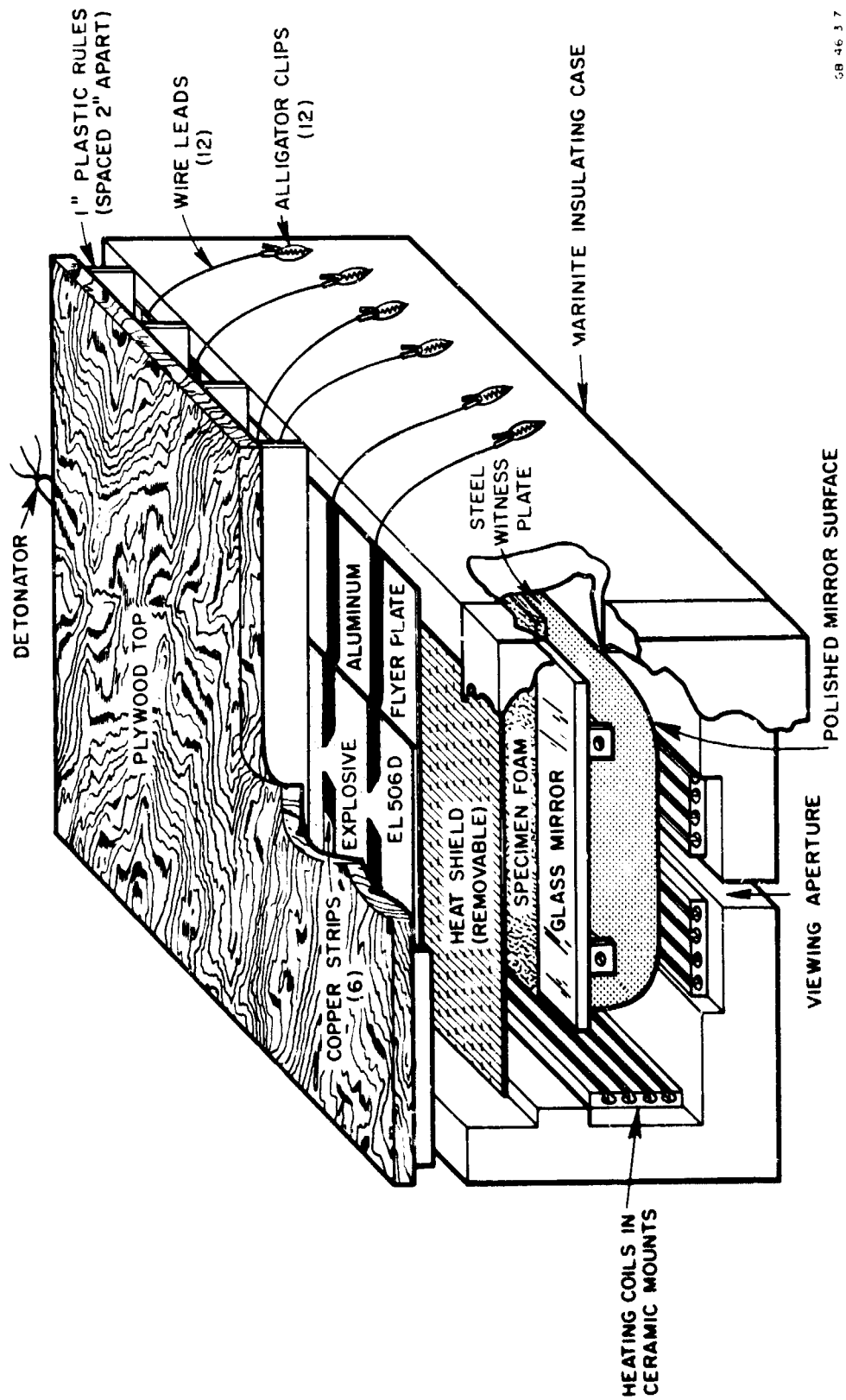


FIG. 22 VIEW OF EXPERIMENT WITH THERMAL ISOLATION

GB 46 3 7

or wholly destroying its elasticity; as a result we sought to preheat 0.67 g/cc polyurethane to approximately 120°C, and 1.4 g/cc aluminum to 400°C. Several technical problems arose in reaching the higher temperature level: to find a glue\* that would hold the curling and cracking foam slabs on to the anvil at high temperature took some time; to avoid deterioration of the quality of the anvil mirror it was vacuum-coated with aluminum. (Gold did not withstand heating so well.) Also the smear camera record from Shot 10,360 (318°C) is blurred by convection currents in front of the anvil mirror; any more experiments at that temperature level should be done with some sort of transparent heat isolation between air in the heating box and air outside.

The preheated foamshots were Nos. 10,331 and 10,332 in polyurethane (CPR) and 10,360 in aluminum. Pertinent data and results are given in Table 1.

Polyurethane at about 115°C transmits a first wave reduced in strength by about 40 percent, although the static yield at 120°C is lessened by 70 percent. Closed-cell aluminum, 1.4 g/cc, at 318°C shows a forerunner stress in the anvil lowered more than 50 percent, while the static proportional limit falls only 30 percent under heating to 426°C. Measurements of average first-wave speeds in preheated material were inconclusive.

#### D. AFTER-SHOT OBSERVATIONS

Even though the smear record has a clear *B*-wave, specimens of the polyurethane foam recovered from the experiment after impact show less than 5 percent residual strain due to the explosively driven compression. When the barrier or flyer is used, there is even no scoring of the struck surface. Beryllium also shows little outward change or residual strain after shocking. Aluminum foam is found compressed to near its unfoamed density; silica and graphite (PT0114) have not been recovered. Samples machine-cut from recovered specimens of polyurethane and aluminum foams show the densities and sound speeds listed in Table 7. All specimens in the experiments mentioned were subjected to a main or *B*-wave except perhaps one, that from Shot 9,892. In the smear record from Shot 9,892 there is a pressure rise of considerable strength coming into the anvil between the first and second reverberations of the *A*-front in the anvil; this second wave is probably a locking wave. Aluminum is recovered with

---

\* Epoxylite, C48644, trade name of Epoxylite Corp., South El Monte, California.

Table 7  
AFTERSHOT DENSITIES AND SOUND SPEEDS OF FOAMS

SHOT NO.	MATERIAL	STARTING DENSITY (g/cc)	PEAK PRESSURE (kbar)	AFTERSHOT DENSITY (g/cc, $\pm 1\%$ )	AFTERSHOT SOUND SPEED (mm/ $\mu$ sec, $\pm 1\%$ )	TYPICAL BEFORE SHOT SOUND SPEED (mm/ $\mu$ sec)
9808	P-C (Polytron)	$\sim 0.67$	1.1 - 4.3	0.672	1.32	1.73
9832	P-C (Polytron)	0.645	5.0	<u>0.673</u>	<u>1.29</u>	
			Average	0.673	1.30	
10260	P-C (CPR)	$\sim 0.714$	0.50	<u>0.716</u>	<u>1.83</u>	2.11
			Average	0.716	1.83	
9834	MD-AO	0.925	0.81	1.94	3.52	2.54
9835	MD-AO	0.927	not measured	3.02	3.62	
9810	MD-AO	0.909	not measured	2.16	3.44	
9803	MD-AO	0.960	1.6	2.06	3.03	
9802	MD-AO	0.939	1.9	2.16	3.37	
9801	MD-AO	0.95	5.0	2.30	3.20	
9800	MD-AO	0.96	12.0	<u>2.06</u>	--	
			Average	2.10	3.20	
9930	MD-AO	1.38	1.4	1.98	3.96	4.75
9933	MD-AO	1.28	8.1	<u>2.32</u>	<u>2.36</u>	
			Average	2.15	3.16	
9892	MD-AK	1.445	1.49	1.90	3.48	4.60
9894	MD-AK	1.46	4.5	<u>2.19</u>	<u>2.49</u>	
			Average	2.04	3.00	
9765	MD-AO	$\sim 0.76$	not measured	2.21	--	--
9792	MD-AO	0.76	20.0	2.04	--	
9809	MD-AO	0.688	6.6	<u>2.10</u>	--	
			Average	2.17		
10082	C-ATJ	1.73	2.6	1.76	1.99	2.32
10084	C-ATJ	1.73	5.7	<u>1.78</u>	<u>2.00</u>	
			Average	1.77	2.00	

densities between 2.0 and 2.2 g/cc or between 72 and 82 percent of the unfoamed density; during the experiments, of course, higher densities may be reached.

After-shot sound speed (1.3 mm/ $\mu$ sec) in polyurethane is markedly lower than sound speed in unshocked material (1.7 mm/ $\mu$ sec), but aluminum is not consistent in this regard. Shocking seems to raise the final sound speed in 0.9 g/cc aluminum but to lower it in 1.4 g/cc aluminum.

Thin sections made from both impacted and unused polyurethane and studied under a petrographic microscope show no differences except that the section from the struck specimen appears to be birefringent. This suggests the possibility of the existence of residual strain.

From flash X-ray shadowgrams we know that 0.67 g/cc polyurethane does compress 40 to 50 percent under explosive impact.\* These pictures show also that the compression lasts at least 17  $\mu$ sec after detonation.

#### E. VALUE OF EXPLOSIVE MOMENTUM

In those experiments described in Table 1 as having standoff, that is, a space between the parallel flyer and foam surfaces, we can later assign an accurate value to the starting momentum in the impact on the foam by subsidiary measurements of the angle between the moving and still portion of the flyer during like detonations. Without this measurement momentum can be related to weights per unit area of explosive and accelerated plate by the Gurney<sup>19</sup> theory<sup>†</sup> and G. R. Abrahamson's observations<sup>20</sup>

\* See Fig. 10, Fowles and Curran.<sup>1</sup> Since detonation speed was about 7.3 mm/ $\mu$ sec and the specimen was 6 inches long, the time interval between the early and late stages of compression is 17  $\mu$ sec. Microphotodensitometer studies of the negative of this shadowgram indicate a compression behind the locking wave in the range mentioned above. This is the region of final strain seen in static compression to ~ 4 kbar.

† This relates final plate speed  $V$  to the superficial charge or explosive density " $c$ " and the superficial plate density " $a$ " as follows:

$$V = \frac{c}{a} \left[ \frac{0.6c_0^2}{0.8 + \frac{c}{a} + 0.2 \left( \frac{c}{a} \right)^2} \right]^{1/2}$$

In our work  $V_0 = I_0$ , input momentum density to the foam and we can rewrite the above expression as

$$\frac{c}{a} = \frac{1 + 0.6 \left[ 1 + 5.33 \left( \frac{c_0}{I_0} \right)^2 \right]^{1/2}}{0.4 \left[ 3 \left( \frac{c_0}{I_0} \right)^2 - 1 \right]}$$

which often can be approximated by

$$\frac{c}{a} = \frac{2}{\sqrt{3}} \frac{I_0}{c_0} \quad \text{i.e., } c = I_0$$

of the Gurney constant,  $G_0$ ; but since this constant strongly depends upon the nature of the material accelerated by the explosive, the amount of explosive momentum delivered to a foam lying against the aluminum barrier at the start of detonation is uncertain within limits.

For instance, a material of density 0.67 g/cc impacted by EL-506D explosive, Abrahamson reports, has a Gurney constant,  $G_0$ , of  $1.88 \pm 0.19 \times 10^5$  cm sec; for aluminum  $G_0 = 2.31 \pm 0.23 \times 10^5$  cm/sec. To put  $1 \times 10^4$  taps of impulse into an aluminum flyer 0.012 inch thick as in our 2-D experiments with standoff, Gurney's formula requires a layer of EL-506D explosive 0.021 inch thick (density 1.4 g/cc). For the experiments without standoff we can use a weighted average value of  $G_0$ , i.e.,

$$\bar{G}_0 = \frac{G_{0Al}m_{Al} + G_{0f}m_f}{M_{Al} + m_f}$$

where  $m$  refers to mass per unit area, subscript  $Al$  means aluminum, and subscript  $f$ , foam. Thus when a 0.012-inch-thick flyer is used against 5 mm of polyurethane foam of 0.67 g/cc density,  $\bar{G}_0 = 1.97$  and the explosive thickness to give  $1 \times 10^4$  dyne sec cm<sup>-2</sup> is calculated as 0.0180 inch. When the flyer alone is impelled, the thickness of explosive for the same momentum density in the same geometry is 0.022 inch.

Values of the abscissa in Figs. 4 and 5 are usually uncertain on two scores: the foregoing theory does not give unchallengeable values of input momentum density  $I_0$  in 2-D experiments, and the foam thickness in the (changing) direction normal to the shock front is unknown. In plotting points in those two figures from the 2-D experiments, we have used one constant ratio between explosive thickness and  $I_0$  for experiments without standoff and another in experiments with standoff, and we have overlooked the greater effective foam thickness due to obliquity of the fronts; the horizontal bars through the points in the figures are estimates of our uncertainties in these respects.

## F. FOAM UNIFORMITY

The rather wide scatter of the reduced data shows, we think, the importance of variation in physical properties among even neighboring sites in one foam block. In the absence of evidence we see no reason to regard density as the only controlling physical characteristic but density

variations are widely found in foam specimens. We have made both X-ray and light shadowgrams through foam layers, and we have measured average densities from small samples cut from neighboring sites. For example, all specimens of the same kind and of approximate densities listed in Table 1 were supplied in single pieces; there is no reason to believe that the variation in average densities seen there does not extend to each single specimen as well. But if we traverse with a microphotodensitometer the X-ray shadowgram, we should see important trends. Figure 23 resulted from two traverses along different axes of a single shadowgram through a 1-inch-thick slab of 0.9 g/cc aluminum. The density variation

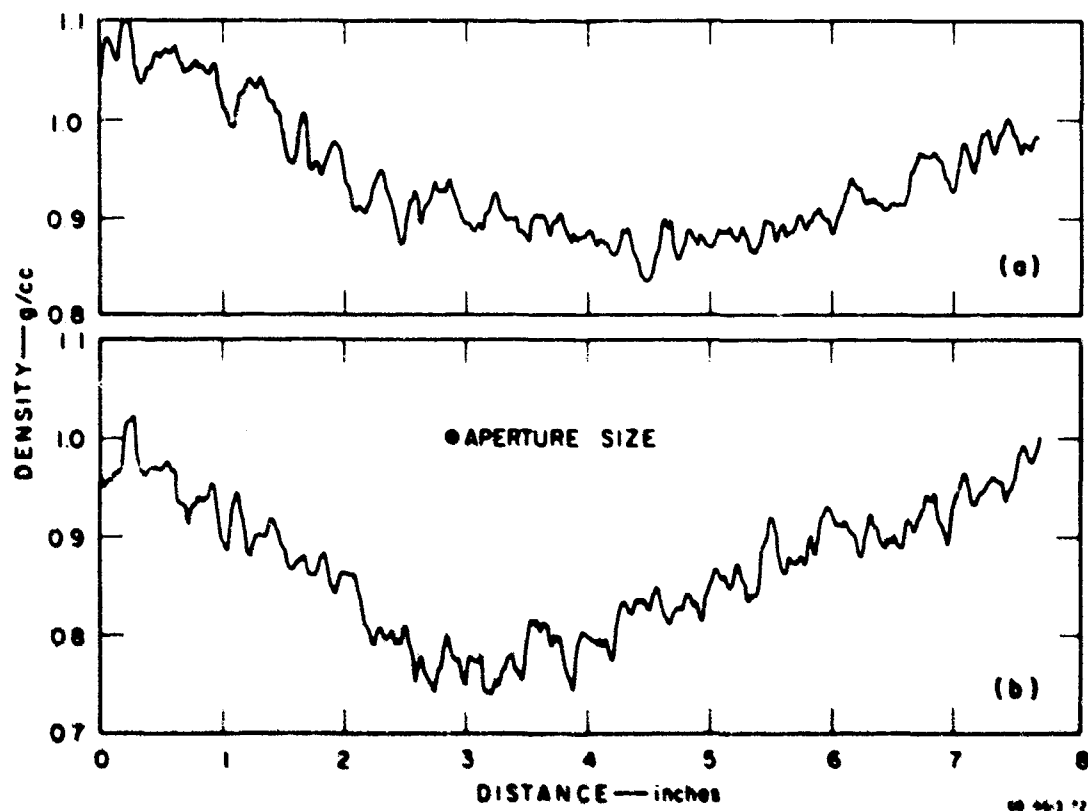


FIG. 23 MICROPHOTODENSITOMETER SURVEY OF X-RAY SHADOWGRAMS OF A THIN FOAM LAYER

from place to place may be as much as 20 percent. All aluminum foam showed obvious outward marks of irregularity in density, especially the lighter density foam. Other foams showed less variation.

We probed our foamed beryllium specimens ultrasonically, and here again considerable irregularity was found in sound speed within one sample. Of four measurements at different sites in one plate  $5 \times 8\frac{1}{2} \times 0.236$ ,

the average was 6.71 mm/ $\mu$ sec; the standard deviation, 0.40 mm/ $\mu$ sec. and the greatest deviation from the mean, 0.54 mm/ $\mu$ sec. Of four cylinders 1 1/8 inch diameter, 1 inch long, the ratio of average density to sound speed through the length of the sample was  $1.52 \times 10^{-6} \pm 0.11$  g sec/cm<sup>4</sup>, the greatest deviation,  $0.16 \times 10^{-6}$  g sec/cm<sup>4</sup>; hence the correlation between average foam density and sound speed was not better than 10 percent.

## 4. THEORY

### A. GENERAL

In the three models used in calculations so far we have assumed a uniform material into which the conventional 1-D shock discontinuities run according to the conservation laws. In all we have taken an equation of state (in effect, a combined Hugoniot and isentropic equation of state) as a simple relation between pressure and specific volume, and, through a linear "elastic" region of small compression in this relation, in all have achieved breakup of a single strong shock into: (1) the fast forerunner behind which strain is small and (2) the main shock behind which strain is great. Entropy change, always concentrated in the main front, is not important in calculation because all isentropes containing any state behind the main front are assumed to coincide. In the simple model, completely set forth by Fowles and Curran<sup>1</sup> and Rempel,<sup>2</sup> the main front is like a snowball, gathering more and more condensed foam behind itself and moving slower and slower, with all parts of the gathered mass moving at the same speed and having the same density. Both the other models are slightly more sophisticated—but not more successful—in allowing waves of small changes to move through the condensed mass.

In the following two sections we present the basic assumptions and some results of 1-D flow calculations by the method of characteristics and by the method of artificial viscosity. The first yielded pressure and particle speed distributions 2.5  $\mu$ sec after impact in a foam half-space struck by a thin metal flyer. The same distributions were derived by the second method. Since the results compared closely and since a code for machine computation by artificial viscosity was available,\* the method of artificial viscosity was used in an attempt to predict the pressure history in the anvil during one of our 1-D experiments.

In the characteristics method the Rankine-Hugoniot jump conditions are satisfied at the leading shock front behind which release waves

---

\* See J. Erskman, Phase 2 of this report.



reverberate. Interface states are found by standard impedance matching techniques in the pressure-particle speed ( $P - u$ ) plane. Locations of fronts and interfaces are followed in the distance-time ( $x - t$ ) plane. In the problem considered the forerunner appears almost immediately upon impact.

## B. CALCULATION BY THE METHOD OF CHARACTERISTICS

Figures 8 and 9 result from a graphical solution of the flow equations carried out in the pressure-particle speed ( $P - u$ ) and distance-time ( $x - t$ ) planes with the help of simplified equations of state. We tried to simulate conditions in a 1 -  $D$  experiment, that is, a solid aluminum flyer plate 0.020 inch thick struck a polyurethane foam half-space at a speed of 0.08 mm/ $\mu$ sec. The foam's original specific volume  $V_0$  was 1.515 cc/g, locked volume  $V_1$  at the elastic limit  $P_e$  was 1.00 cc/g,  $P_e$  was 1.00 kbar, and elastic speed  $U_e$  was 1.65 mm/ $\mu$ sec. The locked foam and the solid aluminum had sound speeds,  $c$ , at zero pressure of 2.12\* and 6.23 mm/ $\mu$ sec, respectively, and both were given equations of state which were single straight lines in the  $P - V$  plane,<sup>†</sup> implying that rarefactions resulting from reflections of shocks at free surfaces were discontinuities.

Thus if  $m$  is the slope of the equation of state, i.e.,

$$c^2 = V_1'^2 \frac{P_e}{V_1' - V_1}$$

and

$$m = \frac{P_e}{V_1' - V_1}$$

( $u$  is the particle speed,  $P$ , the pressure, and  $V$ , the volume), then waves behind the locking front move at speeds

$$|U| = \pm u + V_m^{1/2} = \pm u + c - \frac{V_1'}{c} P$$

Slopes of characteristics for locked foam and aluminum in the  $P - u$  plane are independent of the pressure:

\* Chosen to agree with earlier work using the method of artificial viscosity in which locked foam was treated by an approximate equation of state for lucite.

† This equation of state for the locked foam is shown dashed in Fig. 7.

$$\left| \frac{\Delta P}{\Delta u} \right| = \frac{|U \pm u|}{V} = \frac{c - \frac{V_1'}{c} P}{V_1' - \frac{P}{m}} = \frac{c}{V_1'}$$

Pressure and particle speed in the foam behind the forerunner are related by

$$P = \frac{U_e}{V_0} u \quad \text{if} \quad P \leq P_e$$

In the absence of a forerunner the relation between pressure and particle speed just behind the locking shock in the foam is:

$$P = \frac{1}{2} \frac{c^2}{V_1'^2} \left\{ -V_0 + V_1' + \left[ (V_0 - V_1')^2 + 4u^2 \frac{V_1'^2}{c^2} \right]^{1/2} \right\}$$

if  $P \geq P_e$  where

$$P_e = \frac{V_0 - V_1'}{\left( \frac{V_0}{U_e} \right)^2 - \left( \frac{V_1'}{c} \right)^2}$$

When the locking shock in the foam is running into the elastically strained region, the jump conditions and the equation of state imply immediately behind the shock front:

$$P = \frac{1}{2} \left( \frac{c}{V_1'} \right)^2 \left\{ 2V_1' - V_1 - V_e + \left[ (V_e - V_1)^2 + 4 \left( \frac{V_1'}{c} \right)^2 (u - u_e)^2 \right]^{1/2} \right\}$$

if  $P_e \leq P \leq P_c$ .

Figure 24 shows the relation written above between  $P$  and  $u$  and a few of the early characteristics used in the solution of the problem stated. This solution has not been taken beyond 2.5  $\mu\text{sec}$  of problem time.

### C. CALCULATION BY THE METHOD OF ARTIFICIAL VISCOSITY

In Figs. 8 and 9 (except in the forerunner front) the flow solutions by the method of artificial viscosity (Q-methods)<sup>12</sup> agree closely with

\* The coding for this calculation follows in most particulars that found in Hermann *et al.*<sup>13</sup>

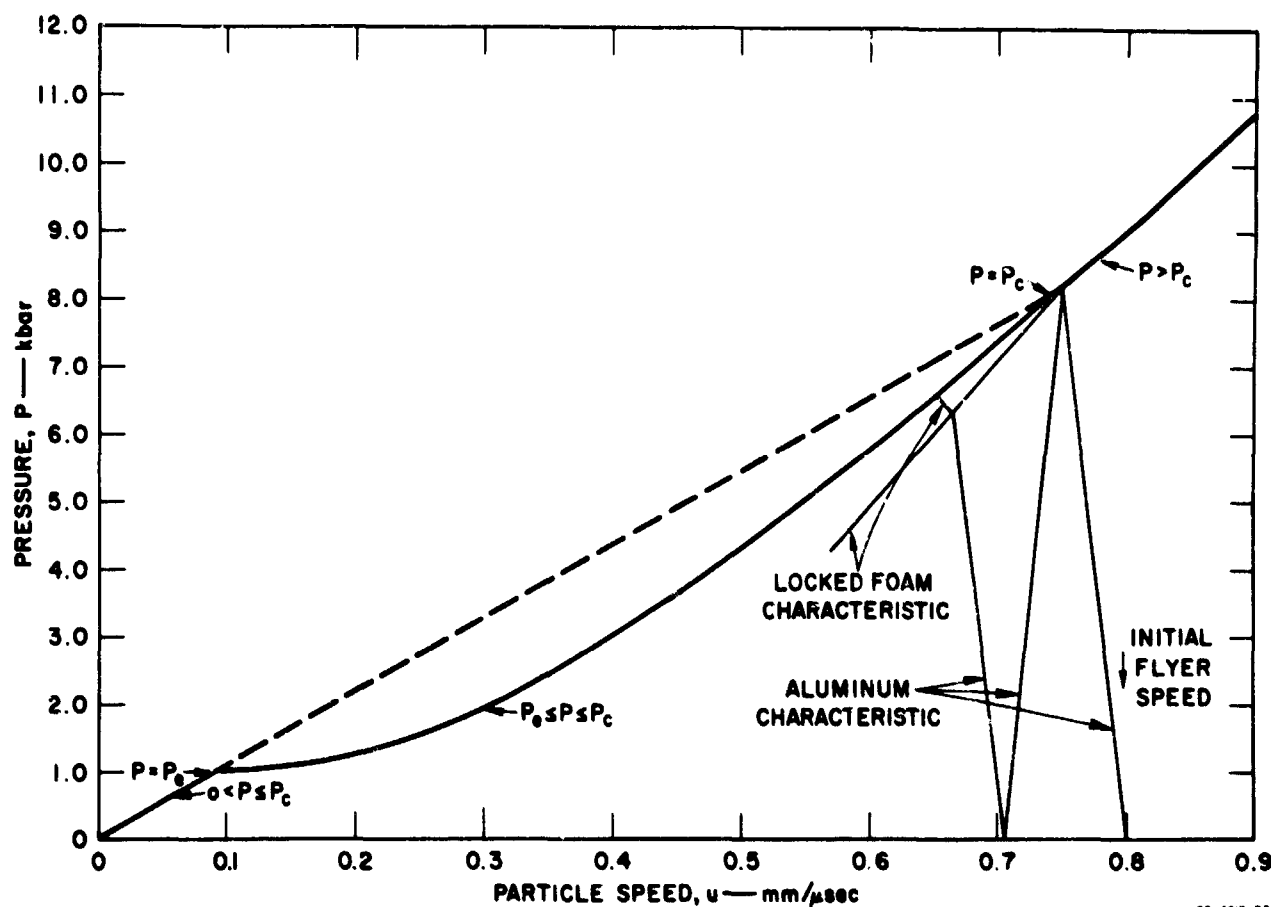


FIG. 24 RELATION BETWEEN PRESSURE AND PARTICLE SPEED JUST BEHIND THE LOCKED FRONT IN POLYURETHANE FOAM HALF-SPACE STRUCK BY ALUMINUM FLYER

those found by the method of characteristics outlined in the foregoing section, although because of the short time covered the test is not a severe one. We think, however, our use of the  $Q$ -method to explore rapidly the effects upon pressure history of certain changes in the equation of state is valid. The only important difference in the forecasts of pressure history between the two calculations lies in the slow pressure rise in the forerunner front expected from  $Q$ -method. The artificial parameter  $Q$  is also high in value in that region. We look upon it as a shortcoming of the  $Q$ -method that results in regions of high  $Q$  are wrong to some unknown extent.  $Q$  is defined as

$$Q = (q^2 |\Delta u| + A c^2) |\Delta u| \frac{1}{V}$$

where  $q$  and  $A$  are free numeric constants,  $\Delta u$  is particle speed difference between adjacent cells of constant mass,  $c$  is local sound speed, and  $V$  is local specific volume.

As seen in Fig. 7, although the equation of state used for locked polyurethane in the  $Q$ -method is more complicated than the simple relation used in the characteristics method, the differences in the pressure range of interest are negligible.\*

Although the distributions shown in Figs. 8 and 9 are uninfluenced by it, a rigid wall at  $x = 5.0$  mm bounded the foam during the calculations by the  $Q$ -method, and Fig. 6 shows the pressure history predicted in the wall by the same computation which gave rise in part to Figs. 8 and 9. There are a number of obvious points of strong disagreement between the predicted and observed histories shown in Fig. 6. We would expect only a 10 to 15 percent lowering of peak stress in the prediction if we gave to the wall the shock impedance of steel; we have sought to lower this peak further by changing the equation of state assumed for the locked foam in such a way as to lower its shock impedance, but this leads to a longer time interval between  $B$ - and  $C$ -fronts (main and reverberation) than observed. The rise time in the  $B$ -front is increased slightly in two different ways: (1) by moving the point  $(V_e, P_e)$  down along the elastic line halfway to  $(V_0, P_0)$  and connecting  $(V_e, P_e)$  with  $(V_1, P_1)$  by a straight line, and (2) by moving  $(V_e, P_e)$  along the elastic line to 0.85 kbar and connecting to the existing equation for locked foam at  $P = 2$  kbar through two second-degree arcs, meeting at  $[P = 1$  kbar,  $V = (V_e + V_1)/2]$  where derivatives  $dP/dV$  on both arcs vanish. Figure 25 illustrates these modifications. In both (1) and (2), the pressure history in the rigid wall begins a slow rise after an interval of constant pressure, but the arrival of the main front is still quite distinct; the  $B$ - $C$  interval is 2  $\mu$ sec too long in case (2) but approximately as seen experimentally in case (1). We can successfully duplicate the failure of the anvil pressure to return to zero within 8  $\mu$ sec after  $A$ -front arrival by choosing a relaxation path for locked foam along the compression path, as for example in case (2). None of the many  $P - V$  constitutive relations tried so far begins to remove the clear pressure relaxation between the  $B$ - and  $C$ -peaks, although the two peaks can easily be made less distinct but farther apart in time.

---

\* It should be noted that when used in the  $Q$ -method the equation represented by Fig. 7 must be supplemented by the inclusion of states along the line  $P = P_e$  between the points  $(V_e, P_e)$  and  $(V_1, P_1)$ , and the provision of paths from these intermediate states to zero pressure, which we have taken parallel to the path from  $(V_1, P_1)$  to  $(V_1, P_1')$ . None of these states is possible in our application of the method of characteristics.

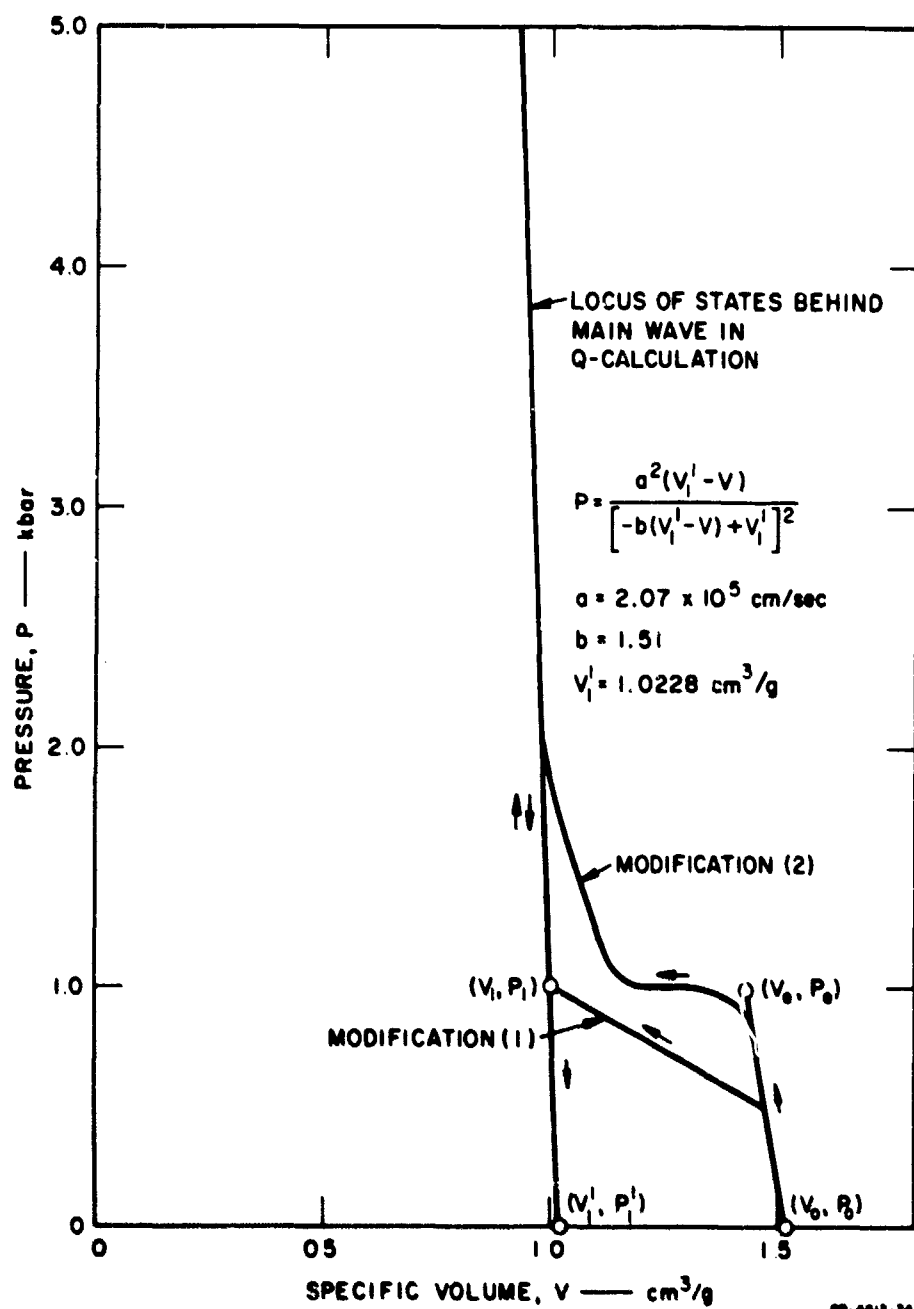


FIG. 25 MODIFICATIONS OF EQUATION OF STATE FOR Q-CALCULATIONS

#### D. INTERPRETATION OF EXPERIMENTAL RESULTS BY THE SIMPLE THEORY

From calculated impact speed and from the peak stresses in the main waves seen in three experiments with 1 - *D* symmetry,<sup>21</sup> we have tried deducing consistent values for average shock speed in the locked foam. If our interpretation of the experiments has been correct in locked 0.67 g/cc polyurethane, the calculations show an average shock speed increase from 0.8 to 1.5 mm/ $\mu$ sec with stress in the range 2 to 4 kbar. The results of the calculation can be seen in Table 8. The computation of those results is explained in the following.

Using the simple theory of elastic-rigid locking behavior (Fowles and Curran,<sup>1</sup> and Rempei<sup>2</sup>), the measured flyer momentum of the 1 - *D* experiments in polyurethane, and the accurately measured forerunner speed in polyurethane, we explore the effect of assuming different values of locked density until we find a range of values in each experiment that leads to calculated time intervals between arrivals of first and second waves (*A - B* intervals) falling within the range actually seen in the same 1 - *D* experiments. Thus in column 6 of Table 8 appear the measured least and greatest values of the *A - B* intervals, and in column 7, the calculated intervals corresponding to each of the values of specific volume in column 8. We see that a locked specific volume between 0.90 and 1.05 cc/g can always be found to produce a calculated *A - B* interval to match any observed value. In fact 1.00 cc/g is a good compromise; so we then calculate particle speed and stress behind the locking wave at the moment of collision of the two locking waves by assuming the locked volume is 1.00 cc/g. Next, assuming the shock speed and density stay constant within the locked mass after this collision and assuming shock impedance of steel is  $4.62 \times 10^6$  g cm<sup>-2</sup> sec<sup>-1</sup>, we compute the value of foam shock impedance corresponding to the observed peak pressure of the main wave (column 7). From this we get the shock speed in column 11. (Sound speeds in two samples of this foam after being subjected to locking shocks were 1.32 and 1.29 mm/ $\mu$ sec, Shots 9808 and 9832, respectively. As noted elsewhere [Table 7] the recovered samples appear to have their original average density.) Our experiments give us a verification of these inferred speeds in locked foam because a third front is reflected back to the anvil from the sharp impedance mismatch at the foam-flyer interface.

Entries in the last column of Table 8 show that the average reverberation speed based on *B - C* intervals is much higher than speeds inferred

Table 8  
DEDUCTION OF SHOCK SPEED IN LOCKED POLYURETHANE (0.67 g/cc)  
FROM MAIN WAVE PRESSURE AND REVERBERATION TIME

1	2	3	4	5	6	7	8	9	10	11	12	13	14
SHOT NO.	KIND OF FOAM	ORIGINAL FOAM DENSITY (g/cc)	ORIGINAL FOAM THICKNESS (mm)	FLYER MOMENTUM ( $10^4$ caps)	OBSERVED A-B INTERVAL ( $\mu$ sec)	OBSERVED PEAK PRESSURE IN B-WAVE (kb)	VALUE OF LOCKED SPECIFIC VOLUME USED IN COMPUTATION (cc/g)	FORERUNNER SPEED $U_c$ (mm/ $\mu$ sec)	PRE-DICTED A-B INTERVAL ( $\mu$ sec)	SHOCK SPEED* $U$ (mm/ $\mu$ sec)	MEASURED B-C INTERVAL ( $\mu$ sec)	ASSUMED DISTANCE TRAVERSED (mm)	SHOCK SPEED† $U$ (mm/ $\mu$ sec)
9155	Polyurethane	0.67	5.0	1.15	1.7 - 2.6	3.25 $\pm$ 0.35	0.90 1.00 1.05	1.65	2.8	0.935 $\pm$ 0.2 0.935 $\pm$ 0.2	1.5 - 2.6	5.85 6.50 6.82	2.25 - 3.90 2.50 - 4.33 2.62 - 4.55
9180	Polyurethane	0.67	10.0	1.15	$\infty$	1.0 $\pm$ 0.1	0.90 1.00 1.05	1.65	$\infty$ $\infty$ $\infty$	-- -- --	-- -- --	-- -- --	-- -- --
9217	Polyurethane	0.67	6.5	1.15	3.0 - 4.9	2.0 $\pm$ 0.25	0.90 1.00 1.05	1.65	5.5 2.7	0.77 $\pm$ 0.2 0.635 $\pm$ 0.2	2.0 - 4.1	7.60 8.45 8.87	1.85 - 3.80 2.06 - 4.22 2.16 - 4.43
9216	Polyurethane	0.67	10.0	2.30	2.6 - 4.9	4.3 $\pm$ 0.8	0.90 1.00 1.05	1.65	6.2 2.6	1.4 $\pm$ 0.6 1.5 $\pm$ 0.6	§		

\* Inferred from measured pressure.

† Inferred from B-C interval.

§ No C-wave (experiment interrupted).

from the computed speed of locked mass and the pressure induced in the anvil by the main wave. The disagreement is so great we are led to doubt whether the third wave originates in the meeting of main wave and anvil, but wonder if it stems instead from a significantly earlier collision of a wall-reflected wave and the main wave. If this is true there should be a fourth wave in our record of anvil motion, and there may have been in Shot 9217; the observation was broken off too soon. However, it is not likely we would have missed the fourth wave in Shot 9155. Furthermore, if we argue that the fourth wave is not seen because the foam has bounced off the anvil before the wave crosses the foam, we must dispute the accuracy or the pertinence of the record of Shot 9155 which shows pressure held on the anvil for a long time after the third wave enters it (Fig. 6). (It is theoretically possible for the locked foam to bounce off the steel wall before the fourth wave reaches it, provided there is substantial increase in the shock impedance of locked material with higher pressure.)

Another way to soften the contrast between columns 11 and 14 of Table 8 is to assume that the pressure behind the main wave when it collides with the wall or the wall reflection of the forerunner is no greater than forerunner stress  $P_r$ . Under this assumption the shock impedance of the locked foam must be greater to give rise to the observed peak B-pressure; but the resulting increase in values of  $U$  in column 11 for Shots 9155 and 9217 amounts to only about 15 percent. Even taking pressure behind the B-front as zero does not wholly reconcile columns 11 and 14.

#### E. FOAM EFFECTIVENESS AS A FUNCTION OF PARAMETERS FROM THE SIMPLE THEORY

When the main wave front strikes the wall reflection of the forerunner just as the front disappears, according to the simple theory, the peak pressure in the anvil is

$$P = P_r \left[ 1 + \frac{V_0}{V_1} \frac{U_r}{U_s} \right] \quad (2)$$

where  $P_r$  = stress in forerunner and  $U_s$  is the shock speed in the locked foam. If the beginning foam thickness is great enough to make  $L_0/U_0 < S^*$ , the reflected wave will pass through the rarefaction fan

\* See Equation (1), Section 2B.



issuing toward the wall from the locked mass at time  $t^*$ , and the second wave on the wall will be elastic and will follow a relaxation of pressure. In other words, for  $l$  slightly higher than that given above, the locked mass is brought to rest with the exertion of pressure at forerunner stress or below on the wall. The complicated calculation needed to express this value of  $l$  exactly is not justified by the accuracy of the model, and we consider  $S$  as giving the approximate "stopping power" of the foam for the locking wave. Furthermore, if we write as a first approximation

$$U_e = K \frac{V_1}{V_0} U, \quad \dagger$$

where  $K$  probably depends somewhat on the kind of material making up the foam, then  $P$  in Eq. (2) becomes the same for all materials which have the same proportionality between distention and reduction of elastic speed due to distention. On this basis, then,  $S$  is the superficial mass density of foam needed to keep pressure on the structure below the value given by

$$P = P_e(1 + K)$$

It is also the superficial density of foam at which increments of foam thickness abruptly become more effective than at lower densities. Letting

$$\alpha = \left( \frac{V_0 - V_e}{V_0} \right)^{1/2} \quad \text{and} \quad \beta = \left( \frac{V_0 - V_1}{V_0} \right)^{1/2}$$

we write stopping power  $S$  as:

$$S = \left[ \frac{I_0}{\left( \frac{l}{V_0} \right)} \right]^* = U_e \frac{\beta^2}{1 + \frac{\alpha}{\beta} - \frac{1}{\beta}} \quad (3)$$

(The asterisk means the quantity is evaluated under conditions such that the collision of the two locked masses takes place at time  $t^*$ .) We can

---

<sup>†</sup> Although they are not conclusive as yet, our results in open-cell aluminum do not make this seem a very good approximation.

thus express the stopping power as a function of three independent parameters from the simplified equation of state, namely  $U_e$ ,  $\alpha$  and  $\beta$ . If  $U_e$  and  $V_0$  are held constant,  $\alpha$  increases with increasing  $P_e$ ;  $\beta$ , the only variable depending on locked volume  $V_1$ , rises with growing distention.  $U_e$  itself, of course, depends both on the slope of the elastic locus and the initial volume:

$$U_e = V_0 \left( \frac{P_e}{V_0 - V_e} \right)^{1/2}$$

As either one of the two variables  $\alpha$  and  $\beta$  is varied through the range  $0 \leq \alpha < \beta$  and  $U_e$  held constant, the right side of Eq. (3) has no maximum; stopping power grows without limit with both increasing distention and increasing elastic pressure. If we take  $\alpha' = (V_0 - V_e/V_1)^{1/2}$  and  $\beta' = (V_0 - V_1/V_1)^{1/2}$  the result is similar, i.e.,

$$S = \left( \frac{P_e}{V_0 - V_e} \right)^{1/2} V_1 \frac{\beta'^2}{1 + \frac{\beta'}{\alpha'} - \frac{\alpha'}{\beta'}}$$

Other things being equal, stopping power increases with final specific volume, slope of the elastic segment of the stress-strain curve, distention  $(V_0 - V_1)/V_1$ , and elastic pressure.

In most foams increasing distentions generally implies falling  $P_e$  and modulus, so there may be an optimum distention which must be found from empirically determined relations between elastic properties and distention. As an illustration of this procedure but not as a demonstration of actual optimization in polyurethane, we will write empirical relations between yield stress and initial density and between modulus and density based on the static measurements of Lindberg, Gates, and Baer<sup>22</sup> in lightweight polyurethane:

$$\frac{P_e}{\frac{V_0 - V_e}{V_0}} = \frac{K_1}{V_0} + A$$

$$P_e = \frac{K_2}{V_0} + B$$

where

$$K_1 = 14.15 \times 10^9 \text{ cm}^2/\text{sec}^2 \quad A = -1.65 \times 10^9 \text{ dyne/cm}^2$$

$$K_2 = 4.74 \times 10^8 \text{ cm}^2/\text{sec}^2 \quad B = -0.674 \times 10^8 \text{ dyne/cm}^2$$

Equation (3) becomes:

$$S = \frac{(K_2 + BV_0)^{1/2} \left( \frac{V_0 - V_1}{V_0} \right)^{3/2}}{\frac{V_0 - V_1}{V_0} + \left( \frac{K_2 + BV_0}{K_1 + AV_0} \right)^{1/2} \left( \frac{V_0 - V_1}{V_0} \right)^{1/2} \left( \frac{K_2 + BV_0}{K_1 + AV_0} \right)}$$

We seek maxima in this function of  $V_0$  so that  $P_e = K_2/V_0 + B \leq P_{e,n}$ , or  $V_0 \geq K_2/(P_{e,n} - B)$ . We are, of course, limited to:  $V_0 \geq V_1$ .

$P_{e,n}$  is the most  $P_e$  can be, if the second pressure jump due to the collision at  $t^*$  is to bring the peak stress in the structure just up to some previously specified limit. If  $V_1 = 1.0 \text{ cm}^3/\text{g}$  and  $P_{e,n} = 1.0 \text{ kbar}$ , the second inequality controls, and in the range  $1 < V_0 < 7$  the function  $S$  has a broad maximum between  $V_0 = 2$  and  $V_0 = 4$ . Row I in the tabulation shows the behavior.

	$V_0 (\text{cm}^3/\text{g})$	1.0	1.33	1.5	2.0	3.0	4.0	5.0	6.0	7.04
I	$10^{-4}S (\text{cm}/\text{sec})$	0		0.922	1.105	1.16	1.08	0.922	0.680	0
II	$10^{-4}S (\text{cm}/\text{sec})$		$\infty$	1.31	1.57	1.79	1.90	1.96	1.99	2.02
III	$10^{-4}S (\text{cm}/\text{sec})$			1.79	1.77	1.48	Imaginary			

Setting  $A = B = 0$  may make the relations between distention and the forerunner parameters more nearly correct and has the effect on  $S$  seen in Row II. (The theory and constitutive relations break down as  $V_0 \rightarrow 1.0$ .) Row III, which also shows little influence of distention on  $S$ , is calculated from a different set of linear relations between modulus and yield stress on the one hand and  $V_0$  on the other. Here quasi-dynamic data for 0.67 and 0.335 g/cc polyurethane is used, specifically  $P_e = 1.0$  and 0.15 kbar, respectively, and  $U_e = 1.6$  and 1.3 mm/ $\mu\text{sec}$ , respectively. These values of  $P_e$  and the values of  $U_e$  for 0.67 g/cc material are reported by Rempel<sup>2</sup> from shock measurements. The value of  $U_e$  for the lighter polyurethane is related to quasi-static compression information also reported by Rempel. Thus  $A = -5.7 \times 10^9$ ,  $B = -0.7 \times 10^9 \text{ dyne cm}^{-2}$ ,  $K_1 = 33.7 \times 10^9$ , and  $K_2 = 2.54 \times 10^9 \text{ cm}^2 \text{ sec}^{-2}$  for Row III.

It is possible foam effectiveness is not highly sensitive to distention. Figure 4 seems to confirm that distention over the range used in our experiments has relatively small bearing on pressure attenuation effectiveness of aluminum foam. The single point in Fig. 5 from 0.335 g/cc polyurethane (Shot 9228) does not appear to be in good agreement with this conclusion.

## 5. CONCLUSIONS AND FUTURE DIRECTIONS

Good methods\* exist to estimate shock response of certain elastic-rigid foams at very high pressures when no forerunner is present, and at very low pressures when no locking wave is present. For the intermediate region of pressure (approximately 0.1 to 6 kbar), when both waves are present and of the same order of magnitude, predictions are less reliable and, in our experience, values forecast of pressure in this region based on general theories are too high. From considerations of pressure wave shape we believe this anomaly may be related to the porous nature of the foam. We have, however, experimentally measured peak pressures transmitted to a steel wall to about 6 kbar, found conditions for double-wave structure, and observed wave shapes produced by impacts carrying momentum densities in the range  $0.6$  to  $3 \times 10^4$  taps in 0.7 to 1.4 g/cc aluminum, 0.67 g/cc polyurethane, 1.1 g/cc beryllium, 1.1 to 1.7 g/cc graphite, and 1.0 g/cc silica foam.

Predictions of pressure histories in the general theories are based on statically measured densities and dynamically measured forerunner speeds and strengths. In the materials studies, forerunner speeds can be related to statically measured moduli within  $\pm 15$  percent; forerunner strengths are two to four times static yields and have not been related to static yields by theory.

In the sense of transmitting the least peak pressure for the least added weight under impact of a given amount of momentum, polyurethane appears to be the best of the foams studied (polyurethane, graphite, silica, beryllium, and aluminum). However, the momentum gain due to the bounce-off of a polyurethane layer from a steel wall is higher than that of other foams, particularly aluminum, where the difference in total momentum passed to the structure by the two foams may be as large as 50 percent. Moreover, polyurethane is subject to a considerable loss of

---

\* Based on the experimentally established Hugoniot of Fowles and Curran.<sup>1</sup>

effectiveness as a pressure attenuator at 100°C, whereas aluminum performance does not deteriorate to the same extent until 300°C is reached. Static data in heated silica point to a possible improvement in high temperature performance.

Improvements in the prediction system will most probably come from the following studies: (1) establishment of the pressure-volume equation of state of foams in the neighborhood of the elastic limit by observing forerunner impacts on a series of anvils of rigidity less than that of steel, (2) removal of the doubt introduced in all static-dynamic correlations by variations in physical properties of foam specimens, (3) cataloging of pressure histories in one material over a wide range of input momenta and foam thickness through the use of 1-D experiments, and finally (4) an attempt to interpret these histories as revealing the interaction of a wall-reflected wave known from (1) above with the main wave and as revealing the nature of shock flow in porous material (as contrasted to a material of uniform density). Although it is not likely that standard methods of analysis, such as the method of artificial viscosity, will be useful in revealing the nature of locking shock motion at low pressures in porous materials, exploration by the method of artificial viscosity of the effects on forecasted main wave shapes of more drastic departures from the simple equation of state than have been studied so far could be informative.

Foam forerunners could provide fruitful fields for investigation of strain-rate effects and the phenomenon of stress relaxation discussed by Duvall.<sup>9</sup>

## REFERENCES

1. Fowles, G. R. and D. R. Curran, AFSWC-TDR-62-22, 1962.
2. Rempel, J. R., AFWL-RTD-TDR-63-3056, 1963.
3. Fowles, G. R., *J. Appl. Phys.* **32**, 1475-1487 (1963).
4. Abrahamson, G. R., extension of work published in Poulter Laboratories Internal Report 009-62, Stanford Research Institute, 1962.
5. Pressman, Z., Poulter Laboratories Technical Report 009-60, Stanford Research Institute, 1960.
6. For a discussion of double shock structure due to rigidity see Rice, M. H., R. G. McQueen, and J. M. Walsh, *Solids State Physics*, F. Seitz and D. Turnbull, eds., Academic Press, Inc., N.Y., 1958, Vol 6, 1-63.
7. See, for example, Figs. 26 and 27 in Ref. 2. Emerging from 5 mm of polyurethane the forerunner shows a rise time of 0.1  $\mu$ sec or less, but after 10 mm of travel it has seemingly broadened to about 0.5  $\mu$ sec.
8. This phenomenon can be seen in Fig. 36 or Ref. 2, as well as in Shots 9891, 9893, and 9931, Fig. 3.
9. Duvall, G. E., "Propagation of Plane Shock Waves in a Stress-Relaxing Medium," *International Symposium on Stress Waves in Anelastic Solids*, Brown University, April 1963.
10. See Shots 9833 and 9894, Fig. 3.
11. Pages 35 to 37 of Ref. 2.
12. Richtmyer, R. D., *Difference Methods for Initial Value Problems*, Interscience Publishers, Inc., N.Y., 1957, Chap. X, especially Sections 9-12; and von Neumann, J. and R. D. Richtmyer, *J. Appl. Phys.* **21**, 232 (1950).
13. Herman, W., E. A. Witmer, J. H. Percy, and A. H. Jones, *Stress Wave Propagation and Spallation in Uniaxial Strain*, ASD-TDR-62-399, 1962.
14. The assumptions of the derivations and the notation are those of Ref. 1, pp.31-44. Momentum is imagined as appearing instantaneously at the free surface of the foam at zero time.
15. See Table X in Ref. 2.
16. Contrast Shot 10,360 with Shots 9894 and 9892, Table 1, and see the results of quasi-static compression in Table 4.
17. Contrast Shots 10,331 and 10,332 with Shots 10,250 and 10,261, Table 1.
18. Shot 9894 in closed-cell aluminum clearly behaved this way. Shots 9832 and 9833 in polyurethane showed a lesser effect but the very Shot 8863 described in Ref. 2 showed relaxation only in the early part of the record.
19. Sterne, T. E., Ballistic Research Laboratories Report No. 648, Aberdeen Proving Ground, Md., 1947.
20. Abrahamson, (Ref. 4) relates the measured superficial impulse density per unit thickness of explosive to material density of thick plates.
21. Shots 9155, 9217 and 9216, described in Ref. 2.
22. Lindberg, H. E., R. W. Gates, and M. J. Boer, *Simulation and Structural Effects of Sharp Pulses*, Stanford Research Institute, Project GND-4356, Final Report, 1964.

**PHASE 2: SOLIDS**

*By*

**J. O. ERKMAN**

*and*

**WM. ISBELL**

## 1. INTRODUCTION

The effects produced in solids by events such as the impact of projectiles and the detonation of high explosives and nuclear devices can be studied directly by performing experiments. In such studies the object may be to observe the physical response of materials at high pressure. Experiments for collecting data on the equation of state of a material are an important example of such work and are usually on a small scale. Other studies are of less fundamental nature and are done to improve or to test the design of a structure or a device. For example, a missile may be damaged or destroyed if a nuclear device is detonated in its vicinity. In such a case, the experimental approach is at least expensive and time consuming, if not virtually forbidden. Because of these reasons, much of the study of the vulnerability of missiles, underground structures, and other installations must be performed by the application of theory to predict shock attenuation. The work reported here is a continuation of an effort to verify the validity of the application of hydrodynamic theory in such studies<sup>1,2</sup> and, where discrepancies are observed, to formulate improved models that will provide more accurate predictions. The term hydrodynamic theory is taken to mean a theory in which material rigidity is neglected and the velocities of waves in the media are hydrodynamic.

At very high pressures, material rigidity is expected to be unimportant so that the principal stresses are approximately equal, and the hydrodynamic theory is a good approximation. For phenomena associated with the shock front itself, hydrodynamic theory seems to be valid at much lower pressures; e.g., in determining the Hugoniot equation of state. As a shock front propagates from its source, it is attenuated. In this report, it is assumed that attenuation is a wave phenomenon in which rarefaction waves overtake and interact with the shock front. If this attenuation is to be calculated, the speed of these relief waves must be known. It cannot be assumed that their speed is always independent of rigidity, even if rigidity can be ignored for the shock transition. An objective of the work reported here is to determine if rigidity is important in the flow behind shocks in some representative solids.



The effects of rigidity on the speed of relief waves can be studied by measuring directly the velocity of the waves. What amounts to the same thing is the study of the attenuation of shock waves. An attempt is made in this work to study both the velocity of the waves and the attenuation caused by them. In previous work, attenuation of shocks was studied in aluminum, copper, rock salt, and other rocks.<sup>1,2</sup> In this work, more observations have been made for both aluminum and copper. A plastic (Armstrong C-7 epoxy) and gold have also been studied. Targets made of these materials are struck by aluminum plates moving with a velocity of about  $0.125 \text{ cm}/\mu\text{sec}$ . This arrangement, which induces an essentially plane wave in the target, is one of the simplest for which flow calculations can be readily performed. Comparison of the results of calculations and experiments determine the extent of agreement with the hydrodynamic theory in each of the several different situations.

## 2. SUMMARY

Attenuation of shock waves was studied in 1060 and 2024 aluminum, OFHC copper, gold, and Armstrong C-7 epoxy. Shock waves were induced in samples of these materials by striking them with aluminum plates traveling about  $0.125 \text{ cm}/\mu\text{sec}$ . Because the strains induced in the specimens were virtually one-dimensional, the experiments could be simulated with a computer code. Comparison of experimental and calculated results indicated that an elastoplastic relation between stress and strain should be used for aluminum, copper, and epoxy. More data are needed before a stress-strain relation can be suggested for gold.

The amplitude of the elastic relief wave in 2024 aluminum was approximately 20 kbar when the maximum stress was 120 kbar. On the assumption that Poisson's ratio is constant, a yield strength value of 5 kbar was inferred (see Sections 4 and 6). This is the yield strength in simple tension, or twice the critical resolved shear stress. For 1060 aluminum, the amplitude of the elastic relief wave was 16 kbar, so that the yield was 4 kbar when the maximum stress was 120 kbar. The relief wave in copper had an amplitude of 27 kbar, so that the yield was approximately 7 kbar for a stress of 160 kbar. These values of the yield strengths are all greater than those observed at engineering stress levels and imply that the yield strength is a function of the stress.

It was impossible to obtain a value of the yield strength directly from the experimental data for either gold or the epoxy. For the epoxy, the calculated attenuation matched the experimental observations fairly well when the yield was assumed to be 1.0 kbar.

Two methods were used for recording the response of materials to shock waves. One employed the smear camera to observe the free-surface motion of specimens shaped like wedges.<sup>3</sup> This technique has been used for a number of years and gives reliable results. As ordinarily used, the technique records only the velocity of the free surface at the instant the shock interacts with the surface. Its use raises the question as to the relation of the free-surface velocity to the particle velocity induced by the shock front.

In an attempt to circumvent some of the disadvantages of the optical technique, a second method of recording response by means of a transducer was used in several experiments. The device consisted of a Manganin wire potted in Armstrong C-7 epoxy.<sup>4</sup> It was calibrated to measure the pressure induced in the epoxy by the transmission of a shock from a specimen into the epoxy. Although the transducer is still in the developmental stage, it was hoped that it would permit the recording not only of peak pressure but also of pressure as a function of time behind the shock front. Measurement of the peak pressure was as good as can be expected, although some transducers gave obviously erroneous results for reasons that are not understood. The transducers do not give the expected response after the passage of the shock front, perhaps because of a hysteresis effect which is being investigated.<sup>5</sup> Presently, the transducers appear incapable of giving the amplitude and arrival time of the elastic relief waves which are implied to exist in the observations obtained with the smear camera.

Detailed behavior of an explosive system such as is used to throw aluminum plates is not understood. Some studies of the system are reported here, but they are far from being exhaustive studies even on the one system which throws aluminum plates at a velocity of 0.125 cm/ $\mu$ sec. Enough data are given to show that the flyer plates are probably not spalling and that their shapes are tolerable. During preliminary studies, reproducibility of the velocities of flyer plates did not appear to be a problem. It became a problem later in the attenuation experiments in which Baratol\* pads were obtained on a new order. Much more work should be done on methods of using explosives for throwing flat, strain-free, unspalled aluminum plates not only at 0.125 cm/ $\mu$ sec, but at greater velocities; methods of throwing and using plates made of other materials should also be investigated.

---

\* Baratol is 67 percent barium nitrate and 33 percent TNT.

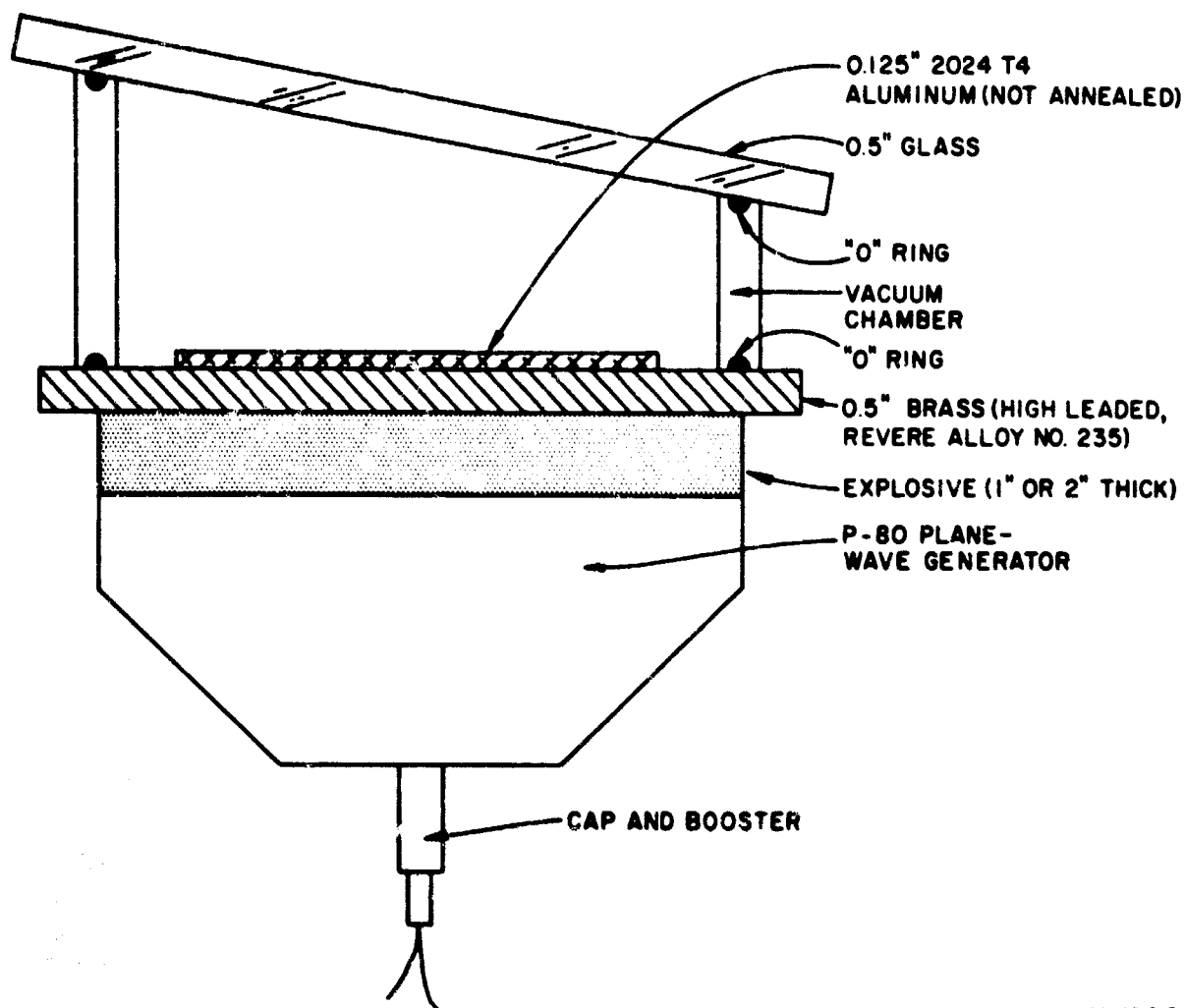
### 3. EXPERIMENTAL ARRANGEMENT FOR STUDYING ATTENUATION OF SHOCKS IN SOLIDS

#### A. FLYER PLATE ASSEMBLIES

All the attenuation experiments were performed by throwing aluminum plates with charges of high explosives. The arrangement used in the experiments is represented in Fig. 1, which shows a plane-wave generator (PWG) and an explosive pad in contact with a brass plate. For most of the work the explosive pad was Baratol. A thermosetting plastic cement about 0.001 inch thick affixed the aluminum plate to the brass plate. The brass plate was used partly because it held back the smoke from the explosive and permitted a clear view of the experiment, and because it also served as a base for the vacuum chamber. The curvature induced in the plate when the chamber was evacuated was negligible. The functions mentioned above could also be achieved by using plates of materials other than brass—for example, aluminum. However, there had to be some separation between the aluminum flyer plate and the brass buffer plate so that, during the time of observation, the target responded only to the impact of the aluminum flyer plate. The impedance mismatch between aluminum and brass is such that the aluminum separates from a brass buffer plate and travels with a considerably higher velocity than the brass.

The 1/8-inch-thick aluminum flyer plates attained a velocity of 0.125 cm/ $\mu$ sec when the explosive pad was Baratol. Greater velocities can be attained by the use of more energetic explosives, such as Composition B-3 or HMX. Use of these explosives may introduce other problems, however. One of the desirable features of explosively driven plates is that the plate have a large useful diameter. When an 8-inch-diameter plane-wave generator is employed, the useful diameter of the flyer plate may be as large as 4 inches.

If the strain induced in a target by the impact of a high-speed plate is to be one-dimensional, the plate should be flat and oriented parallel to the surface of the target at the time of impact. This is difficult to achieve, especially when the flyer plate is as much as 4 inches in diameter. Several shots were fired to determine an acceptable method of driving plates.



GA-4613-7

FIG. 1 FLYER PLATE ASSEMBLY

for the attenuation studies. In these shots, a flat glass mirror was held about 1/2 inch from and parallel to the initial position of the aluminum flyer plate. The shot was suitably illuminated and the record of the collision was taken by the smear camera.

Results of six of these shots, where the deformation is given as a function of the diameter of the plate, are given in Fig. 2. The scale for the deformation is enlarged with respect to the ordinate. Each plate should be visualized as moving from right to left so that the center of the plate is the last part to reach a target. In Shots 9886, 9887, and 9902, the original diameter of the aluminum plates is  $4\frac{1}{2}$  inches. Shot 9902 shows a fairly good plate, the center of which lags the most forward part by 0.015 inch. Because the velocity of the plate was 0.125 cm/ $\mu$ sec, the plate first struck the edges of the target and then,

approximately 0.3  $\mu$ sec later, struck the center. The useful diameter of the plate was under 4 inches. Results of Shots 9886 and 9887 are worse in that the delay of the center was greater and the useful diameter was less.

In order to obtain plates with larger useful diameters, 6-inch-diameter plates were used in the following three experiments. The lag of the centers in these shots was determined by drawing a chord 4 inches long across the profile. This chord represented the maximum dimension of the target for most experiments. In Shot 9938, the center lag was about 0.011 inch or 0.2  $\mu$ sec; in Shot 10,017, 0.013 inch or 0.3  $\mu$ sec; and in Shot 10,018, 0.015 inch or 0.3  $\mu$ sec. Each of these shots gave delay

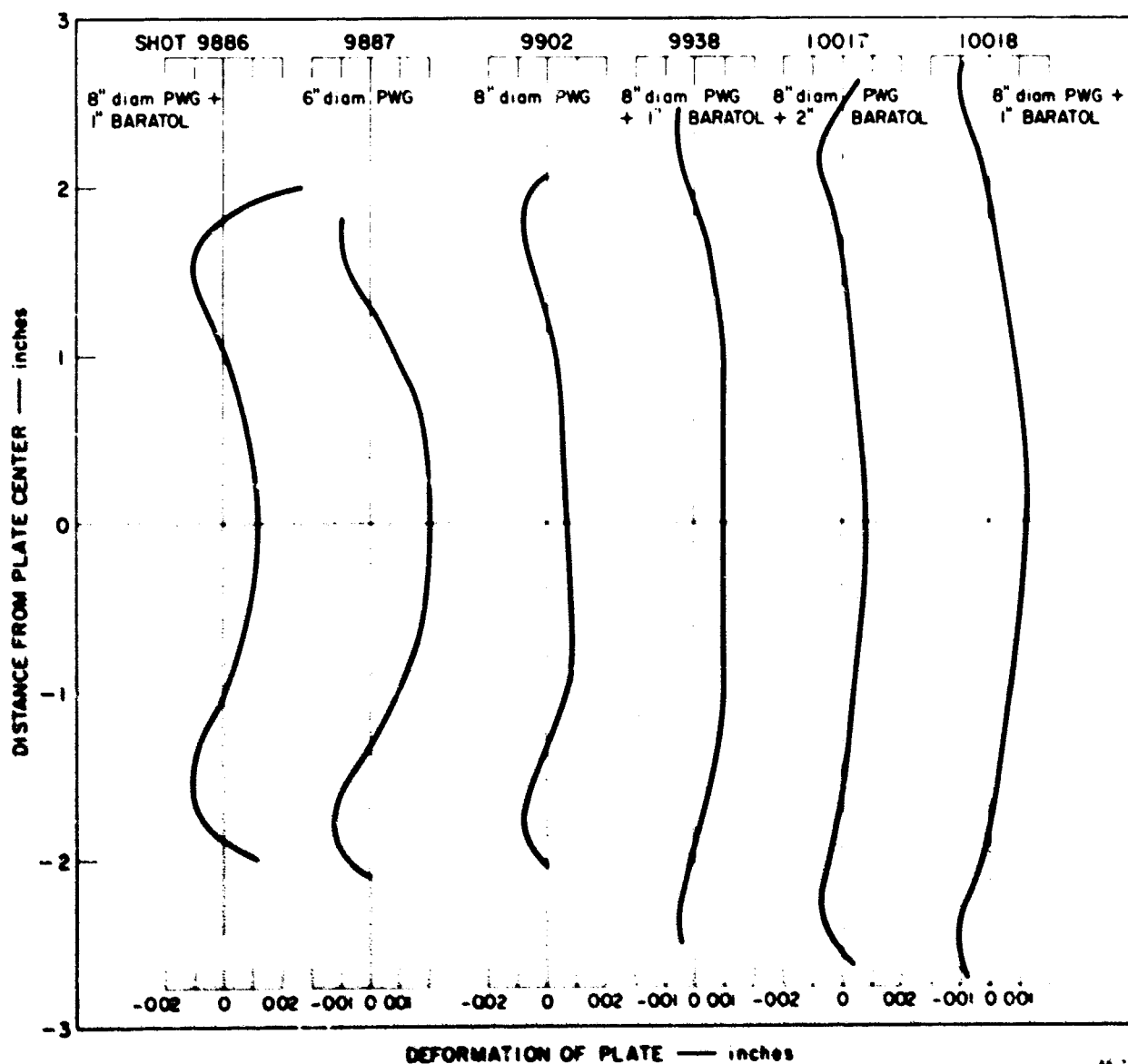


FIG. 2 RESULTS OF FLYER PLATE PLANARITY TESTS

times for the center less than or as good as the times for Shot 9902, the best of the shots using 4½-inch-diameter plates. As expected, the useful diameter of the plates was improved also. No great advantage was given in Shot 10,017 by using 2-inch-thick Baratol. The combination of an 8-inch-diameter PWG and a 1-inch-thick pad of Baratol was used as a reasonable compromise in the attenuation experiments which followed. Reproducibility of such a system is inferred by comparing the duplicate Shots 9938 and 10,018, the lag times of which were 0.2 and 0.3  $\mu$ sec, respectively.

Previous studies showed that aluminum plates projected by a driving assembly containing a pad of Composition B-3 did spall.<sup>2</sup> Those studies involved the recovery of flyer plates as well as the use of the flash X-ray camera. A description of the mechanism which produces the spall is given in Appendix I. The event has been simulated by the use of a computer code, and the results based on a fracture strength of 30 kbar indicate that the aluminum plate should spall.

At the beginning of this project it was not known if the use of Baratol between the PWG and the brass plate, Fig. 1, would cause the aluminum flyer plate to spall. Previous experience showed that the problems associated with the recovery of the flyer plates after they had been accelerated to a high velocity by an explosive charge were many, and that misleading results could be obtained. Three methods were used for determining if the flyer plate had spalled.

The first method used the high-speed framing camera. The flyer plate was thrown across the field of view of the camera, and the event was back-lighted. Although great attention was given to the control of the detonation produce gases, no useful records were obtained because of obscuration by these gases.

Another method for determining spallation employed the flash X-ray camera. A double flash unit was used, and each unit was flashed at predetermined times after the flyer plate was put into motion. These records (see Fig. 3) show that the flyer plates remained intact when Baratol was used as the explosive (or a bare plane-wave generator which used Baratol as the low-velocity explosive). As a test, a shot was also fired using Comp B-3, and a clear indication of spalling was obtained, as shown in Fig. 4.

The third method used a pressure transducer which is being developed at Stanford Research Institute.<sup>4</sup> It was reasoned that if the plate spalled

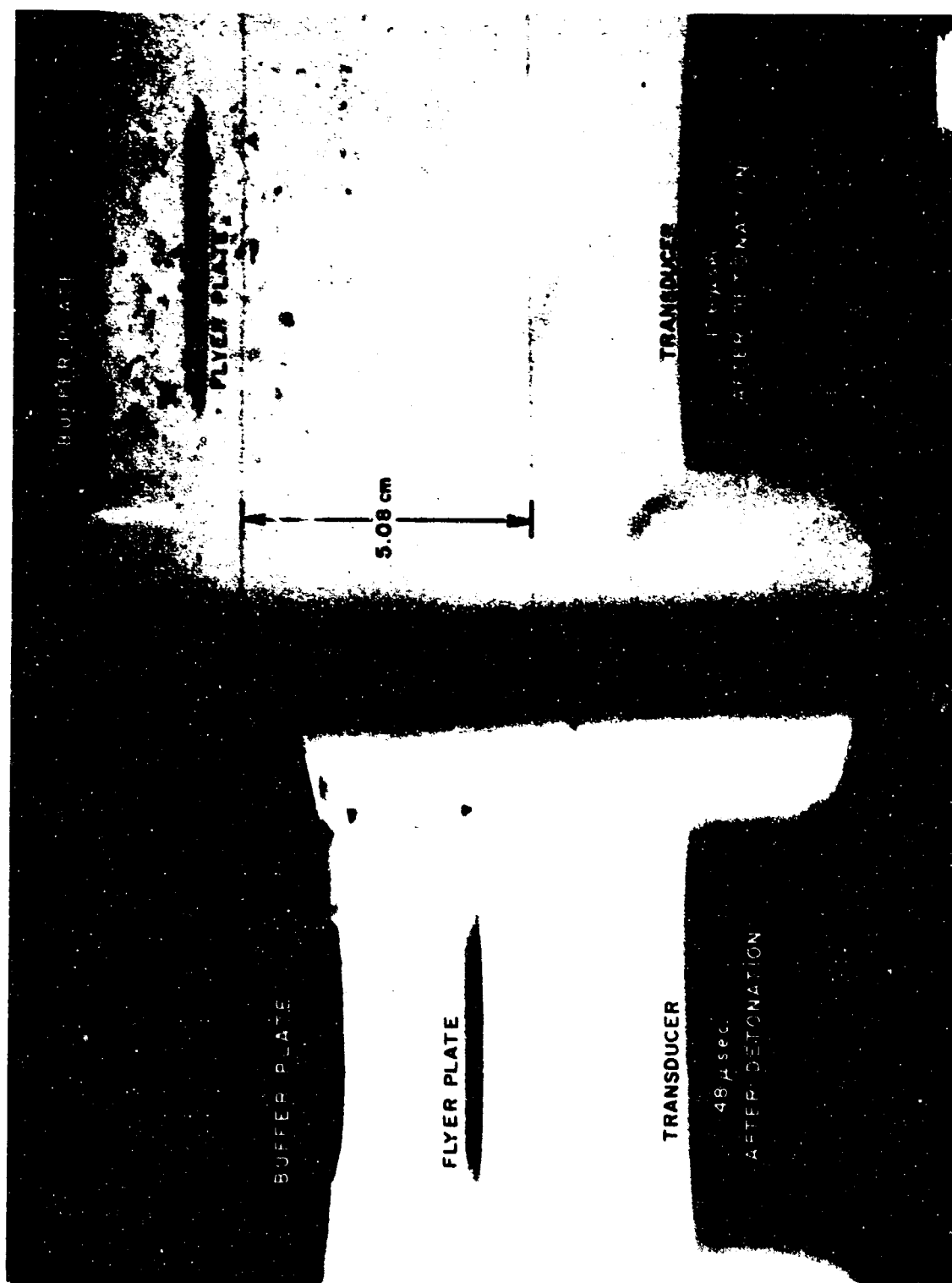


FIG. 3 X-RAY PICTURES OF FLYER PLATES IN MOTION  
(a) Shot 9813 — 6-inch diam PWG



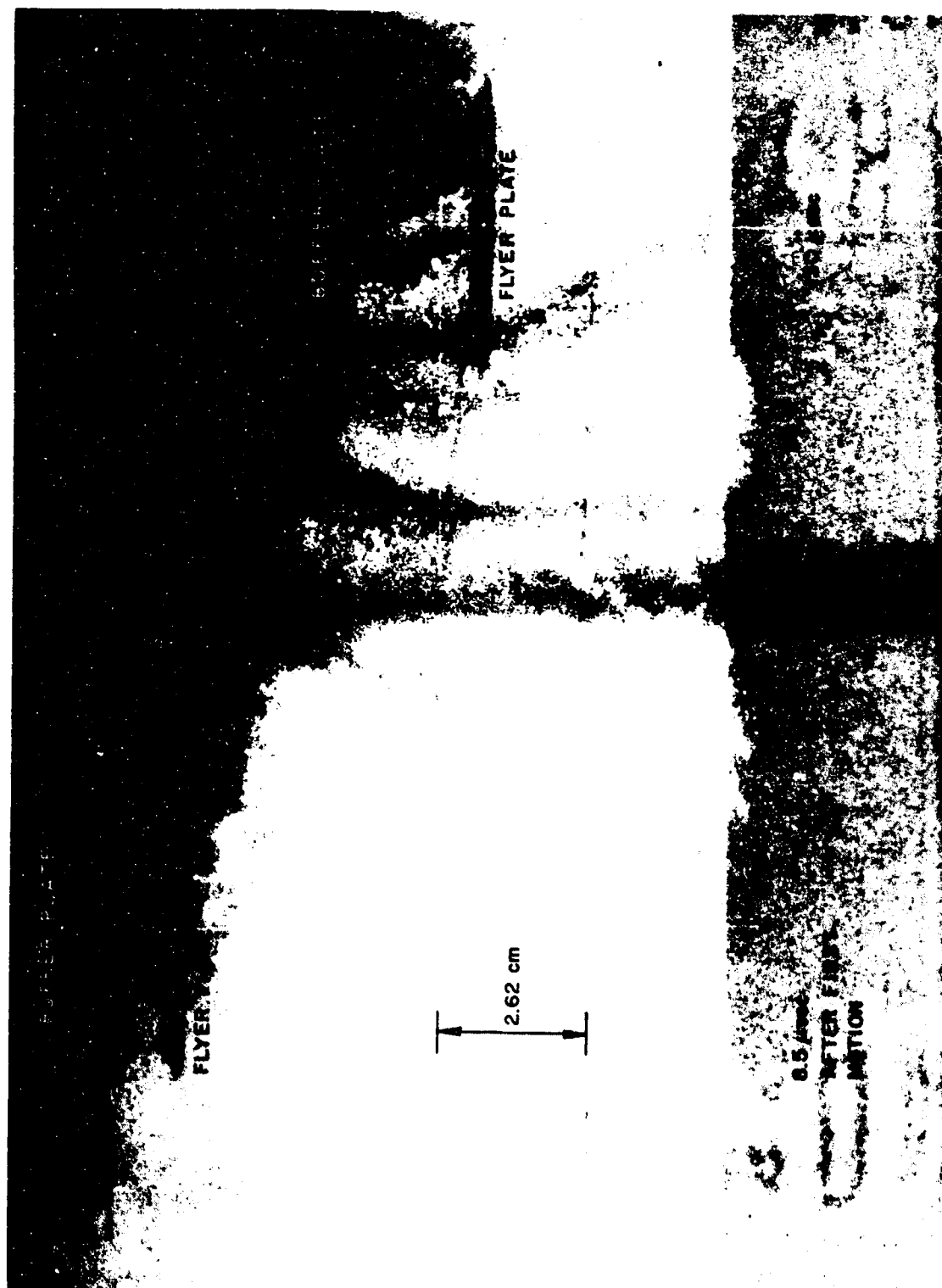


FIG. 3 X-RAY PICTURES OF FLYER PLATES IN MOTION  
(b) Shot 9767 — 6-inch diam PWG + 1-inch Baratol



FIG. 4 X-RAY PICTURE OF SPALLED FLYER PLATE (Shot 9768)

before hitting the transducer, the transducer record should show a second shock. When Baratol was used in the explosive train, the transducer record showed only one pulse. For the shot in which Comp B-3 was used, the record did show a second increase in pressure. Hence the transducer confirmed the X-ray record, because both instruments were used simultaneously, as indicated in Fig. 3(a).

The plate thrown by Baratol had a velocity of approximately  $0.125 \text{ cm}/\mu\text{sec}$ , which is adequate for many experiments. Use of Comp B-3 resulted in flyer plate velocities of  $0.19 \text{ cm}/\mu\text{sec}$ . Such flyer plates would be useful if some way can be developed to prevent the plates from spalling. A possible method is to introduce a layer of plastic between the brass plate and the aluminum flyer plate. This system was simulated by a computer code with encouraging results. The calculated results also indicate that the plastic will not seriously interfere with the experiment. The computed results should be confirmed by experimental results before the system is used.

## B. METHODS OF RECORDING FOR ATTENUATION EXPERIMENTS

The smear camera was used in previous work to record the free-surface motion of specimens in which attenuating shock waves were being studied. A simple way of recording the free-surface velocity was to mount a small, partially reflecting mirror close to the surface being watched. Both the mirror and the surface beneath it were illuminated. When the shock arrived at the surface of the specimen, the reflectance of the surface changed, and the arrival time of the shock was thereby recorded on the film in the camera. Because the surface was accelerated by the shock, it soon crossed the gap and collided with the mirror, which caused another change in the intensity of the light reaching the smear camera. Thus the flight time of the free surface of the specimen across the gap was recorded. This method of obtaining the velocity of a free surface is not satisfactory when the shock wave is nonuniform. In such a case, the free surface does not stay in uniform motion, so that some average velocity is obtained by this technique. The gap technique was employed with specimens cut in the shape of wedges so that any variation of the free-surface velocity with the distance of travel of the shock in the specimen could be observed. The results of such experiments are still regarded as being fairly reliable.

More reliable results should be obtainable, however, with the optical lever arm technique, in which targets were in the shape of wedges and the surface facing the camera was polished to a mirror finish.<sup>3</sup> This requirement restricts the technique to homogeneous materials whose surface takes a polish. The camera was not focused on the surface of the specimen but was focused on the light source reflected in the mirror surface of the specimen. The light source was covered with a mask with alternate transparent and opaque spaces (Fig. 5). As the shock wave hit the free surface of the specimen, the surface was turned, and the image of each grid line was displaced. As shown in Appendix II, the displacement of the grid line and the velocity of the shock along the inclined surface of the specimen give the particle velocity induced in the specimen by the shock front. The advantage of this method is that the velocity of the surface is recorded at the appropriate time—at the time of breakout of the shock front, and thus there is no averaging, as was mentioned above for the gap method. A disadvantage is the necessity for differentiating the curve defined by the termini of the straight lines on the record, see Fig. 6. If the flyer plate were perfectly flat and were oriented parallel to the target at the time it hits, the curve described above would have no inflection points; that is, the shock front would travel along the inclined surface of the wedge (see Fig. 5) at constant velocity, or at a continuously decreasing velocity. Curvature of the flyer plate can cause an inflection in the curve, so that the apparent velocity increases near the thick end of the wedge, even though the pressure carried by the shock is being attenuated. This inflection makes it difficult to differentiate the curve and is probably the chief source of error in the analysis of the records. Otherwise, the analysis requires knowledge of the camera writing speed, which is known to a precision of about 0.5 percent; of the camera magnification, which is determined from each record to a precision of about 1 percent; and of the displacement of each trace, which is measured to about 5 percent.

Both the gap method and the optical lever arm method give information about the free surface of the target. It is usually assumed that the free-surface velocity is twice the velocity of the particles immediately behind the shock front prior to the time of incidence of the shock on the surface. This assumption was used in the analysis of the records because it simplified the calculations. The error introduced was of the same order as the experimental error.



FIG. 5 WEDGE AND LIGHT-SOURCE COVER MOUNTED ON VACUUM CHAMBER

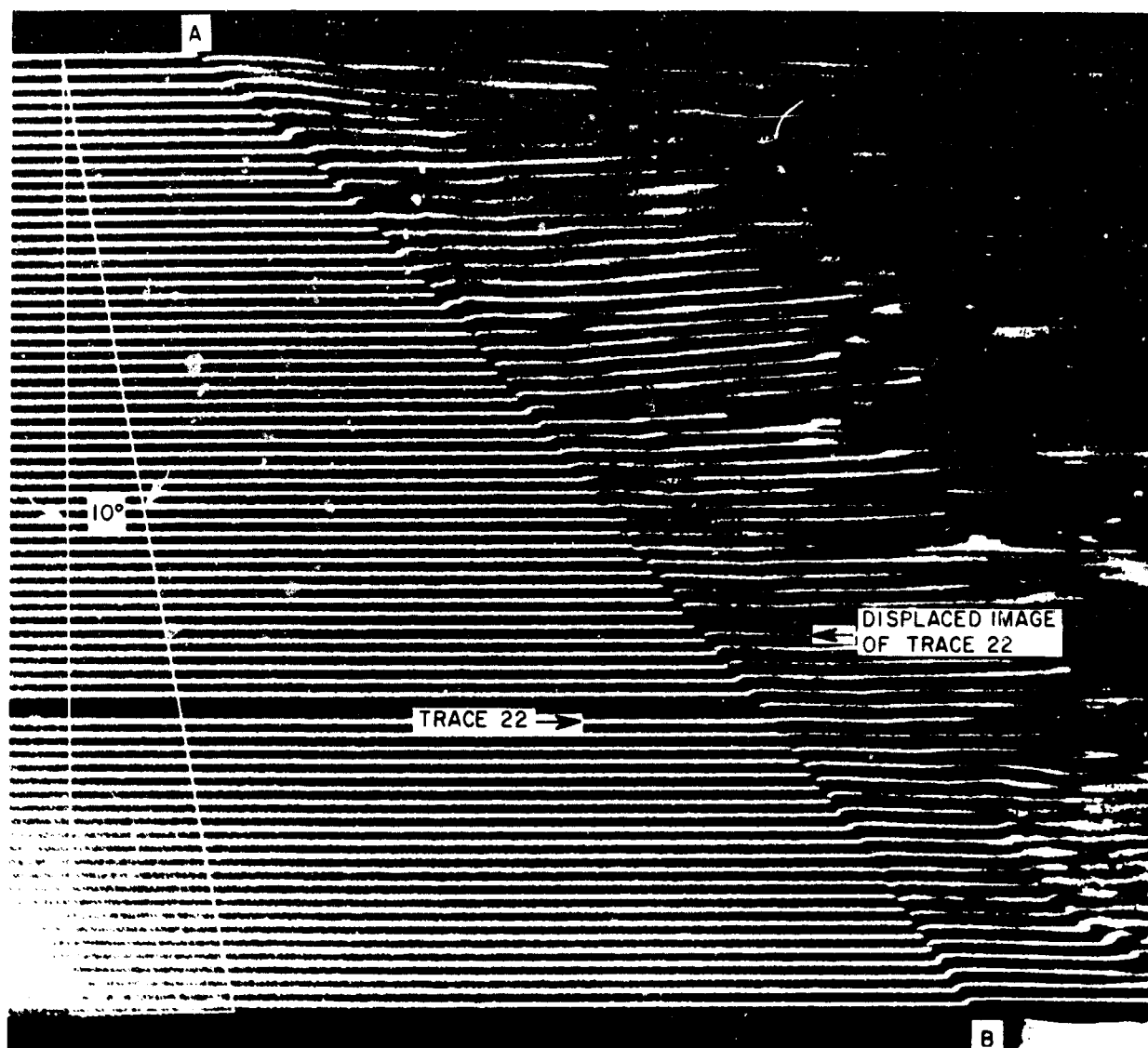


FIG. 6 SMEAR CAMERA RECORD OF AN OPTICAL LEVER SHOT

A transducer was also used in studying the attenuation of shock waves. The device, which was developed at Stanford Research Institute, consisted of a Manganin wire cast in C-7 epoxy manufactured by Armstrong Products Company.<sup>4</sup> Prior to the recording time, a constant current was passed through the Manganin wire. As the wire was compressed by the shock, its resistance changed. Signal leads were connected to the wire, Fig. 7, so that the resistance change could be monitored by an oscilloscope as a change in voltage. The device was calibrated to a pressure of about 200 kbar, and the relation between pressure and the resistance was found to be linear. The calibration experiments depended on the use of the smear camera to determine the input to the transducer and on knowledge of

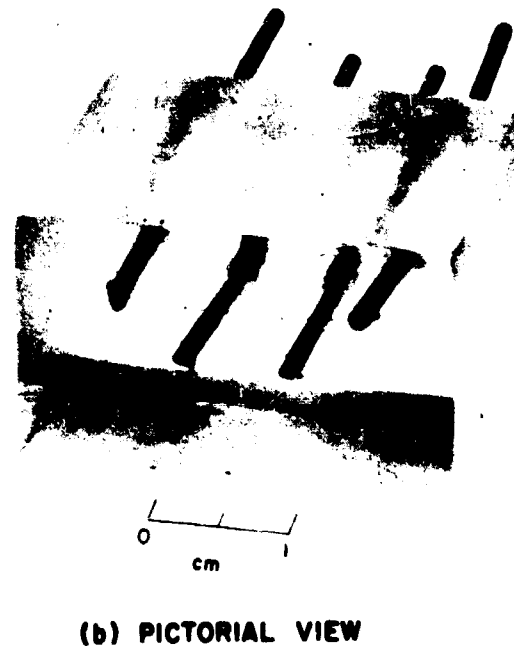
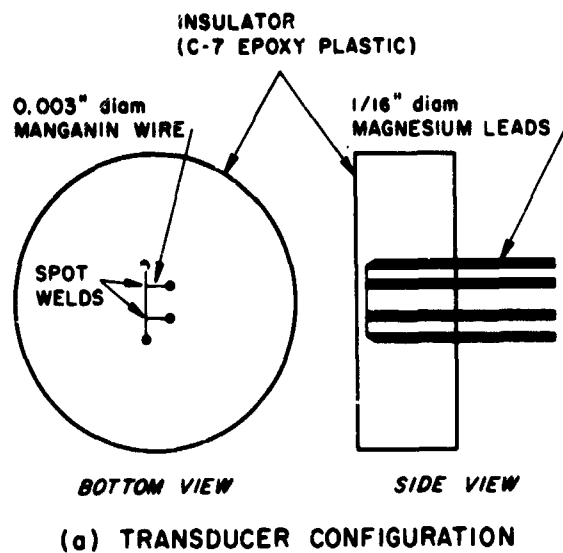


FIG. 7 CONSTRUCTION OF MANGANIN WIRE TRANSDUCER

the equation of state of the epoxy and of the material used to transmit the shock into the transducer.

The response of the transducer was adequate to record accurately the arrival of the shock wave. The transducer also appeared to respond to changes in pressure after the passage of the shock front; this is the chief attraction in the use of transducers in the study of attenuating shock waves. Accurate records showing pressure as a function of time would be helpful in determining the velocity of the initial relief wave behind a shock front. If the relief wave is elastic, transducer records should be useful in measuring the strength of the wave. These data would be helpful in formulating models for the relation between stress and strain for the solids being studied.

Application of the transducer to the study of attenuation of shock waves in solids was accomplished by placing the transducer on the surface of the specimen being studied. The Manganin wire was separated from the interface by about 0.1 cm of the epoxy. In order to expedite the work, three transducers were mounted together, as shown in Fig. 8(a). One transducer was placed at the surface of the specimen. The other two were placed in holes machined into the specimen. This was relatively easy to accomplish because the wires could be positioned, and the epoxy could

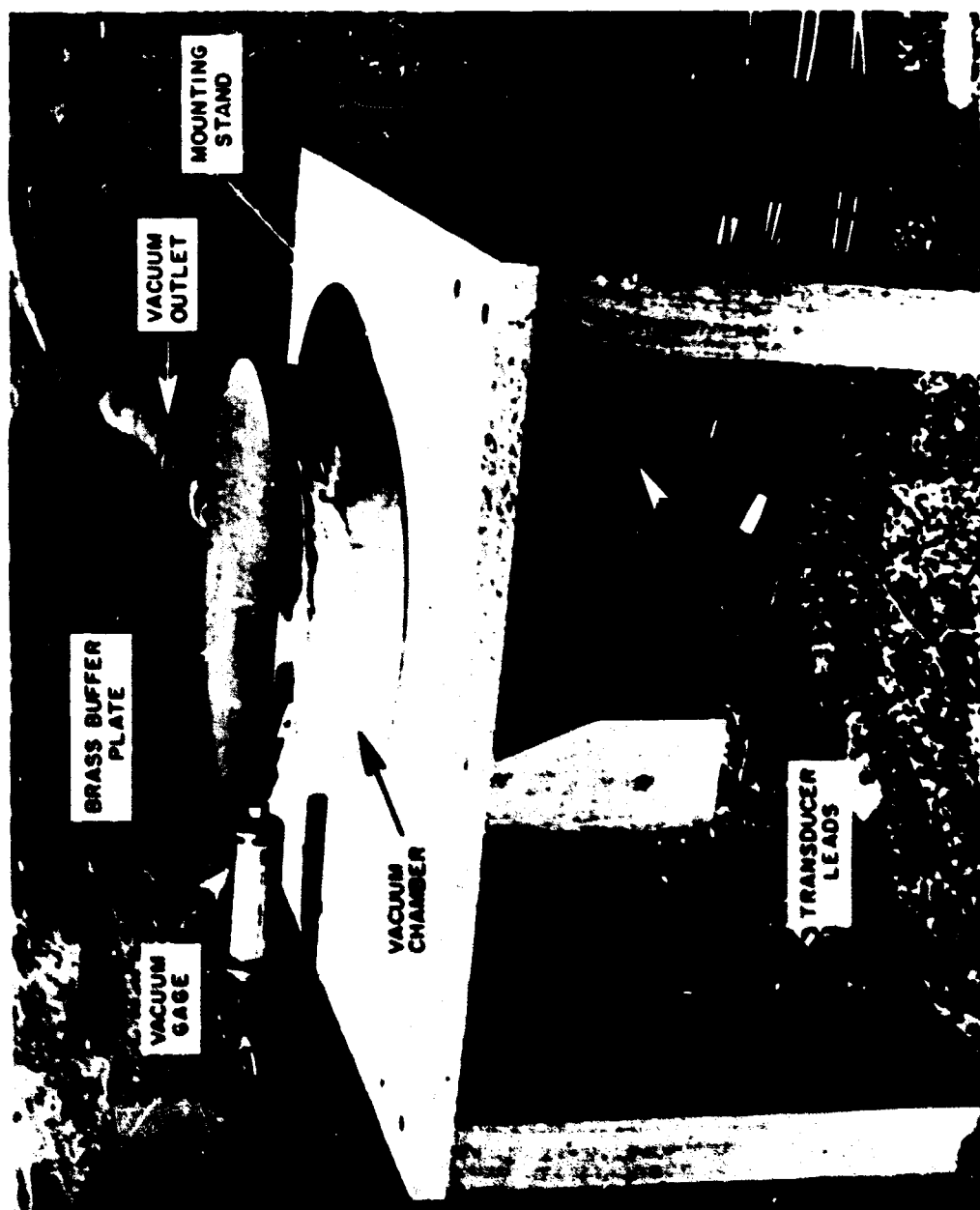


FIG. 8 ARRANGEMENT OF THREE TRANSODUCERS FOR A SINGLE SHOT  
(a) Top View



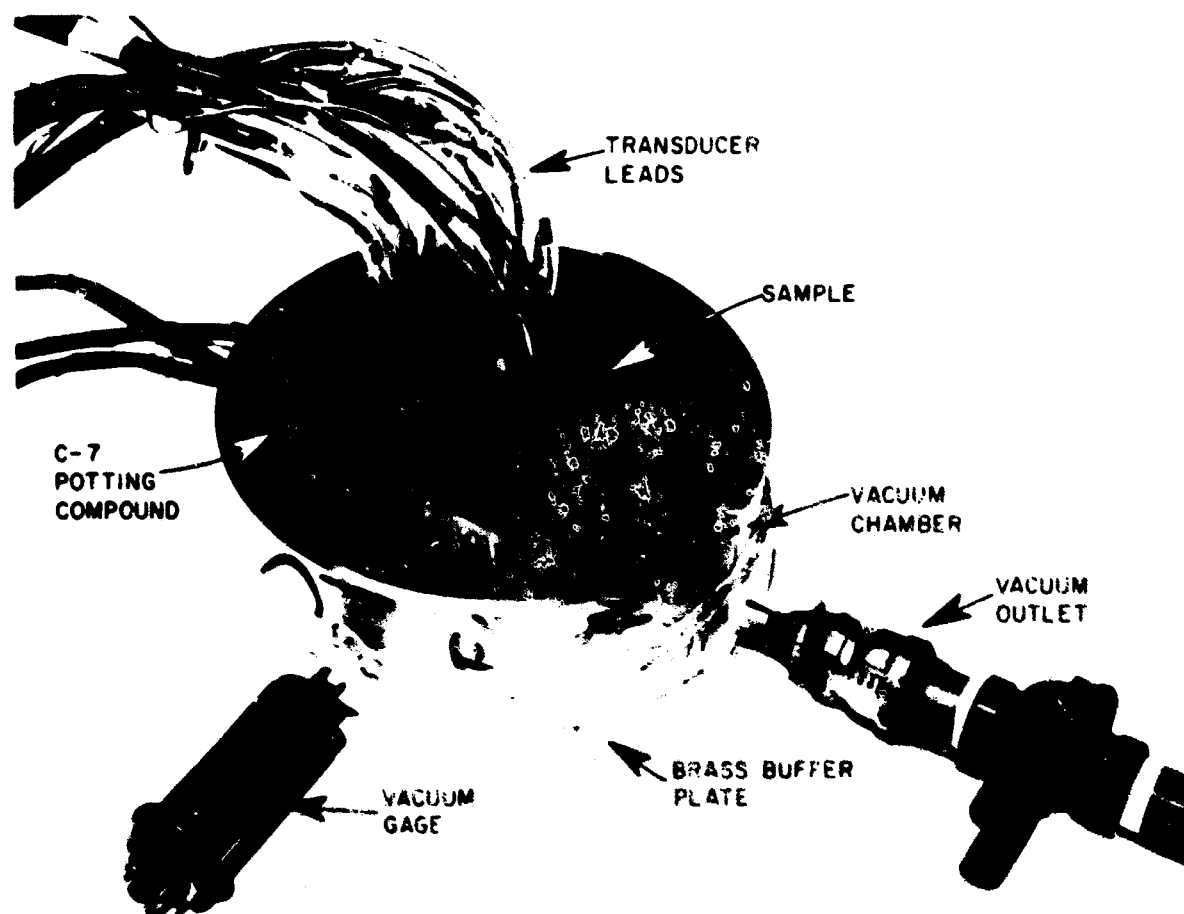


FIG. 8 ARRANGEMENT OF THREE TRANSDUCERS FOR A SINGLE SHOT  
(b) Bottom View — Assembly Ready for Mounting of Explosive

then be poured to the desired thickness. The hardened epoxy was sufficiently rigid so that it and the specimen formed the top of the vacuum chamber. Figure 8(b) shows an assembly ready for loading with explosive.

Each transducer was connected to two oscilloscopes. The primary oscilloscope was set up to record the signal induced in the transducer by the application of a source of constant current to the transducer. This current was turned on a few microseconds before the shock front reached the transducer. The primary scope also showed the signal due to the change of resistance of the Manganin wire as it was compressed. This stratagem made it unnecessary to measure either the resistance of the transducer or the current induced in it by the power supply; it was only necessary to assume that the power supply gave a constant current. Any change in the voltage output of the gage due to the application of pressure to the wire

is proportional to the change in resistance of the gage. Hence a record such as that shown in Fig. 9 was analyzed by first measuring the deflection  $A$  to  $B$ , and then a point could be read off the signal resulting from compressing the transducer, such as point  $C$ . The ratio of  $BC$  to  $AB$  gave the relative change of resistance of the transducer. A calibration curve was then used to obtain the pressure.

Because the record of the signal given by the primary scope was relatively small, a secondary scope was used to display the signal after it had been amplified. This gave a record which could be analyzed more accurately.

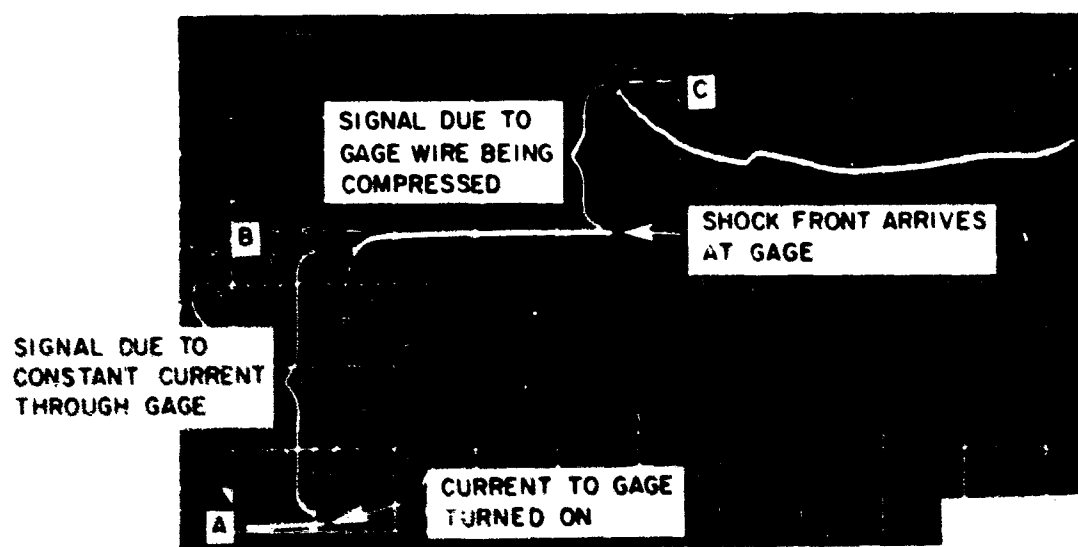


FIG. 9 TYPICAL TRANSDUCER RECORD

## 4. RESULTS OF WEDGE EXPERIMENTS

### A. C-7 EPOXY WEDGE-SHAPED SPECIMEN

The optical lever arm technique which requires the use of a specimen in the shape of a wedge is described in Section 3B. A record for such a shot is shown in Fig. 6 and the complications introduced in the analysis due to the curvature of the flyer plate are also discussed in Section 3B. This record was further complicated because of a slight bend in the wedge near the apex. The specimen, made of C-7 epoxy, was mounted in the cover of the vacuum chamber so that it had to support the force exerted by normal atmosphere. This force produced in the thin portion of the wedge some deformation which made the record somewhat unreliable near the symbol A in Fig. 6. Otherwise the data obtained from the record were readily reducible.

The curve from A to B in Fig. 6 is a record of the travel of the shock front along the inclined surface of the specimen. In order to obtain the velocity of the shock along this surface, the curve must be differentiated. This was done by reading the time and distance coordinates of the end of each undeflected trace in a Vanguard Motion Analyzer (VMA). Where lines were omitted on the grid, synthetic data were generated by averaging the results of the two adjacent lines. The data were then differenced in order to determine if any errors are detectable, and any obvious errors were corrected. Next, the data were smoothed by use of a 5-point smoothing formula, following which a 5-point differentiation formula was used to obtain the slope. Application of the appropriate reduction factors then gave the velocity of the shock along the surface of the wedge.

The displacement of the traces were also read on the VMA, and these data were also differenced and smoothed in order to minimize errors. The method for obtaining the shock-induced particle velocity is discussed in Appendix II. Peak pressure could then be determined from Hugoniot data for the material concerned.

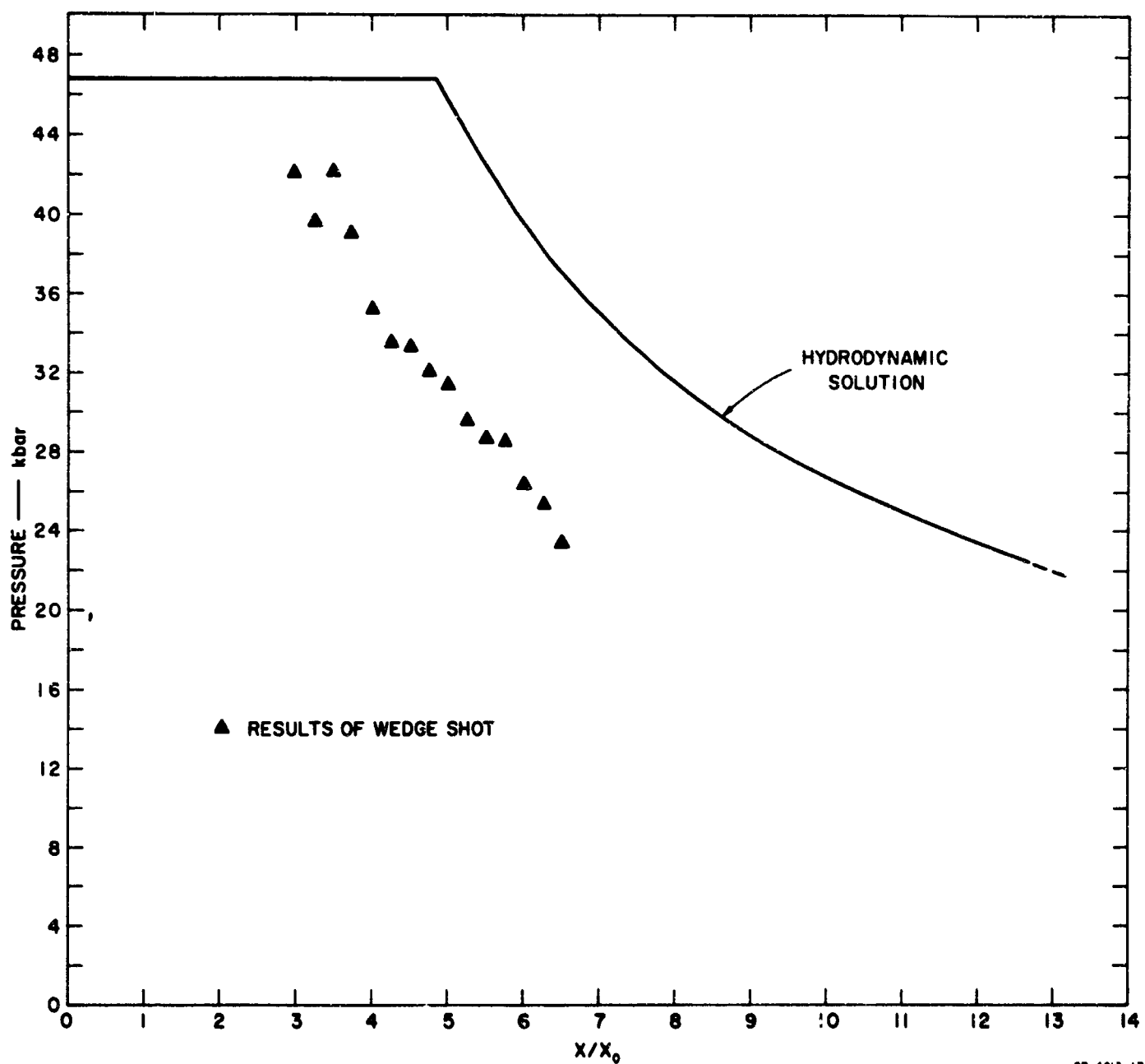


FIG. 10 PRESSURE IN C-7 EPOXY vs.  $x/x_0$  ( $x_0$  is thickness of flyer plate)

Results for the C-7 epoxy wedge are given in Fig. 10, which shows the shock-induced particle velocity as a function of the distance into the C-7. The record was unreliable near the thin end of the wedge, as noted above, so no reliable values of the particle velocity were obtained for values of  $x/x_0$  less than approximately 3.\* An impedance "mismatch" solution gave a pressure of about 46 kbar in the absence of any attenuation.

\* It was convenient to divide the distance the shock had traveled into the specimen,  $x$ , by the thickness of the flyer plate,  $x_0$ , which was 0.322 cm for most experiments reported here.

Hence attenuation of the shock commenced at a distance of about 2.5 times the thickness of the aluminum flyer plate. The hydrodynamic calculation, which will be described later, predicted that attenuation started at 4.9.

## B. ALUMINUM WEDGE-SHAPED SPECIMEN

Specimens were fabricated from both 2024-T4 and 1060 aluminum. After being machined, the 2024 specimens were heat treated in an air atmosphere at 775°F for three hours, and were then cooled at 500°F at a rate of 50°F per hour. Specimens cut from 1060 aluminum were held at a temperature of 650°F for one-half hour.

Smear camera records showing the free-surface motion of aluminum and copper are shown in Figs. 11(a) and (b). The undeflected traces did not terminate along a monotonic curve, as was observed for the C-7 wedge. That the record for copper showed less curvature than the record for aluminum was accounted for on the basis that shock velocity is less in copper than in aluminum. When a curved flyer plate hits a target, a phenomenon occurs which is analogous to refraction in optics. The shock is curved more than the flyer plate if the shock velocity is greater than the velocity of the flyer plate. Hence analyses of wedge experiments become easier for materials having low shock velocities. Conversely, greater flyer plate velocities give records which are more easily analyzed (assuming that the shock velocity does not increase as fast or faster than the flyer plate velocity).

It should be noted that all records are not as clear as those shown in Fig. 11. For some experiments the displaced traces were so smeared that individual traces could not be recognized, and measuring the trace displacement was impossible. The cause of such smearing is not clear. It has been attributed to a poor polish on the face of the specimen or to residual polishing material on the surface. Errors in focusing the camera may be responsible, or curvature of the displaced surface may depend in a critical manner on the wedge angle.

Results were obtained from the record for the metal wedges in the same way as described for the C-7 epoxy wedge above. Results for two shots using annealed 2024 aluminum target wedges are shown in Fig. 12(a). Because what appeared to be very early attenuation was observed in earlier work, Shot 10,227 was designed to give data at a few plate thicknesses into the target. This was accomplished by using a small wedge angle.

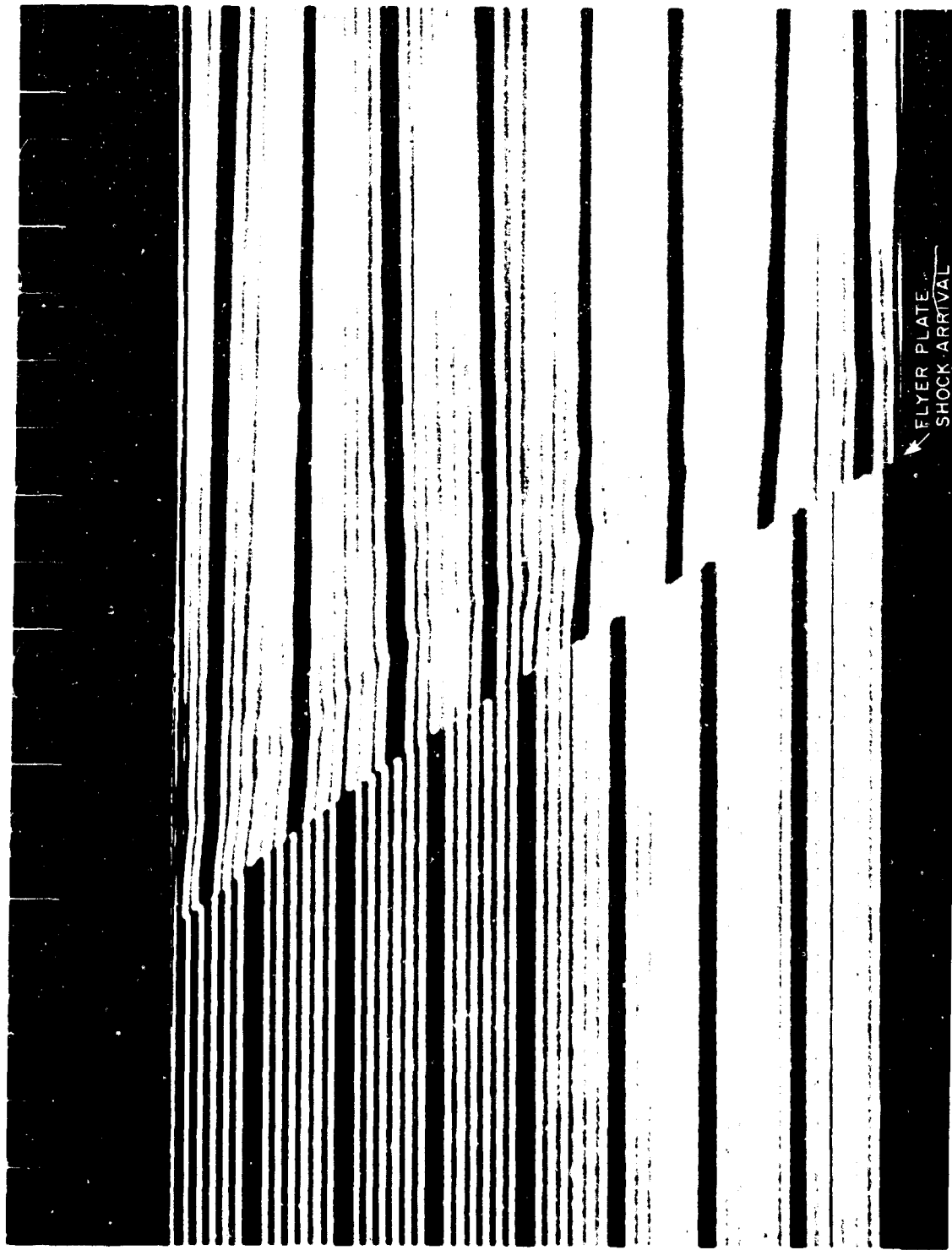


FIG. 11 RECORD OF MOTION OF FREE SURFACES OF ALUMINUM  
AND COPPER WEDGES  
(a) Aluminum (Shot 10,353)

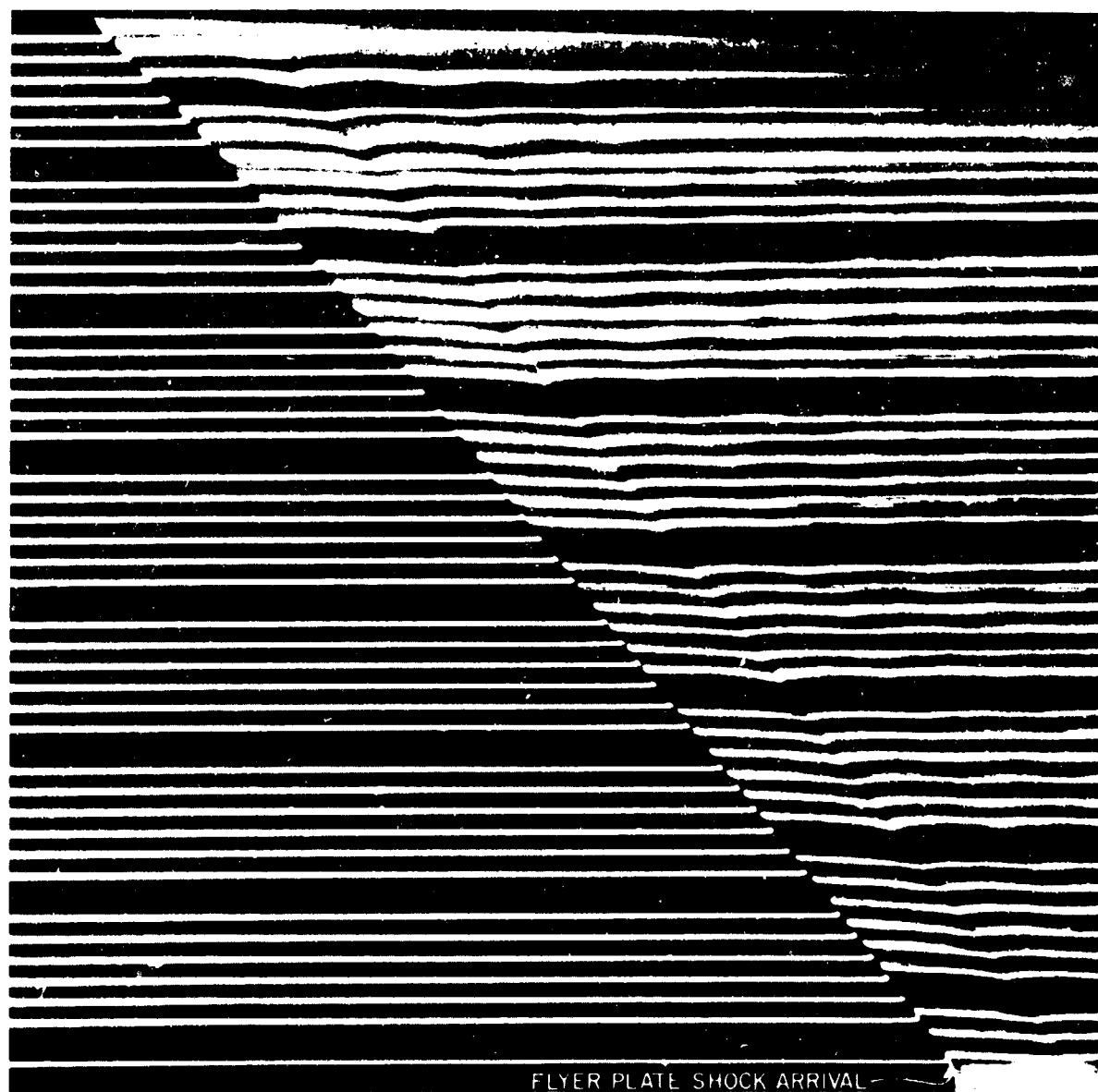


FIG. 11 RECORD OF MOTION OF FREE SURFACES OF ALUMINUM  
AND COPPER WEDGES  
(b) Copper (Shot 10,366)

This shot shows what can be called attenuation at about 5 plate thicknesses; at 3 plate thicknesses the results compare favorably with the hydrodynamic solution which will be described later (in this region it amounts to an impedance mismatch solution using only Hugoniot data).

The apparent attenuation exhibited by the data from Shot 10,227 did not appear in the earlier analysis.<sup>7</sup> There, differentiation was performed graphically, and apparently that method smoothed the data to an extent greater than the numerical method employed later.

Because no attenuation was observed in the preliminary analysis of Shot 10,227, another experiment, Shot 10,354, was designed to yield data for greater values of  $x/x_0$ . The results are given in Fig. 12(a); the particle velocity is surprisingly high at values of  $x/x_0$  near 5. All shots are designed on the assumption that the explosive systems give reproducible flyer plate velocities, which are measured in separate

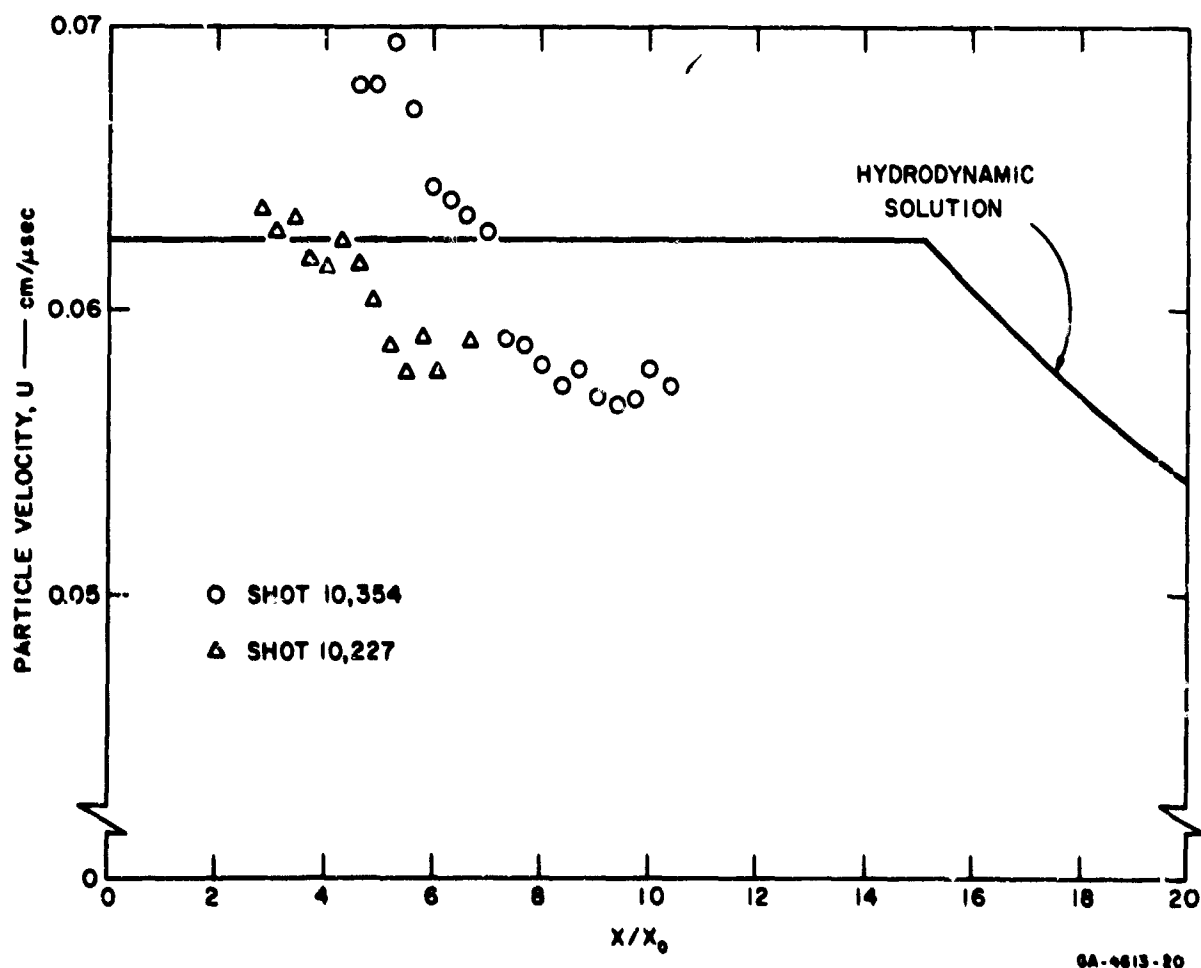


FIG. 12 PEAK PARTICLE VELOCITY IN ALUMINUM vs.  $x/x_0$   
(a) 2024 Aluminum



experiments. Plate velocities have been observed in attenuation experiments at a cost of more difficulty in design of the experiment and in less satisfactory records of the motion of the free surface of the specimen. The present results show that reproducibility is not good when Baratol is used. The average of the four points near 5 plate thicknesses gives a particle velocity of close to  $0.068 \text{ cm}/\mu\text{sec}$ . If no attenuation at this thickness is assumed, a flyer plate velocity of  $0.136 \text{ cm}/\mu\text{sec}$  is implied. In a later experiment, it was observed that an 0.040-inch-thick aluminum plate achieved a velocity of  $0.133 \text{ cm}/\mu\text{sec}$ . Hence the unexpectedly high values of particle velocities in Shot 10,354 may be due to the inadvertent use of a charge of Baratol, which was capable of giving greater velocities.

In Shot 10,354 attenuation commenced between 5 and 6 plate thicknesses, in fair agreement with Shot 10,227. Averaging the first four points for Shot 10,354 gives a particle velocity of  $0.068 \text{ cm}/\mu\text{sec}$ , which corresponds to a stress of 120 kbar on the Hugoniot for aluminum. At  $x/x_0$  approximately 8, the particle velocity is approximately 0.058, and the stress is 100 kbar. If this attenuation is entirely due to the elastic relief wave, the value of the yield strength,  $Y$ , is approximately 5 kbar, or about twice that expected for 2024 aluminum under more ordinary conditions. The relation between the yield strength and the amplitude of the elastic relief wave is given in Section 6.

Results of two shots using annealed 1060 aluminum are shown in Fig. 12(b). Attenuation in Shot 10,226 commenced at 5 or 6 plate thicknesses. The results agree well with the hydrodynamic solution for small values of  $x/x_0$  also. Results of Shot 10,353 show unexpectedly high values of the particle velocity at about 5 plate thicknesses. As before, this must indicate that the flyer plate had a velocity greater than expected— $0.125 \text{ cm}/\mu\text{sec}$ . If this is true, attenuation in 1060 aluminum commences at about 5 or 6 plate thicknesses, just as it does in 2024 aluminum. The data are not precise enough to determine to a fractional part of a flyer plate thickness the point at which attenuation commences.

In Shot 10,353, the particle velocity drops from about 0.067 to  $0.059 \text{ cm}/\mu\text{sec}$  in the vicinity of  $x/x_0$  of about 7. By using the same Hugoniot as was used above for 2024 aluminum, the stress dropped from 118 kbar to 102 kbar, so that the value of  $Y$  is about 4 kbar. In both cases, the value of  $Y$  is approximate, and it is not certain that its value for 1060 aluminum is really smaller than it is for 2024 aluminum.

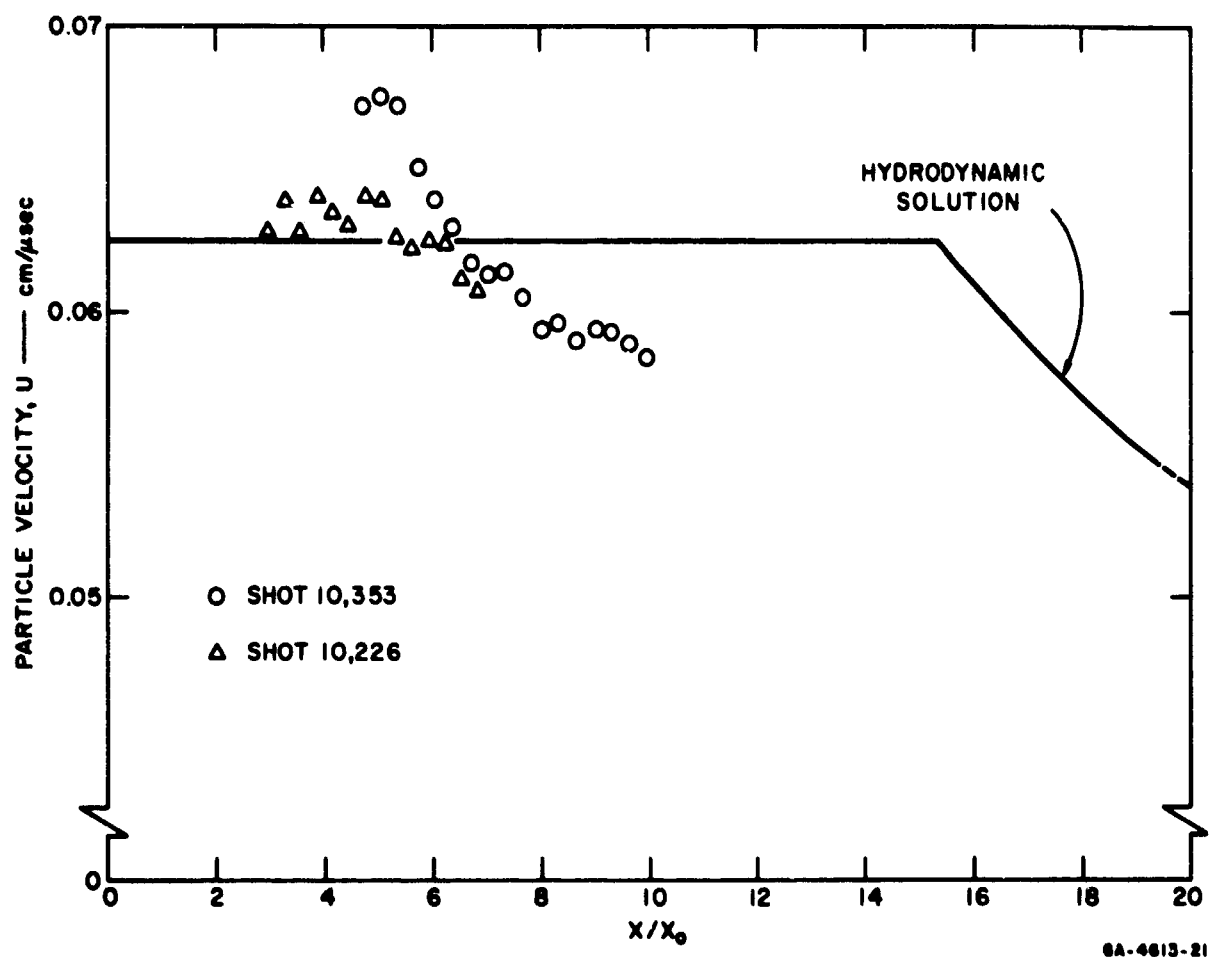


FIG. 12 PEAK PARTICLE VELOCITY IN ALUMINUM vs.  $x/x_0$   
(b) 1060 Aluminum

### C. COPPER WEDGE-SHAPED SPECIMEN

Copper specimens were cut from forgings of OFHC copper having a density of 8.94 g/cc. Principal impurities in the copper were 0.001 percent silver and possibly 0.002 percent nickel (from semiquantitative analyses). After machining and polishing, the samples were heat treated at a temperature of 1100°F for an hour in an atmosphere of dry hydrogen.

Results of two experiments in which aluminum flyer plates hit copper targets are shown in Fig. 13. As pointed out previously, the lesser value of the shock velocity in copper made it easier to analyze records from copper experiments than those from aluminum experiments. Results of Shot 10,366 are in reasonable agreement with the hydrodynamic solution out to 6 plate thicknesses. There is an indication that the flyer plate velocity may have been greater than 0.125 cm/ $\mu$ sec. Shot 10,365 indicated that some attenuation occurs at 5.5 to 6 plate thicknesses. Hence this pair of copper shots gave results which are more consistent than are the

results from either pair of aluminum shots referred to above. Better reproducibility in this case, as compared to the aluminum shots, may be because the two copper shots used Baratol which was from the same order.

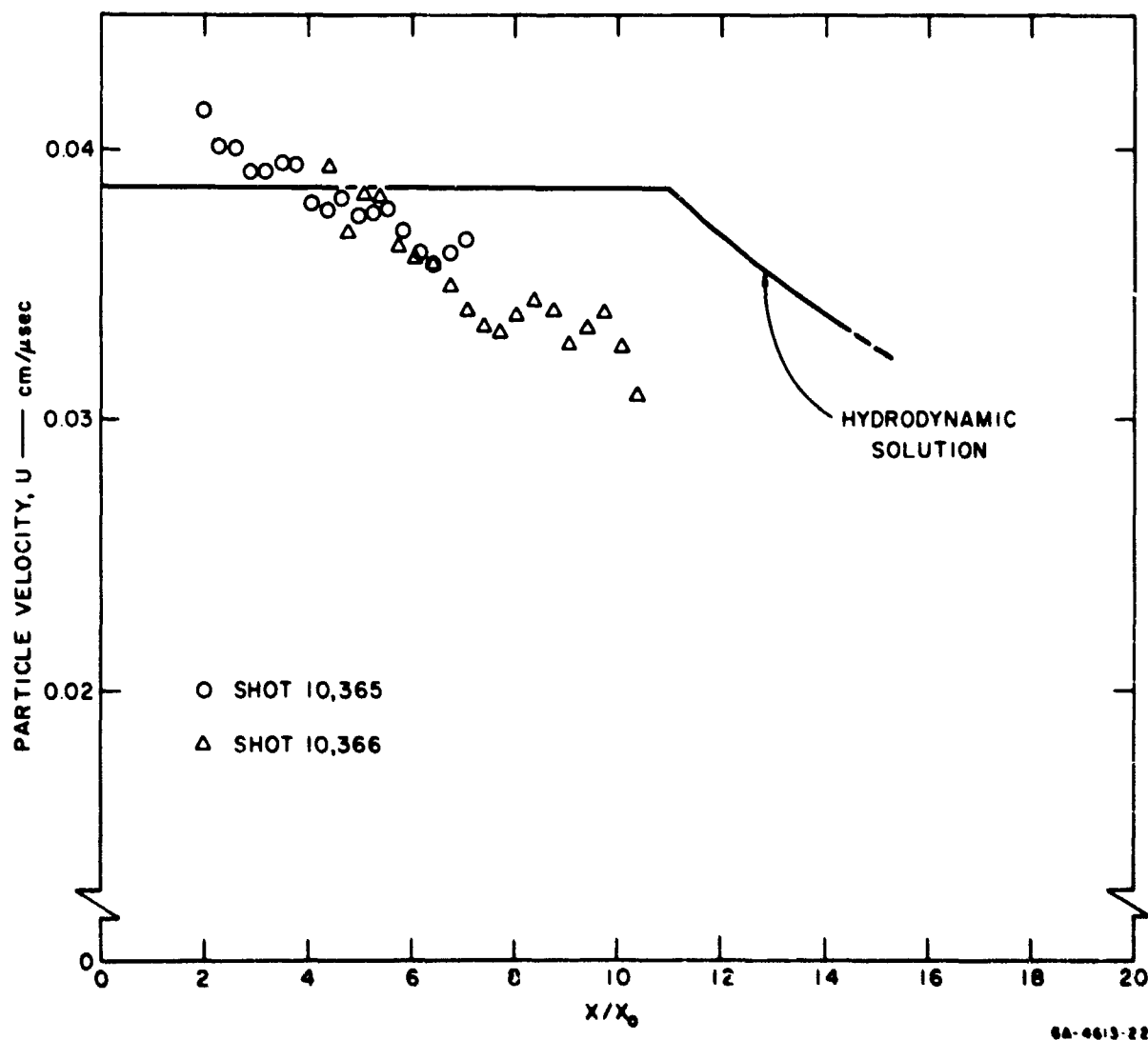


FIG. 13 PEAK PARTICLE VELOCITY IN COPPER vs.  $x/x_0$

The peak particle velocity for copper attenuates from approximately 0.04 to approximately 0.034 cm/ $\mu$ sec between 3 and 7 plate thicknesses. By using the Hugoniot for copper, the stress attenuates from 163 kbar to 136 kbar, or 27 kbar. If this is due entirely to the elastic wave in copper, the reverse yield strength is about 7 kbar. The precision of the data may be inferred from the scatter in the results shown in Fig. 13. The scatter is about 0.002 cm/ $\mu$ sec near  $x/x_0 = 8$ , or about 13 percent.

#### D. GOLD WEDGE-SHAPED SPECIMEN

The gold wedge was made from 99.99 percent gold by Western Gold and Platinum Company, Belmont, California. After casting, the gold was reduced 50 percent in thickness by rolling and then was machined into the required shape. After the inclined surface was polished, the material was softened by heating to 650°C for one hour. Because the sample was small (3 inches long), it was placed inside a vacuum chamber rather than being molded into the top cover of the chamber, as were the other wedge-shaped samples. Because of the size of the sample, the flyer plate was also reduced to 0.040 inch in thickness. This flyer plate was observed to have a velocity of 0.133 cm/ $\mu$ sec, for which the probable error is less than 1 percent.

Results for the gold shot are shown in Fig. 14 along with the results of the hydrodynamic calculations. At  $x/x_0 = 3.3$ , the experimental results give a particle velocity of 0.028 cm/ $\mu$ sec which agrees well with predicted value, 0.0288 cm/ $\mu$ sec. Some attenuation takes place between values of  $x/x_0$  of 3.3 and 6.9, the particle velocity being reduced from 0.028 to 0.024 cm/ $\mu$ sec. These values of particle velocities correspond to Hugoniot pressures of 190 and 159 kbar, respectively. This is interpreted as being the amplitude of the elastic relief wave for gold at the pressures referred to above. As was done for aluminum and copper, a value of the yield strength,  $Y$ , is inferred. For gold, Poisson's ratio  $\nu$  is 0.42,<sup>9</sup> so that  $Y$  is about 4 kbar. (See Section 6 for the method for calculating the conversion factor.)

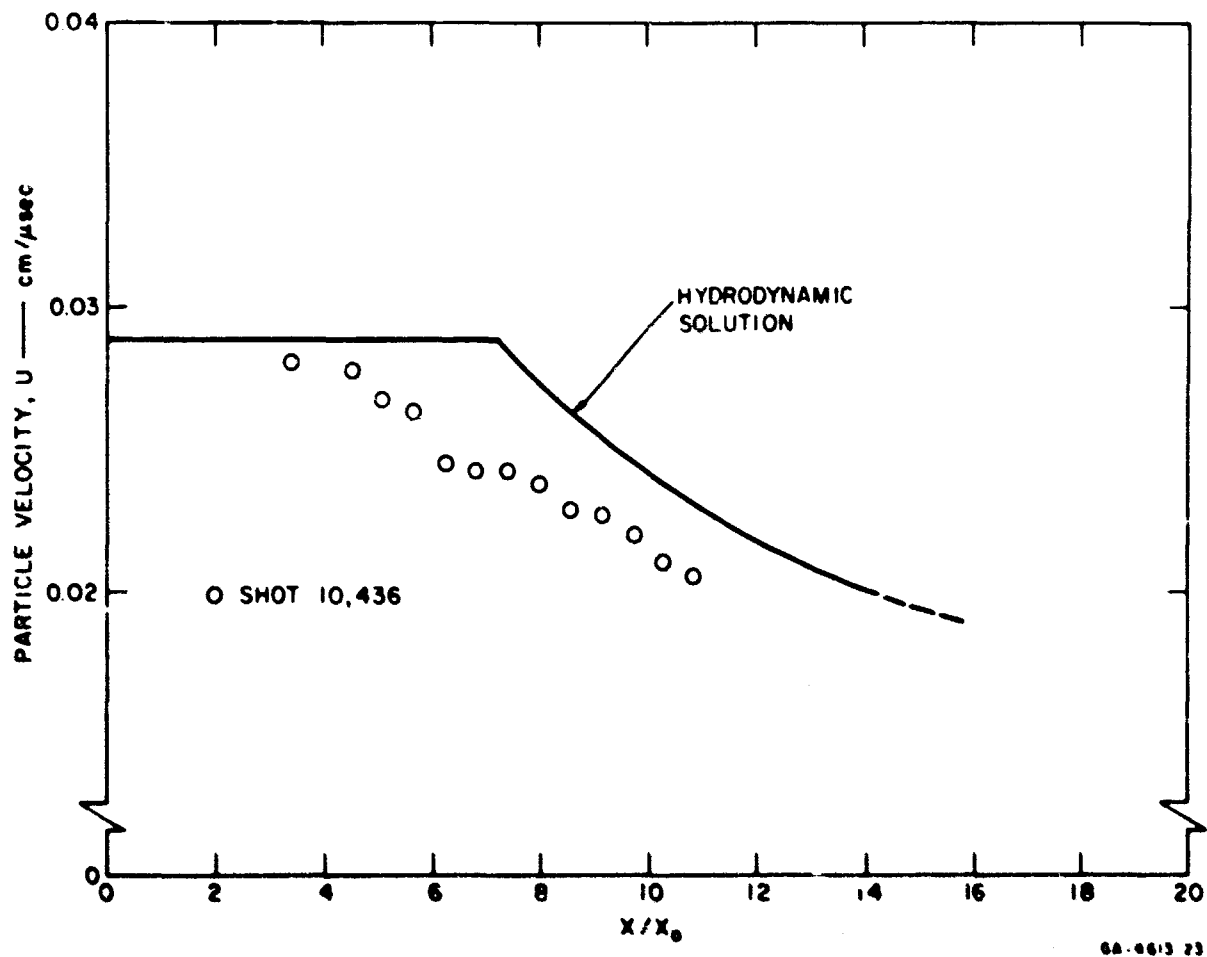


FIG. 14 PEAK PARTICLE VELOCITY IN GOLD vs.  $X/X_0$

## 5. RESULTS OF EXPERIMENTS USING GAGES

### A. C-7 EPOXY SPECIMENS

A typical gage record is shown in Fig. 9 and a brief description of the method of analysis was given in Section 3B. Three gages were included in each shot, also as described in Section 3B. Results of experiments in which "bare gages" were hit by aluminum plates are given in Fig. 15. The term bare gage is applied to the arrangements in which no material other than C-7 separates the flyer plate from the Manganin wire. Because these wires were located at different depths in the C-7, attenuation of peak pressure could be observed. In the experiments the oscilloscopes were triggered individually, so that the relation in time of one record to another is not known accurately. Placement of the records in Fig. 15 (and in subsequent figures) is therefore arbitrary, being based on calculations which will be described later. Some indication of the reproducibility of results can be obtained by comparing the curves for which values of  $x/x_0$  are 0.92 and 0.95. These differ about 6 percent in peak pressure and have considerably different shapes. This latter disagreement is particularly distressing because it indicates that these gages cannot be relied upon to give the shape of the pulse.

The envelope of the curves shown in Fig. 15 shows that some attenuation takes place between  $x/x_0 = 1.9$  and  $x/x_0 = 2.9$ . This is in fair agreement with the results of the wedge experiment shown in Fig. 16 where attenuation is observed at  $x/x_0 = 3$ . At  $x/x_0 = 6$ , the wedge experiment gives a pressure of about 26 kbar which agreed well with the 27.5 kbar given by the gage at  $x/x_0 = 5.8$ , Fig. 16.

### B. ALUMINUM SPECIMENS

When gages were used on metal targets, the Manganin wire was separated from the surface of the specimen by about 0.1-cm-thick C-7 epoxy, as noted in Section 3B. Results of gages mounted on targets of 1060 aluminum are shown in Fig. 17(a). Reproducibility can be checked by comparing the results of the gages located at 7.82 and 7.83 (three significant figures are used in order to identify the curves, not to indicate the accuracy of the

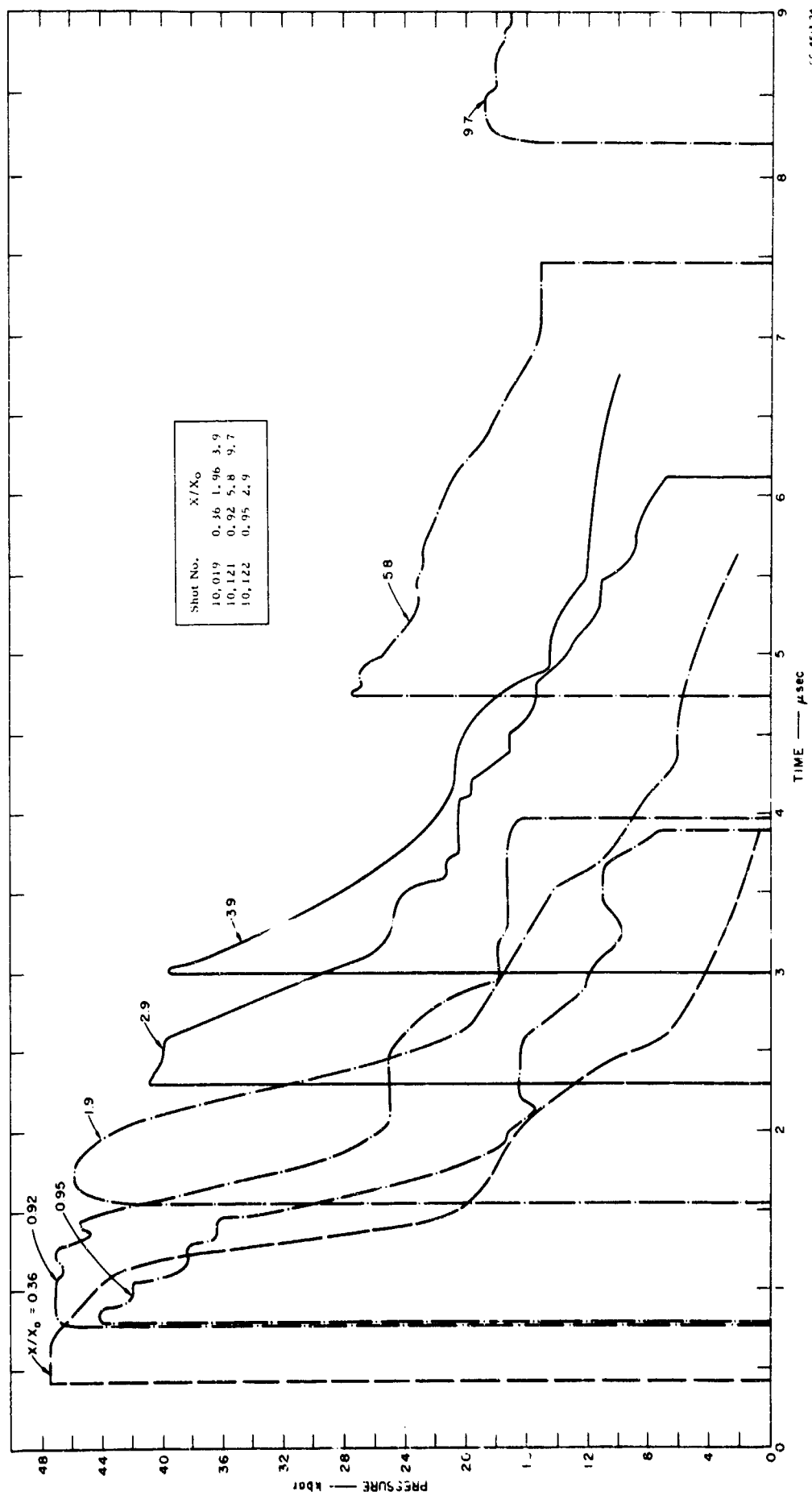


FIG. 15 PRESSURE vs. TIME FROM GAGES HIT WITH ALUMINUM PLATES

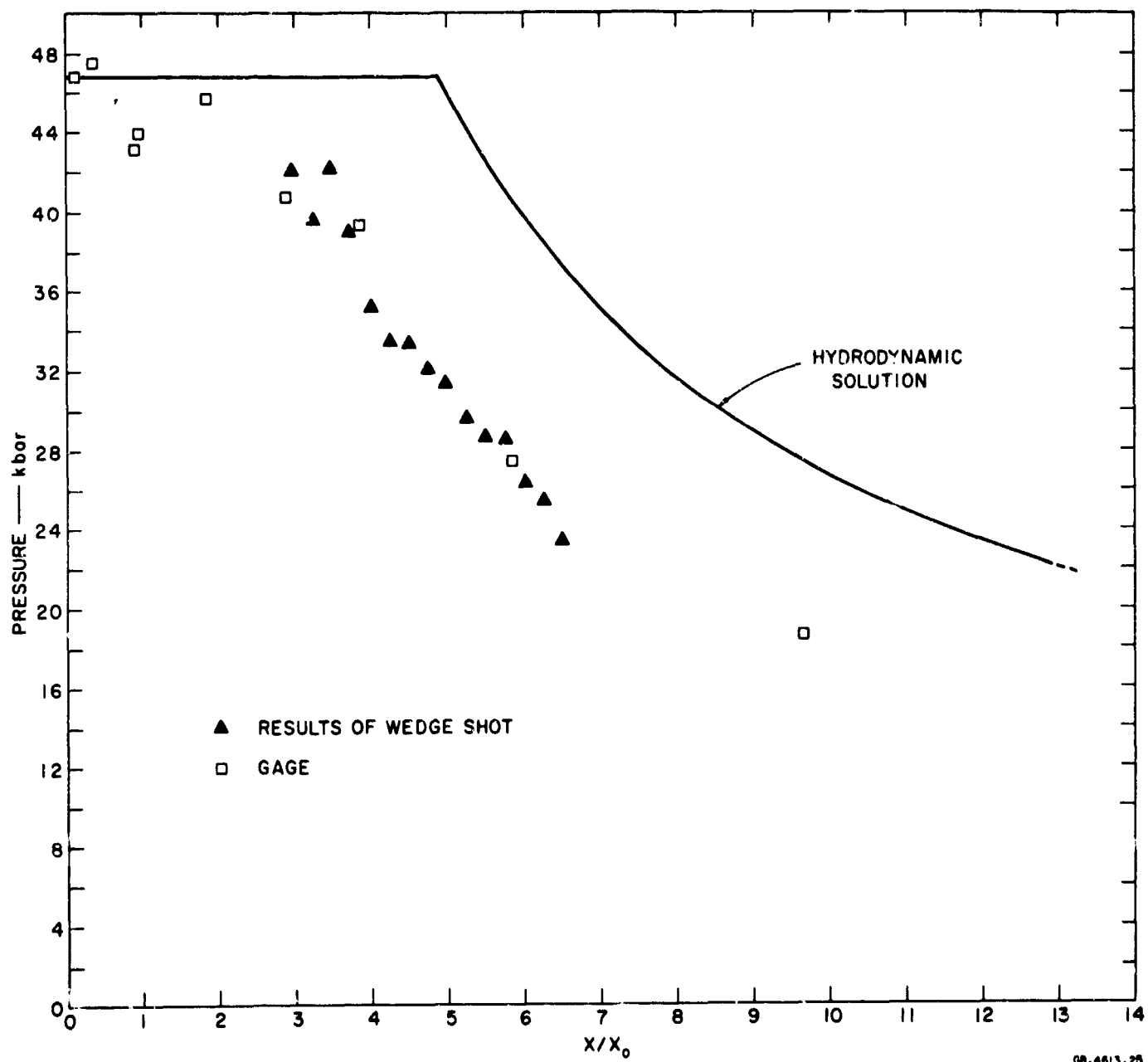


FIG. 16 PRESSURE IN C-7 EPOXY vs.  $x/x_0$ . RESULTS FROM OPTICAL AND TRANSDUCER SHOTS



depth of the wire in the epoxy). These two curves are separated on the time scale more than warranted so that the curves can be more easily distinguished and reproducibility is seen to be good. Considering the envelope of the curves, the gage at 3.9 appears to have been erratic. If this gage is ignored, the gage records suggest that attenuation in 1060 aluminum starts at values of  $x/x_0$  between 3 and 5. This is somewhat earlier than was indicated by the wedge experiments, Figs. 12(a) and 12(b).

Results for annealed 2024 aluminum are presented in Fig. 17(b) where attenuation appears to commence for a value of  $x/x_0$  of about 4 or 5. At least the pulse top is no longer flat for gages located at 3.9 and 4.9, which is one indication that an elastic relief wave has overtaken the shock front. The flat top exhibited by the gage at 7.9 could be explained by use of the elastoplastic model for relating stress to strain. This is discussed in a later section where results of calculations are compared with experimental results.

For experiments with aluminum targets, the peak pressure observed for thin targets was observed to be 51 kbar. When bare gages were struck by flyer plates, the peak pressure was 45 kbar. This difference in response has not been explained, and the records presented in Figs. 17(a) and 17(b) have normalized to 45 kbar.

The impedance mismatch of aluminum and C-7 epoxy is relatively large so that a strong relief wave was reflected back into the aluminum at the aluminum-epoxy interface. This relief wave interacted with the wave from the back side of the flyer plate and put a portion of the aluminum in a state of tension. The tension was apparently great enough to cause the aluminum to fracture or spall. This is the explanation of the relatively long tails on the waves, like that shown by the gage at 7.9 in Fig. 17(b). That portion of the record beyond 5.5  $\mu$ sec is due to the spalling of the aluminum target. This phenomenon is also observed for copper targets and will be discussed when computed profiles are compared with experimental profiles.

### C. COPPER SPECIMENS

Results for gages on copper are shown in Fig. 18. An impedance match solution showed that a pressure of 30 kbar should be induced in the C-7 epoxy when the copper target was thin. The gage on the thinnest copper target gave a pressure of 36 kbar for reasons that are not understood.

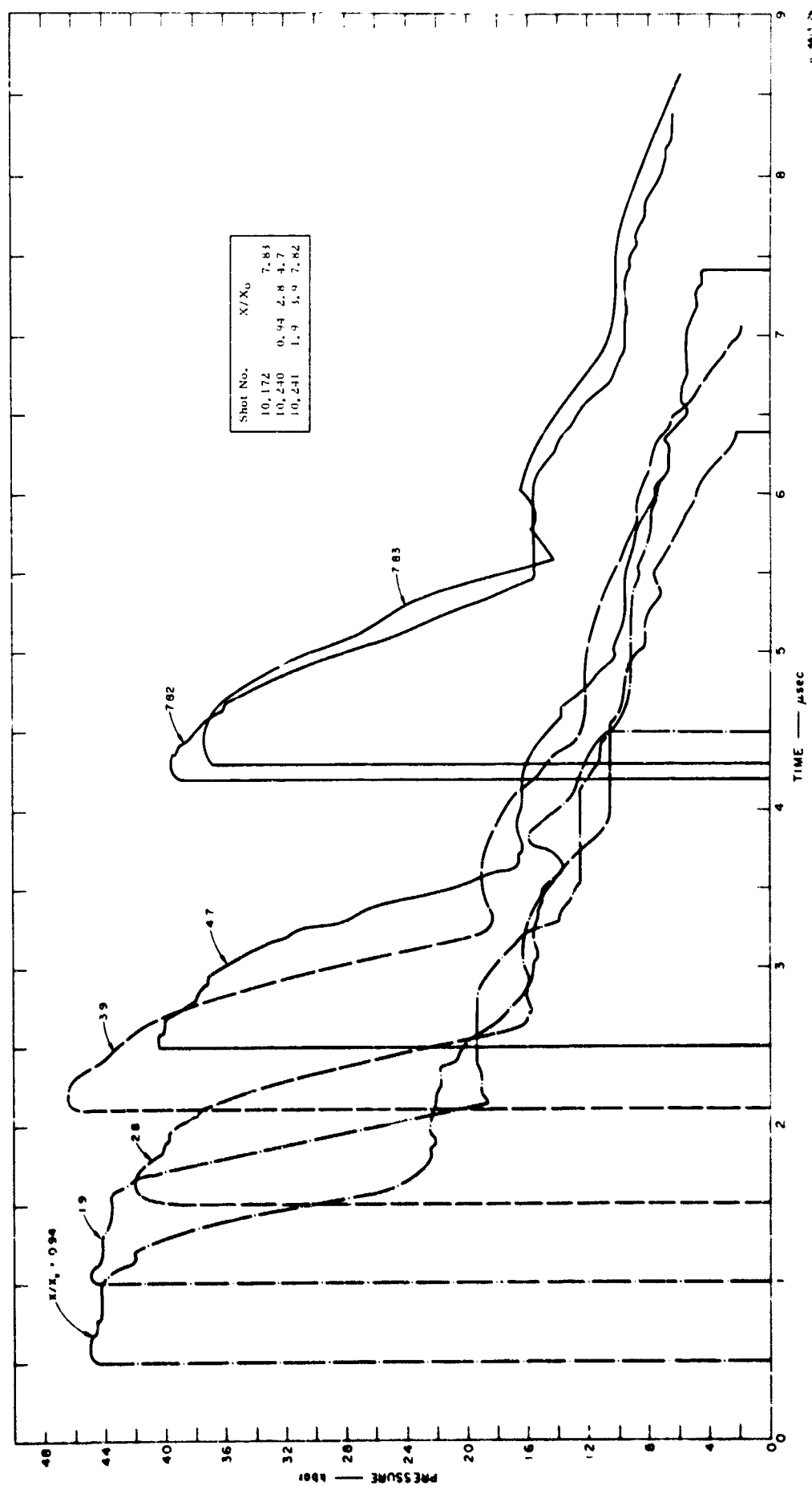
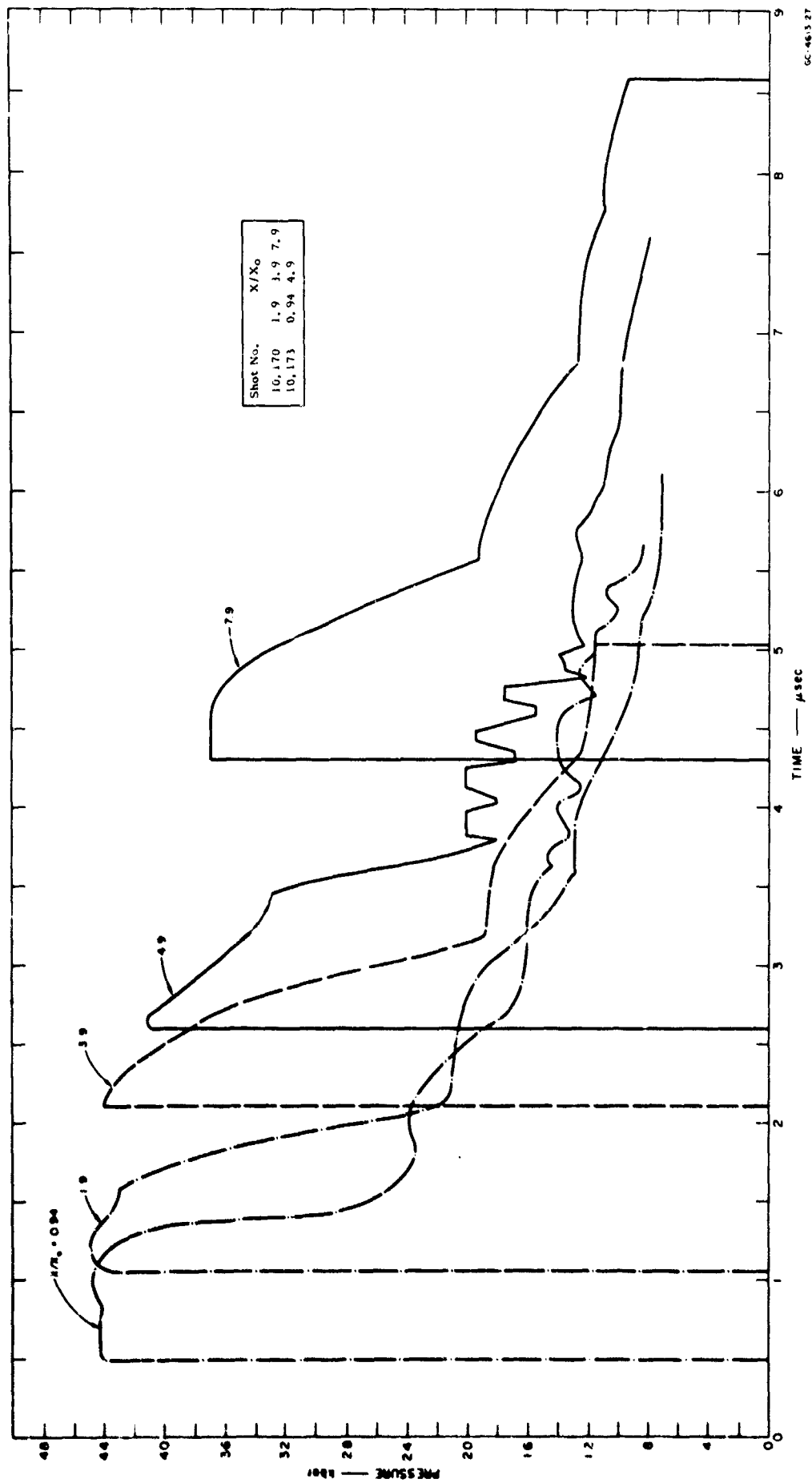


FIG. 17 PRESSURE FROM GAGES ON ALUMINUM SPECIMENS vs. TIME  
(a) 1060 Aluminum



GC-4613.27

FIG. 17 PRESSURE FROM GAGES ON ALUMINUM SPECIMENS vs. TIME  
(b) 2024 Aluminum

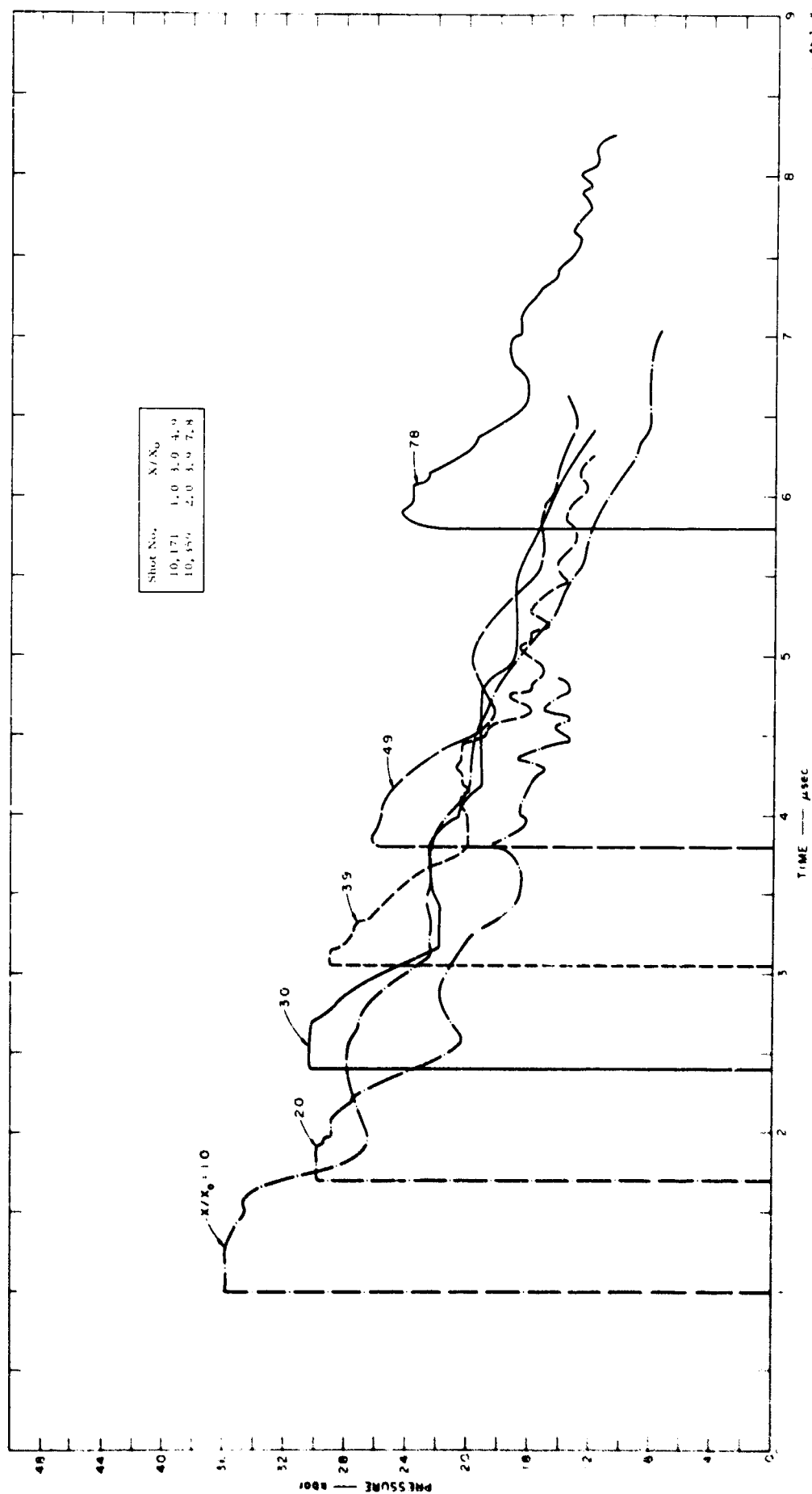


FIG. 18 PRESSURE FROM GAGES ON COPPER SPECIMEN vs. TIME

Because the gages at 2.0 and 3.0 gave the expected pressure, assuming no attenuation, it is probable that the gage at 1.0 malfunctioned. Assuming that the gage at  $x/x_0 = 1$  did malfunction obviates the necessity for normalizing the remaining records. The gage records (Fig. 18) show some attenuation of the peak pressure at 4.9 plate thicknesses which is a somewhat smaller value than that obtained from the wedge experiments (Fig. 13).

The impedance mismatch between copper and C-7 is greater than that for aluminum and C-7. Hence spalling should be even more probable for the copper targets. That the copper did spall was inferred from the long tail on the pressure profiles. It was also inferred from the reloading which is shown by most of the profiles in Fig. 18. For example, the profile of the gage at 2.0 shows approximately 1 kbar reloading of the gage at a time of about 2.8  $\mu\text{sec}$ . This reloading was caused by the sudden fracture of the copper which released compression waves on each side of the break.

## 6. CALCULATION OF ATTENUATING SHOCK WAVES

The major uncertainty in the calculation of attenuating shock waves in solids is the lack of information concerning the equation of state of solids. Much work has been done on the assumption that solids behave as fluids above some limiting pressure or stress. The work reported here was performed in an attempt to determine if departure from fluid behavior could be observed. In order to do this, the results of the experiments reported in Section 5 must be compared with calculated results.

In some of the calculated results, the material is assumed to behave hydrodynamically, i.e., material rigidity is neglected. Pressure is related to density by

$$P = A \left[ \left( \frac{\rho}{\rho_0} \right)^K - 1 \right], \quad (1)$$

where  $P$  is the pressure,  $\rho$  is the density, and  $\rho_0$  is the density at zero pressure. Values of the constants  $A$  and  $K$  are obtained by requiring the equation to fit the Hugoniot data of the medium. No adiabats are derived, it being assumed that, for the materials observed and for the pressures encountered, the adiabats are not distinguishable from the Hugoniot curves. Thus the term "hydrodynamic" is used in a restricted sense.

Table 1 gives the values of  $A$ ,  $K$ , and  $\rho_0$  for the materials for which calculations have been performed. The source of the data used in determining the values of  $A$  and  $K$  is also given for each case. Data for the C-7 epoxy range from about 0.04 to 0.08 Mbar. For this material, the pressure encountered in the experiments was 0.046 Mbar or less.

Table 1  
VALUES OF CONSTANTS FOR MURNAGHAN  
EQUATION OF STATE

MATERIAL	$\rho_0$ (g/cm <sup>3</sup> )	$A$ (Mbar)	$K$	SOURCE
C-7 Epoxy	1.18	0.205	4.54	Reference 4
Aluminum	2.785	0.196	4.10	Reference 1
Copper	8.9	0.301	4.71	Reference 1
Gold	19.24	0.305	5.79	Reference 8

Determinations of the constants for aluminum and copper have been reported previously. For gold, the data given by Rice *et al.*<sup>8</sup> was used in determining the values of constants.

The computer code which employs Eq. (1) to represent the equation of state uses a finite difference scheme based on the method of characteristics. Results of this code are identified with the label "hydrodynamic solution" in the figures where results are reported. For a small distance, i.e., a small value of  $x/x_0$ , the results amount to an impedance mismatch solution.

In order to account for the early attenuation of shock waves induced by the impact of high-speed aluminum plates, an elastoplastic relation between stress and strain is assumed. This model has the notable feature that the initial attenuation in the situation described above is accomplished by an elastic relief wave. The velocity of this wave is considerably greater than the velocity of the following plastic waves. The model is described graphically in Fig. 19 where Hugoniot data are assumed to

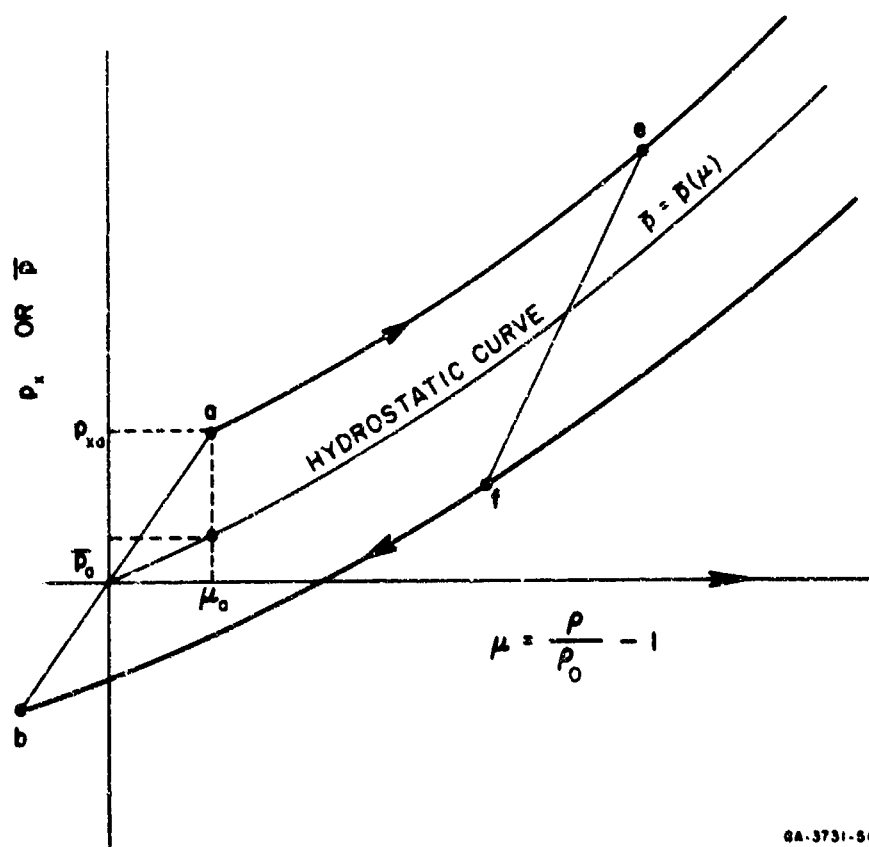


FIG. 19 ELASTOPLASTIC EQUATION OF STATE

lie along the curve  $ae$ . This curve is related to the hydrostatic curve by the relation

$$p_x = \bar{p} + \frac{2}{3} Y \quad , \quad (2)$$

where  $p_x$  is the stress along the curve  $ae$ , and  $p$  is the hydrostatic pressure. The variable  $Y$  represents what is usually called the yield stress in simple tension and is twice the maximum resolved shear stress. The curve  $bf$  is displaced from the hydrostat by  $(-2/3) Y$ .

Comparisons of theory and experiment based on this model with constant yield strength show improvement in agreement over that obtained with the fluid model; however, significant differences still remain. Good agreement can be obtained by assuming that the yield strength is a function of the hydrostatic pressure

$$Y = Y_0 + M(\bar{p} - \bar{p}_a) \quad , \quad (3)$$

where  $Y_0$  and  $M$  are constants,  $\bar{p}$  and  $\bar{p}_a$  being defined in Fig. 19. The hydrostatic curve is represented by

$$\bar{p} = A\mu + B\mu^2 + C\mu^3 \quad (4)$$

where  $\mu = \rho/\rho_0 - 1$ ,  $\rho$  is the density and  $\rho_0$  is the density at normal pressure. Combinations of values of the constants for aluminum, copper, and C-7 are given in Table 2. Hugoniot data for aluminum and copper were taken from Rice *et al.*<sup>8</sup> while values of  $Y_0$  and  $M$  were estimated from attenuation experiments. Data for C-7 epoxy were obtained from Keough.<sup>4</sup>

Table 2  
VALUES OF CONSTANTS FOR ELASTOPLASTIC  
EQUATIONS OF STATE

MATERIAL	$Y_0$ (Mbar)	$M$	$A$ (Mbar)	$B$ (Mbar)	$C$ (Mbar)	$\rho_0$ (g/cc)
Aluminum	0.0025	0.055	0.755	1.29	1.197	2.785
Aluminum	0.0025	0.0	0.743	1.74	0.329	2.785
Aluminum	0.0	0.0	0.765	1.66	0.428	2.785
Copper	0.0007	0.031	1.49	0.546	11.85	8.936
C-7	0.0	0.0	0.0782	0.196	0.221	1.18
C-7	0.0006	0.0	0.0585	0.301	0.0726	1.18
C-7	0.001	0.0	0.0528	0.328	0.0379	1.18



Poisson's ratio was assumed to be 1/3 for the metals and 0.4 for C-7, the same as for lucite.<sup>9</sup> Both the bulk and shear moduli are expressed in terms of Poisson's ratio,  $\nu$ , and Young's modulus,  $E$ , and do not appear explicitly in the equations describing the elastoplastic model. Poisson's ratio is assumed to be independent of pressure, and  $E$  is represented by

$$E = -3(1 - 2\nu) V \frac{d\bar{p}}{dV} , \quad (5)$$

where  $V$  is the specific volume.

The elastic relief wave decreases the stress from  $p_{xe}$  to  $p_{xf}$ , Fig. 19. This change in stress<sup>10</sup> is given by

$$p_{xe} - p_{xf} = \frac{1 - \nu}{1 - 2\nu} (Y_e + Y_f) . \quad (6)$$

If  $Y$  is not strongly dependent on the pressure, and  $\nu = 1/3$ , the usual result is obtained for which

$$p_{xe} - p_{xf} = 4Y . \quad (7)$$

The assumption that Poisson's ratio,  $\nu$ , is a constant is not supported by an experimental observation. The change in stress carried by the elastic relief wave is dependent on the value  $\nu$ , see Eq. (6). The elastic longitudinal sound speed also depends on  $\nu$ , as shown in the following. Sound speed  $c$  is defined as

$$c = \sqrt{\frac{dp_x}{d\rho}} \quad (8)$$

The elastic sound speed is obtained by using the relation between  $p_x$  and  $\rho$  which connects points  $e$  and  $f$  in Fig. 19. The relation<sup>10</sup> is

$$p_{xe} - p_x = 3(1 - \nu)(\bar{p}_e - \bar{p})/(1 + \nu) , \quad (9)$$

where  $p_{xe}$  is the stress at point  $e$ , Fig. 19, and  $\bar{p}_e$  is the hydrostatic pressure at the  $\mu_e$ . Use of Eq. (4) and the definition of  $\mu$  permits Eq. (9) to be written so that  $p_x$  is a function of the density,  $\rho$ . The

expression for the sound speed then becomes

$$c_1 = [-3V^2(1-\nu)(d\bar{p}/dV)/(1+\nu)]^{1/2}, \quad (10)$$

where  $V$  is the specific volume. By use of Eqs. (2) and (3), the hydrostatic pressure  $\bar{p}$  can be replaced by the stress  $p_x$ . There results

$$c_1 = \{3(1-\nu)(dp_x/d\rho)/[(1+\nu)(1+2/3M)]\}^{1/2} \quad (11)$$

where  $dp_x/d\rho$  is the derivative of the upper curve, Fig. 19, which represents the Hugoniot data. In the computer code where the difference scheme is based on the method of characteristics, sound speed is simply  $(dp/d\rho)^{1/2}$ , where  $p$  vs.  $\rho$  represents the Hugoniot data and the derivative is evaluated by using Eq. (1). For  $\nu = 1/3$ , the elastic sound speed, from Eq. (11), is

$$c = \sqrt{\frac{3}{2\left(1 + \frac{2}{3}M\right)}} \cdot \frac{dp_x}{d\rho} = \sqrt{\frac{3}{2\left(1 + \frac{2}{3}M\right)}} c_{\text{hydro}}, \quad (12)$$

so that the elastic sound speed is always greater than the hydrodynamic sound speed,  $c_{\text{hydro}}$ . The elastic sound speed is reduced a few percent when  $M$  is not zero ( $M = 0.055$  for aluminum).

Any variation of  $\nu$  with pressure would affect both the amplitude of the elastic wave, Eq. (6), and its velocity, Eq. (11). As pointed out above, it is not known if the value of  $\nu$  depends on the stress. If it increases with stress, the speed and amplitude of the elastic relief wave are both increased.

The computer code which uses the elastoplastic model for the equation of state employs the method of integrating the flow equations given by von Neumann and Richtmyer.<sup>11</sup> This method uses an artificial viscosity term which smears the shock front over a few cells or meshes. Both linear and quadratic terms are used in the expression for artificial viscosity,

$$Q = [1.7^2\Delta U + 0.1c]\Delta U/V, \quad (13)$$

where  $c$  is the speed of sound (the code uses the elastic sound speed),  $V$  is the specific volume and

$$\Delta U = U_{j+1} - U_j, \quad (14)$$

is the difference in particle velocities in two adjacent cells. This relation is used only when the material is being compressed, i.e., for  $\Delta U < 0$ . Otherwise, the value of  $Q$  is taken to be zero.

Most of the calculations presented in the remainder of this report were obtained by use of the artificial viscosity code (the  $Q$ -code). Each set of results is identified with the values of  $Y_0$  and  $M$  used in the equation of state for that set. Where both  $Y_0$  and  $M$  are zero for both projectile and target, the results should agree with results obtained with the previously described characteristics code. The agreement is not exact because Eqs. (1) and (4) cannot give the same results, and because of the smearing of the shock front by the  $Q$ -code.

## 7. COMPARISON OF RESULTS OF CALCULATIONS AND RESULTS OF EXPERIMENTS

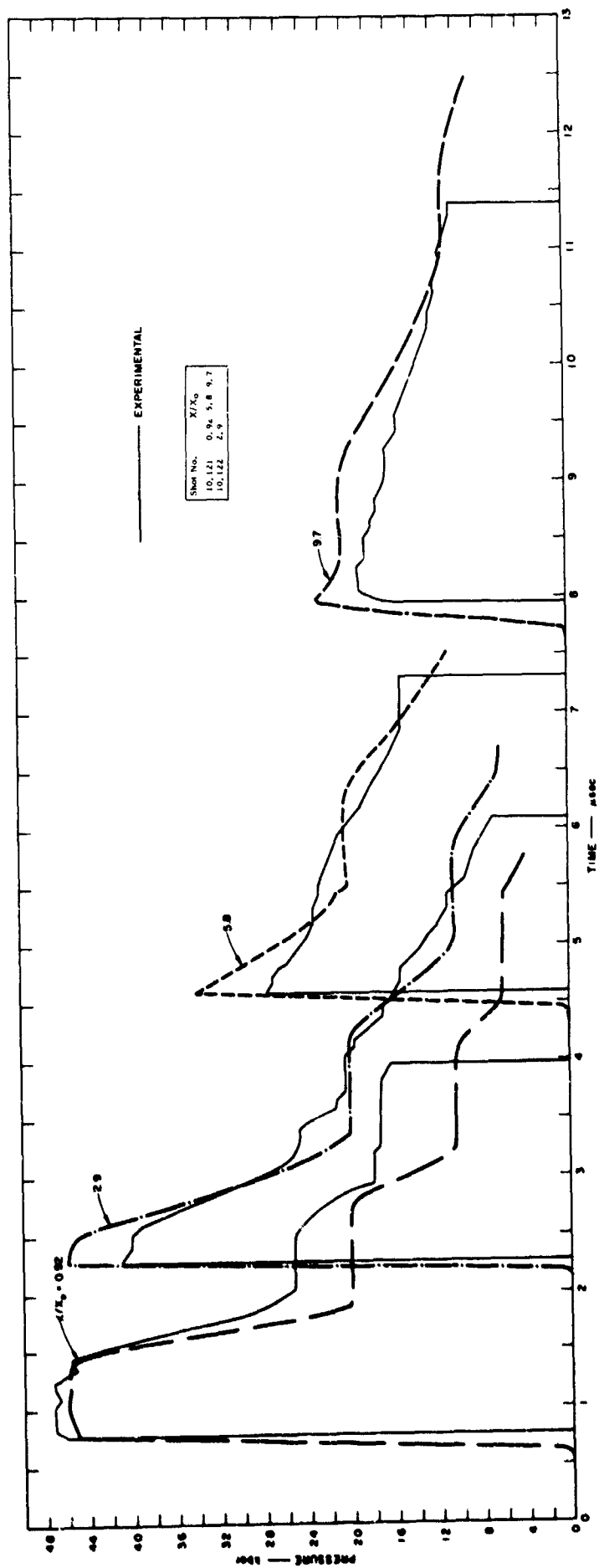
### A. C-7 EPOXY

Some comparisons of calculated results with experimental results have been made in the figures discussed above. The calculated results were obtained by a computer code using the method of characteristics and a simple hydrodynamic equation of state; i.e., rigidity was not included. The comparisons show that early attenuation occurred in all the experiments. In this section, results obtained by the artificial viscosity code are compared with the experimental results. The artificial viscosity code has the advantage that rigidity can easily be included in the equation of state. However, rigidity need not be included in the equation of state for the *Q*-code. Results obtained using hydrodynamic representations of the equations of state of both aluminum and C-7 epoxy are given in Fig. 20(a) for four different locations in the epoxy.

Experimental data from four gages are superimposed in Fig. 20(a) on the results of the calculations. Gage data showed greater attenuation of peak pressure than did the results of calculations. This is viewed as evidence that the flow is not hydrodynamic. The situation was improved very little by adding rigidity to the equation of state of aluminum [see Fig. 20(b)]. These results led to the inclusion of rigidity in the equation of state of C-7 epoxy also.

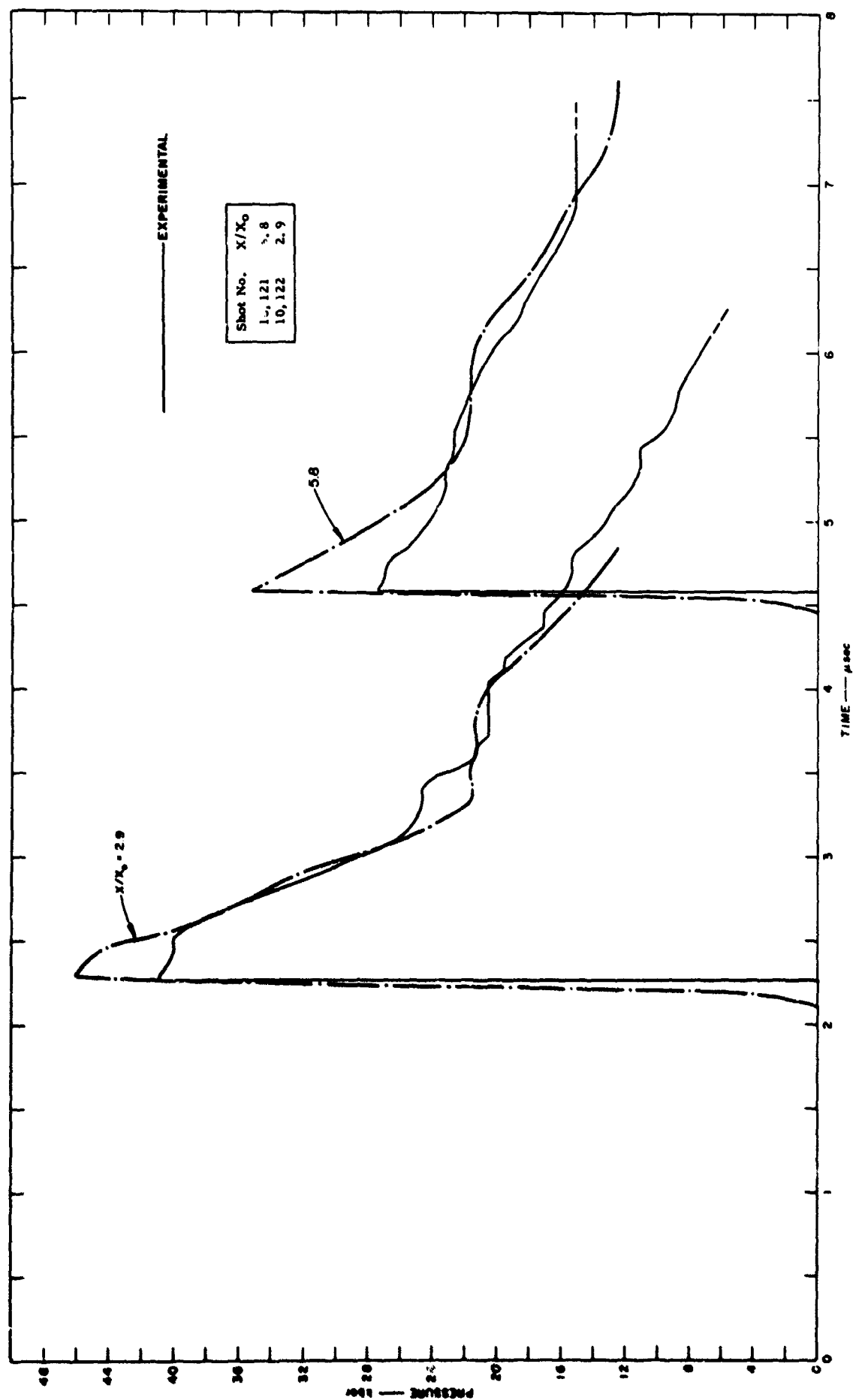
Calculated peak pressures agree more closely with those from the gages when the yield in C-7 is assumed to be 0.6 kbar, Fig. 21(a). Fair agreement of pulse shapes is also obtained. Even closer agreement is obtained for peak pressure by increasing the value of the yield in C-7 to 1.0 kbar, Fig. 21(b). Pulse shapes are in somewhat better agreement also. In both cases  $Y$  is assumed to be independent of pressure; i.e.,  $M = 0$ .

Results for C-7 epoxy are summarized in Figs. 22(a) and 22(b) which show the peak pressure as a function of distance of penetration of the shock front into the epoxy. Figure 22(a) shows the results of using the hydrodynamic equation of state in the *Q*-code for both aluminum and C-7, i.e.,  $Y_0$  and  $M$  were zero for both materials. These results differ from



(a) HYDRODYNAMIC EQUATIONS OF STATE FOR BOTH ALUMINUM AND C-7

FIG. 20 COMPARISON OF CALCULATED WAVE PROFILES WITH RESULTS OF GAGES FOR C-7 EPOXY



(b) HYDRODYNAMIC EQUATION OF STATE FOR C-7, ELASTOPLASTIC EQUATION OF STATE FOR ALUMINUM

FIG. 20 COMPARISON OF CALCULATED WAVE PROFILES WITH RESULTS OF GAGES FOR C-7 EPOXY

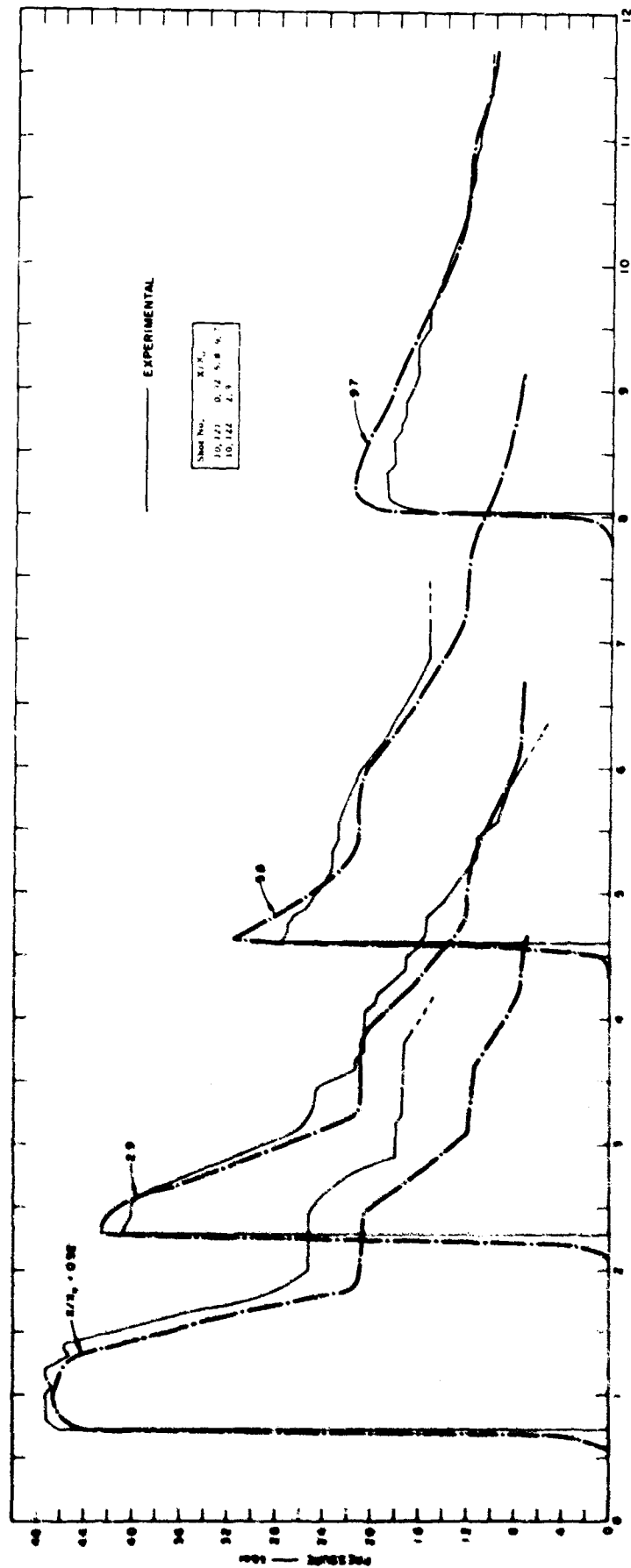


FIG. 21 COMPARISON OF CALCULATED WAVE PROFILES WITH RESULTS OF GAGES FOR C-7 EPOXY ELASTOPLASTIC EQUATION OF STATE FOR ALUMINUM ( $\mu = 0.058$ )

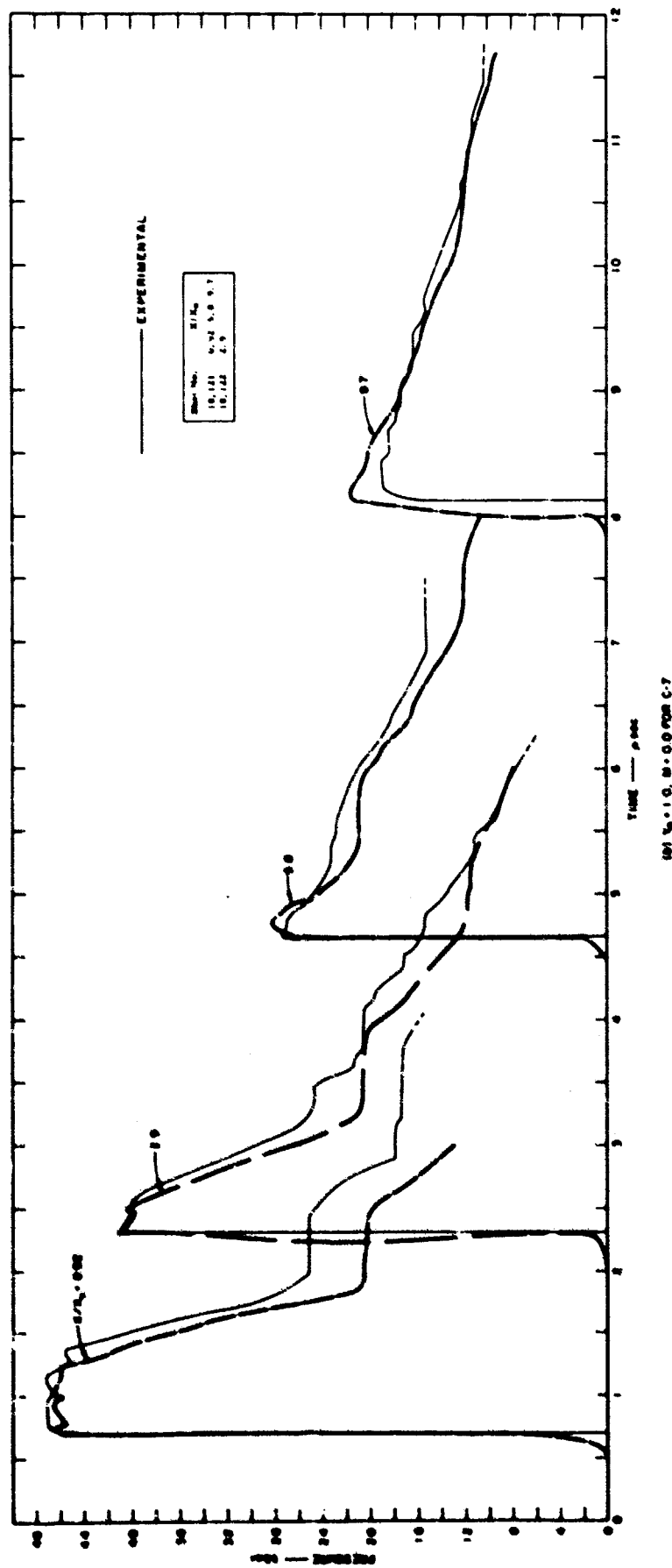


FIG. 21 COMPARISON OF CALCULATED WAVE PROFILES WITH RESULTS OF GAGE:  
FOR C-7 EPOXY. ELASTOPLASTIC EQUATION OF STATE FOR ALUMINUM  
 $m = 0.002$



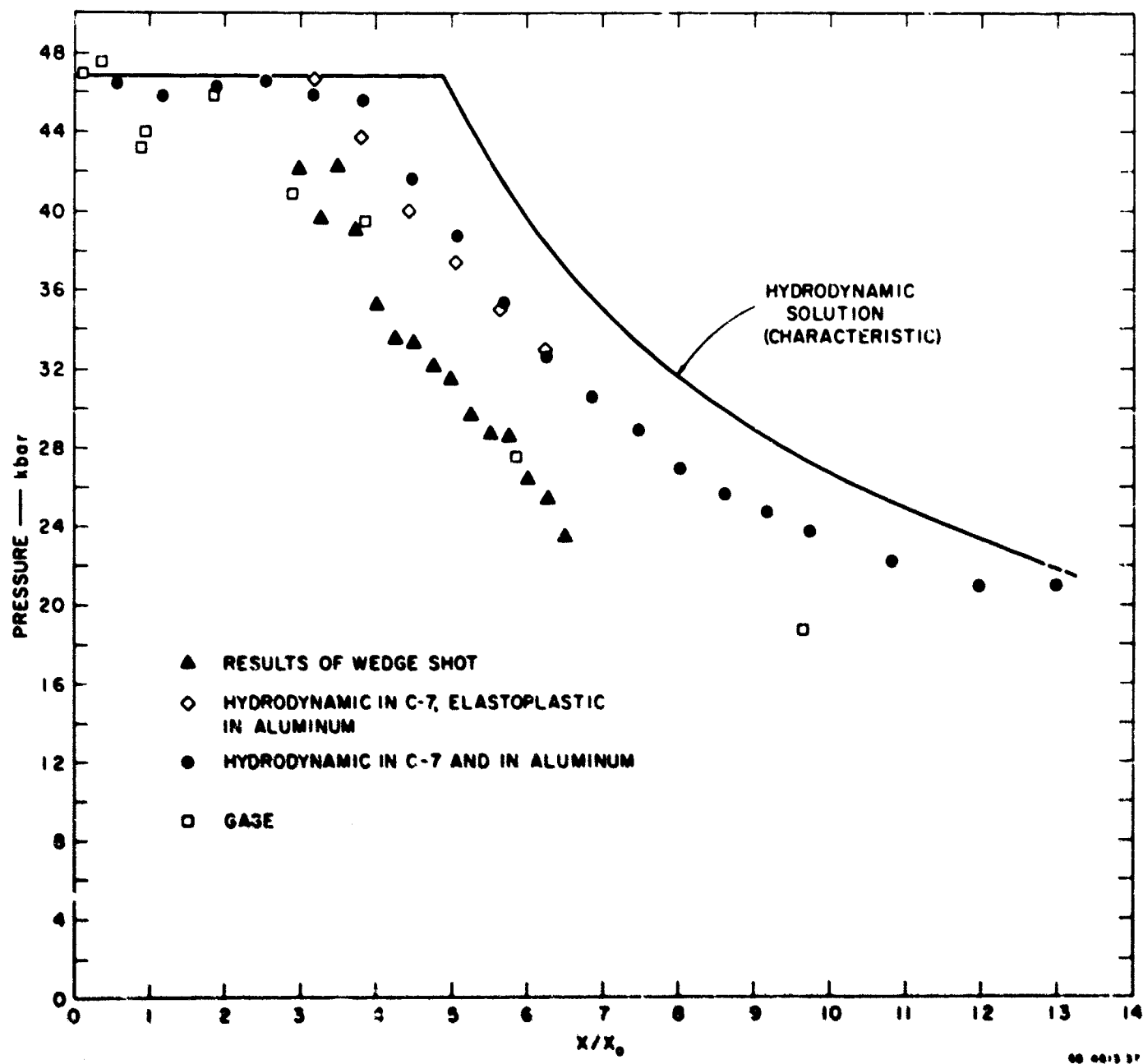


FIG. 22 PRESSURE IN C-7 EPOXY vs.  $x/x_0$  FROM EXPERIMENTS AND CALCULATIONS  
(a) Hydrodynamic Equation of State for C-7 Epoxy

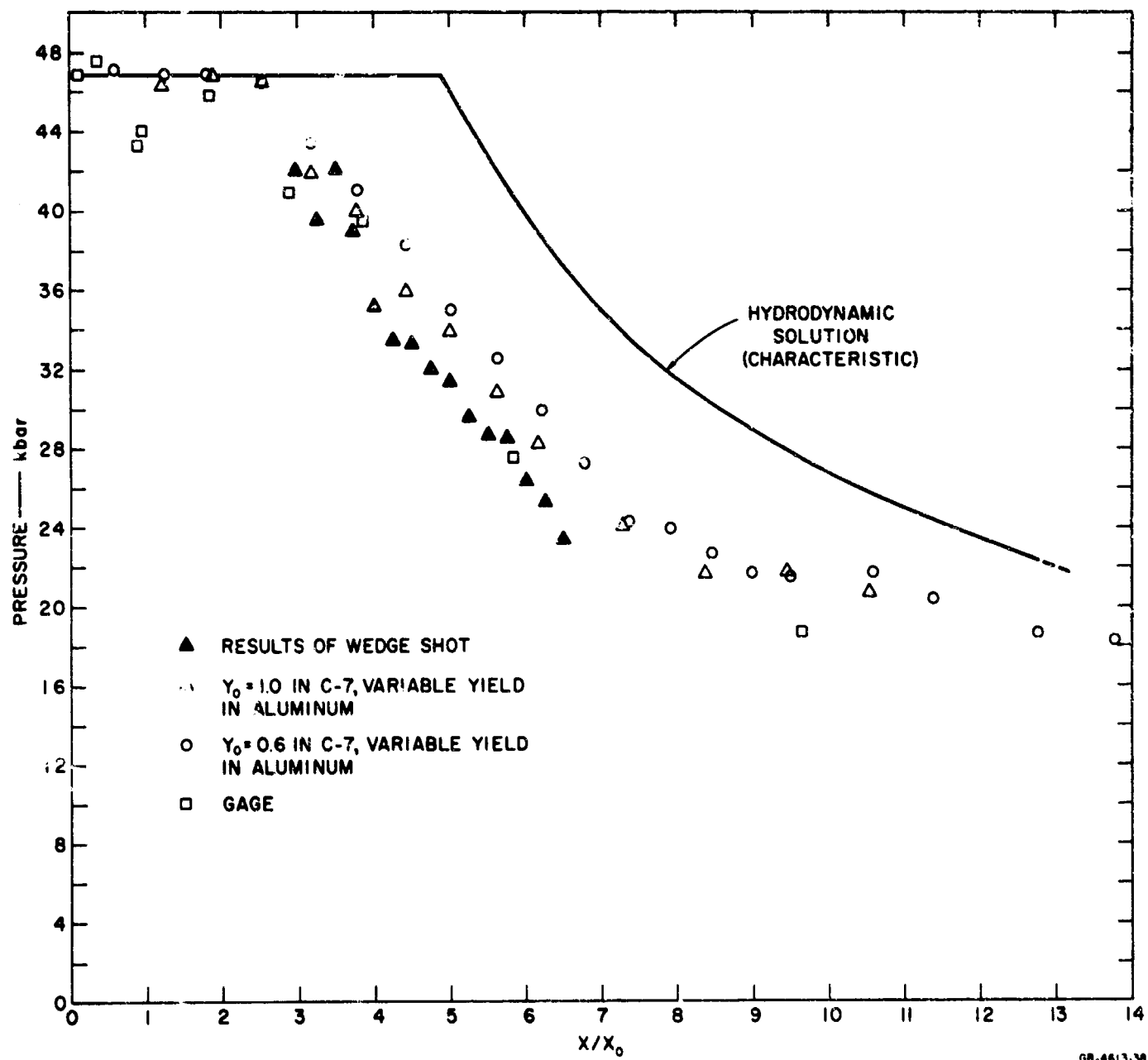


FIG. 22 PRESSURE IN C-7 EPOXY vs.  $x/x_0$  FROM EXPERIMENTS AND CALCULATIONS  
(b) Elastoplastic Equation of State for C-7 Epoxy

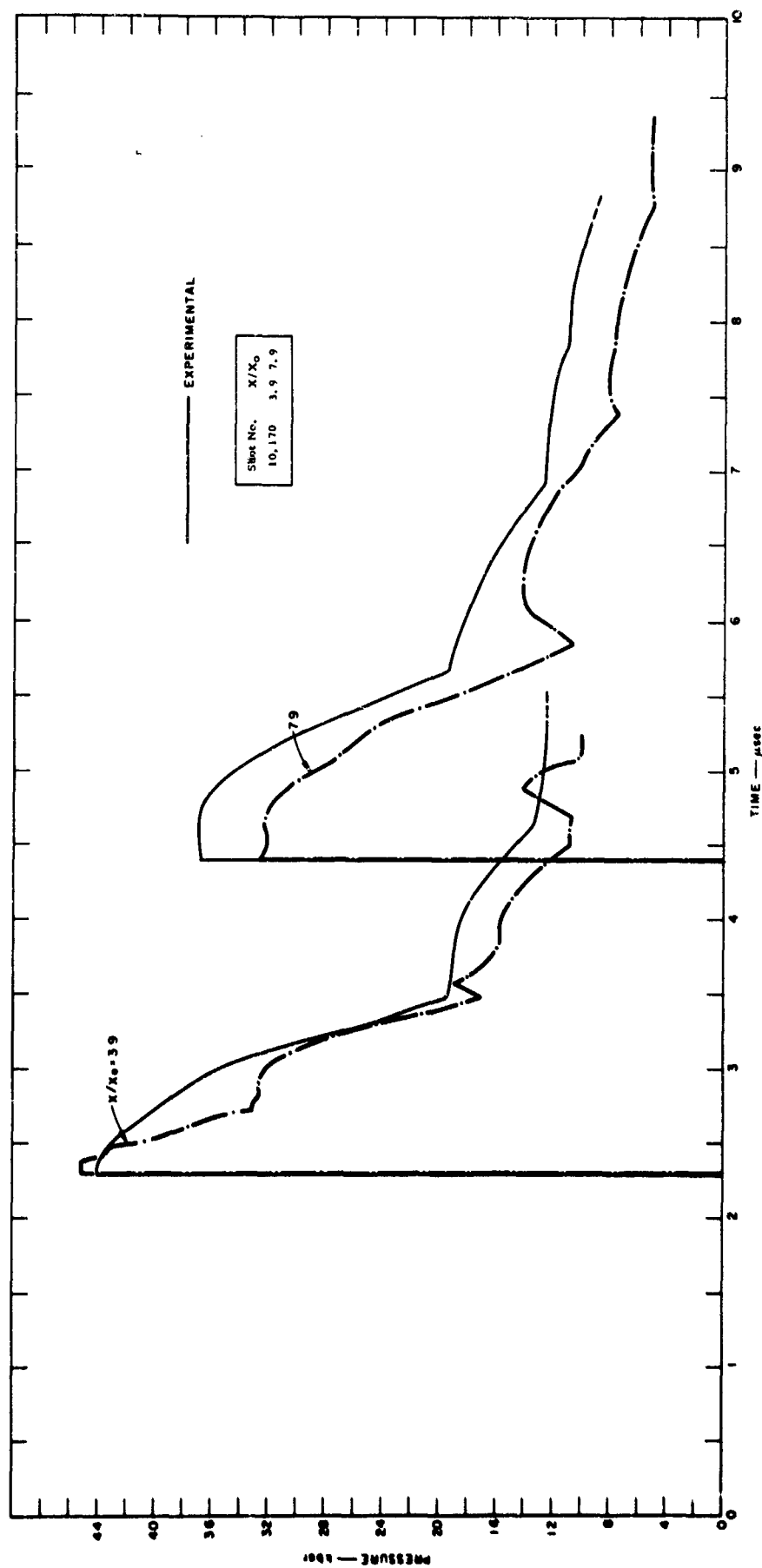
those obtained by the use of the code using the method of characteristics. Part of the disagreement (about half) is due to the fact that the equations of state are slightly different, see Eqs. (1) and (4). The remainder of the disagreement must be due to the way in which the artificial viscosity code operates. Apparently the true velocity of the leading edge of a rarefaction is not preserved by the code.

Including rigidity in the equation of state of aluminum changed the calculated results very little, Fig. 22(a). Thus the difference between the experimental and calculated results shown in Fig. 22(a) must be due to a poor representation of the equation of state of the epoxy. Figure 22(b) summarizes the results obtained by the inclusion of rigidity in the equation of state of the epoxy. The calculated results using  $Y = 1.0$  kbar,  $M = 0$  agree fairly well with the experimental data.

## B. ALUMINUM

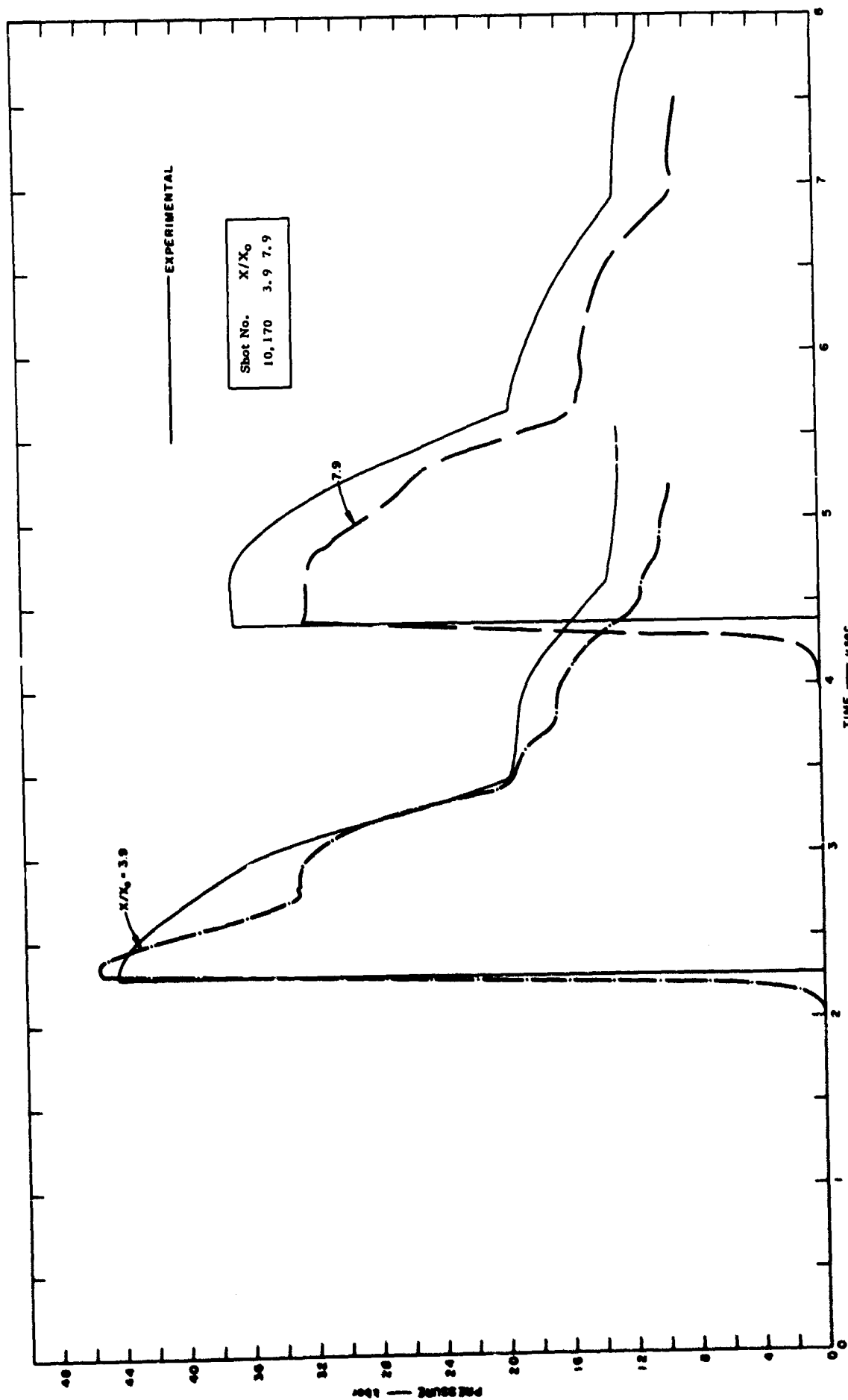
An attempt was made to calculate the response of gages on both aluminum and copper targets. As discussed above, the gages on thin aluminum targets gave unexpectedly high pressures, so that all the data were normalized for aluminum targets. This unexplained behavior of the gages makes the comparison of calculated and experimental results of questionable value. Such comparisons are made however for two gages in Fig. 23(a) which show that the calculated peak pressures for  $x/x_0 = 3.9$  are in fair agreement. Agreement is not so good when the aluminum specimen is 7.9 times as thick as the flyer plate. Of some interest is the reloading of the gage for the calculated results, at times of  $4.9 \mu\text{sec}$  for the thin target and  $5.9 \mu\text{sec}$  for the thick target. There is no indication of this reloading in the two gage records. This appears to be evidence that too great a strength at fracture (15 kbar) was used in the calculation.

The calculated results shown in Fig. 23(b) were obtained by using 5 kbar for the strength of the material at fracture. The shapes of the calculated pulses now agree with the gage records much better than in Fig. 23(a)—at least as far as the later parts of the pulses are concerned. These results do not prove conclusively that the spall strength of aluminum is closer to 5 kbar than to 15 kbar. One reason for this is the necessity for extrapolating the equation of state of aluminum to negative pressure, which raises questions which will not be discussed in this report. A spall strength for annealed 2024 aluminum of 10 kbar is consistent with results reported by Butcher *et al.*<sup>12</sup>



(a) 15-ibar SPALL STRENGTH

FIG. 23 COMPARISON OF CALCULATED WAVE PROFILES WITH RESULTS OF GAGES FOR ALUMINUM TARGETS



(b) 5-500 SPALL STRENGTH

FIG. 23 COMPARISON OF CALCULATED WAVE PROFILES WITH RESULTS OF GAGES FOR ALUMINUM TARGETS

When the relation between stress and strain is assumed to be elastoplastic, the initial relief of pressure is always elastic. This relief is accomplished by a wave which is visualized as showing little, if any, dispersion. Its effect should be virtually that of a rarefaction shock and should carry a pressure drop of about  $4Y$ . For a pressure of about 100 kbar, Eq. (2) gives a value of  $Y$  of 7.5 kbar. Thus the shock in aluminum should be overtaken by an elastic wave and the interaction should reduce the pressure by about 30 kbar. Following the interaction, the profile of the wave may again be almost flat, as it was just following the impact of the flying plate. The "Q"-code handles this interaction fairly well as shown in Fig. 23(a). In the first calculated profile, the elastic wave has not overtaken the shock front. But its interaction reduces the pressure by 10 kbar about 0.3  $\mu$ sec after the shock front reaches the gage. This is the effect of the 30-kbar wave in the aluminum mentioned above which, because of the impedance mismatch, propagates into the epoxy as a 10-kbar wave.

The record of the gage at  $x/x_0 = 3.9$  is inappropriate when compared with the results of the calculations referred to above. From the slope,  $dp/dt$ , of the back side of the wave, it appears that the initial relief wave is more dispersed in time than the following wave. The effect described above as virtually being a rarefaction shock is not observed. The decay is not as rapid as the results given by the Q-code, which is expected to smear out such shock-like effects. If elastic relief waves are involved in the flow, their arrivals are not apparent in the records from the gages.

None of the gage records obtained indicates clearly the arrival of the elastic relief wave. This may be due to the inability of the gage to respond to a sudden release in pressure. Some "hysteresis" has been reported in other experiments in which the pressure on the gage was relieved in a controlled situation.<sup>5</sup>

For the second profile shown in Fig. 23(a), the calculated results show that the elastic relief wave has attenuated the shock to a pressure of 32 kbar in the epoxy. The top of the wave is relatively flat, as is the top of the profile given by the gage. Here the gage record is consistent with the elastoplastic model and is inconsistent with the hydrodynamic model which always gives a triangular profile after the initial flat top has attenuated.

### C. COPPER

Results of calculations are shown in Fig. 24 for three thicknesses of copper targets. Spall strength is arbitrarily taken to be 5 kbar and the copper spalled in several places for each example. Spalling started in each case about  $0.2 \mu\text{sec}$  after the shock front hit the gage. This means that the fractures occurred very close to the copper-epoxy interface. Calculated and experimental results agree reasonably well over most of each pulse. This is surprising because of the complications introduced into the calculations by the necessity for permitting the material to spall. Spall strengths of 24 and 28 kbar are reported.<sup>12</sup> Use of such values for the spall strength would increase the calculated reloading at the gage position.

As in the case for aluminum targets, the experimental results for copper do not show the characteristics of elastoplastic flow. Note the shape of the top of the calculated pulse shown by the gage at 3.9. There is an initial spike and then a flat portion from  $3.2 \mu\text{sec}$  to  $3.5 \mu\text{sec}$ . This shape is expected from the use of the elastoplastic model. The gage at 3.9 does not show this shape, or the gage may not be able to respond to such a sudden release of pressure.

As in the case for aluminum targets, the gage on the thick copper target does not show the sharp peak characteristic of the attenuation predicted by hydrodynamic theory.

### D. GOLD

No calculations were performed for gold in which the elastoplastic equation of state was used. However, a value of the yield strength,  $Y$ , was derived from the experimental data in Section 4D. It was necessary to use a handbook value, 0.42, for Poisson's ratio for hardened gold to convert from the amplitude of the supposed elastic wave to a value of  $Y$ . The value of  $Y$  was found to be 4 kbar, so that it is expected that the yield strength for gold is also dependent on the stress.

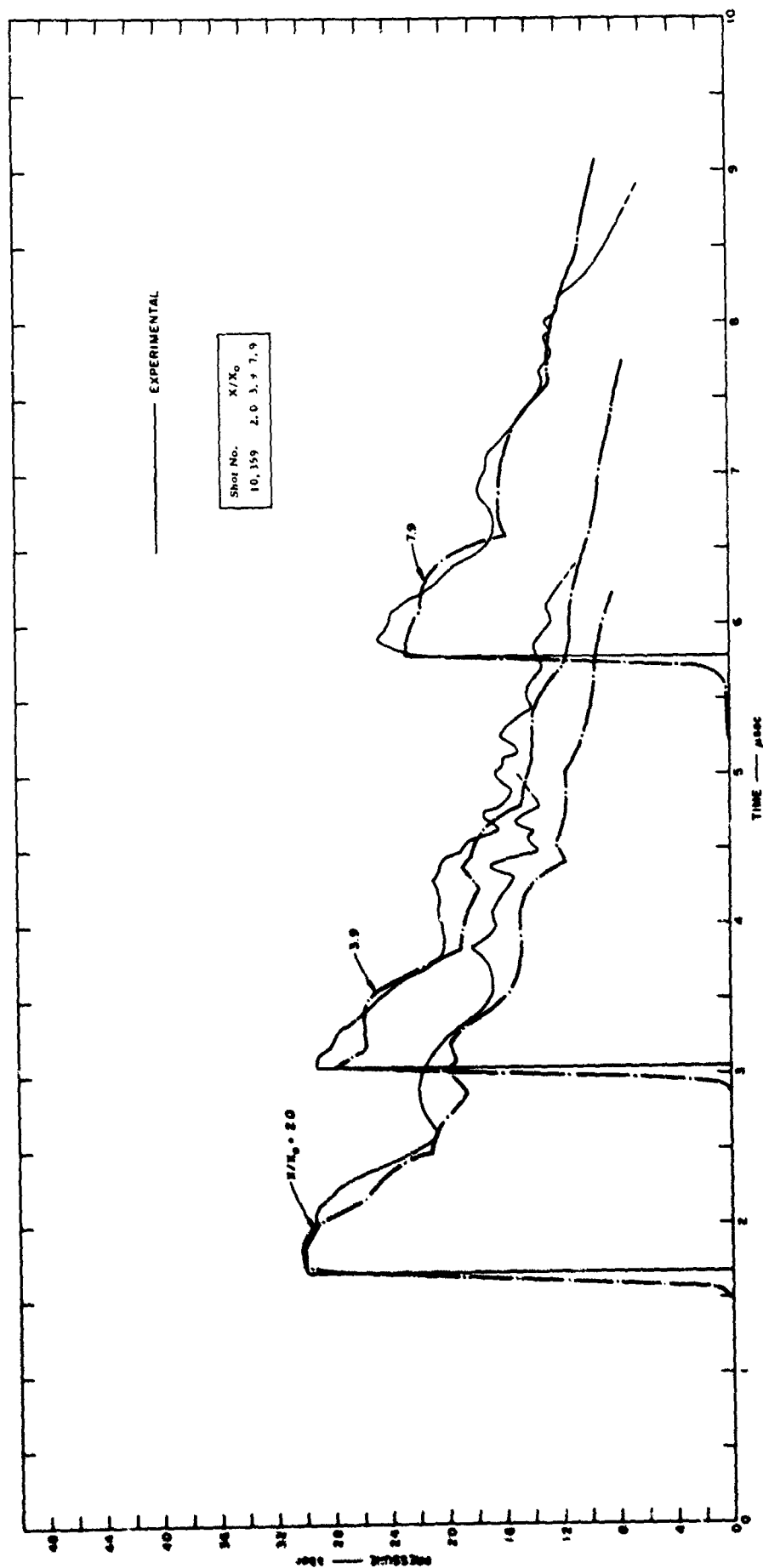


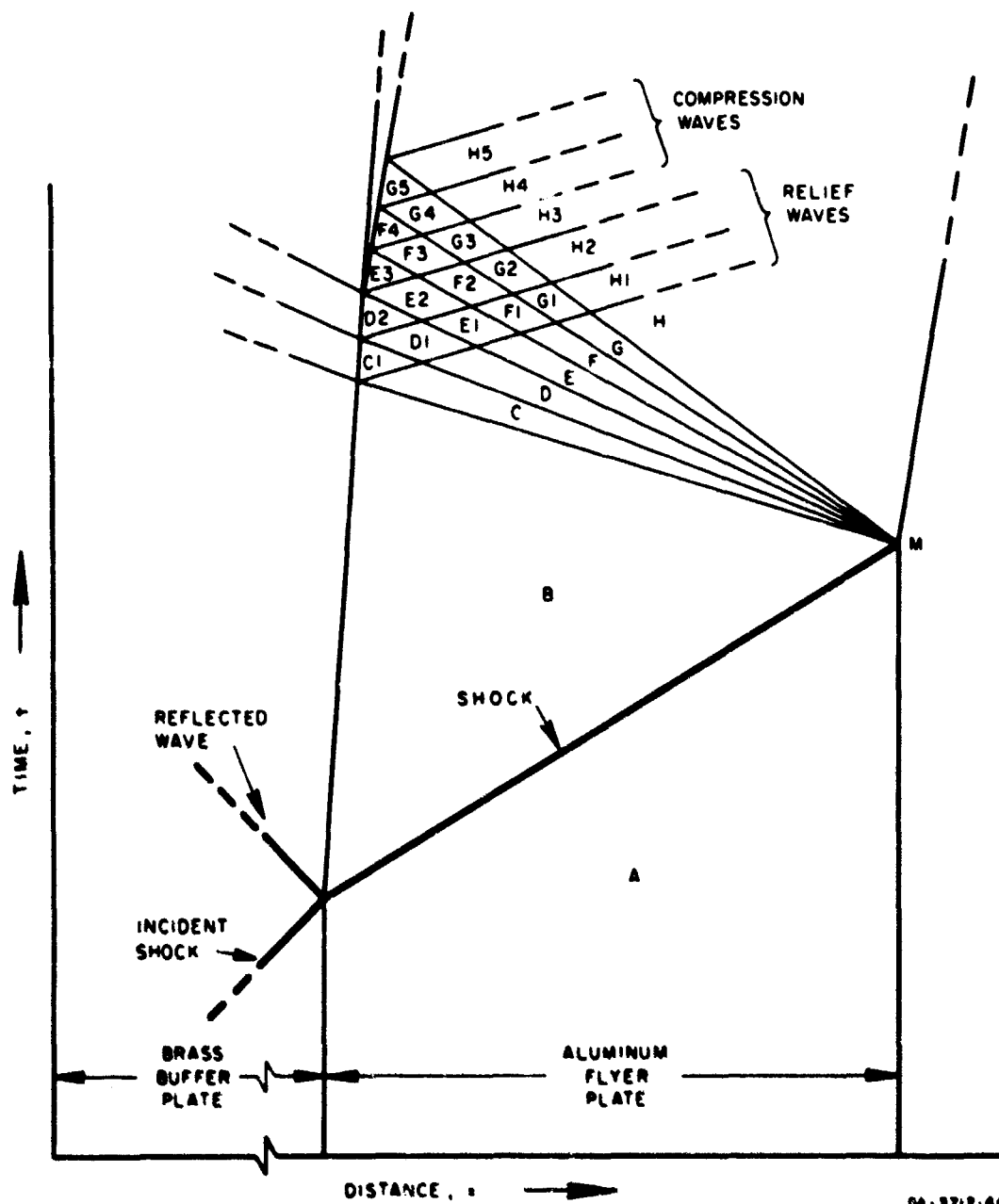
FIG. 24 COMPARISON OF CALCULATED WAVE PROFILES WITH RESULTS OF GAGES FOR COPPER TARGETS. SPALL STRENGTH ASSUMED TO BE 5 Kbar IN COPPER



## APPENDIX I

### MECHANISM CAUSING FLYER PLATES TO SPALL

It is possible that the flyer plates may spall, i.e., fracture into two or more pieces, because the material in the flyer plate is put into a state of tension at the instant that it is separating from the brass buffer plate. This possibility exists even though the wave entering the aluminum from the brass has a constant state behind the shock front, i.e., the shock is a uniform shock. Furthermore, no bonding is necessary at the interface for the production of a tensile stress in the flyer plate. As shown in Fig. I-1, the shock wave reflects from the free surface of the flyer plate as a rarefaction fan. In the figure the rarefaction wave is assumed to consist of a succession of small waves, each being represented by a line which divides the area in the  $(x,t)$  diagram into fields. When a wavelet reaches the interface, each in turn is transmitted into the brass and reflected into the aluminum. The reflected wavelets are also rarefactions. At some time the part of the flyer plate adjacent to the brass will acquire a higher velocity than the brass, and the interface will open up. Thus, the field marked *E3*, for example, will have a stress-free boundary. The fields labeled *F3*, *G3*, and *H3* are reached from field *E3* by successively crossing elements of the original rarefaction centered at the point *M*. Thus the fields named must have successively lower pressures than field *E3*, which is stress-free. These fields then represent locations in the plate which are in a state of tension. Using the method of characteristics, the basis for drawing Fig. I-1, Fowles and Curran<sup>6</sup> estimated the maximum tension to be 35 kbar when the flyer plate was driven at a velocity of 0.19 cm/ $\mu$ sec. The spall threshold for aluminum may be well below 35 kbar, so that the plate fractures soon after it starts to move. The estimate may not be reliable, however, because the equation of state of aluminum had to be extrapolated into the negative pressure region, and also because the work has indicated that hydrodynamics is not reliable as a method for calculating flow in solids.



GA-3712-44

FIG. I-1  $(x,t)$  DIAGRAM OF FLYER PLATE DRIVEN BY A BRASS BUFFER PLATE

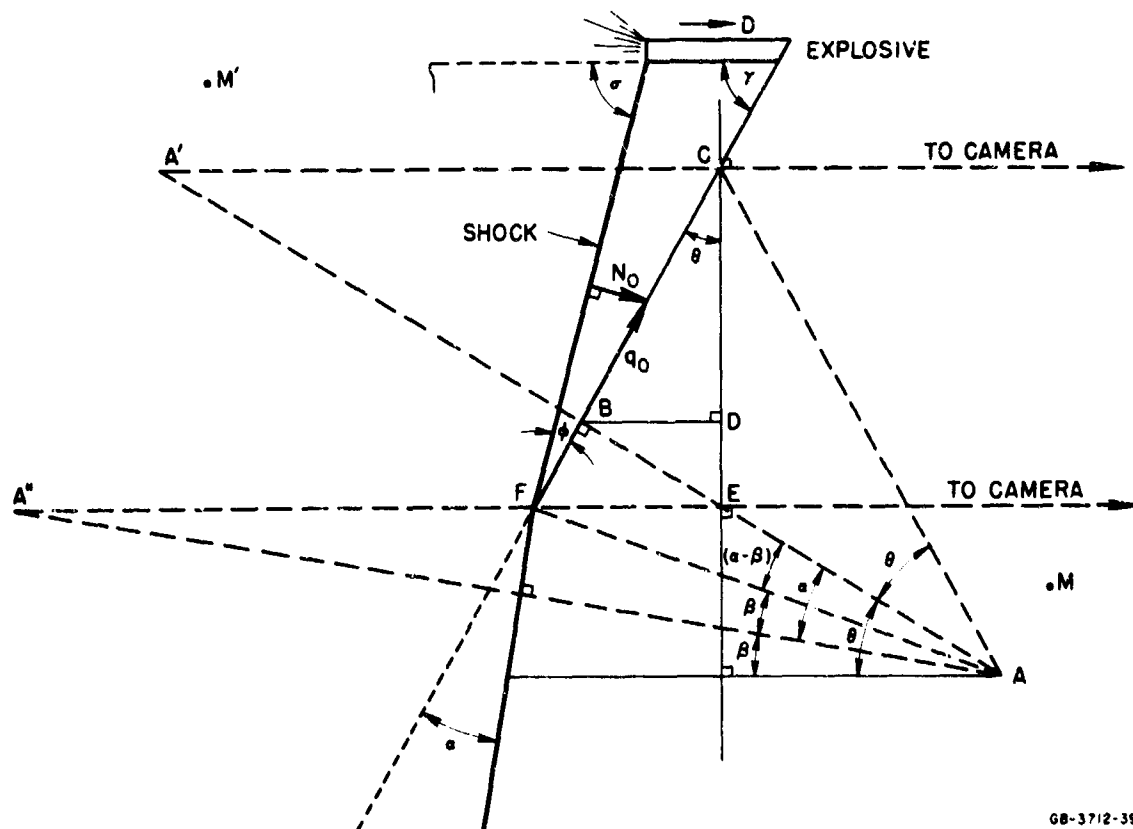
Figure I was drawn for illustrative purposes which required the fields to be large enough for labeling. The angular width of the rarefaction fan is probably much smaller than shown, and the triangular region including fields C1, G1 and G5 is much smaller than in the drawing. Thus the field of maximum tension, field #3, begins very close to the interface. If there are no time effects, the spall fracture, if any, should occur very close to the rear of the flyer plate.

If the shock is not uniform, the flyer plate can be caused to spall by the interaction of the rarefaction fan centered at the point *M* in Fig. I-1 with the rarefaction following the shock front. If the shock wave is sufficiently peaked, the spall fracture can form near the front of the plate, whereas the spall caused by the mechanism described above should occur near the rear of the flyer plate. Thus for a nonuniform shock wave the plate can fracture at almost any location.

## APPENDIX II

### THE OPTICAL LEVER ARM TECHNIQUE

The optical lever arm technique as described by Fowles<sup>3</sup> is applicable when a portion of a reflecting surface is abruptly bent through a small angle by the arrival of a shock wave. Light from the point source, Point A in Fig. II-1, is reflected in the undisturbed surface and has an image at the point A'. The shock, whose normal velocity is  $N_0$ , contacts the free surface at F and deflects the surface through the angle  $\alpha$ . Also in Fig. II-1, the image of the light source A is reflected in the deflected



GB-3712-39A

FIG. II-1 GEOMETRY FOR OPTICAL LEVER ARRANGEMENT

surface and is located at A''. This image is not fully illuminated because the camera accepts a cone of light from a point source and point F must move upward before the full cone is reflected in the deflected surface to the camera. In Fig. II-1 the axis of the camera is horizontal, and

normals to the original and deflected surfaces are inclined at the angles  $\theta$  and  $\beta$  to the horizontal. The distance,  $d$ , between points  $A$  and  $B$  is known, and the displacement of the traces on the film is proportional to the distance  $\overline{CE}$ . From Fig. II-1 it is evident that

$$\begin{aligned}\overline{BC} &= d \tan \theta \\ \overline{CD} &= \overline{BC} \cos \theta = d \sin \theta \\ \overline{BF} &= d \tan (\alpha - \beta) \\ \overline{DE} &= \overline{BF} \cos \theta = d \tan (\alpha - \beta) \cos \theta \\ \overline{CE} &= a = \overline{CD} + \overline{DE} \\ \theta &= \alpha + \beta\end{aligned}$$

so that

$$\tan (2\alpha) = \frac{(a/d) \cos \theta}{1 - (a/d) \sin \theta} \quad . \quad (\text{II-1})$$

The value of  $a$  must be obtained from the displacement,  $J$ , of the trace on the film, so that the magnification of the optical system is needed. Suppose another source of light is at the point  $M$ , Fig. II-1, at a distance  $G$  from the source  $A$ . The images of sources  $A$  and  $M$  as seen in the undisturbed surface appear to be separated by a distance  $G \cos \theta$ . On the screen of the Vanguard Motion Analyzer the two sources are separated by a distance  $Z$ , so that the magnification is  $G \cos \theta / Z$ . Thus the quantity  $a$  is found to be

$$a = (JG \cos \theta) / Z \quad .$$

Equation (II-1) then becomes

$$\tan (2\alpha) = \frac{(JG \cos^2 \theta) / Zd}{1 - (JG \sin \theta \cos \theta) / Zd} \quad . \quad (\text{II-2})$$

Where the value of  $\theta$  is zero, the result reduces to that obtained by Fowles. The velocity of the free surface in the direction of the normal to the original surface is

$$u_n = q_0 \tan \alpha \quad . \quad (\text{II-3})$$

where  $q_0$  is defined in Fig. II-1.

This is not the true velocity of the surface, because particles will move perpendicularly to the undisturbed surface only if the angle  $\phi$  is zero. A better approximation is given in the following paragraph.

As the shock advances, the point  $F$  in Fig. II-1 moves past point  $C$  and the image  $A'$  disappears. Until that time, the image  $A'$  is recorded on the film as a streak because of the rotation of the mirror in the smear camera. Many light sources are used in a shot, and the termini of the streaks as viewed in the undeflected surface define a curve on the film (Figs. 5 and 6 in the main report). Differentiation of this curve gives the velocity  $q_0$ , the "apparent velocity" of the shock along the free surface. Previous analyses used the nomenclature of one-dimensional shock wave theory;<sup>3</sup> oblique or two-dimensional shock wave relations are preferred here. Referring to Fig. II-2, and using the nomenclature of Courant and Friedrichs,  $q_0$  is the velocity of the oblique shock and  $\phi$  is the angle between the vector  $q_0$  and the shock line.<sup>13</sup> The velocity of flow behind the shock is represented by the vector  $q_1$ , which intersects  $q_0$  at the angle  $\delta$ , the angle of turning of a streamline at the shock. The velocity,  $u_1 = N_0 - N_1$  is the particle velocity behind the shock wave.

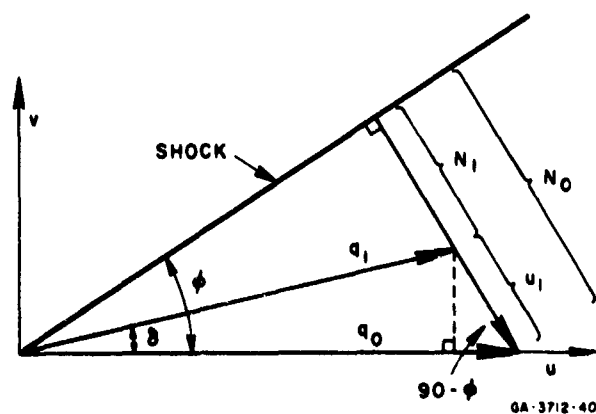


FIG. II-2 DIAGRAM OF TWO-DIMENSIONAL SHOT

From the diagram,

$$\tan \delta = \frac{u_1 \cos \phi}{q_0 - u_1 \sin \phi} \quad (\text{II-4})$$

from which

$$u_1 = \frac{q_0 \sin \delta}{\cos (\phi - \delta)} \quad (II-5)$$

Hydrodynamic theory predicts the angle of turning of the free surface to be twice the value of  $\delta$ , i.e.,  $\alpha = 2\delta$ . Thus the value of  $\delta$  is obtained from the optical lever arm equation. The value of  $\phi$  can be determined for the two-dimensional experiments by referring to Fig. I-1, where the shock is represented by a straight line for convenience. If the wedge angle is represented by  $\gamma$ , then

$$\sigma = \gamma + \phi \quad .$$

The detonation advances toward the apex of the wedge with the velocity  $D$  while point  $F$  moves with the velocity  $q_0$ . Using the sine law

$$D/\sin \phi = q_0/\sin (180 - \sigma) = q_0/\sin \sigma \quad .$$

Eliminating  $\sigma$  gives

$$\tan \phi = \frac{D \sin \gamma}{q_0 - D \cos \gamma} \quad (II-6)$$

so that Eq. (II-5) can be solved for the particle velocity immediately in back of the shock front. Thus values of  $u_1$  may be found for many points on the face of the wedge.

The components of velocity,  $N_0$  and  $N_1$  are related to density and pressure by the conservation of mass and momentum equations

$$\rho_0 N_0 = \rho_1 N_1 \quad (II-7)$$

$$\rho_0 N_0^2 + P_0 = \rho_1 N_1^2 + P_1 \quad (II-8)$$

In these equations,  $\rho$  is the density and  $P$  is the pressure, the subscript 0 refers to the state in front of the shock, and subscript 1 refers to the state behind the shock.

In addition,

$$u_1 = N_0 - N_1 \quad (II-9)$$

so that

$$P_1 - P_0 = \rho_0 N_0 u_1 \quad . \quad (II-10)$$

But

$$N_0 = q_0 \sin \phi$$

so that

$$P_1 - P_0 = \rho_0 q_0 u_1 \sin \phi \quad . \quad (II-11)$$

Thus the pressure of the shock wave can be calculated for any point on the wedge face. The density behind the shock is obtained from the relation

$$1 - \frac{\rho_0}{\rho} = \frac{u_1}{q_0 \sin \phi} \quad . \quad (II-12)$$

When the value of the angle  $\phi$  is nearly 90.0 degrees, the quantity  $q_0 \sin \phi$  becomes equal to  $N_0$  and the results are the same as those derived by Fowles.<sup>3</sup> The use of the oblique shock relations obviates the annoying question about the direction of the motion of the free surface.

In the case of the one-dimensional experiments, it is not possible to calculate the value of the angle  $\phi$ , that is, the angle of incidence of the shock on the wedge face is not known, principally because of the curvature of the flyer plate. For this reason, those experiments do not yield equation of state data. The wedge angle is used as an approximation in the analysis so that an approximate value of the particle velocity  $u_1$  is obtained. An approximate shock velocity,  $N_0$ , may then be calculated if the equation of state of the specimen material is known. A new approximation to the value of  $\phi$  is then obtained from

$$\sin \phi = N_0/q_0 \quad (II-13)$$

where  $q_0$  is known from the camera record. Thus, a closer approximation for the value of  $u_1$  can be obtained.



## REFERENCES

1. Erkman, John O., Hydrodynamic Theory and High Pressure Flow in Solids, Stanford Research Institute, Project No. PGU-3712, Technical Summary Report No. 2, 1962.
2. Erkman, John O., Hydrodynamic Theory and High Pressure Flow in Solids, Stanford Research Institute, Project PGU-3712, Final Report, 1963.
3. Fowles, G. R., "Shock Wave Compression of Hardened and Annealed 2024 Aluminum," *J. Appl. Phys.* **32**, 1475-1487 (1961).
4. Keough, D. D., Pressure Transducer for Measuring Shock Wave Profiles, Stanford Research Institute, Project No. GPU-3713, Final Report, 1963.
5. Keough, D. D., R. F. Williams, and D. Bernstein, "Piezoresistive Pressure Transducer," paper to be presented at Annual Meeting of ASME, New York, November 1964.
6. Fowles, G. R. and D. R. Curran, Experimental Testing of Shock-Attenuating Materials, AFSWC-TDR-62-22, 1962.
7. Erkman, John O., Stanford Research Institute, Project No. GSU-4613, Quarterly Progress Report No. 4, 1964.
8. Rice, M. H., R. G. McQueen, and J. M. Walsh, *Solid State Physics*, F. Seitz and D. Turnbull, eds., Academic Press, Inc., New York, 1958, Vol 6, pp. 1-63.
9. Gray, Dwight E., ed., *American Institute of Physics Handbook*, McGraw-Hill Book Co., Inc., New York, 1957.
10. Duvall, G. E. and Roy C. Alverson, Fundamental Research in Support of VELA-UNIFORM, Stanford Research Institute, Project No. PGU-3731, Semiannual Technical Summary Report No. 4, 1963.
11. Von Neumann, J. and R. D. Richtmyer, "A Method for the Numerical Calculation of Hydrodynamic Shocks," *J. Appl. Phys.* **21**, 232-237 (1950).
12. Butcher, B. M., L. M. Barker, D. E. Munson, and C. D. Lundegren, "Influence of Stress History on Time Dependent Spall in Metals," *AIAA Journal*, **2**, 977-990 (1964).
13. Courant, R. and K. O. Friedrichs, *Supersonic Flow and Shock Waves*, Interscience Publishers, Inc., New York, 1948.

Unclassified

Security Classification

## DOCUMENT CONTROL DATA - R&amp;D

(Security classification of title, body of abstract and indexing annotation must be entered when the overall report is classified)

1. ORIGINATING ACTIVITY (Corporate author) Stanford Research Institute Menlo Park, California		2a. REPORT SECURITY CLASSIFICATION Unclassified	
		2b. GROUP	
3. REPORT TITLE SHOCK ATTENUATION IN SOLID AND DISTENDED MATERIALS			
4. DESCRIPTIVE NOTES (Type of report and inclusive dates) Final Report 1 August 1963 through 1 November 1965			
5. AUTHOR(S) (Last name, first name, initial) Rempel, J. R.; Erkman, J. O.; Schmidt, D. N.; and Isbell, W. M.			
6. REPORT DATE February 1966	7a. TOTAL NO. OF PAGES 176	7b. NO. OF REFS 13	
8a. CONTRACT OR GRANT NO. AF29(601)-6040	9a. ORIGINATOR'S REPORT NUMBER(S) WL-TR-64-119		
b. PROJECT NO. 5710			
c. Subtasks: 15.018, 15.032	9b. OTHER REPORT NO(S) (Any other numbers that may be assigned this report) SRI Project GSU-4613		
d.			
10. AVAILABILITY/LIMITATION NOTICES Distribution of this document is unlimited.			
11. SUPPLEMENTARY NOTES		12. SPONSORING MILITARY ACTIVITY Air Force Weapons Laboratory (WLRP) Kirtland AFB, New Mexico 87117	
13. ABSTRACT PHASE 1. FOAMS. Results of optical measurements of peak pressures in the 0.1- to 6-kbar range transmitted through 3- to 12-mm-thick layers of certain foams, namely, 0.7 to 1.4 g/cc aluminum, 0.67 g/cc polyurethane, 1.1 g/cc beryllium, 1.1 and 1.7 g/cc graphite, and 1.0 g/cc silica, are presented. The peak pressures scale approximately linearly with the ratio of superficial momentum density to superficial mass density of foam; the validity of the scaling and the scale factor depend strongly on the kind of foam. The effect distention on scaling relations in aluminum is slight but is somewhat greater in graphite. Of the foams considered, polyurethane transmits the least peak pressure per unit of added weight but shows the greatest tendency to increase the delivered momentum through rebound. Present theory fails to predict accurately peak pressure or wave shape for observed shocks but the condition under which the transmitted shock is an elastic forerunner only can be predicted fairly reliably.  PHASE 2. SOLIDS. Attenuation of shock waves is studied in specimens made of 1060 and 2024 aluminum, OFHC copper, gold, and Armstrong C-7 epoxy. The strains induced in the specimens are virtually one-dimensional. Comparison of experimental and calculated results indicate that an elastoplastic model for the relation between stress and strain should be used for aluminum, copper, and epoxy but more data is needed to determine the stress-strain relation for gold.			

Unclassified

Security Classification

14. KEY WORDS	LINK A		LINK B		LINK C	
	ROLE	WT	ROLE	WT	ROLE	WT
Shock propagation						
Shock attenuation						
Hugoniot						
Equation of state						
Dynamic response						
Distended materials						
Elastic-plastic						

### INSTRUCTIONS

1. **ORIGINATING ACTIVITY:** Enter the name and address of the contractor, subcontractor, grantee, Department of Defense activity or other organization (*corporate author*) issuing the report.

2a. **REPORT SECURITY CLASSIFICATION:** Enter the overall security classification of the report. Indicate whether "Restricted Data" is included. Marking is to be in accordance with appropriate security regulations.

2b. **GROUP:** Automatic downgrading is specified in DoD Directive 5200.10 and Armed Forces Industrial Manual. Enter the group number. Also, when applicable, show that optional markings have been used for Group 3 and Group 4 as authorized.

3. **REPORT TITLE:** Enter the complete report title in all capital letters. Titles in all cases should be unclassified. If a meaningful title cannot be selected without classification, show title classification in all capitals in parenthesis immediately following the title.

4. **DESCRIPTIVE NOTES:** If appropriate, enter the type of report, e.g., interim, progress, summary, annual, or final. Give the inclusive dates when a specific reporting period is covered.

5. **AUTHOR(S):** Enter the name(s) of author(s) as shown on or in the report. Enter last name, first name, middle initial. If military, show rank and branch of service. The name of the principal author is an absolute minimum requirement.

6. **REPORT DATE:** Enter the date of the report as day, month, year; or month, year. If more than one date appears on the report, use date of publication.

7a. **TOTAL NUMBER OF PAGES:** The total page count should follow normal pagination procedures, i.e., enter the number of pages containing information.

7b. **NUMBER OF REFERENCES:** Enter the total number of references cited in the report.

8a. **CONTRACT OR GRANT NUMBER:** If appropriate, enter the applicable number of the contract or grant under which the report was written.

8b, 8c, & 8d. **PROJECT NUMBER:** Enter the appropriate military department identification, such as project number, subproject number, system numbers, task number, etc.

9a. **ORIGINATOR'S REPORT NUMBER(S):** Enter the official report number by which the document will be identified and controlled by the originating activity. This number must be unique to this report.

9b. **OTHER REPORT NUMBER(S):** If the report has been assigned any other report numbers (*either by the originator or by the sponsor*), also enter this number(s).

10. **AVAILABILITY/LIMITATION NOTICES:** Enter any limitations on further dissemination of the report, other than those

imposed by security classification, using standard statements such as:

- (1) "Qualified requesters may obtain copies of this report from DDC."
- (2) "Foreign announcement and dissemination of this report by DDC is not authorized."
- (3) "U. S. Government agencies may obtain copies of this report directly from DDC. Other qualified DDC users shall request through \_\_\_\_\_."
- (4) "U. S. military agencies may obtain copies of this report directly from DDC. Other qualified users shall request through \_\_\_\_\_."
- (5) "All distribution of this report is controlled. Qualified DDC users shall request through \_\_\_\_\_."

If the report has been furnished to the Office of Technical Services, Department of Commerce, for sale to the public, indicate this fact and enter the price, if known.

11. **SUPPLEMENTARY NOTES:** Use for additional explanatory notes.

12. **SPONSORING MILITARY ACTIVITY:** Enter the name of the departmental project office or laboratory sponsoring (paying for) the research and development. Include address.

13. **ABSTRACT:** Enter an abstract giving a brief and factual summary of the document indicative of the report, even though it may also appear elsewhere in the body of the technical report. If additional space is required, a continuation sheet shall be attached.

It is highly desirable that the abstract of classified reports be unclassified. Each paragraph of the abstract shall end with an indication of the military security classification of the information in the paragraph, represented as (TS), (S), (C), or (U).

There is no limitation on the length of the abstract. However, the suggested length is from 150 to 225 words.

14. **KEY WORDS:** Key words are technically meaningful terms or short phrases that characterize a report and may be used as index entries for cataloging the report. Key words must be selected so that no security classification is required. Identifiers, such as equipment model designation, trade name, military project code name, geographic location, may be used as key words but will be followed by an indication of technical context. The assignment of links, rules, and weights is optional.

AD 628796

Research and Technology Division  
AIR FORCE WEAPONS LABORATORY  
Air Force Systems Command  
Kirtland Air Force Base  
New Mexico

2 March 1966

ERRATA

WL-TR-64-119:

SHOCK ATTENUATION IN SOLID AND DISTENDED MATERIALS  
(Unclassified Report) February 1966

Cover:

Change Technical Report No. WL-TR-65-119 to read:

"TECHNICAL REPORT NO. WL-TR-64-119"

*C. W. Haig*  
C. W. HAIG  
Chief, Reports and Data Branch  
Technical Information Division